SOME INVESTIGATIONS OF THE BEHAVIOUR OF A ROTATING ARC DISCHARGE.

'Thesis submitted in accordance with the requirements of the University of Liverpool for the degree of Doctor in philosophy by Joseph Spencer.'

MARCH 1987

ABSTRACT

The investigations of a rotating arc discharge in stationary Sulphur hexafluoride during the peak current and current zero phases of arcing show that it is a complex interaction of many primary parameters.

The information gathered from experimental investigations leads to some simplifications about the arcs aerodynamic and electrical behaviour over a range of arc currents (3kA - 18kA), normalised magnetic fields (35mT/kA-113mT/kA) and two different phase angles (47°and 80°). At current zero photographic data helps to normalise the arc's conductance and leads to a useful comparison between different operations.

Simplifying the arcs behaviour leads to an arc model which can describe the arc's aerodynamic and electrical behaviour and is sufficiently accurate during the peak current and current zero phases of arcing that it can predict the thermal performance of the arc discharge for different operating conditions.

CONTENTS

1 INTRODUCTION

The successful operation of a circuit breaker requires control of the arc discharge during the high current phase of arcing and the current zero phase. The efficiency of the circuit interrupter can be improved if the most influential parameters are identified and then improved.

The aim of this work is to investigate those parameters which control a magnetically rotated SF_6 arc discharge between annular electrodes for one half cycle of simulated sinusoidal fault current and the effects upon the arc's behaviour of changing such parameters during peak current arcing and at current zero.

Those parameters investigated during the peak currrent and current zero periods are; the arc current, magnetic flux density, the phase difference between the exciting current and resultant magnetic flux, rotational velocity, the arc length and the critical rate of recovery voltage (rrrv) after current zero.

The experimental results are obtained on a model test circuit breaker using a tuning capacitive/inductive power circuit. The peak current varied from 3kA to 18kA and the normalised magnetic flux density changed between 35mT/kA and 113mT/kA for two phase difference angles (47° and 80°). The static pre-arc pressure did

not vary from 0.7 atmospheres above ambient.

A pair of parallel voltage probes monitors the arc voltage during rotation and an estimate of the electric field strength is calculated from these results. This information correlates with further evidence obtained through high speed photographic methods and other arc voltage measurements which enables some simplifying assumptions to be made about the electric field.

The shape of the arc during the half cycle is monitored by a high speed photographic technique and an image converter technique during arcing. The shape revealed by these techniques helps to simplify the arc's behaviour during the peak period of arcing and is most useful for describing the pre-current zero and post current periods of arcing. This image converter method enables the path of arc reignition to be determined and leads to further simplication of the arc's description.

The complex interaction of the magnetic field and the arc current is investigated. Although the primary interaction of these two parameters is to cause arc rotation, there is a secondary interaction which can cause arc instabilities. These instabilities occur for a particular set of conditions, these are identified and the implications of such instabilities assessed.

The non-uniformity of the magnetic field within the

arcing coil is examined with particular attention to its interaction with the arc current. Those Lorentzian forces arising from the three dimensional orientation of both the arc current and the magnetic field are assessed and the principle and most dominant forces identified.

The thermal performance of the interrupter is examined and those parameters which have the most influence upon it identified and discussed in relation to the arc velocity, length, electric field strength, magnetic, flux density and phase difference angle. The thermal performance results are analysed further and are recast and presented in a more convenient form.

To highlight the effects of the major influencing parameters upon the arc's behaviour an approximate theoretical model using a three zone description is presented. The model uses the momentum and energy conservation equations to describe the arc column in terms of its temperature, area, electric field, velocity and its withstand voltage at current zero. This model is particularly useful because it is not only describes the arc's behaviour during the peak current period but describes the behaviour of the arc at current zero and beyond for various imposed rate of rise of recovery voltages (including free recovery conditions). Despite the complex interaction of many

factors it is possible to derive a model of the arc column with a blend theoretical and experimental information.

2.1 GENERAL ARC PROPERTIES

An arc is an electrical discharge sustained by current flowing between two electrodes. It has three physically distinct regions corresponding to the two electrode regions and an inter-connecting plasma column. The arc is distinguishable from other electrical discharges by the relatively high current densities and gas temperature in both the electrode and column regions. The only arcs which are discussed are the high pressure discharges (i.e. $\geq$ 1bar).

2.1.1 ELECTRODE REGIONS

Electrode phenomena arc essentially junction phenomena associated with the problem of transferring current between a metallic conductor, in which electrons arc the only charge carries, and a gaseous conductor in which charges of both polarity are free to move. The two electrode regions, called the anode and cathode regions, exhibit similar characteristics of high electric and thermal fields, relatively high current densities and electrode jets consisting of gas and electrode vapour.

The physical phenomena occuring at each electrode are different.

At the cathode, electons are extracted from the electrode, rapidly heated and accelerated into the arc plasma, whilst at the anode the electrons are decelerated, cooled and collected by the anode.

The cathode region is generally more important in affecting the column properties than the anode region because of the thermal emission processes which affect the magnitude of the characteristics already mentioned. The voltage potential at the cathode is between 8 to 20 volts; that at the anode is only 1 to 12 volts and this is dependant upon the electrode material (1). These potential drops are known as cathode - and anode - fall voltages respectively and occur over very short distances (10^{-5} m) (2,4) from the electrode surfaces.

The electric field strengths are therefore extremely large and are believed to exceed 10^{9}v/m at the cathode and 10^{6} - 10^{7}v/m in the anode region (2).

Another important feature is the high thermal gradient which exists because of the difference in magnitude between the high temperature in the arc column and the relatively lower temperature at the electodes. It is impossible to measure the temperature in these regions directly but within a few mean free paths of the electrodes an estimate of 6000°k has been made (4). However this could be higher if the current flow contraction near the electrodes is considered.

This contraction causes the temperature at the column ends of cathode - and anode - fall regions, to be larger than that observed at the arc column axis midway between the electrodes (3) and will increase this temperature gradient between those fall regions and the arc column.

This contraction, due to magnetic pinch forces, causes an increase in current density above that observed in the arc column. The current density in the cathode fall region is about 10^{10} - 10^{11} A/M^2 and in the anode fall region about 10^8 - 10^9 A/M^2 (1). The reason for the uncertainty in the current densities is because of the difficulty in measuring these densities directly so that recoarse has to be made to somewhat indirect measurement techniques.

The variation in the current density between the plasma column and the electrode regions causes a change in the radial magnetic pinch force acting upon the arc plasma (5) which creates a negative pressure gradient directed away from the electrode surface. If this pressure gradient is sufficiently it causes gas and electrode vapour, formed in high current arcs, to flow in the form of jets away from the electrode. This flow can cause contamination of the plasma column.

2.1.2 COLUMN REGION

Transition from the electrode regions to the column region takes place through transition or contraction zones where the properties are a mixture between those seen in the electrode and column regions. Provided that the electrode gap is large enough, the formation of an arc column occurs relatively free from electrode influences. The overall properties of this column at high pressure are dominated by thermodynamic properties of the host gas. Since the arc plasma may be considered to be in thermal equilibrium (but not always) (5). The arc plasma properties are then governed by temperature and pressure relationships for that particular gas.

The magnitude of the electric field and current densities can vary in this column region depending upon the external constraints imposed upon the arc column. Typically the electric field is between 100v/m - 10^4v/m (5) and the current density between 10^6 - 10^7 A/M^2 (5). These values are several orders of magnitude lower than those occurring at the electrodes.

The external constraints imposed upon the arc column gives rise to two types of arcs called axis-symmetric and non-axis-symmetric arcs.

Axis-symmetric arcs have a radial temperature profile symmetrical about the arc's axis. Such profiles are observed in free burning, wall stabilised and gas blast arcs.

The wall stabilised arc is confined by a wall surrounding the entire cylindrical boundary of the arc. The temperature profile is radially symmetrical with the temperature at the boundary being equal to that at wall. The principle energy loss mechanism, which governs the behaviour of the arc column, is the radial energy transport (5).

The free burning arc has no wall constraints and simply expands radially outwards until controlled only by natural convection, magnetic pumping forces and the arc current (5). The temperature near the boundary is nearly ambient. Any imposed gas axial flow, supplied by external means, will cause contraction of the arc boundary because of the forced convection losses (5). Provided the flow is laminar then the temperature profile remains axis-symmetric (5).

If this imposed flow is directed transverse to the column then the induced pumping produces internal vortices which in turn cause the radial temperature profile to become distorted so that it is no longer symmetrical about the arc's axis (5).

Similar pumping and internal vortices occur if an external transverse magnetic field is applied to the arc column (5). The thermal and electrical structures of the arc column are non-symmetric. The arc column bends in the direction of the Lorentz force and if there are no external constraints, the arc column moves freely under the Lorentz action. Energy is convected away by either the arc moving through the gaseous medium or the medium flowing passed the arc column (5).

By loosing energy the column is cooled and controlled. This control mechanism of convective energy lose is utilised in the designs of Commercial circuit breakers (5). The most common form of gas filled circuit breaker is the method of extinguishing the arc by forcing gas axially along the length of the column (5). However, recent development of circuit breakers using transverse flow and magnetic fields for arc extinction has created a new avenue for circuit breaker manufacturers and the electricity services.

2.2 SULPHUR HEXAFLUORIDE FILLED CIRCUIT BREAKERS

SF_6 circuit breakers operate on basically the same principle as air blast breakers which is to control and condition the arc discharge during the high current phase of arcing in preparation of exstinction at current zero.

It is only in the methods used in achieving this aim that there is considerable research activity on the part of Industry and Universities.

There are two broad categories - that using an axially blow arc quenching technique and that employing transverse flow and magnetic fields aided quenching. Axial blown arc devices can be subdivided into "mono-blast", "duo-blast", and "puffer type" arc interrupters (4).

2.2.1 TWO PRESSURE MONO-FLOW INTERRUPTERS

Operation of two pressure, mono-flow circuit breaker requires the transfer of gas from a high pressue reservoir to a low pressue tank. This gas flow is coaxial with the arc discharge and passes through a nozzle or an orifice, which causes axial acceleration of the flow (57). The constraining influence of the nozzle or orifice produces an increase in pressure gradient at this point (57).

The essential geometric difference between a nozzle and an orifice is the profile. A nozzle has a slow divergent contour down stream of the throat which is not present for an orifice (57) also the orifice tends to have a shorter upstream inlet region. These contours affect the flow conditions which inturn influence the arc's electrical. This behaviour is now summarised.

A nozzle used to constrain the flow in this type of interrupter has a steep angle at the inflow end of the nozzle and a more gentle outflow angle. The first effect of the nozzle produces a converging subsonic accelerating flow towards the throat of the nozzle, whilst the outflow angle casuses the flow to decelerate and diverge becoming supersonic (57). Constraining an arc discharge in such a flow causes the arc's diameter to vary axially. This variation in arc area alters the electrical properties of the discharge which arc manifest as a change in current density, electrical field strength and temperature profile (57). These properties are most affected at the throat of the nozzle where the axial acceleration and axial pressure gradient ($\delta p / \delta z$) arc maximum (57).

The oriface arc is constrained in a similar way to the nozzle arc. The flow is accelerated more forcibly in the oriface and the resultant pressure gradient increase is greater. The dominant energy loss mechanism in the high pressure upstream region is the kinetic flow, whereas downstream of the throat radial convection dominates because of the kinetic energy flow and radially expanding arc core (57). However, for the nozzle arc because of the divergance in the downstream section, the important losses are due in part to turbulent effects (57).

2.2.2 DUO-FLOW INTERUPTERS

In duo flow interupters the arc burns between two nozzle shaped electrodes. The central portion of the arc column which lies between the two electrodes is subjected to a radial flow which then flows through each nozzle electrode. The centre of the arc discharge is exposed to the highest pressue. At the throat region the electrical properties are greatly affected causing an increase in current density, electric field strength and axis core temperature.

The existance of a large axial pressure gradient and a high arc core temperature causes a strong axis acceleration of the arc plasma. The resultant axial plasma flow is maintained by a cold radial gas flow into the arc. The entrained gas is heated by heat exchange and absorbing radiation.

The principle energy loss mechanisms are convection processes at the central region and straining conduction and turbulent processes in the nozzle throat regions of the arc column. The properties are similar for both mono and duo flow interrupters but with a duo flow system there is twice the flow of a mono system.

2.2.3 PUFFER INTERRUPTERS

Whereas a two pressure interrupter always has a pressurized tank of gas, the Puffer breaker generates the pressure needed to cause gas flow through the nozzle just prior to the instant the breaker is required to operate. This flow can be generated by either using a piston arrangement or a self-pressurising technique.

The piston method relies upon the opening mechanism to move a piston arrangement causing a pressure rise in an enclosed chamber. The gas is then released through exhaust ports and flows through a contoured nozzle co-axially with the plasma flow. The nozzle is designed to give similar flow conditions which exist in a two pressure arrangement, ensuring that the flow upstream of the throat is converging and accelerating.

The effects of these flow conditions upon the arc's electrical properties is similar but not identical to that of the two pressure system and are greatly affected by conditions at the nozzle throat.
The self pressurising circuit breaker relies upon the arc heating of the gas in an enclosed volume to generate the required pressure to sustain a nozzle flow. This flow contributes in a major manner to the energy loss from the arc column.

2.2.4 ROTATING ARC CIRCUIT BREAKER

Previous circuit interrupters have used the principle of axially cooling the arc by an accelerating flow through a nozzle or orifice. The concept of a rotary arc circuit breaker differs from the axial configuration in that the gas flow is transverse to the arc column. The gas flow can either be induced by external means or can be a relative flow with respect to a moving arc column. The simplest possible arrangement for circuit breaker use is an arc rotating under the influence of a magnetic field. Under the action of the magnetic force the arc rotates through cool gas, the energy from the arc heats the cooler gas consequently extracting energy from the arc.

There are three practical electrode arrangements which can be used in rotary arc interrupters; these consist of parallel ring electrodes, cylindrical electrodes positioned co-axially one inside the other and the third a similar co-axially arrangement but the inner electrode is positioned at the entrance plane of the outer ring electrode.

The interaction between the arc current and applied magnetic field gives rise to a lorentz force which is orthoganol to both arc current and magnetic field.

The arc column moves into the cool gas in front of it, heating the gas and leaving a relatively warm area behind the arc, called the wake. This wake is dissipated mainly by turbulent mixing with the surrounding gas.

The removal of energy from the arc column through forced convection controls and conditions the arc discharge in preparation for current interruption at current zero. However, the arc columns interaction with the surrounding mediumn and applied magnetic field is complicated as described in chapter 5. A major requirement for circuit interruption is the ability to control and condition the discharge. Cross flow arc control has only been recently introduced as a means for circuit interruption. Previously such arc control was used in arc heaters which utilised d.c. rather than a.c. control. Consequently investigations reported in the literature are mainly for direct current, steady state arc conditions with few specific application mentioned about circuit breakers. However, recently this technique has been adopted by a number of switchgear manufacturers for circuit interruption, but no indication of the major factors nor any theory describing the interrupters thermal performance has been reported.

Theories describing axi-symmetric arc behaviour are well documented but clearly show that formulating a rigorous model is extremely difficult even for this relatively easier situation. Selected theories are discussed in the next section. Non-axisymmetric arc behaviour is also discussed for various combinations of magnetic and flow fields.

2.3 AXI-SYMMETRIC ARC THEORY FOR CIRCUIT BREAKER

A description of arc behaviour in a circuit breaker environment is facilitated through the establishment of an arc model. Cassie (6) in 1939 first proposed such a model. Several other arc models, each becoming more sophisticated in their physical representation and mathematical complexity, have been developed.

This review discusses the earlier models of Cassie, Mayr and Browne (6,7,8 respectively) and the subsequent modification introduced by Frind (9,10) to Mayr's model. Departing from these traditional models, the discussion follows the development of those models using boundary layer analysis which significantly altered the theoretical description of the arc. Such models were developed by Swanson and Roidt (11-17), the Brown Boveri group (21-26), Lowke and Tuma (27-33) and an integral analysis method proposed by Cowley and Fang (34-40).

Two good reviews have been published in the past by Lee (41), covering the earlier models from Cassie to 1939 to 1969, and by Fang (42) discussing the boundary layer approach to modelling the arc's behaviour from 1970 to 1982.

Common to most high pressure arc models is the assumption that the conductivity of a given gaseous medium is a unique function of temperature and pressure. Experimental evidence suggests that this a valid assumption for most (but not all) operating conditions particularly if the medium does not become contaminated by electrode vapour. Therefore the proposed models only describe the arc column behaviour and usually neglects electrode effects. For various proposed arc models specific assumptions have been introduced to simplify the mathematical difficulties and the complex physics.

2.3.1 CASSIE'S MODEL.

Cassie's model was published in 1939 (6). From a mathematical and physical point of view this model involves three basic assumptions:

(i) The temperature within the cylindrical arc column is uniform with a finite electrical conductivity inside the column and ambient outside. The energy density per unit volume (q) is constant.

(ii) Changes in the total current supplied by the external circuit are accommodated by a change in the arc cross-sectional area (A).

(iii) The power dissipated per unit volume (N) from the arc column is proportional to the cross-sectional area (i.e. $N = \lambda A$, λ = const)

The resulting theoretical description for the electrical behaviour of the arc discharge is;

$$R\frac{d}{dt}\left[\frac{1}{R}\right] = \frac{1}{\theta_c}\left[\frac{e^2}{E_0^2} - 1\right] \qquad (2.1)$$

Where θ_C= Cassie time constant $=\lambda/q$; e = instantaneous arc voltage and $E^2_0 = \lambda/\sigma$ = steady state voltage

The advantage of such a model is the ease of use and understanding. However the model has serious misleading implications for the arc's behaviour at current zero. The constant electrical characteristic (E_0 independent of I), constant energy densites with the arc and the dominance of convection losses lead to a good qualitative description of the arc during the peak current regime but during current zero this is no longer true.

This deficiency became apparent and a newproposal by Mayr was published.

2.3.2 MAYR'S MODEL

Mayr's model is essentially for low current arcs where conduction rather than convention dominates. Mayr assumed that:

(i) The cross-sectional area of the arc column remains constant.

(ii) The arc temperature changes to accommodate any change in the arc current. This temperature change causes the electrical conductivity (σ) to change according to the Saha's equation.

$$\sigma = \text{constant}\, T^{3/4} \exp\left(-\alpha'/T\right) \qquad (2.2)$$

Where α' = gas constant and T = temperature

(iii) The stored energy per unit volume (q) is independant of arc geometry and is only a weak function of temperature. This leads to the result that the stored energy per unit length (Q) is constant (Q_o).

Mayr's equation for the electrical behaviour of the arc is given as;

$$R\frac{d}{dt}\left[\frac{1}{R}\right] = \frac{1}{\theta_m}\left[\frac{W}{N_o} - 1\right] \qquad (2.3)$$

Where θ_m = Mayr time constant = Q_o/No; W = energy input

The time constant θ_m is the ratio of stored energy (Q_o) to dissipated energy (No) and is constant because of the initial assumptions.

Essentially with the assumptions of constant cross-sectional area and temperature variation, this type of model describing arc behaviour is a thermal conduction dominated and is useful in describing the low current, current zero period of arcing. Difficulty arises after current zero, when determining whether or not reignition has occured, since the ultimate sign is an increase in arc area. Mayr's model will not demonstrate this phenomena because temperature rise by itself is not sufficient to indicate that reignition has occurred.

The parameters E_0 and No in both the Cassie and Mayr models respectively, are quantities which depend upon the geometry and flow conditions existing within the arc device. The time constant θ, is dependent upon the nature of the surround mediums and the dissipation term, λ or No (Cassie or Mayr model respectively).

The Cassie and Mayr models are useful for obtaining qualitative descriptions of the arc's electrical behaviour if used for the peak current regime and current zero regime of arcing, respectively. Browne (8) produced a composite model which combined both models each describing the arc's behaviour during a particular phase.

2.3.3 BROWNE'S COMPOSITE MODEL

Browne's method used Cassie's description before current zero and Mayr's afterwards, linking the $^{di}/_{dt}$ before current zero with a $^{dv}/_{dt}$ afterwards.

Applying a current ramp waveform ($I(t) = I\omega t$) to Cassie's model modifies equation (2.1) to;

$$\frac{d}{dt}\left[\frac{1}{R^2}\right] + \frac{2}{\theta_c}\left[\frac{1}{R^2}\right] = \frac{2}{\theta_c}\left[\frac{I(t)}{E_0^2}\right] \qquad (2.4)$$

The resistance of the arc column at current zero is described in terms of the arc voltage (E_0), the peak current (I), the circuit frequency (ω) and the arc time constant (θ_c).

$$R_0 = \frac{\sqrt{2}\,E_0}{I\omega\theta_c} \qquad (2.5)$$

The arc resistance at current zero is used as a starting condition in Browne's modified Mayr equation. Imposing a restrike voltage after current zero modifies the Mayr equation to:

$$\frac{dR}{dt} - \frac{1R}{\theta_m} = -\frac{E^2(t)}{Q_0} \qquad (2.6)$$

and has the general solution

$$R = \left[\exp\left(\frac{t}{\theta_m}\right)\right]\left[R_0 - \frac{1}{N_0\theta_m}\int_0^t E^2(t)\exp\left(\frac{-t}{\theta_m}\right)dt\right] \qquad (2.7)$$

The arc resistance after current zero (2.7) is a combination of the supplied restrike voltage and, most important, is related to the current zero arc resistance, hence is a function of di/dt.

For successful arc reignition the differential of R in equation (2.7) must be negative. Using a linear voltage ramp for E (t), the critical restrike voltage is,

$$\left(\frac{dE}{dt}\right)_{crit} > \frac{R_o e^{t/\theta} N_o}{2\theta_m[\theta_m e^{t/\theta} - \theta_m - t]} \qquad (2.8)$$

This useful expression for circuit breaker design has the disadvantage that E_o and N_o are dependant upon geometry and imposed flow conditions and θ_c, θ_m arc gas dependant quantities. The effect of these dependancies upon the above parameters must be known before equation (2.8) can be fully utilised for predictive purposes.

2.3.4 FRINDS EXTENSION OF MAYRS MODEL

Frind proposed the use of a modified form of the Elenbans-Heller equation (2.9). Using a relationship between electrical conductivity and the heat flux derived by Maecker (4.3) (2.10)

$$\sigma E^2 + \left(\frac{1}{r}\frac{d}{dr} rk\frac{dT}{dr}\right) - dc_p\frac{dT}{dt} = 0 \qquad (2.9)$$

and

$$S(T) = \int_0^T k(T)dt \qquad (2.10)$$

Mayr's time constant becomes for a thermal conduction cooled arc,

$$\theta_F = \frac{r_o^2}{(2.4)^2 k} \qquad (2.11)$$

Where K = thermal conductivity and r_o = arc radius
This modification although dependant upon geometry suffers from the same difficiencies as the Mayr model.

Although Frinds time constant agrees reasonably well with those measured experimentally by Yoon and Spindle (44) for SF_6, the agreement with air is poor.

	SF_6	AIR
θ. Calculated (9,10)	1.3	3
θ. Measured (44)	0.8	80

Despite the obvious simplicity of such models they were to be replaced by methods using boundary layer analysis. It was hoped that these models would overcome the difficiencies of previous models.

2.3.5 SWANSON AND ROIDT'S ARC MODEL

Swanson and Roidt's new approach for the arc's description takes the radial variation of properties into account. The energy equation is derived from conservation considerations and is given by,

Thermal Storage *Radial Convection* *Axial Convection*

$$\rho \frac{\delta h}{\delta t} + \rho U_r \frac{\delta h}{\delta r} + \rho W_a \frac{\delta h}{\delta x} =$$

Expansion cooling *Radiation* *Radial diffusion*

$$\left[1 - \rho\left(\frac{\delta h}{\delta \rho}\right)_T\right] W \frac{dp}{dx} - Q(p,T) + \frac{1}{r}\frac{\delta}{\delta r}\left[r\left(\frac{\mu}{P_r} + \frac{\rho_t \varepsilon_m}{P_{rt}}\right)\frac{\delta h}{\delta r}\right]$$

Joule heating

$$+ \sigma E^2 \qquad (2.12)$$

This equation written in the above form is essential incorrect. This is a result of expressing the thermal storage term as $\rho \frac{\delta h}{\delta t}$ *, correction to the equation is possible in two ways. The first requires changing the thermal term to* $\rho c_p \frac{\delta T}{\delta t}$ *and the second removal of the expansion cooling term. However , the influence of this error has been lessened because one or both terms have been neglected during further analysis.*

The method of solution adopted requires that during the peak current regime, the arc temperature remains constant and changes in thermal storage are effected by arc area changed, the energy conservation is simplified, under this assumption, neglecting parts of the thermal storage terms which are influenced by temperature changes. This is expressed more formally as;

$$R^2 \frac{\delta}{\delta t} \int_0^1 \rho W(h-h_e)\eta\delta\eta \quad << \quad \left[\int_0^1 \rho W(h-h_e)\eta\delta\eta\right]\frac{\delta R}{\delta x}^2 \qquad (2.13)$$

and

$$R^2 \frac{\delta}{\delta t} \int_0^1 \rho W(F-F_e)\eta\delta\eta \quad << \quad \left[\int_0^1 \rho W(F-F_e)\eta\delta\eta\right]\frac{\delta R}{\delta x}^2 \qquad (2.14)$$

The energy equation can now be simplified to

$$\gamma\frac{\delta R}{\delta t}^4 + \frac{\delta R}{\delta x}^4 + \xi R^4 = C I^2(t) \qquad (2.15)$$

Swanson and Roidt solved equation (2.15) for a linear ramp towards current zero. However, difficulty arose when current zero approached since the losses attributed to conduction and turbulence became more effective than other losses. The simplifying assumptions (2.13 and 2.14) were revised.

$$R^2 \frac{\delta}{\delta x} \int_0^1 \rho W(h-h_e)\eta\delta\eta \quad >> \quad \left[\int_0^1 \rho W(h-h_e)\eta\delta\eta\right]\frac{\delta R}{\delta x}^2 \qquad (2.16)$$

and

$$R^2 \frac{\delta}{\delta t} \int_0^1 \rho W(F-F_e)\eta\delta\eta \quad >> \quad \left[\int_0^1 \rho W(F-F_e)\eta\delta\eta\right]\frac{\delta R}{\delta t} \qquad (2.17)$$

Essentially equations (2.16) and (2.17) imply that any change in thermal storage is due to a change in temperature rather than arc area.

Experimentally this is not true because Walmsley (47) and Lewis (48) have observed relatively rapid changes in the arc area within four micro-seconds of current zero (0.6 $mm^2/\mu s$ for di/dt of $14A/\mu s$). Within the same time period, Smith et al (49) recorded a decrease in arc temperature from $8700^{\circ}k$ to $7100^{\circ}k$, a substantial change.

A further two assumptions are used to obtain a soluble energy equation. The first is the introduction of the heat flux potential ($\dot{\tilde{S}}$), and the second is the assumption of a Bessel function profile of $\dot{\tilde{S}}$. The latter may describe the temperature profile before current zero but afterwards there could be a large deviation away from this because of relatively large changes in arc temperature compared to small changes in arc area (42)

$$\gamma\frac{\delta\dot{\tilde{S}}^2}{\delta t} + \frac{\delta\dot{\tilde{S}}^2}{\delta x} + \xi S^2 = \overset{*}{C}I^2(t) \qquad (2.18)$$

Equation (2.18) is solved for a linear voltage ramp after current zero Swanson (17). The rate of rise of recovery voltage (RRRV) predicted by Swanson and Roidt did not agree with experimental results but adjustment of a turbulence parameter led to an improved agreement.

This disagreement is not entirely due to the incorrect modelling of turbulent effects but is more probably due to the effect of the current assumption about arc area ($\delta A/\delta t = 0$).

Despite problems with this model it did lead to a furtherence of the art of modelling by using boundary layer analaysis techniques to describe electric arc plasma columns. However Swanson and Roidt used the over-simplified assumptions of Cassie and Mayr about arc area and temperature at current zero, although in a slightly modified way.

2.3.6 BROWN BOVERI GROUP MODEL.

This model was proposed by the BBC group after extensive experimental investigations on arcs in gas flow (21-26). A two zone approach has been adopted describing the high temperature conducting arc and the cold gas regions. To simplify the arc model, these zones are sub-divided into two categories, upstream and downstream, and further assumptions are introduced. For the upstream region these are:

(i) Axial heat conduction is neglected compared to convection.

(ii) In the momentum equation, only the most dominant term is included.

(iii) The radial pressure gradient is constant across the boundary region of the arc and the cold gas region and this is small compared to that in the axial direction and is therefore neglected.

The implications of this is that the axial pressure gradient determines the axial velocity component and that radial momentum need not be considered. However, the radial velocity is determined by the mass balance.

In the downstream region additional effects have to be included, which are:

(i) The temperature distribution is axisymmetrical but is dependent upon axial position (Z):

(ii) For supersonic flow velocities within the nozzle the kinetic energy of the gas contributes significantly to its total energy content but the contribution to the overall kinetic energy of the radial velocity component may be neglected:

(iii) The terms describing the radial flow of heat and the axial momentum contain contributions due to turbulent mixing effects.

The physical quantities used in the energy, mass and momentum equations are radially averaged but have an axial variation (this requires a knowledge of the temperature distribution within the arc). Integrating these equations over the cross-sectional area of each zone produces the following equations:

ARC ZONE

$$\frac{d(m_1 h_1)}{dz} + q\overset{o}{h}(r_1) = IE - 2\pi r_1 W - U_1 \quad \textit{ENERGY} \qquad (2.19)$$

$$\frac{d(m_1 v_1)}{dz} + qv(r_1) = -A_1 \frac{dp}{dz} - 2\pi r_1 S \quad \textit{AXIAL MOMENTUM} \qquad (2.20)$$

$$\frac{dm_1}{dz} = -q \quad \textit{MASS} \qquad (2.21)$$

COLD GAS ZONE

$$\frac{d(m_2 \overset{o}{h}_2)}{dz} + q\overset{o}{h}(r_1) = IE - 2\pi r_1 W - U_2 \quad \textit{ENERGY} \qquad (2.22)$$

$$\frac{d(m_2 v_2)}{dz} + qv(r_1) = -A_2 \frac{dp}{dz} - 2\pi r_1 S \quad \textit{AXIAL MOMENTUM} \qquad (2.23)$$

$$\frac{dm_2}{dz} = q \quad \textit{MASS} \qquad (2.24)$$

Where,

$$m_1 = \rho_1 v_{z1} \; ; \; m_2 = \rho_2 v_{z2} A_2 \; ; \; q = 2\pi r_1 \rho(r_1) \left[v_r(r_1) - v_z(r_1) \frac{\delta r_1}{\delta z} \right] \qquad (2.25)$$

and,

Arc cross-section: $A_1 = \pi r_1^2$

Cold gas flow cross-section: $A_2 = \pi(R^2 - r_1^2)$

Stagnation point enthalpy: $\dot{h} = h + v^2/2$ (2.26)

radial heat flux across the arc boundary:

$$W = -\left[(k+k_t)\frac{dT}{dr}\right]_{r_1}$$

radial flux of axial momentum across the arc boundary:

$$s = -\left[(\eta+\eta_t)\frac{dv_z}{dr}\right]_{r_1}$$

The method of solution for equations (2.19-2.26) is given by Hermann et al (22). The model shows that there are three different types of radial energy transport from the arc to the surrounding region which are radiation, conduction and turbulent mixing. However, only a small fraction of this energy increases the cold gas velocity (i.e. kinetic energy). The largest fraction is used to raise the temperature (i.e. enthalpy) of the radially inflowing gas to the arc region from the surrounding cold gas region. As a result the rate of radial mass inflow is limited by the magnitude of the radial energy flux.

The elementary processes are coupled to one another. The radial transport of energy determines the axial variation of the enthalpy stagnation point and therefore the arc temperature.

This temperature together with the arc radius determines the radial temperature gradient and as a result, the radial energy flux. The radial mass flow (-q) determines the axial increase of the axial mass flow in the arc.

The assumption imposed by the authors limits the use of the model. The temperature and velocity profiles are assumed to be the same shape, although allowed to vary with time both in radial extent and magnitude this affects the predicted RRRV characteristic. Treatment of the arc properties as being axially uniform makes it difficult to estimate the effect of turbulence. Finally there are six parameters (two radiation parameters, effective arc length, two turbulence parameters and the ratio C/p_o for the pressure distrubution) which are difficult to calculate either from experimental results or by theoretical arguments.

2.3.7 THE LIVERPOOL-CAMBRIDGE ARC MODEL

A more general and rigorous approach to arc modelling was adopted by Cowley (36) in 1974. This analysis is the boundary layer integral method which rigorously formulates the arc conservation equations of mass, momentum and energy together with the external flow equations in a non dimensional form.

In the model three regions are considered:

(i) The arc core (electrically and thermally conducting):

(ii) The thermal area (thermal conducting only):

(iii) The external flow (external flow conditions):

The main assumption, applicable to all three regions, is the similarity between the radially integrated properties of various types of arcs. This eliminates the need for a detached knowledge of the radial structure of the arc, once scaling laws for the various integrals have been established. The methods also lends itself to the mixing of theoretical arguments and experimental considerations such as the description of change in radiation loss from electrode contamination.

The various radial integrals of various arc plasma properties are expressed as "Characteristic areas", as defined in table (A.1) Jones and Fang (57).
The integral arc and external flow equations then become:

MASS

$$\frac{\delta}{\delta t}\left[\rho_{\infty}(A-\theta_{\delta})\right] + \frac{\delta}{\delta z}\left[\rho_{\infty} v_{\infty}(A-\theta_{d})\right] = 0 \quad (2.27)$$

MOMENTUM

$$\frac{\delta}{\delta t}\left[\rho_{\infty} v_{\infty}(\theta_{\delta}-\theta_{d})\right] - \rho_{\infty}\theta_{\delta}\frac{\delta v_{\infty}}{\delta t} + \frac{\delta}{\delta z}(\overset{*}{\rho}\overset{*}{v}^{2}\theta_{m}) - v_{\infty}\rho_{\infty}\theta_{\delta}\frac{\delta v_{\infty}}{\delta z}$$

$$= \frac{\mu I^{2}}{8\pi}\frac{\delta}{\delta z}(\ln\theta_{B}) \qquad (2.28)$$

OVERALL ARC ENERGY

$$\frac{\delta}{\delta t}\left[\overset{*}{\rho}\overset{*}{h}\theta_{\Delta} + 1/2\overset{*}{\rho}\overset{*}{v}^{2}\theta_{m} + 1/2\rho_{\infty}v_{\infty}^{2}(\theta_{\delta}-\theta_{d})\right] - \rho_{\infty}\theta_{\delta}\frac{\delta}{\delta t}(h_{\infty}+1/2v_{\infty}^{2}) +$$

$$\frac{\delta}{\delta z}(\overset{*}{\rho}\overset{*}{h}\overset{*}{v}\theta_{h} + 1/2\overset{*}{\rho}\overset{*}{v}^{3}\theta_{ke}) - \rho_{\infty}v_{\infty}\theta_{d}\frac{\delta}{\delta z}(h_{\infty}+1/2v_{\infty}^{2}) = EI - \overset{*}{Q}\theta_{Q}$$

(2.29)

CORE ENERGY

$$\frac{\delta}{\delta t}\left[\overset{*}{\rho}\overset{*}{h}\phi_{\Delta} + 1/2\overset{*}{\rho}\overset{*}{v}^{2}\phi_{t}\right] + \rho_{l}(\phi_{l}-\phi_{\delta})\frac{\delta}{\delta t}(h_{l}+1/2v_{l}^{2}) -$$

$$\rho_{\infty}\phi_{l}\frac{\delta}{\delta t}(h_{\infty}+1/2v_{\infty}^{2}) + \frac{\delta}{\delta z}\left[\overset{*}{\rho}\overset{*}{h}\overset{*}{v}\phi_{h} + 1/2\overset{*}{\rho}\overset{*}{v}^{3}\phi_{ke}\right] + \rho_{l}(\phi_{l}-\phi_{\delta})\frac{\delta}{\delta z}(h_{l}+1/2v_{l}^{2})$$

$$- \rho_{\infty}\overset{*}{v}\frac{\delta}{\delta z}(h_{\infty}+1/2v_{\infty}^{2}) = -2\pi\overset{*}{h}(k/C_{p})Nu + 2\pi\overset{*}{\eta}\overset{*}{v}v_{l}C_{\eta} + EI$$

(2.30)

CONDUCTANCE

$$I = \overset{*}{\sigma}E\theta_{c} \qquad (2.31)$$

EXTERNAL FLOW

$$\rho_{\infty} \frac{\delta}{\delta t}(1/2 v_{\infty}^2) + \rho_{\infty} v_{\infty} \frac{\delta}{\delta z}(h_{\infty} + 1/2 v_{\infty}^2) = 0 \qquad (2.32)$$

Where, ϕ *represents the characteristic arc core areas,*

η *is viscosity,*

C_η *is the friction factor,*

Nu *is the Nusselt number.*

Subscript " ∞ *" and "I" represents cold flow and arc core edge respectively, Superscripts "*" represents characteristic values.*

Equations (2.27 - 2.32) are in a general form which can be simplified and applied to a specific situation depending upon the constraints imposed upon the arc column. The set of equations are closed by shape factors which are related to the thermal area of the arc (i.e. $\Lambda_\alpha = \theta_\alpha / \theta_d$ *where* α *represents any subscripts given in table A.1). These shape factors reflect the influence of the shape and magnitude of temperature and standard velocity profiles (but not there radial extent). The actual velocity profile is related to the standard profile* $V_1(r,x,t)$ *through the velocity magnitude factor (g).*

$$v - v_{\infty} = g(v_1 - v_{\infty}) \qquad (2.33)$$

The shape factors calculated from the standard velocity profile are known as primary standard shape factors and are assumed to be uniquely related to the shape factor correlation parameter χ . A proper choice of χ leads to a universal relationship between shape factors and the correlation parameter. The success of the integral method is largely dependant upon this assumption and the unique relationship $\Lambda_{\alpha 1} = f(\chi)$ for any type of arc (34,37). Work carried out on computer simulated arc's (52,53) and experimantal results (54) indicates that this is true if the Nusselt number (Nu) is chosen as the correlation parameter. However, the choice of dynamic power loss and arc conductance per unit length as correlation parameters are unsatisfactory for predicting the transient arc behaviour (18,19,20).

From the conservation equations a simplified model for the current zero can be formulated by assuming negligible radiation loss and known pressure distribution ($\Theta_\delta << A$). A single non-dimensional equation results (2.34) which can be solved with a linear current ramp before current zero and a voltage ramp afterwards.

$$\frac{1}{v_\infty}\frac{\delta}{\delta T}\left(\frac{\Theta_\delta}{\alpha}\right) + \frac{\delta}{\delta z}\left(\Lambda_h \frac{\Theta_\delta}{\alpha}\right) = \frac{I^2}{\left(\frac{\Theta_\delta}{\alpha}\Lambda_c \alpha\right)} \qquad (2.34)$$

where $\alpha = A/A_t$, A_t = the throat area, Θ = non-dimensional overall area.

This model is sufficiently detailed to give information about the electric field strength, thermal area, conducting radius and the influence of current distortion prior to current zero due to circuit interation. A similar dependence is predicted of the RRRV upon di/dt and ambient pressure (P_o) as experimentally observed. This model (2.34) is not likely to be accurate at high value of di/dt's nor at high pressures.

2.3.8 CONCLUSIONS

Despite the large amount of experimental information about axisymmetric arcs there is no totally satisfactory arc model yet available. Each author is forced to make resource to simplifying assumptions about describing the arc's behaviour in axial flow. However the models describing the arc's behaviour have become sufficiently rigorous to allow qualitative description of the arc's steady-state and transient behaviour.

Replacing the axial gas flow with mutual orthoganal magnetic and flow fields considerably changes the arcs behaviour. Such arcs have distorted electrical, thermal and plasma flow fields which may show departures from symmetry about the arc's axis. The theoretical description of such arcs is extremely difficult because of the non-symmetric profiles and

until the present work was limited to the steady state description.

Such arcs in transverse field are considered further and methods of solution of cross flow arc equations are discussed.

2.4 NON-AXISYMMETRIC ARC BEHAVIOUR AND THEORY

2.4.1 ARC DISCHARGE ENVIRONMENTS

Interest has increased in the various technical applications of an electric arc discharge in crossed convective and magnetic fields. This has created a demand for the development of a sufficiently accurate arc model which would enable the arc's behaviour to be predicted under various imposed conditions. Apart from purely scientific interest, a study of this type of arc discharge is desirable in view of its applications in many kinds of power devices such as switchgear, gas heaters, arc furnaces, welding apparatus, plasma torches etc.

The importance of high pressure arcs in transverse flow and magnetic fields has been the subject of experimental and theoretical investigations. Review by Uhlenbusch (55), Stablein (56) and Jones and Fang (57) give a good overall view of experimental and theoretical investigations of the arc discharge under the influence of either transverse magnetic fields only, imposed

cross flow only or a combination of mutually orthoganol transverse magnetic and flow fields.

Free from electrode effects and constraining walls, the arc column responds in a number of ways to any imposed condition. An imposed magnetic field would cause the arc column to bend and move in the direction of the Lorentz force ($\underline{j} \times \underline{B}$) (fig.2.1). Gas flow opposing the Lorentz force will retard the movement of the cloumn eventually producing a straight column when the net force is zero (fig.2.2). Increasing the flow even further or removing the magnetic field causes the arc column to bend and move in the direction of flow (fig.2.3).

The arc's aerodynamic, electrical, plasma flow and thermal structures are also influenced by the external conditions. Experimental and theoretical investigations have been concerned with examining the electrical and thermal structures of the arc, the induced plasma motion within the arc column, the interaction of the arc plasma with the surrounding gas and electrode influences upon the arc's movement.

2.4.2 ARC COLUMN BEHAVIOUR

Subjecting an arc to cross flow or a transverse magnetic field causes disturbance of the internal plasma flow within the column and subsequently alters

the electrical and thermal profiles. A wall stabilised d.c. arc exposed to a transverse steady state magnetic field exhibits plasma disturbances under the action of a Lorentzian force ($\underline{j} \times \underline{B}$).

This force causes mass to flow in a plane perpendicular to the arc's axis and results in a convective energy transport mechanism distorting the previously symmetrical temperature profile in the direction of the Lorentz force (55,56). The induced flow within the arc plasma forms a double vortex whereby mass is transported back from the leading edge of the arc boundary (upstream) through the relatively cooler gas near to the impervious constraining wall and re-enters the arc at the opposite side (downstream) (figure 2.4). A similar plasma flow occurs within free burning arcs exposed to balanced magnetic and gas flow fields.

The formation of vortices within the plasma of an arc balanced in mutually orthoganol transverse fields was first thought to be determined by the Reynolds number of the external flow (Malgham and Benenson 66) but this was replaced later by a parameter (P) relating the magnetic forces to viscous forces (Fischer 62). For a balanced arc column sustained between two electrodes neglecting electrode effects, this votices parameter is,

$$P = \frac{IB}{\eta U} \qquad (2.35)$$

Where, I is the arc current, B applied magnetic field, η is visocity and U is flow velosity.

Vortices formation is favoured by either large arc currents and magnetic fields or low flow velocities and low viscosity (i.e. low temperature at the arc boundary). For low values of P the external flow partially penetrates the arc column and the temperature isotherms elongate in the direction of imposed flow. If P is large then a double vortex is generated (fig 2.4) and the isotherms extend laterally outwards perpendicular to the incoming flow.

For weak or no external magnetic field the self magnetic field of the arc is important in determining the existance of back flow. Fischer (62) showed this new parameter (P') to be,

$$P' = \frac{\mu_0 I^2 d}{\eta U D^2} \qquad (2.36)$$

where d is the maximum displacement of the arc centre line from the electrode centre line and D is the effective diameter. This parameter of Fischers is similar to that used by Uhlenbush (55).

$$\beta = \frac{\mu_0 I^2 \overset{*}{r}}{\bar{\eta} U D^2} \left(\frac{L}{D}\right)^2 \qquad (2.37)$$

Where $\overset{*}{r}$ represents arc column displacement, L arc length and D arc diameter, $\bar{\eta}$ mean visocity.

Equations (2.36,2.37) represent the ratio of the self magnetic force to friction force, formation of a double vortex being favoured by a large arc current, a large arc deflection, small flow velocities and small arc diameters. A further condition for the formation of vortices, although implied in equation (2.36) but explicit in equation (2.37), is that the arc length (L) must be greater than the arc diameter (D).

Such flows within the arc plasma disturb the isothermal and electrical structures of the arc. Experimental observation of these structures were undertaken by Baker and Benenson (67) and Sebald (68). Although they used different gases their results showed remarkable similarity between the two thermal structures. They show a lateral broadening of the temperature profile indicating the presence of back flow and calculating the back flow parameter (P) confirms this observation. Sebald (68) thus calculated the flow field from his temperature profile which clearly demonstrates a double vortex (fig.2.4) and two

stagnation points. These stagnation points occur upstream and downstream of the arc column. The flow lines terminate and originate at these stagnation points separating the vortices from each other and also from the by-passing external flow.

Further observations show that the external flow circumvents a region which far exceeds the luminous region of the arc column. This circumvention caused by the generated mass flow alters the arc's shape from circular to that of an elipse so altering the flow resistance of the arc column, which can nolonger be considered as a cylindrically heated solid body in a flow.

Plessl (69) examines an arc which is curved into approximately a semi-circle and rotating through stationary gas (fig.2.5). The temperature distribution was determined by spectroscopic means without resorting to symmetrical properties but considers the local thermodynamic equilibrium deviations. The distrubutions obtained by Plessl (fig.2.6.) show a deviation from radial symmetry as a result of movement through the surrounding gas medium. An increase in the arc's velocity causes further deformation and the isotherms which extend further in the direction of the Lorentz force becoming more compressed at the leading edge of the arc column.

A maximum plasma temperature of 4200°k was ovserved for a gas mixture of 40% hydrogen, 60% nitrogen.

An increase in the rotational velocity did not cause the maximum arc temperative to change, however, the electric field strength decreased from 90 v/m to 76 v/m for rotational frequencies of 30 Hz and 60 Hz respectively. The implication of this constant temperature and decreasing electric heating power is that reduced cooling occurs with increasing velocity. This reduction in arc cooling is accompanied by an increase in the total electrical conductance of the arc mainly caused through the cross-sectional area of the discharge increasing with the speed of rotation.

The plasma flow field in this experimental arrangement is extremely complex and is a result of the interaction of the arc plasma with the surrounding stationery gas and applied magnetic fields. Figure (2.6.) show that the flow field is composed of 6 votices and 6 stagnation point. This is a result of three basic processes.

(i) a mass flow through the arc in the direction of deflection caused by inhomogeneous heating due to the arc's curvature

(ii) a closed double vortex in the cross-sectional plave of the arc caused by the rotational movement

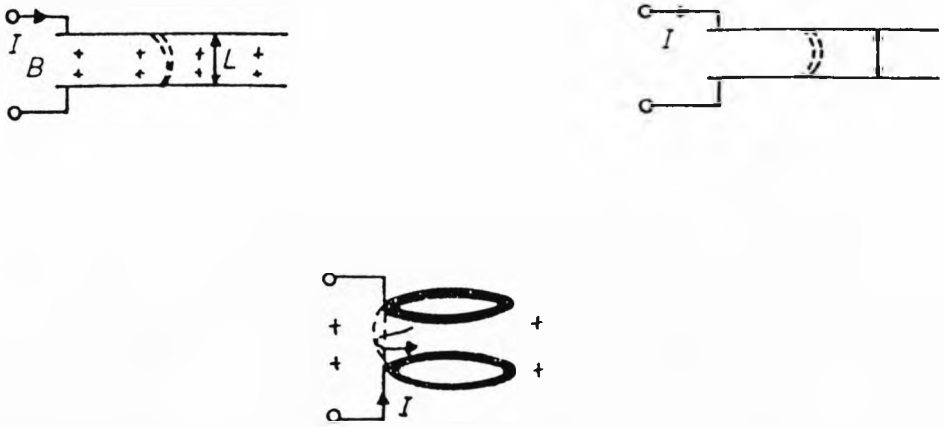

FIGURE 2.1. Lorentz Force Control Only.

FIGURE 2.2. Lorentz And Gas Flow Control.

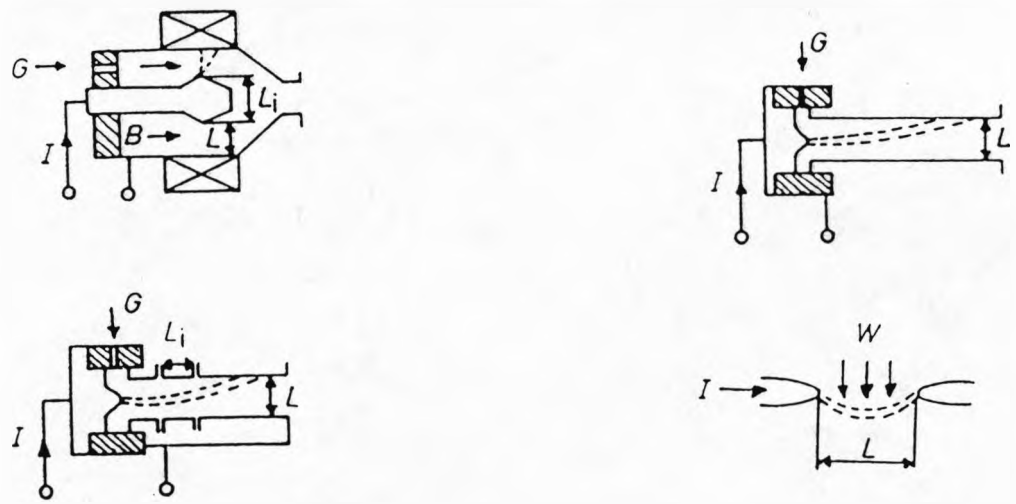

FIGURE 2.3. Gas Flow Control.

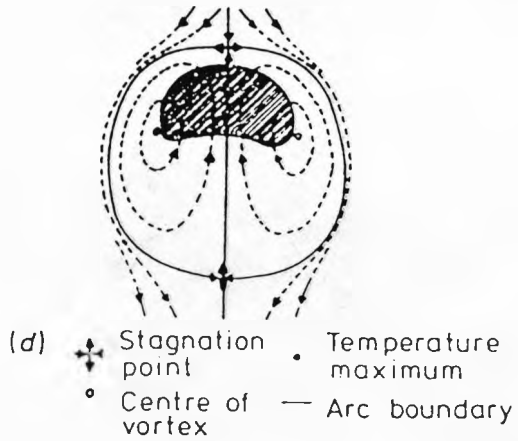

FIGURE 2.4. Double Vortex Formation.

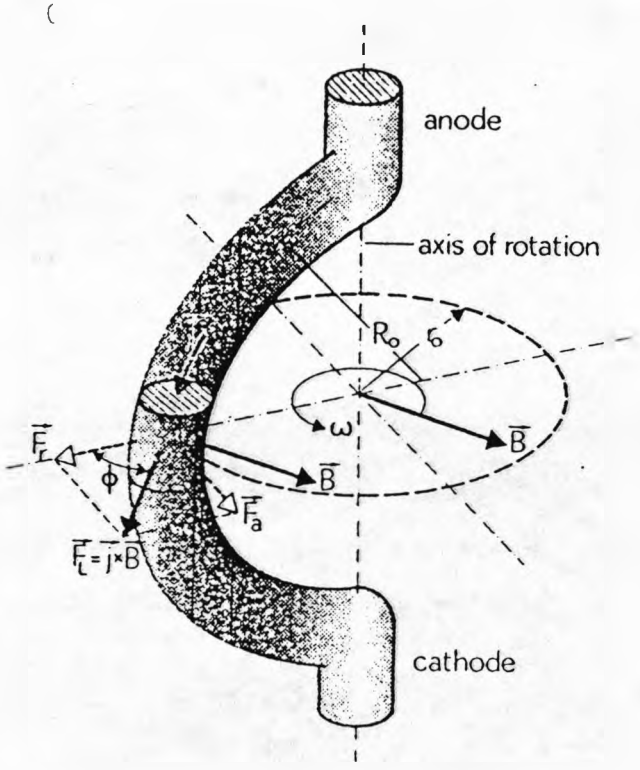

FIGURE 2.5. Rotating Arc.

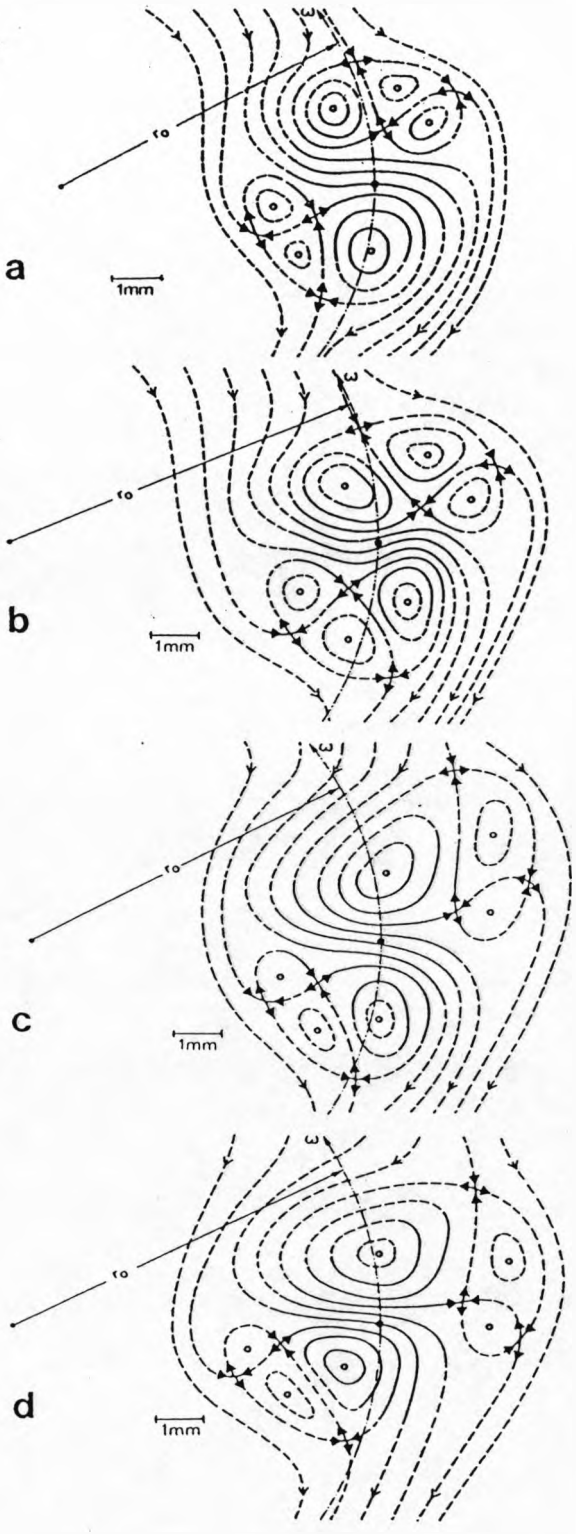

FIGURE 2.6. Flow Calculations.

(iii) the decay of unstable shear layers in the flow field, which causes the formation of a further two additional pairs of vortices (69)

From the flow field it can be seen that cool gas is entrained on one side of the arc and emerges at the other side aligned with the apparent external flow. The complexity of the plasma flow structure and the entrainment of the external flow for low current arcs causes changes in the arcs thermal structure and cross-sectional area. There are no similar results available for the behaviour of high current arcs, however the same changes in the thermal structure are likely but with reduced flow entrainment. These changes alter the areodynamic behaviour of the arc column.

2.4.3 AERODYNAMIC PROPERTIES

For arcs of sufficiently high current, external flow and magnetic field the plasma column's behaviour is similar to a heated solid current carrying rod of a specified characteristic diameter because the external flow circumvents the arc's boundary and of course alters it's internal structures. The control of the arc column, in either a balanced confiruration or an arc rotating through stationary gas may be described through a consideration of the momenteum conservation.

This involves two forces, the magnetic driving force and the retarding drag force. The magnetic force per unit length of arc column is given by reference (69) as

$$F = IBSin\theta \qquad (2.38)$$

Where I is the arc current, B the applied magnetic field and θ the angle between the current direction and the applied magnetic field. The opposing drag force per unit length of arc column is (55).

$$F_D = 1/2\, C_D D\, \rho_i U_{\infty}^2 \qquad (2.39)$$

Where C_D is the drag coefficient, D the characteristic arc diameter perpendicular to the flow, ρ_i is the density of the surrounding flow and U_{∞} is the velocity of the gas relative to the arc column. For steady operating conditions, this relative velocity maintains a straight arc under balanced flow-magnetic conditions or controls the arc velocity for a quasi steady arc magnetically rotating through the stationary gas. This velocity is related to other areodynamic and electrical properties through equations 2.38 and 2.39.

i.e.

$$U_{\infty} = \sqrt{\frac{IB}{1/2\, C_D D\, \rho_i}} \qquad (2.40)$$

Thus, the magnitude of U_{∞} *is proportional to the square root of applied magnetic field and arc current and inversely proportional to the square root of the drag coefficient arc diameter and mass density of the surrounding gas. Guile et al (72) proved the functional relationship between* U_{∞} *and B but could not obtain the same dependence between* U_{∞} *and I. This descrepency arises from the accompanying increase in arc diameter with increasing arc current and if this factor is considered then I and D have the correct functional influence upon* U_{∞} *. The drag coefficient is not an independant variable but affected by the degree of interaction between the arc plasma and the surrounding gas. A comparison between this coefficient for low current arcs and that for cylindrical bluff bodies (* fig.2.7 *) shows good correlation for low Reynolds number. However for large Reynalds number (strong flow conditions) the drag coefficient for an arc corresponds to that of an elliptical body in a similar flow. This elliptical arc shape was confirmed by Roman and Myers (70) even for low current arcs in a moderate Reynolds number flow. Above 1000A the drag-coefficient remains approximately constant (55,71) at 1.2 for air and 1.7 for* SF_6*(74).*

An important parameter to examine is the mass density of the surrounding gas in which the arc either rotates or is in a balanced condition.

A less dense gaseous medium, obtained by using different gases or by heating the medium, will thus reduce the drag force acting upon the arc column and as a result the column will either bend and become un-balanced or rotate at a greater velocity until the net force is once again zero.

As a result of a relative movement of gas past the arc, a symmetrical wake forms downstream within which vortex shedding occurs at the inner side of the wake boundary. In addition no flow is detectable near to the centre of the wake (70). The occurrance of vortex shedding is represented by the Strouhd number (fD/U_{∞}, f is the frequency of shedding, D is the diameter of the arc and U_{∞} is the velocity of the surrounding flow. For a Reynolds number of 10^4 and 300 amp arc the Strouhal numbers obtained were between 0.3-0.4 which greatly differs from those obtained for solid cylinders (0.2) under the same operating conditions. The corresponding wake dimensions also differ; a larger wake forms behind an arc column than for a bluff body having the same transverse dimension. This larger wake is a result of the temperature difference between the boundaries of the arc (approx 6000k) and that of the solid cylinder (1600k). An increase in surface temperature of a solid cylinder produces a wider wake as observed by Roman and Myers (70).

More detailed experimental and theoretical investigations were undertaken by Kopainsky and Schade (73). They examined the wake created by an arc rotating through stationary gas. A maximum wake temperature of 1900k for a 4.8kA, SF_6 arc was measured using a shock wave technique. The wake's thermal structure changed little over one arc revolution and it was observed to extend isotropically (neglecting the arcs length, the wake formed a diverging sphere) throughout the electrode gap. At relatively low gas pressures (but above atmosphere pressure), there are large irregularities in the wake boundary which at higher pressures disappear, the wake boundary becomes more regular (74).

The energy transfer from the wake is achieved by turbulent mixing with the surrounding cold gas. This mass mixing, better known as wake mass entrainment, causes the wake to expand the mass entrained across the boundary is (73).

$$\frac{\dot{m}}{dx}_{x=} \; 2\alpha d\rho \left|U_w\right| (\rho/\rho_w)^{1/2} \qquad (2.41)$$

Where ρ_w is the average wake density, ρ is the cold gas density, U_w is the wake velocity. α is an empirical constant experimentally calculated to be 10^{-3}. This differs from that determined for wakes behind unheated solid obstacles at 0.2.

The difference is due to the absence of heat transfer for those values obtained for unheated solid bodies.

The thermal decay of the wake by turbulance and thermal conduction occurs very slowly (>>10ms) (73). Because of this slow decay rate the arc may rotate through its own wake (73). The upstream gas density is now reduced and the arc column accelerates until the drag and the Lorentz forces become balanced (2.40). Measurements by Kopainsky and Schade (Fig 2.8) show the arc velocity variation with time. The initial rise in arc velocity is caused by transients in the arc current and magnetic field values but after this tranisition the arc velocity again increases as it enters its own heated wake. After several revolutions the arc rotated within a homogeneously heated environment with a steady velocity of 800m/s.

2.4.4 ELECTRODE INFLUENCES

For arcs moving between electrodes seperated by more than 5 cms with a velocity above 50 m/s, the dominant forces controlling the arc movement are aerodynamic. With electrode gaps less than 5cms, the arc movement becomes increasingly electrode dominated.

Guile et al (72) investigated this phenomena for electrode spacings upto 12cms, steady magnetic fields upto 1.75 tesla and d.c. arc currents upto 20kA.

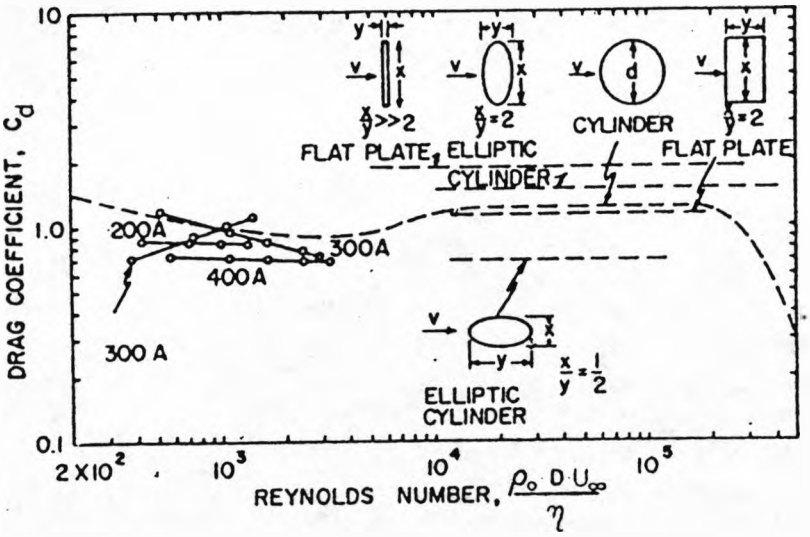

FIGURE 2.7. Drag Coefficient.

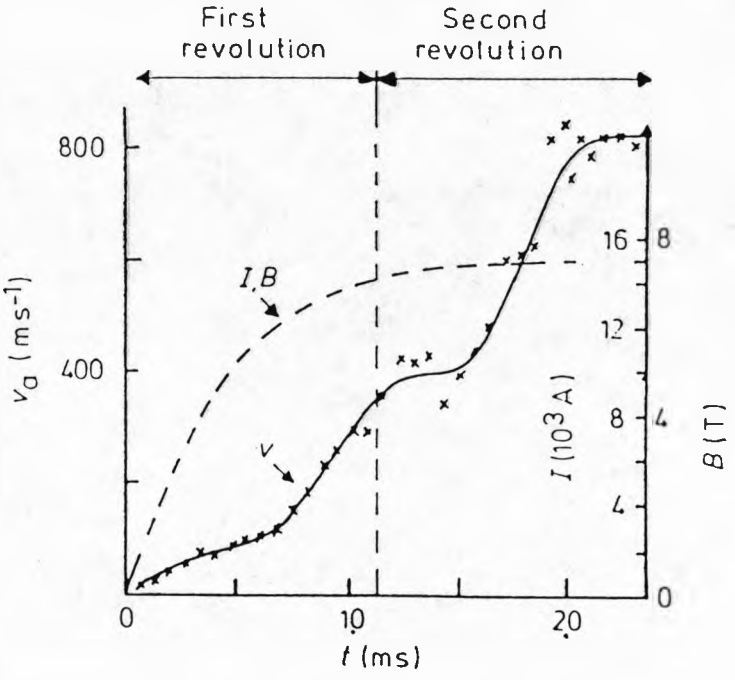

FIGURE 2.8. Arc Velocity.

For electrode spacings greater than 5 cms the arc velocity is constant (75) but below this value a decrease in spacing causes an increase in arc velocity by a factor of between 2 and 3. At some critical spacing (2mm-3mm) the arc velocity then decreases with a decrease in electrode gap (72). This reversed in the velocity/gap trend is a result of two factors. The first involves electrode jets interference and contamination of the arc plasma so causing the arc column to become "stiff" and increasing its resitance to more. The second factor is the distortion of the applied magnetic field by the field generated by the flow of current through the arcing electrodes. If the experimental conditions are changed, resulting in plasma jet formation, then the trend reversal will occur for a larger electrode gap. A larger critical gap is required if the magnetic field or ambient gas pressure is reduced and if the arc current is increased or if the electrode material is changed from brass to copper (75).

Significant changes in the arc velocity are observed for different electrode materials and the surface condition of the electrodes. An arc moves faster on drawn copper electrodes than on drawn brass, the difference at 100A is 100% and at 5000A 45%. However an arc moving on ground brass electrodes has a similar velocity characteristic to that on drawn copper (72).

These differences are a result of the complex mechanism of arc root transfer from one arcing site to another and is strongly dependent upon electrode material and the condition of those electrodes. Ideally smooth, polished surfaces promote high velocity arcs rather than rough, contaminated surfaces which restrict the movement of the arc root.

2.4.5 ARC SHAPE

For sufficiently long arcs, free from electrode effects, the shape of the arc column is controlled by the external magnetic and drag forces. An arc column rotating in an annular gap between two concentric electrodes has a complex involute shape (fig.2.9). Adams (76) develops a simple model for describing the involute shape of such an arc column. Treating the arc as a solid current carrying conductor with uniform current density in an imposed magnetic field, the velocity of each element of the arc column is given by equation (2.40). This velocity is constant for and perpendicular to each element but has a different direction for each element because of the involute shape. The shape of the arc column is defined by a radial position (r) and the angle (θ) which r substends with the root attachment point on the inner electrode (fig.2.9). The equation describing the shape is;

$$\theta = \left(\frac{r^2}{C^2} - 1 \right)^{1/2} - \cos^{-1} \frac{C}{r} \qquad (2.42)$$

Where C is a constant given by;

$$C = \frac{1}{\omega} \left(\frac{IB}{1/2 \rho D C_D} \right)^{1/2} \qquad (2.43)$$

and W is the angular frequency of the arc element.

Since the constant C is the ratio of the areodynamic and electromagnetic forces, the shape of the arc column is independent of the absolute values of these two forces. The predicted arc shape agreed with those shapes observed during arcing (76). Predicting the arc shape for small gaps is not possible because of electrode influences which cause the previously steady motion of the arc to become unsteady and so affecting the arc's shape.

2.4.6 ARC STABILITY

Deviation from rotational symmetry of an arc column exposed to transverse magnetic fields causes convection and momentum transport between the arc column and the surrounding gas. Through this transport the arc moves and changes its geometry until it reaches a stable, balanced configuration.

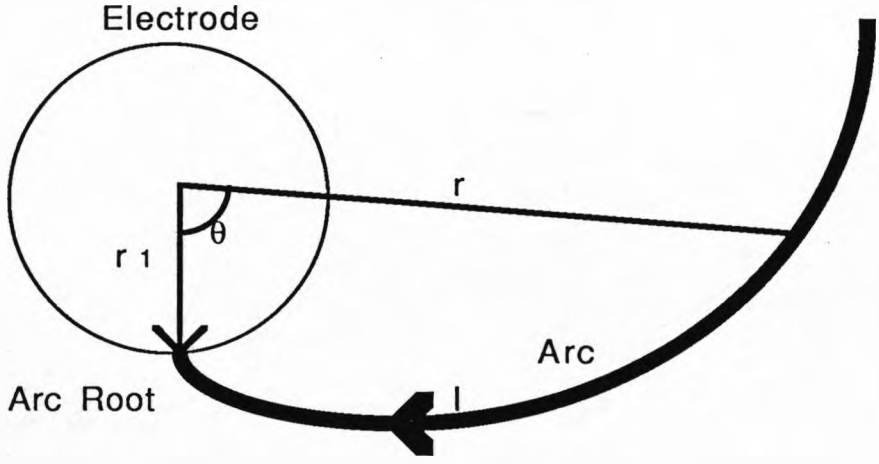

FIGURE 2.9 Arc Shape.

A suitable stability criterion can be formulated by inspection of the momentum transport mechanism and a knowledge of the arc's cross-sectional area. This approach eliminates the need for detailed knowledge of the energy dissipation mechanisms, the temperature distributions and the axial shape of the arc.

A kink which forms in the arc column will either grow or decay (i.e. it is unstable or stable respectively) depending upon the imposed condition. For a balanced arc column, in mutually orthaganal magnetic and gas flow fields, the stability criterion is given by Schrade (77) as,

$$1 + \beta - 2\lambda^2 - 2\cos^2\alpha \quad \begin{matrix} > \\ = \\ < \end{matrix} \quad \begin{matrix} \text{Stable} \\ 0 \quad \text{Indifferent} \\ \text{Unstable.} \end{matrix} \qquad (2.44)$$

β is the ratio of the average static pressure to magnetic pressure, λ is the ratio of average self-magnetic field to applied magnetic field, α is the azimuthal angle between the applied magnetic field and the radius of curvature vector.

The direction of least stability is parallel to the applied magnetic field (i.e. $\alpha = 0$ or $\alpha = \pi$) and the onset of these instabilities is caused by high arc currents (high λ) and applied magnetic fields (small β).

Any kink which forms under these conditions will grow causing an increase in the arc voltage. If the deformity becomes sufficiently large then it may eletrically short itself producing a new straighter arc column. However, if the arc roots are free to move then under an unstable operating condition the whole arc will move in the direction of greatest instability. The effect of such instabilites must be examined for the present geometry and their importance and implications accessed.

2.4.7 NON-AXISYMMETRIC ARC THEORY

A theoretical description of an arc cloumn requires solution of the energy and momentum conservation equations. Many methods have been employed to solve these conservation equations, each method becoming more sophisticated than the previous method. A "Linearization" method adopted by Lord (58), which was subsequently improved by Hodnett (59), describing the arc as an impenetrable hot gaseous cylinder whose electrical and thermodynamic properties were radially averaged. Outside the cylinder these properties were fixed by the ambient temperature and pressure. Although their results showed the generation of a double vortex structure within the arc plasma, their method failed to predict the transition in the arc's shape which occurs under such conditions.

A more advanced analysis was proposed by several authors (60,61,62 and 63) and allowed the decoupling of the energy and momentum conservation equations. Knowledge of either the flow field or temperature distribution within the arc leads to the solution of the energy conservations or momentum conservation equation respectively. This method is useful and lends itself to an iterative solution because all that is needed is an initial estimate of either the flow field or arc temperature distribution. A solution is obtained once both equations are satisfied simultaneously. These results obtained describing the temperature and flow fields are in good agreement with those determined experimentally (78,74) and the overall interaction between the arc plasma and surrounding gas is also correctly predicted (Section 2.4.2).

The development of the "Similarity" method by Yas'ko (64) adopts a similar philosophy to the method developed for axisymmetric arcs by Cowley and Fang (Section 2.3.7). No detailed knowledge of the arc's temperature distribution and surrounding flow field is required but are eliminated by the use of non-dimensional parameters.

The arcs areodynamic, electrical and thermondynamic behaviour can be predicted by solution of the non-dimensional equations given by Yas'ko (64) and Nicolas and Keuthe (65).

MOMENTUM:

$$\overset{*}{\rho}(\underline{\overset{*}{W}}.\text{grad})\underline{\overset{*}{W}} = \frac{P_o}{\rho_o W_o^2}\,\text{grad}\overset{*}{P} + \frac{j_o B_o L}{\rho_o W_o^2}\,\underline{\overset{*}{j}} \times \underline{\overset{*}{B}} \qquad (2.45)$$

$$\text{div}(\overset{*}{\rho}\underline{\overset{*}{W}}) = 0 \qquad (2.46)$$

ENERGY:

$$\frac{\rho_o W_o h_o}{j_o E_o L}\,\overset{*}{\rho}\underline{\overset{*}{W}} \cdot \text{grad}\overset{*}{h} + \frac{\rho_o W_o^3}{j_o E_o L}\,\overset{*}{\rho}\underline{\overset{*}{W}} \cdot \text{grad}(1/2\,\underline{\overset{*}{W}}^2) - \frac{\lambda_o T_o}{j_o E_o L^2}\,\text{div}(\overset{*}{\lambda}\,\text{grad}\overset{*}{T}) + \frac{Q_o}{j_o E_o}\overset{*}{Q} = \underline{\overset{*}{j}}\,\underline{\overset{*}{E}} \qquad (2.47)$$

MAXWELL:

$$\text{curl } B = \frac{\mu_o j_o L}{B_o}\,\overset{*}{j} \qquad (2.48)$$

OHM'S LAW:

$$\overset{*}{j} = \frac{\sigma_o E_o \overset{*}{E}}{j_o} \qquad (2.49)$$

Where the astericks indicate non-dimensional numbers (obtained by dividing dimensional variable by the appropriate sealing value; e.g. $\overset{*}{\rho} = \rho/\rho_o$, $\overset{*}{W} = W/W_o$ *etc). The assignment of subscripts indicates reference values and L is a reference length.*

Non-dimensional numbers can easily be idenfified from equations (2.45-2.49) and their physical significance can be readily identified.

For example, from the momentum conservation equation (2.45), two non-dimensional numbers can be written;

$$\Pi_p = \frac{P_o}{\rho_o W_o^2} \quad \text{and then} \quad \Pi_{em} = \frac{j_o B_o L}{\rho_o W_o^2}$$

The first number (Π_p) represents the ratio of pressure to inertial effects and the second (Π_{em}) is the ratio of magnetic to inertial forces. The energy equation (2.47) gives four non-dimensional coefficients;

$$\Pi_h = \frac{\rho_o W_o h_o}{j_o E_o L} \qquad \Pi_{ac} = \frac{\rho_o W_o^3}{j_o E_o L} \qquad \Pi_{hc} = \frac{\lambda_o T_o}{j_o E_o L^2} \qquad \Pi_r = \frac{Q_o}{j_o E_o}$$

These parameters reflect the conversion of electrical energy ($j_o E_o L$) into various other forms; convective ($\rho_o W_o h_o$); kinetic $\rho_o W_o^3$; thermal conduction $\lambda_o T_o$ and radiation Q_O.

The remaining two equations produce a further two non-dimensional parameters.

$$\Pi_m = \frac{\mu_o j_o L}{B_o} \quad \text{and} \quad \Pi_E = \frac{\sigma_o E_o}{j_o}$$

These two coefficients give the relationship between self ($\mu_o j_o L$) and external (B_o) magnetic fields and the process of charged particle transfer in the electric field (E_O), respectively.

A combination of various non-dimensional parameters leads to the elimination of those properties which are difficult to measure experimentally (64).

This results in the formulation of two important characteristics involving the arc velocity (2.46) and the arc voltage (2.47).

$$\Pi'_u = \mathbf{f}(\Pi'_p, \Pi'_{em}, \Pi'_h, \Pi'_{ac}, \Pi'_{hc}, \Pi'_r, \Pi'_m \ldots\ldots\ldots) \qquad (2.46)$$

$$\Pi_v = \mathbf{f}(\Pi'_p, \Pi'_{em}, \Pi'_h, \Pi'_{ac}, \Pi'_{hc}, \Pi'_r, \Pi'_m \ldots\ldots\ldots) \qquad (2.47)$$

The magnitude of these various non-dimensional parameters indicates the relative importance of the physical process involved. An advantage of these characteristics is that they can be used to correlate experimental results obtained under different operating conditions by defining the appropriate non-dimensional parameters (Yas'ko 64).

An example given by Yas'ko (64) for an arc driven by an external magnetic field between two parallel electrodes shows that the velocity characteristic (2.49) was in fair agreement with experimental data, i.e.

$$U/B = 4.27\,(l/Bl)^{0.45} \qquad (2.49)$$

However, the experimental velocities are best correlated by equations (2.49) and (2.50)

$$U/B = 1.45 \times 10^{-2}\,(l/Bl)^{0.66} \qquad (2.50)$$

where l = arc length.

The voltage characteristic (2.51) agrees well with the experimental data.

$$(VI/I) = 1.06 \times 10^{4} (I/BI)^{-0.55} (B^{2})^{-0.19} \qquad (2.51)$$

At the expense of loss of detailed information about the flow and temperature distributions a description is obtained of the arc's behaviour in terms of the characteristic parameters.

2.5 CONCLUSION

Many experimental and theoretical investigations have been undertaken on axisymmetric arcs. During the past 50 years much knowledge has been gained from experimental investigations leading to a further understanding of the various physical processes occuring within the arc column and the interations between the electrically conducting arc plasma and the thermally conducting flow. Theoretical descriptions of the axisymmetric arc has considerably developed from Cassie and Mayr's simple and convenient models into the more rigorous boundary larger models formulated during the seventies. These incorporate the "Integral Analysis method" while results in reasonable agreement with experimental data not only for steady state conditions but also for transient arcing conditions.

Investigations of non-axisymmetric arc behaviour have indicated a complex interation between the arc plasma and the surrounding gas for a given set of imposed

magnetic and glas flow fields. For low velocities the external flow partially penetrates the arc column distorting the isothermal and electrical structures in the direction of flow, whilst for large flow velocities the external flow circumvents the arc plasma with a simultaneous generation of vortices within the plasma. There is also distortion of the isothermal and electrical structure of the arc which extends in a lateral direction perpendicular to the incoming gas flow. The arc shape becomes elliptical rather than circular. Theoretical and experimental investigations have hitherto only considered this interaction for steady state arcing conditions.

Little information has been published about rotary arcs in circuit breakers where the conditions are non steady. To describe the behaviour of such a rotating arc in a transient situation requires the assilutation of information available about axisymmetric arcs, circuit breaker arc theory and arc heater theory. With the aid of new experimental results, an attempt to describe the transient behaviour of a non-axisymmetric rotating arc is undertaken in this thesis.

3. EXPERIMENTAL SYSTEM

The experimental system can be divided into two parts. Firstly there is the experimental test facility which describes the synthetic test circuit, its timing control, the construction of the rotary arc circuit breaker and the sulphur hexafluoride gas handling system. Secondly, the measurement system describes those diagnostic techniques used to gather data about the electrical and magnetic conditions within the arc environment during the peak current and current zero regimes of the arc sustaining waveform. During the same periods photographic records were taken.

3.1 EXPERIMENTAL TEST FACILITY

3.1.1 CONSTRUCTION OF TEST BREAKER

The annular contact and coil yoke of the interrupter consisted of a cylindrical copper tube 70 mm diameter and 65 mm in length. At each end of the tube there was a raised flange whose purpose was to ease the transfer of the arc from the fixed contact to the arcing surface of this tube. The nominal thickness of the tube wall was 3.6 mm.

A tinned copper winding is securely fastened to this copper former by three screws which were placed in tapped, countersunk holes in the copper former. This tinned copper strip was 50 mm wide and 0.42 mm thick. A length of this strip was wound onto the former with insulating material placed between each turn. After a

sufficient number of turns had been wound onto the former and a metal fixing collar was secured around the turns. Onto this collar was bolted the fixed contact. Fig (3.2) shows the resulting arrangement.

The coil system was clamped to one of the incoming bushings which also provided electrical contact and mechanical support for the coil. The other bushing provided a similar service for the moveable contact which was connected to the external operating mechanism and was allowed to pivot about the axis of the bushing (fig 3.2).

A viewing port was provided at one end of the enclosing tank allowing for end on photographic investigations of the arc within the coil (fig 3.2). An inspection plate was also fitted to the side of the tank which allowed for easy access to the interior. Both the viewing port and the inspection plate were made gas tight by the insertion of gaskets. The coil arrangement was housed in a gas tight chamber which had a volume of 14×10^3 cms^3.

3.1.2 GAS HANDLING SYSTEM

The gas handling system allowed for the evacuation of the test vessel of either air or SF_6 and for changing spent gas for new. It is important to remove air from the chamber before filling with SF_6 and to remove "arced" SF_6 gas before opening the vessel in order to

reduce the effect of contaminants. Spent SF_6 gas was vented to the outside atmosphere via an exhaust tube and the chamber flushed with air several times before opening and cleaning. After each day's testing the gas was discarded and the vessel left under vacuum overnight.

3.1.3 SYNTHETIC TEST CIRCUIT.

The synthetic test circuit comprises of a ringing capacitor/inductor circuit tuned to a frequency of 110Hz (fig 3.1). The capacitor bank consists of two parallel banks of 1.37mF, 16kV maximum charging voltage and 2.4 mF, 20kV maximum charging voltage. Resistors were provided in series with each capacitor bank (not shown) which limits the discharge current from each set if a direct short occurs between the high potential terminals of each bank and experimental earth. The parallel connection results in a total capacitance of 3.77mF, a maximum charging voltage of 16kV a peak current of 40kA and a total stored energy of 0.48mJ.

In series with the capacitors are three ignitrons each connected in parallel with one another. The first ignitron (Bk 394) is in series with a 250 Ω resistor which provides a small initiation current to the test breaker whilst its contacts separate. The second ignitron (the forward biased Bk 194) provides the first sinusoidal current pulse through the 0.55 mH, 100kA inductor to the test breaker. The third ignition (the commutating Bk194) provides a second negative current

pulse but whose amplitude is reduced by 30% because of power disspation from the arc and the test circuit. However, if the test breaker interrupts the current at the end of the first half cycle then a transient voltage appears across the two electrodes, stressing the previously conducting region. The rate of rise of this voltage is controlled by the voltage remaining on the capacitor bank, the series inductor in the circuit and the stray capacitance inherent arross the electrode gas of the test breaker ($1_{n}F$). This rate of rise of recovery voltage (RRRV) can be controlled for a fixed bank voltage and series inductor by adding parallel capacitance across the terminals of the test breaker.

The peak current of the sinusoidal current pulse, for a given frequency, is controlled by the bank charging voltage.

Any remaining charge on the bank after arc extinction can be removed by pneumatic dumps shorting the capacitor back terminals through a dump resistance.

3.1.4 CONTROL AND TIMING SEQUENCE

Energising the trip coil on the spring loaded opening mechanism starts the arcing sequence. After energising the trip coil but before the opening mechanism begins to open the initiation ignitron is triggered from an electronic unit producing a 200V, 10 μs voltage pulse which is stepped upto a 1.5kV, 20 μs voltage pulse. A

small initiation current (8-32A's) flows through the over-damped circuit to the fixed contact of the interrupter and through the moveable contact which it houses (fig 3.2). The moveable electrode (or poker) moves away from the fixed contact drawing a low current arc as it does so. When the poker reaches its furthermost point of travel the second ignition is triggered allowing current to by-pass the initiation ignition, which, now turns off. The current is now a sinusoid because of the under-damped character of the circuit. At the same instant the arc transfers from the fixed contact to the arcing surface of the coil (fig 3.2). Current now flows through the windings of the coil, through the copper former and to the poker via the arc.

Before the current in the first half cycle has returned to zero the third, commutating ignitron is triggered. This ignitron switches on and remains on, by providing an isolated mains supply to the holding anode, it does not conduct any current from the capcitor bank until the current has returned to zero in the second ignitron. This system eliminates the need for accurate timing (less than 0.5 μs) and results in either a smooth commutation of current at current zero or correct application of stressing voltage after current zero.

A schematic diagram of the current waveform is shown by figure (3.3). The initiation current (i_1) is between 8A to 32A and flows for between 15-19 ms (t_1). The magnitude of i_2 and i_3 can be varied between 2kA and 40kA and this current flows for approximately 4.5 mS per half cycle. A further half cycle can be supplied if needed by the commutation ignitron but the peak current (i_3) is less than (i_2).

Various timing pulses for ignitron and oscilliscope triggering were provided by electronic delay units, whose delays were variable from 100 nS to 100 mS. Reproducible signals were therefore provided which were relatively insensitive to spurious triggering.

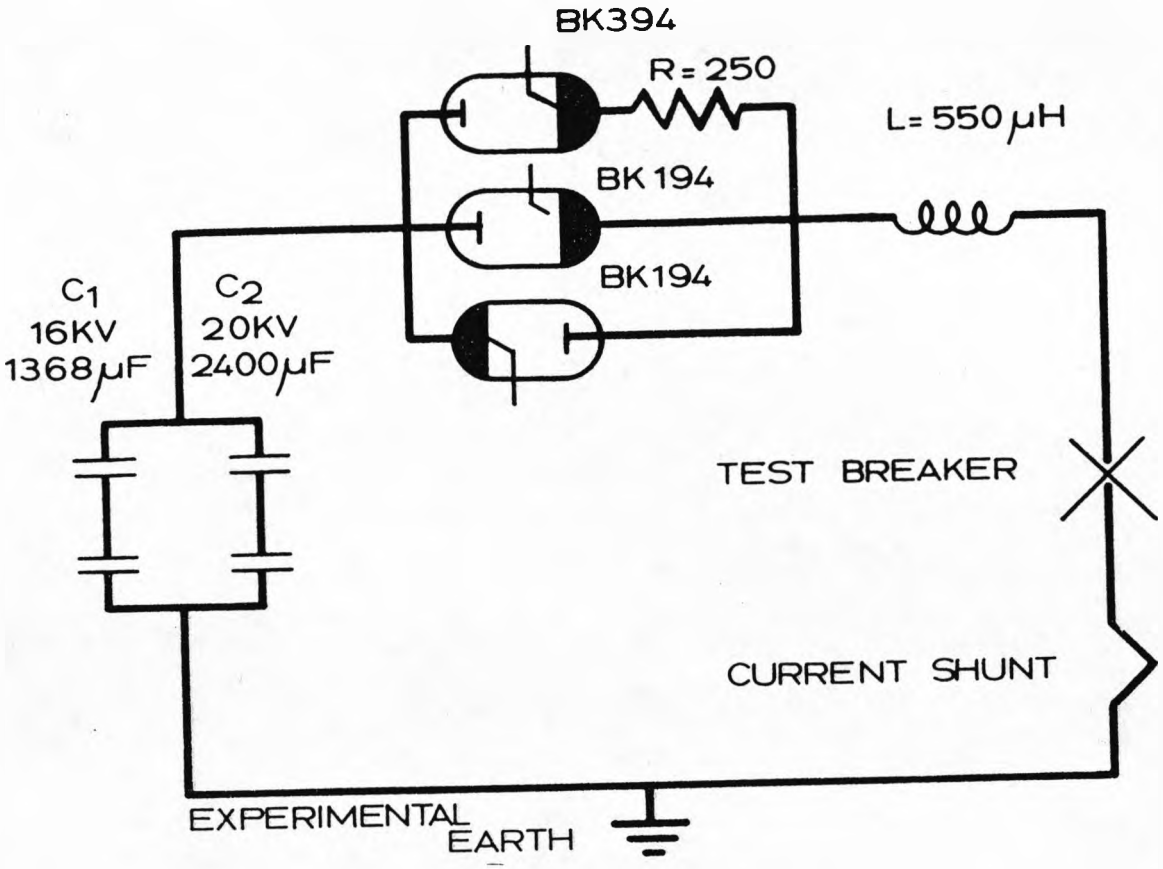

FIGURE 3.1. Synthetic Test Circuit.

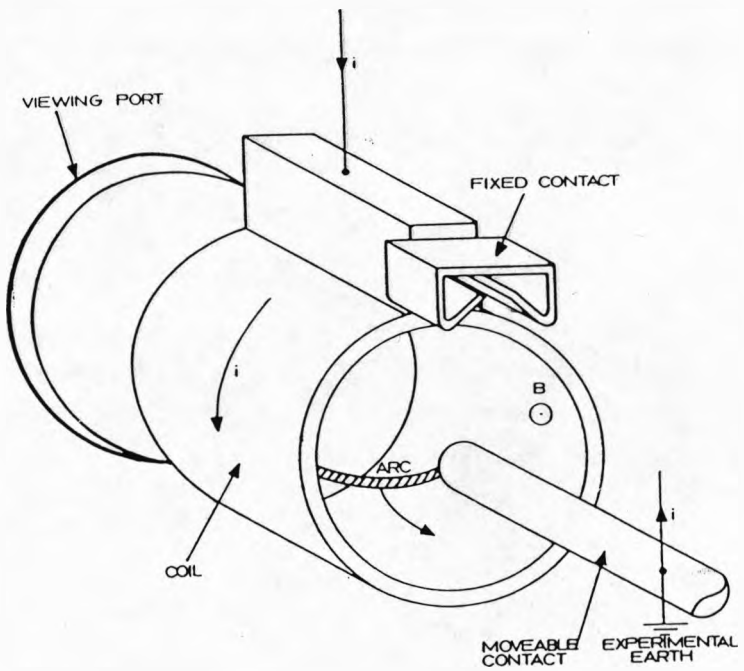

SCHEMATIC OF CIRCUIT AND COIL ARRANGMENT

FIGURE 3.2. Coil Arrangement.

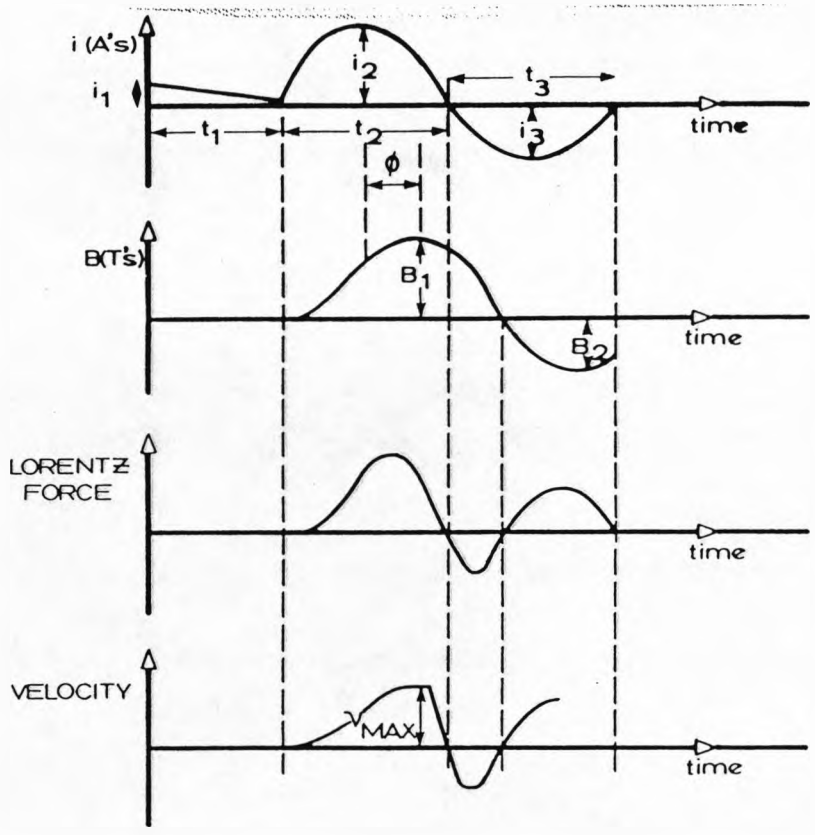

FIGURE 3.3. Typical Waveforms.

3.2 MEASURING SYSTEM

3.2.1 GENERAL COMMENTS

The measurements of electrical parameters of arc discharges requires adoptation of conventional measuring techniques. Even for relatively simple measurements of current, voltage and pressure this is not easy. There are many complex aspects which need to be assessed before equipment can be electrically connected to a high power source.

Generally a measuring system consists of a transducer of some description (i.e. current shunt, voltage probes, photomultiplier tubes etc), an interconnecting cable and a recording device (e.g. oscilloscope) which has a choice of pre-amplifiers. Each part of this system has its own unique problems when connected together or when measuring rapid changes in the arc parameters.

It is convenient to divide any investigation into two zones. The first zone is the peak current period during which time several kilo-amperes of current flow and the arc voltage is only a few hundred volts. The duration is relatively lengthy, 10 ms depending upon the frequency of the sinusoid. The second zone is the current zero period. During this time only a few amperes of current flow and the applied voltage after current zero is many kilo volts.

During this period there are large rates of change associated with both the arc current and voltage. The time scale of the current zero investigation is approximately 10 micro-seconds duration.

Many measurement problems are common to both the peak current and current zero periods. They fall broadly into four categories;

a) Electrostatic, electromagnetic and mechanical noise

b) Experimental earth and mains isolation

c) A common signal return path

d) Amplifier de-saturation and frequency response

These four categories are discussed in general in the following sections but are later discussed in more detail with specific emphasis to the experimental environment used throughout the investigation.

3.2.1.1 ELECTROSTATIC, ELECTROMAGNETIC AND MECHANICAL NOISE PROBLEMS.

Electrostatic, electromagnetic and mechanical noise interference are the three most common types of noise interference present on a measuring system connected to a high power source and test circuit breaker. An interference signal is superimposed onto any measurement signal causing an error in the recorded signal. This noise problem is not unique to the transducer and it affects the other two links, both the interconnecting cable and the recording device.

Vibrational noise, generated by various mechanical movements during the opening operation of the test breaker, essentially affects the transducer rather than the other two parts of the system. Reducing or eliminating this type of noise involves a trial and error method. Most important is correct positioning of the transducer device and correct housing in a vibration dampening supportive holder connected to the test head. One or both of these methods would eliminate such interference.

Electromagnetic induced noise is a problem associated with the high current phase of arcing. An induced voltage signal is superimposed on the real signal because there is an interference sensitve loop. A typical loop is shown on fig (3.4). This is the arrangement used for differential arc voltage measurements on the test breaker. However it is clear from the diagram that the outer sheaths near to the probes are not connected together. An interference loop exists between A-a-b-B and during arcing a voltage is induced on these sheaths. Shorting these sheaths together at the probe end will considerably reduce the amount of interference. Two further precautions can be taken to ensure noise elimination; firstly routing coaxial cable along the similar paths and secondly providing an extra screening sheath which is shorted at both ends and connected to experimental earth.

Electrostatic interference problems occur after the arc current ceases to flow. The interference caused by electric field induction within a loop sensitive to such induction produces a further signal which superimposed upon the actual signal. A similar screening technique should be used as for electromagnetic interference but also proper positioning of the probe or probes is essential. They should be placed as near as possible to the low potential terminal where the electric field strength is a minimum (79).

To protect the recoding equipment from both electrostatic and electromagnetic inference a copper shielding cabinet is placed around such equipment. The cabinet must be experimentally earthed and the equipment electrically powered through electrically isolated supplies.

3.2.1.2 EXPERIMENTAL EARTH AND MAINS ISOLATION

It is of paramount importance on any high current, high voltage test circuit that there is only one earth point. This earth is know as an experimental earth and is usually connected to a copper rod placed in the foundations of the building. Although the mains earth is connected in a similar way at the sub-station the interconnecting cable is long having considerable impedence and limited fault current capability (≈30A).

However, the earth rod used in the laboratory is situated near to the experimental system with a much shorter and a much lower impedence cable capable of carrying several kA. If a fault occurs on the rest system then several kilo-amperes may flow to earth through this system without cable damage on the mains earth system.

To eliminate any mains earthing or mains looping problems caused by powering equipment from either the same phase or different phases of the mains supply, 1:1 isolation transformers are used. Although the mains earth is connected on the primary side of the transformer there is no electrical connection with the secondary. The earth associated with this side of the isolation transformer is the experimental earth.

Equipment must only have one earthing point which is the experimental earth. Any connection to another earth causes current to flow through the introduced earth loop causing distortion of the real signal. Therefore great care is taken before connecting pieces of equipment together including the triggering signals. Each electronically produced trigger signal is always passed through a 1:1 pulse transformer providing electrical isolation.

Although the importance of one experimental earthing point for all pieces of equipment is of paramount importance, this can cause further measurement problems because usually there is only one signal return path.

3.2.1.3 A COMMON SIGNAL RETURN PATH

Unfortunately, because of the principle of one point earthing which eliminates possible earth loops and induced voltage loops, all probe signals return to experimental earth via one cable sheath. Figure (3.4) shows differential voltage probe measurements and current measurement. The return signal from the current shunt flows through the outer sheath of the interconnecting cable. Also through this cable flows two further signal currents from the voltage probes. These induce an E.M.F. in the current measuring loop due to the coupling between the core/sheath and the resistive voltage drop of the sheath.

Taylor and Wang (79) calculated this error for their system on the basis of an arc current of 0.1 A, recovery voltage of 10 kV, signal frequency of 0.1 MHz, a five metre length of cable and a cable impedence of 13×10^{-3} Ω/m. Their percentage error was 0.6%. For the present experiment system a similar assessment is made for this error at a signal requency of 1 MHz, cable length 2 m and arc current of 0.5 Amperes.

The percentage error is 0.8%. This level of error is acceptable in the experimental arrangements used but attention must be paid to this phenomena if longer cables are used, if the frequency of the signals are high (i.e. >10MHz) or a small ohmic value of current shuht is used (<10 mΩ).

3.2.1.4 AMPLIFIER DE-SATURATION AND FREQUENCY RESPONSE

Amplifier saturation is a problem which is caused by measuring large signals during the peak current phase of arcing (such as arc current) and then measuring relatively small signals during the current zero period. Some protection against saturation can be afforded by a diode clipper arrangement (See Section 3.2.2.2) but the emphasis is placed upon the time for the amplifier to become de-saturated. The choice of pre-amplifier is important not only for its response to high frequency signals (> 1MHz) but also for its de-saturation time. The amplifier must be able to recover sufficiently quickly so that it gives accurate measurements at current zero.

The frequency response of the amplifier should be greater than the highest frequency which is present during arcing. This is usually determined by either the current decay or by the rate of rise of recovery voltage. Usually the bandwidth of such amplifier is of the order of 16 MHz.

3.2.2 CURRENT MEASUREMENT

During one half cycle of arcing the arc current varies from kilo-amperes at peak current to just a few amperes at current zero. To investigate both regimes accurately the experimental investigation is divided into a peak current study of the arc and a current zero study.

The position of the current shunt in the circuit is shown by figure (3.1), one terminal is connected directly to experimental earth. The choice of shunt is dependent upon the magnitude of the current and the time period under investigation.

3.2.2.1 PEAK CURRENT MEASUREMENT

A coaxial current shunt of 1.038 mΩ resistance, a bandwidth of 500 kHz and a pulsed current rating of 100kA was used during this period. The design of the shunt is similar to that investigated by Grundy (80). This current shunt is a four terminal device connected in series with the power circuit and has two connections across its resistive element for measuring purposes. The potential difference between the measurement terminals of a low value ohmic shunt is,

$$v(t) = Ri(t) + L\frac{d(t)}{dt} \pm M\frac{di(t)}{dt} \qquad (3.1)$$

The shunt used in this investigation and those used by various other experimentalists (80,81,82,83) has a low mutual inductance and low self inductance obtained by good shunt design. During this peak current period the di(t)/dt is not too large. Therefore the second and third terms on the RHS of equation (3.1) are negligible and the whole equation approximates extremely well to,

$$v(t) = Ri(t) \qquad (3.2)$$

The low ohmic values of this shunt was chosen on the basis to give good signal to noise ratio and to minimise heating. A current shunt between 0.5 mΩ and 10 mΩ is ideal for such investigations.

A BNC coaxial cable of 2m length connected the measuring terminals of the shunt to the oscilloscope. It is advisable when connecting low output impedence (1.038 mΩ) measuring apparatus to a high input impedence (10 MΩ) monitoring equipment to insert a 50 Ω termination onto the input to the oscilloscope. This impedence matching stops the formation of refelected waves in that cable. Using a mismatched termination can cause an appreciable error (33% with a 75 Ω terminator).

Amplifier saturation is not a problem during this period because peak voltage is only approximately 20 volts well within the normal operating range of the

Tektronix 1A1 pre-amplifier. The bandwidth of this amplifier was DC to 50 MHz and has a rise time of 7 nS.

3.2.2.2 CURRENT ZERO MEASUREMENT

Current measurement during this period is hampered by a large rate of change of current prior to current zero and small post arc currents there after. To investigate this period accurately a larger ohmic value shunt with an improved bandwidth is required. A 19.83 mΩ current shunt with 2 MHz bandwidth and a rise time of 170 nS was used for the current zero investigation arc. The design of this shunt is reported by Champman (84) and is the design recommended by Schwab (83). Briefly the construction of this shunt consists of a large number of narrow resistive strips connected electrically in parallel and lying along the shunt axis. A current return path is provided by a number of insulated wires connected electrically in parallel placed on top of the resistive elements.

The maximum current rating of this shunt was 20 kA (this is the limit imposed by the BNC connectors). For this current level 400 volts would be applied to the pre-amplifier of the oscilloscope, which would not only cause saturation of the amplifier by also cause permament damage. A diode clipper eliminates this problem.

Figure (3.5) shows schematically a diode clipper arrangement. There are two sets of two diodes, each set is placed back to back so that both forward and reverse protection is given to the amplifier. The saturation voltage of each diode is approximately 0.4 volts so that the amplifier would only see about 0.8 volts on a 100 mv sensitivity, causing little saturation. A 50Ω termination is used on the input to the clipper and the output of the clipper device is placed onto the input of the pre-amplifier.

The choice of diodes for the clipper is important. They must have a low capacitance (2pF) and an extremely small leakage current. The rise time of the clipper was 15 nS.

3.2.3 VOLTAGE MEASUREMENT

Both the overall and local arc voltage were measured during one half cycle of arcing. In each case the arc voltage was measured differentially, so eliminating any other circuit voltage drops.

3.2.3.1 OVERALL ARC VOLTAGE

Connecting the voltage probes across each bushing of the circuit breaker would result in a misleading voltage due to the summation of two components, arc and coil voltage.

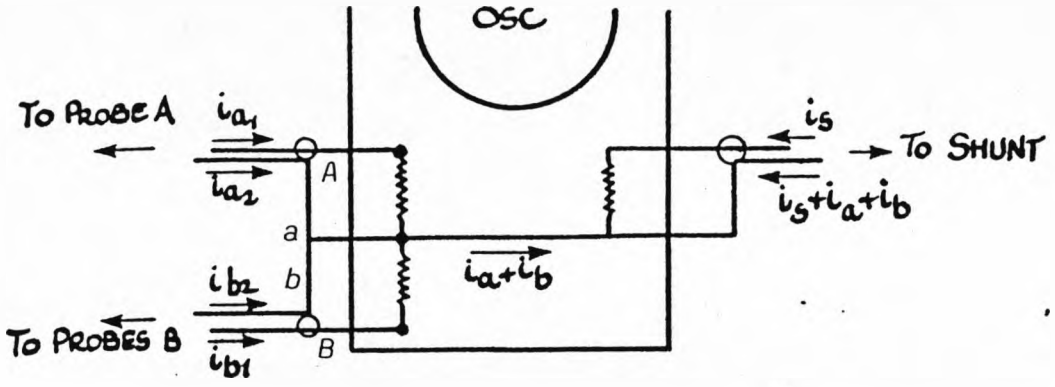

FIGURE 3.4. Voltage Probe Layout And Signal Return Path.

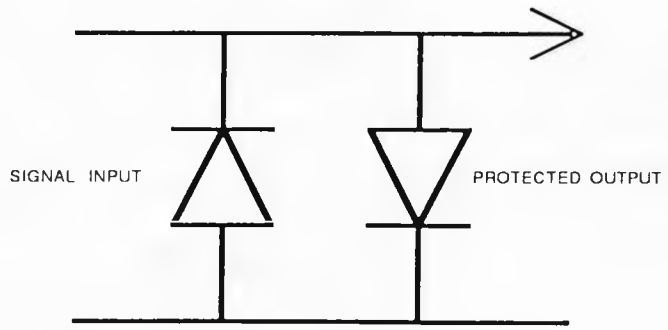

FIGURE 3.5. Diode Clipper Circuit.

$$v(t) = R_a(t)i(t) + L\frac{d(t)}{dt} + R_c(t)i(t) \qquad (3.3)$$

ARC VOLTAGE + COIL VOLTAGE

the last two components represent the voltage drop across the magnetic field producing coil. To eliminate this voltage which is 20 volts for a 3kA peak current, an electrically and thermally insulated cable was securely fastened into a drilled hole on the copper core surface. The insulation provided for this cable had to withstand large transient voltages at current zero and also had to afford protection from any thermal blasts eminating from the arcing area. Ceramic beads were first placed onto the wire and then two sheaths of PTFE sleeving were fitted on top. This was sufficient to prevent excessive thermal blast damage during arcing and to stop electrical breakdown between the inner cable and any low voltage points (e.g. the circuit breaker casing).

The other end of the interconnecting cable was attached to a high voltage feed through insulator. This feed through was a modified long-reach spark plug capable of withstanding 20 kV. A high voltage probe could easily be connected to the other side. The copper/tungstan core of this feed though did not affect the frequency response of the voltage measuing system.

A second voltage probe was connected to the other electrode via the low potential bushing, eliminating the voltage drop across the remaining cable and current shunt. The voltage drop across the electrode was negligible (< 0.1 volts).

Both voltage probes were 1000 dividers (Teletronix type P6015). Compensation elements terminated the coaxial cable at the oscilloscope amplifier end. This compensating termination matched the cable impedence to the input of the oscilloscope so that it was possible to measure fast voltage transient. If correct compensation was afforded then the voltage probes, rated at 40kV, had a frequency response of DC to 50 MHz.

A differential amplifier was used to measure the arc voltage (i.e. voltage probe 1 - voltage probe 2). A suitable differential amplifier for this purpose is a type G Tektronic pre-amplifier. This amplifier has moderate gain and good frequency response (D.C. to 20 MHz).

3.2.3.2 LOCAL VOLTAGE MEASUREMENT

Two parallel tungsten wire probes were placed axially into the arcing coil (figure 3.6). They were held inside the coil volume by two PTFE clamps which also served as spacers and insulators.

The separation distance between these wire probes was 1 cm. The probe wires were brought out from the sealed arcing chamber via an insulating perspex plate which fitted the recess at the viewing port. Two Tektronics 40 kV voltage probes (P6015) were connected to the probe wires via adjustable connectors and supported by two clamps.

To ensure good electrical contact between the arc plasma and the probe wires, a biasing 3.9 kΩ resistor was connected to experimental earth from each wire. The resistance value chosen was sufficient not only to give good electrical contact but also to keep the electrical disturbance of the arc plasma to a minimum. The maximum probe current was less than and 50 mA for each probe wire.

Each wire probe voltage was monitored by 1000:1 voltage probes whose signals were fed into a type G pre-amplifier operating in non-differential measuring mode.

3.2.4 MAGNETIC FIELD MEASUREMENT

The spatial and temporal variation of the magnetic flux density within the coil volume was measured by a search coil measuring 4 mm cubed. A copper shorting strap placed between the cylindrical copper core arcing surface and the moveable arc contact allowed a pulsed

sinusoidal current to flow through the coil producting a magnetic field.

The search coil monitored this field at several radial and axial positions as a function of time. Positioning the search coil within the arcing volume at a specific location was achieved by a matrix locator and clamp arrangement. This matrix fitted over the viewing port apperature so that the magnetic search probe could be positioned in any axial position and a number of discrete radial positions. Using a different orientation of the search coil, both radial and axial field strengths could be successfully measured.

The output signals from the search coil were integrated and stored in a digital storage oscilloscope. A hard copy of both the magnetic flux variation and exciting current was obtained via an X,Y graph plotter. The bandwidth of the entire system was sufficient to give accurate measurement of the magnetic field at the 110 Hz exciting frequency. The spatial resolution was sufficiently good which allowed for a good graphical representation of this field.

3.2.5 PRESSURE MEASUREMENTS

Pressure changes within the enclosed arcing chamber were measured by a piezoelectric transducer (Kistler 601 A). This was mounted within a hollow nylon

insulator which was connected to a stainless steel tube (4 mm internal diameter), whose other end was exposed to any pressure transients in the test vessel (figure 3.7). The stainless steel tube served two other function which were to protect the piezoelectric transducer from the effects of arc radiation and also from the arc decomposition products. This protection was achieved by an "L" shaped tube.

The exit of this tube was situated in a removable inspection plate, 13 cms from the floor of the arc vessel and 15 cms from the rear. During arcing, any pressure changes which occured were transmitted to the piezoelectric transducer via the column of gas inside the inter-connecting tube. The force exerted upon the piezoelectric crystal causes the stress within the crystal to change the electric field. These field changes which gave rise to a flow of charge were fed into a charge amplifier (Kistler 5001) via a short length of low leakage coaxial cable. Thus, the charge developed is proportional to the change in pressure. The output signal from the amplifier is monitored by a Tektronix 1A1 pre-amplifier.

This experimental arrangement has already been successfully on gas blast circuit breakers. This arrangement could measure aerodynamic oscillations upto a frequency of 180 kHz.

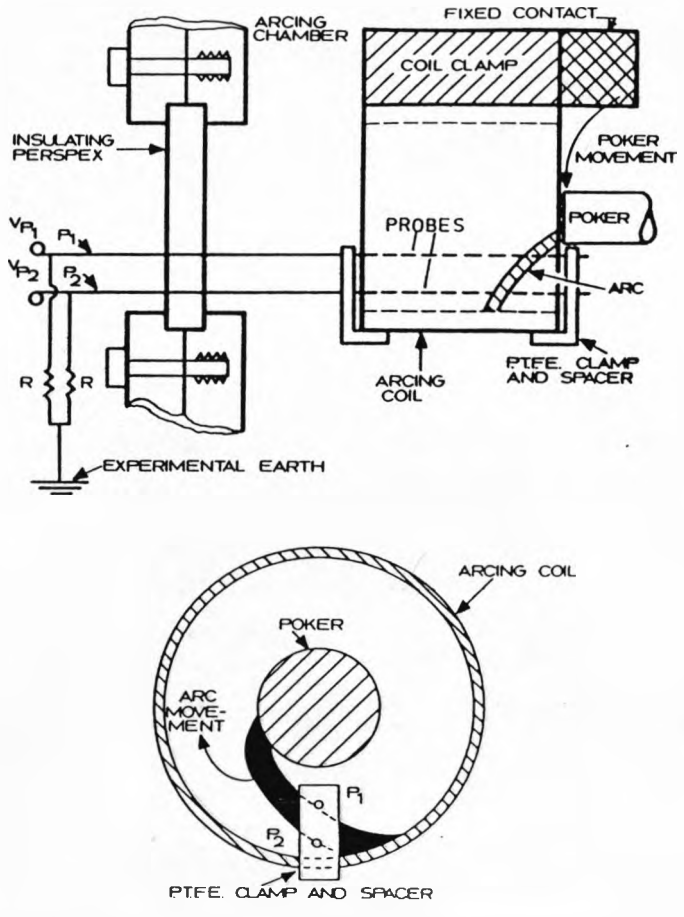

FIGURE 3.6. Local Voltage Probe Measurement.

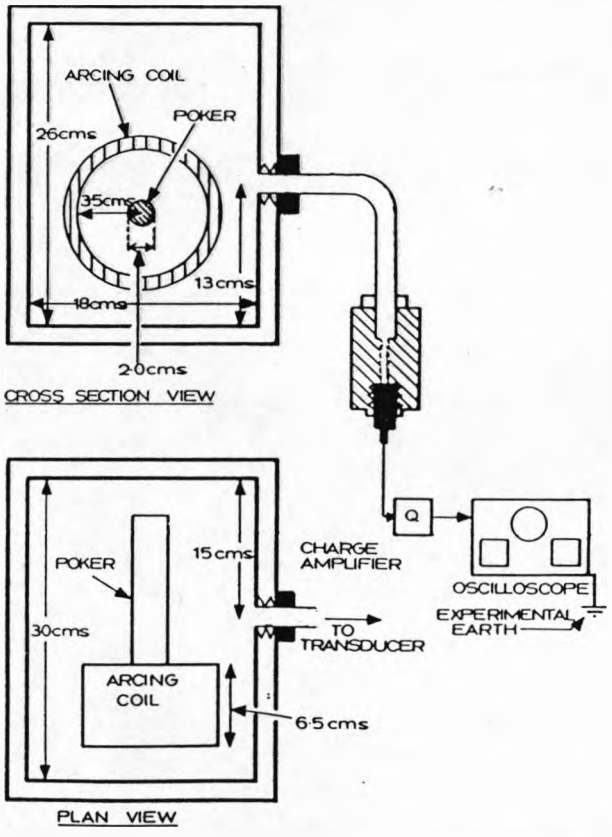

FIGURE 3.7. Pressure Measurement.

3.2.6 FIBRE OPTIC/PHOTOMULTIPLIER SYSTEM

Fibre optic and photomultiplier systems were used to monitor the arc shape and movement. The main disadvantages with using a conventional photomultiplier tube and lens system are the precise degree of alignment and careful electrical screening of the photomultiplier tube which are required. To eliminate these problems a fibre optic cable can be used in conjunction with a glass collimating system.

3.2.6.1 FIBRE OPTIC CABLE AND COLLIMATING SYSTEM

The fibre optic cable used in this investigation was an acrylic monofibre type of cable. The peak spectral response was 6000A and the acceptance angle was 60°. For short lengths of optic cable the attenuation was not a serious problem (500dB/kM). The actual length of fibre used in this investigation was 2 metres. A black plastic sleeve was placed over the entire length of cable so that no ambient light could enter the optical core.

The collimating system consisted of a length of capillary tubing with an internal diameter of 0.6 mm. Both the internal surface of this tube and its external surface were blackened. This was necessary to stop interference caused by ambient light and reflections from the internal surface of the capillary tube. The

optic cable was fixed at the far end of the collimating tube in a light tight housing. The need for critical alignment between cable and tube was not necessary but some care was taken to locate the fibre fairly accurately.

The collimating tube was secured into a persepex disc, which had its outer surfaced blackened. The whole arrangement (figure 3.8) fitted into the viewing port with a bolted flange. A stainless tube was added to the system which gave protection from any thermal blasts and decomposed sulphur hexaflouride products during arcing.

The collimating system was such that half way into the arcing coil the area of view was 0.94 mm^2. This area of view varied from 0.64mm^2 to 1.3mm^2 corresponding to zero axial penetration into the coil to full (6cms) penetration, respectively.

3.2.6.2 PHOTOMULTIPLIER SYSTEM

An EMI type 6255A photomultiplier tube having a 13 stage venetian blind arrangement was used through out the investigation. The spectral response was determined by the S12 type photocathode material (Cs_3SbO). Its peak quantum efficiency was at 3900A (19%) with a typical current per lumens of 70 MA. The quantum efficiency did not fall below 8% for a range of

frequencies between 330A and 5400A. This system had an overall sensitivity of 2000 A/IM.

A 1MΩ resistor connected each dynode to the next. This resistor value was sufficiently large so that the maximum anode current (1mA) could not be exceeded (typical anode current 120 μA). A high voltage zener diode connected the cathode to the first dynode, this prevented the maximum voltage rating of this first stage (300v) from being exceeded. The voltage applied to the photomultiplier did not exceed 1.5 kV which was below it maximum rated valued of 2.5 kV.

A light diffuser placed before the photomultiplier window allowed for sufficient dispersal of light over a large area of the cathode window thus avoiding localised damage to the electron emitting surface due to the high density of light intensity.

The rise time of this system was 390 nS. The signals were monitored through a Tektronix 7A15 conventional pre-amplifier having a bandwidth of D.C. to 75 MHz and a rise time of 4.7 nS. This pre-amplifier was coupled to a 7704A Tektronix digital storage oscilloscope.

3.2.7 OSICILLOSCOPE RECORDING SYSTEM

Three oscilloscopes were used for various parts of the investigation - Tektronic type 556, Tektronic type 7704A and Gould OSA.

For fast transient measurements of current and voltage the two digital oscilloscope proved to be inadequate, mainly because the chopping rate of these oscilloscopes was only 100 kHz. However, the type 556, a dual beam oscilloscope, could accurately measure these transients without the problems of beam chopping arising. As well as measuring fast transients at current zero the 556 proved useful for recording the current, voltage, pressure and the output from the photomultipler system during the whole half cycle of arcing. Whilst the storage oscilloscopes could record the magnetic field, localised voltage probe measurements and photomultiplier measurements.

All the oscillographic equipment was powered through 1:1 isolation transformers and if triggered externally a 1:1 probe transformer provided isolation.

3.2.8 HIGH SPEED PHOTOGRAPHY

Conventional high speed photographs of the arc column were taken with a Dynafax camera. This camera used a metre length of tri-pan, 400 ASA film which rotated on a drum. The image from the objective lens was relayed to an octagonal rotating mirror by a system of stationery mirrors. An image is produced onto the film through two relay lenses and an exit diamond stop. The exposure times were controlled by the framing rate and the type

of exit diamond stop used. The maximum obtained exposure time at full framing speed of 35,000 frames per second and for an (3/32)" diamond stop was 0.75 μs, the time between frames was 28.6 μs and the overall writing time on the film (before which the event must have finished to prevent overwriting) was 6.4 mS. In practice a diamond stop of (3/16)" was used altering the exposure time to 1.5 μs and a frame speed between 10,000 - 20,000 frames a second. This camera examined the arcing period for either one or two half cycles of arcing. Stopping the camera aperature down to f-22 gave the maximum depth of field possible and also had the advantage that there was no interference from ambient light during the period the camera shutter was open.

However, this camera was unsuited for accurate current zero photography and recourse to image converter photograph was made.

3.2.9 IMAGE CONVERTER PHOTOGRAPHY

The IMACON (image converter) camera system is a particularly useful diagnostic tool for current zero photography because of its sensitivity to low light levers. However, the camera has to be protected from the effects of radiation during the peak current period. A mechanical shutter provided this protection. Specifications are detailed in section (3.2.9.2).

3.2.9.1 IMACON SYSTEM

The IMACON camera is essentially an opto-electronic device is shown schematically in figure (3.9). Light emanating from the arc was focused by an F/2 objective lens onto the curved surface of the photocathode. The photocathode has a spectral response of S11 (which has a peak efficiency at 3900A). Electrons emitted by light impinging on the photocathode are focused by high voltage elastrostatic lenses and are accelerated towards the photocathode by high voltage accelerating plates. An image is produced on the photo-anode (P11 spectral response) which then is transposed onto polaroid 3600 ASA black and white film by a F/1.2 double coated relay lens. A plug in unit (type 9B) controls the exposure times and delay times between the 3 consecutive frames. The exposure times are variable for each frame from 0.15, 1.0, 2.0, 5.0 and 10 μs. The second and third frames have a modified delay control giving a variable delay between 3 and 500 μs. This unit can produce three consecutive frames each of which appear at different positions on the polaroid film due to a stepped high voltage applied to the deflection plates. A monitor signal enabled frames to be precisely timed and the exposure of each frame to be determined.

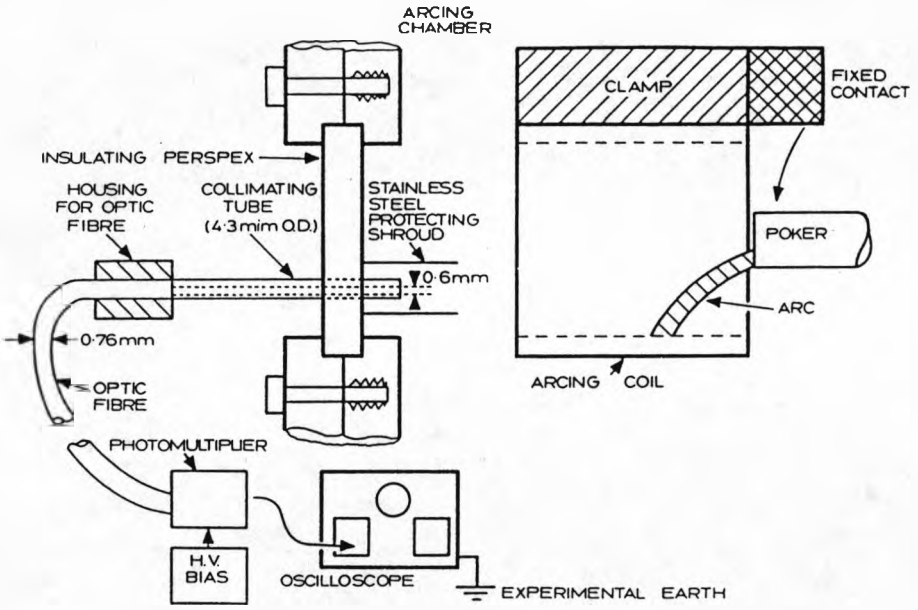

FIGURE 3.8. Fibre Optic Measurement.

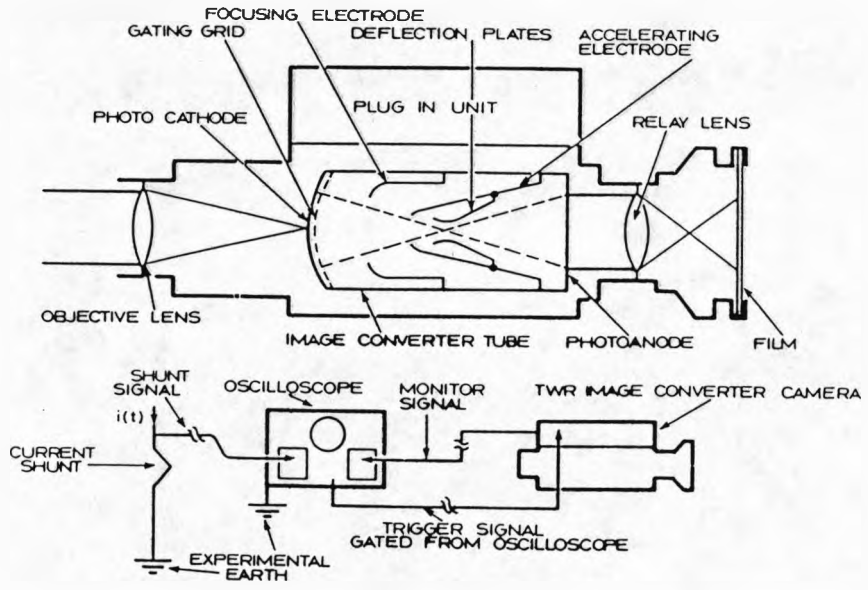

FIGURE 3.9. IMACON System.

3.2.9.2 SHUTTER SYSTEM

A protection shutter system was used infront of the photocathode of the IMACON. This prevented the intense light during peak current arcing from affecting the sensitive photocathode. The capping shutter was modified by adding an external spring which aided opening of the shutter. The aperature setting on this shutter arrangement could be varied from an f-stop of 4.5 to 32. The maximum opening speed indicated on the shutter mechanism was 1/500th of a second. With the modified synchro-compass shutter system this was improved to the extent that the shutter opened fully in 190 us for an f-stop of 22. This was the maximum opening time recorded during tests.

During normal operation the shutter system was fully open no earlier than 620 μs before current zero, protecting the photocathode from the damaging light intensity during the peak current period of arcing.

3.2.9.3 TIMING CONTROL SEQUENCES

The capping shutter opened more than 620 us before current zero but was always fully open at current zero. This was electrically timed from standard electronic delay unit.

The electronic shutter on the IMACON was operated from the Teltronix 556 oscilloscope through the gate facility.

This gate signal was actuated when the arc current had fallen to a predetermined level set by the triggering circuit on the 556 oscilloscope. This method allowed for accurate timing of the frames (± 500 ns) during the current zero period and could be checked on the oscilloscope by monitoring signal from the IMACON.

4. EXPERIMENTAL RESULTS

4.1 PEAK CURRENT RESULTS

The peak current investigation is divided into four sub-sets each covering a particular aspect of the peak current period. The four sub-categories correspond to investigations of the magnetic field, the electrical behaviour of the arc, it's areodynamic behaviour and it's apperarence during arcing. Information gained from the peak current period of arcing should identify the important parameter which need to be considered in the development of a theoretical model of a rotating arc.

4.1.1 MAGNETIC FLUX

4.1.1.1 CALIBRATION OF MAGNETIC FLUX MEASURING SYSTEM

The search coil used for monitoring the magnetic flux density was placed in a known uniform magnetic field generated by a long solenoid.

The integrated waveform representing the magnetic field was displayed on a digital storage oscilloscope. Figure (4.1) shows a typical waveform obtained from such tests. The calibration factor for the entire system can be calculated from such measurements and for this particular arrangement was found to be 10mV 1.604m T figure (4.1).

4.1.1.2 SPATIAL VARIATION OF MAGNETIC FIELD

Typical magnetic field and current waveforms produced during excitation of the interrupter coil by the L-C power source without arcing are shown on figure (4.2). The peak exciting current during the first half cycle was 850A. The peak value of subsequent half cycles decay because of losses in the ringing circuit. The magnetic field shown on figure (4.2) is the axial component which is 71.5mT for 850 amperes exciting current. The peak magnetic field decreases each half cycle not only because of the decaying exciting current but also because of the sudden energising of the coil. As a consequence of both these effects the ratio of peak current to peak magnetic field changes and the displacement in time between successive current and magnetic flux peaks varies. To standardise the magnetic field measurements, two criteria have to be defined.

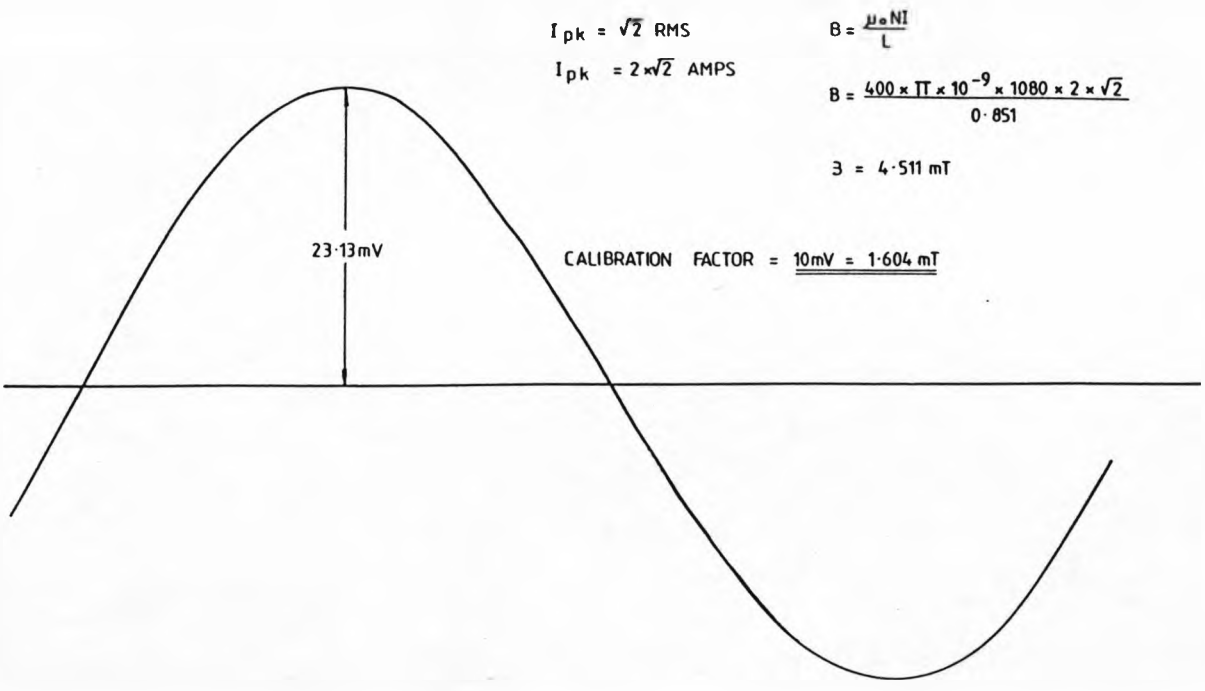

FIGURE 4·1. CALIBRATION OF MAGNETIC FIELD MEASURING SYSTEM

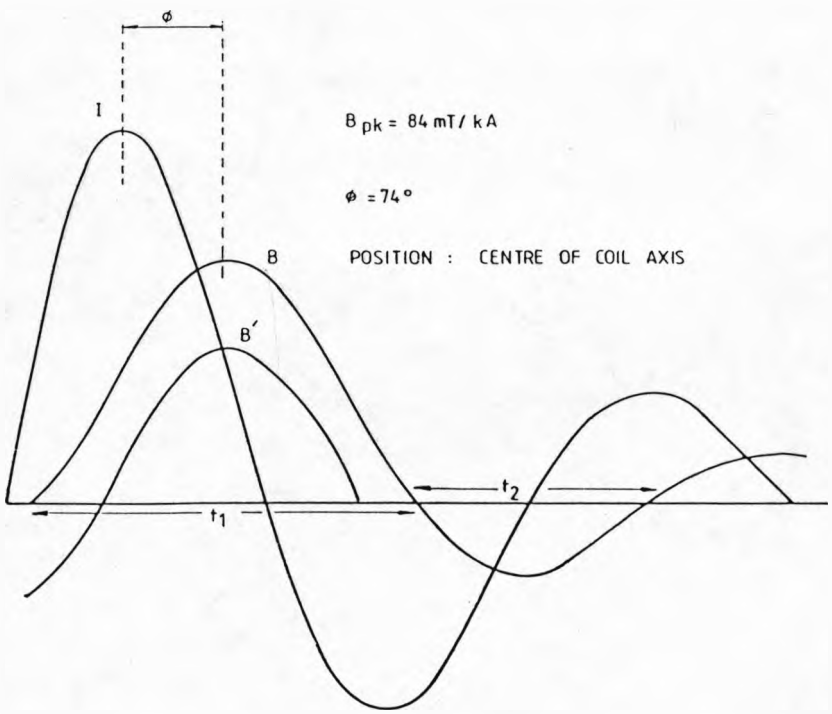

FIGURE 4·2. AXIAL MAGNETIC FLUX COMPONENT

The first criterion is the normalisation of the magnitude of the first peak of the magnetic field with respect to the first current peak. Of course the ratio of peak magnetic field to peak current (i.e. x Test per kilo ampere) will vary during subsequent half cycles. The second criterion defines the phase angle between current and magnetic field. This angle is quoted in degrees (one half cycle is 180 degrees) and is that angle which separates the first peak of current and magnetic flux. This angle subsequently increases for each half cycle (figure 4.2).

Thus each coil can be characterised by these two critera. The results of figure (4.2) correspond to the axial magnetic field component at the centre of the coil which has a ratio of 84mT/kA and a phase difference of 74°. Measurements at additional locations within the coil lead to a magnetic map showing normalised axial flux as well as normalised radial flux components within the coil volume. Figure (4.3) shows some typical lines of magnetic flux generated within the cylindrical coil. This field is non-uniform because of the end effects of the short coil. A typical pattern of the axial and radial field components is shown on figure (4.4). The axial field component is orientated in the same direction throughout the entire coil volume. However the orientation of the radial

component changes. In cross-section 1 (figure 4.4) the field is directed radial outwards from the coils axis but in cross-section 3 its vector direction becomes reversed and is directed radially inwards.

It is convenient to specify a convention which defines the direction of positive or negative field orientation. For a positive radial field the magnetic flux direction must be radially inward and is negatively orientated if the field is radially outward. Figure (4.5) demonstrates this convention graphically.

The axial components of the induced magnetic flux is the most dominant. Its spatial variation is shown on figures (4.6, 4.7, 4.8, 4.9). This field is non-uniform and varies both axially and radially. Figures (4.6, 4.7) show the axial variation within the cylindrical volume for 5 positions corresponding to the left and right hand side of the coil, the top and bottom of the coil and the axis of the coil. The axial field (B_Z) decreases from a maximum at the mid axial position of the coil to a lower finite value at the end of the coil. This decrease in B_Z is significant and for the example on figures (4.6, 4.7), the decrease is on average 48%. The axial field near to the surface of the copper annular electrode measured at four locations (left, right, top and bottom) show reasonable similarity to each other.

The axial field measured at these location is greater than that measured on the axis of the coil. This radial increase of B_z is 20% for cross-section 2 (positioned at the mid axial point figures (4.3, 4.4), between 10% and 20% for cross-section 1 and approximately 30% for cross-section 3 (figures 4.8, 4.9). There is a significant difference between the radial variation observed at cross-section 1 and that ovserved at 3. This discrepancy is caused by the added magnetic field produced by the current flowing through the temporary making contact between the poker and annular copper former (figure 4.3).

The phase difference (ϕ) between the exciting current and the axial component of the induced field varies both axially and radially. Mid-way into the coil volume the phase difference is a maximum and decreases for all locations towards the end of the coil. On the axis this variation is from 85° to 77° over a 3 cm distance (figure 4.10). At a position mid-way into the coil volume the phase difference is greater on the left hand side of the coil than the right hand side. There is a similar trend between the top and bottom locations. However, this difference disappears towards the coil's open end at which point the phase difference of all four radial locations tend to the same value.

For these four locations there is a substantial decrease in ϕ, but on the axis this decrease is not as large resulting in the phase difference on the axis at the end of the coil becoming larger than that at the radial positions.

This radial variation is depicted on figures (4.12, 4.13) for all three cross-sections. The least undisturbed profile is cross-section 3 which is situated far enough away from the current flow through the poker electrode and making strap. The phase difference is greatest on the axis of the coil at station 3 and decreases radially outwards. The profile at station 1 should be similar to that at 3 and it is so if the coil is reversed so that station 1 is the furthest point away from the poker electrode. These added influences generally increase the phase difference angle at the left and top positions and decrease it at the centre, bottom and right positions for stations 1 and 2. The profile at section 2 should have a parabolic shape similar to that at station 3 but the magnitude of ϕ will be larger throughout that radial cross-section.

Although the magnitude of B_z is insensitive to small additional imposed magnetic fields, the phase difference angle is more susceptible to such change.

Figure (4.14) highlights the sensitivity of Φ to a imposed supplement field (B_S). Although B_S is less than one fifth of B_Z' the change in B_Z is small, 8%, but the change in the phase difference angle is larger at 16%.

The radial component of the magnetic field also has a spatial variation within the cylindrical volume. The strengh of this component is at maximum 10% of the axial field for the same location and because of the small size of this component it is easily distorted by any additional induced fields. To minimise this interference each end of the coil volume was individually tested so that each end was positioned away from the poker electrode. This distortion can be seen by comparing measurements taken at cross-section 1 shown on figure (4.17). 1a shows the composite radial field produced by the coil and any other induced field, whilst 1b is the field measured when the coil has been rotated through 180° and is not affected by interference due to other magnetic fields.

The radial field is a maximum at either end of the coil but at one it is directed radially inwards and at the other radially outwards (figure 4.15, 4.16). This field should be zero at the centre of the coil but because of the distortion of the magnetic field due to the uneven distribution of eddy currents in the copper

annular electrode this field is zero at a point off-centre of the coil. The field on the axis is small compared to that measured at the four radial positions (figures 4.17, 4.18). Radially across any cross-sectional station this field is a maximum at the core surfaces and zero near the coil axis. At both core surfaces the field is always in the same sense, ie. inward or outward.

The phase difference angle varies little with axial position and is relatively constant between 70°and 80° with only the top and bottom measurements showing an axial decrease (Figure 4.19). The radial variation shows a similar trend with only a radial decrease in 0 for three locations (top, axis and right) the others remain constant at 80°(Figure 4.20).

4.1.1.3 TEMPORAL VARIATION OF FIELD

The magnetic field set up in the cylindrical gap of the annular copper electrode is the product of two separate mmfs. The first mmf is produced by the pulsed sinusoidal current through the coil windings and copper former; the second mmf is a result of eddy currents generated in the copper core by the exciting current. Where as the exciting current varies sinusoidally the eddy currents grow more gradually at the rate governed by the resistivity of the coil yoke. This latter

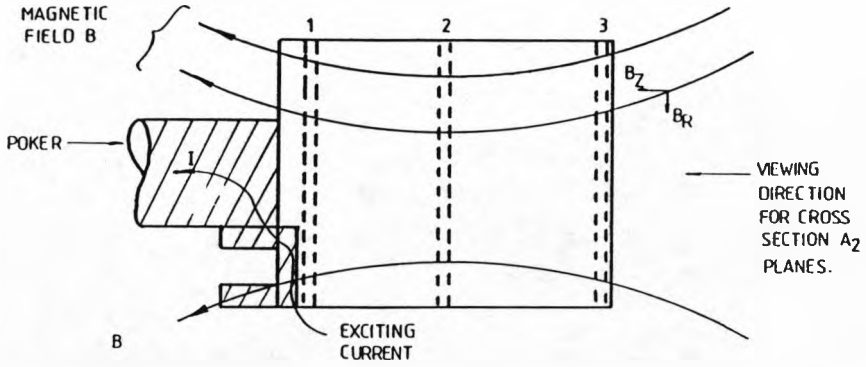

FIGURE 4·3 MAGNETIC FIELD

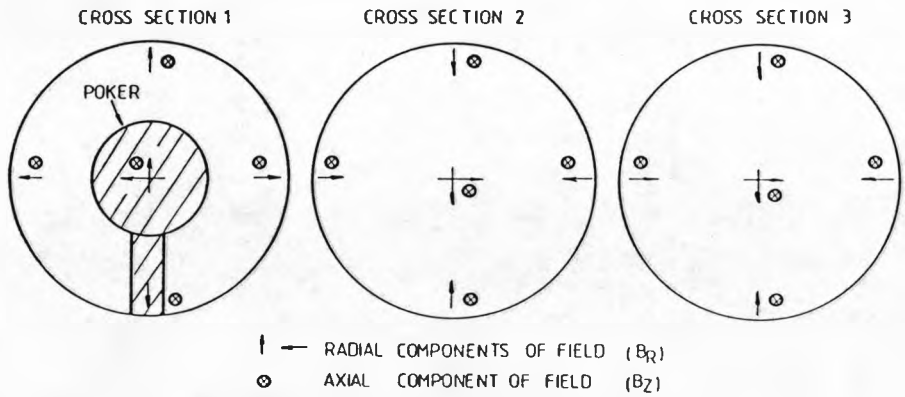

FIGURE 4·4 EXPERIMENTALLY MEASURED FIELD DIRECTION

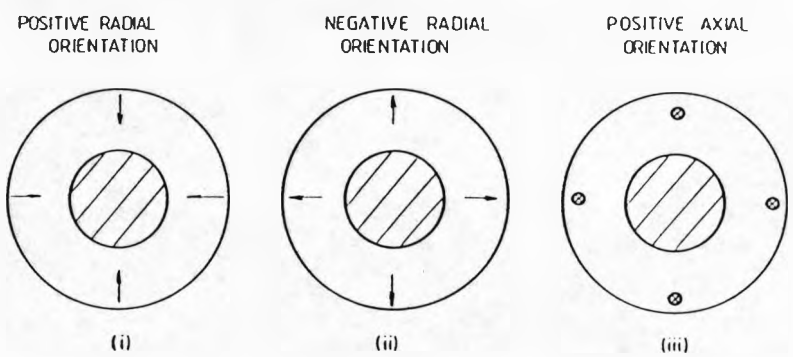

FIGURE 4·5. DEFINING FIELD ORIENTATION

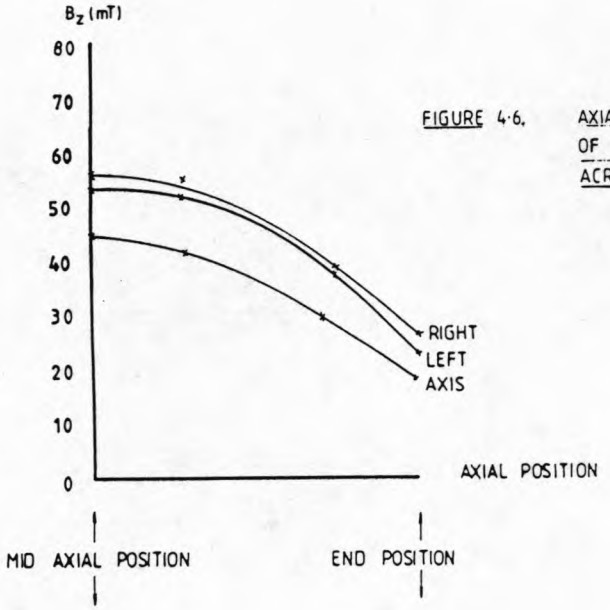

FIGURE 4·6. AXIAL VARIATION OF B_z HORIZONTALLY ACROSS THE COIL

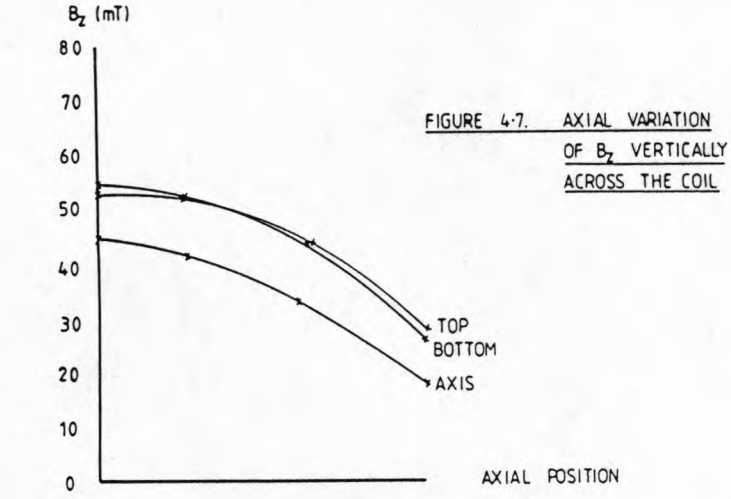

FIGURE 4·7. AXIAL VARIATION OF B_z VERTICALLY ACROSS THE COIL

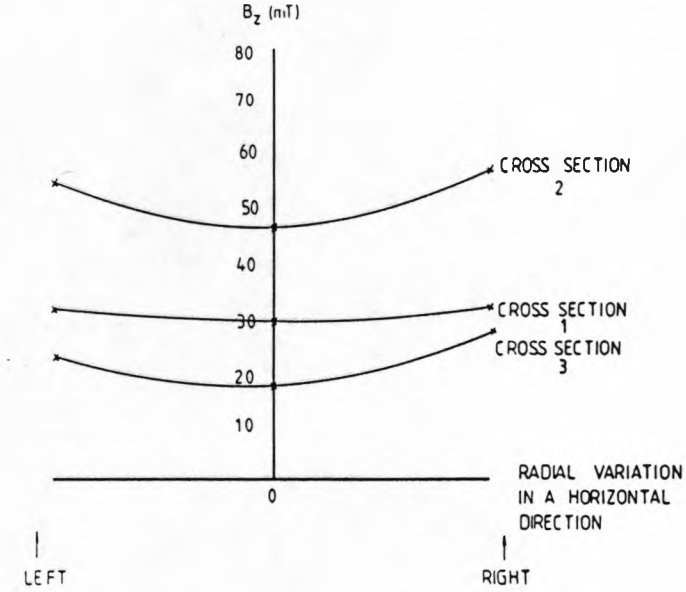

FIGURE 4·8. RADIAL VARIATION OF B_z FOR 3 AXIAL POSITIONS

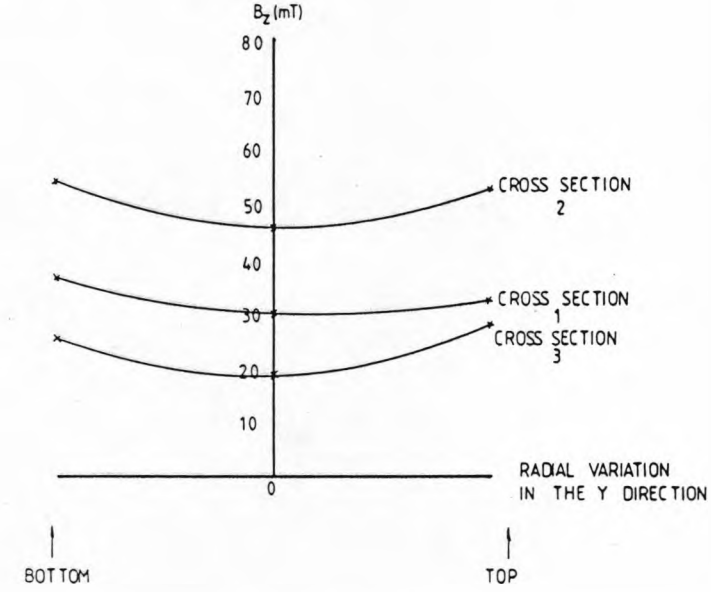

FIGURE 4·9. RADIAL VARIATION OF B_z FOR 3 AXIAL POSITIONS

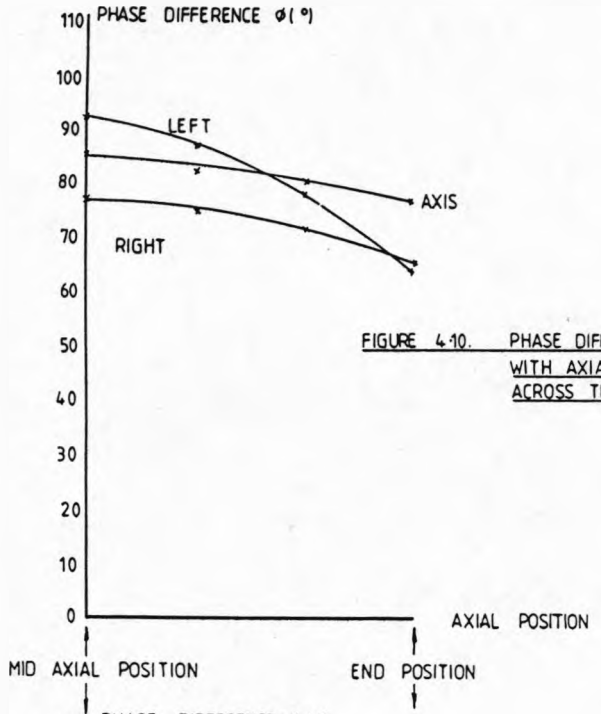

FIGURE 4·10. PHASE DIFFERENCE ANGLE CHANGE WITH AXIAL POSITION HORIZONTALLY ACROSS THE COIL

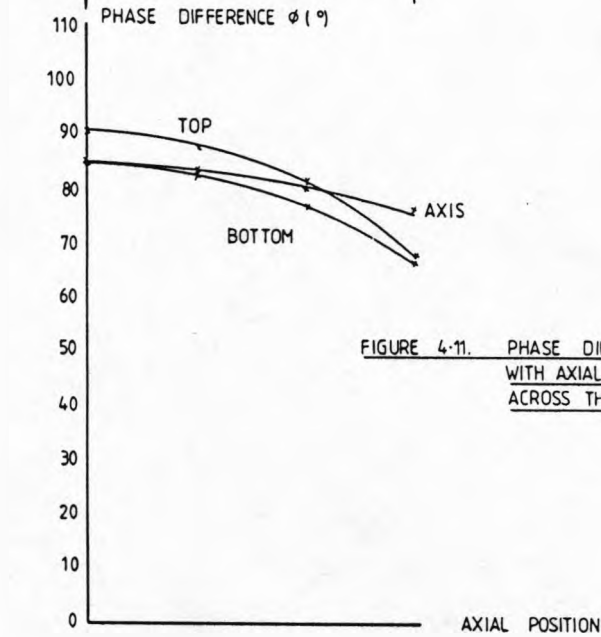

FIGURE 4·11. PHASE DIFFERENCE ANGLE CHANGE WITH AXIAL POSITION VERTICALLY ACROSS THE COIL

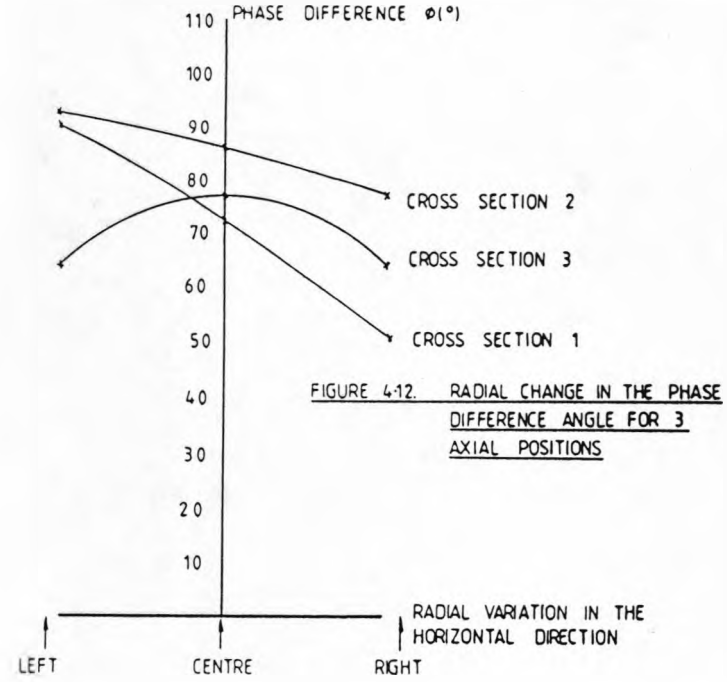

FIGURE 4·12. RADIAL CHANGE IN THE PHASE DIFFERENCE ANGLE FOR 3 AXIAL POSITIONS

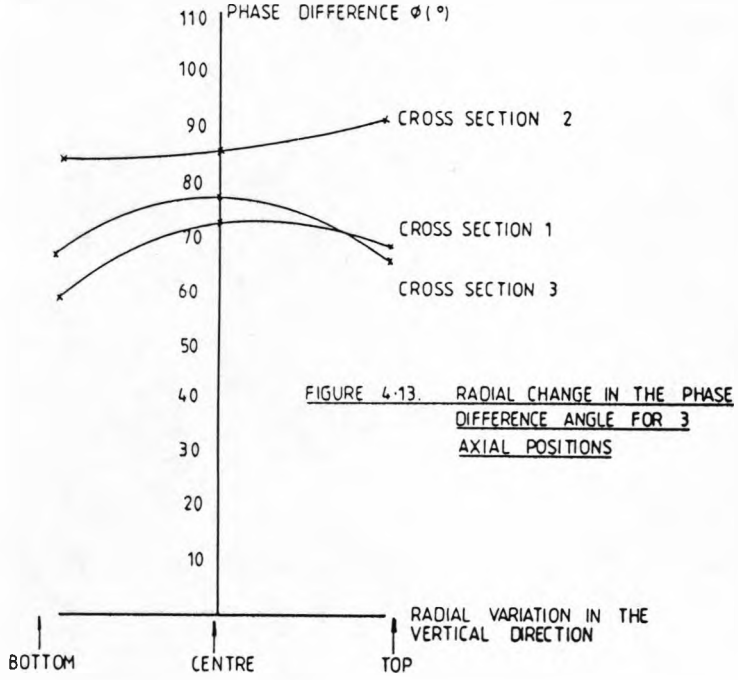

FIGURE 4·13. RADIAL CHANGE IN THE PHASE DIFFERENCE ANGLE FOR 3 AXIAL POSITIONS

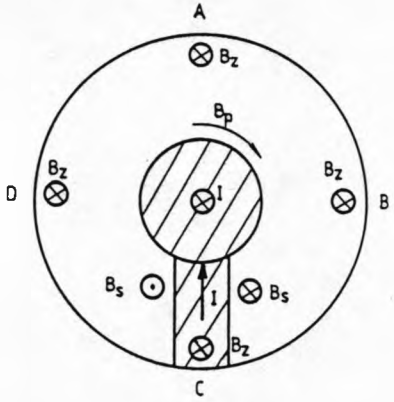

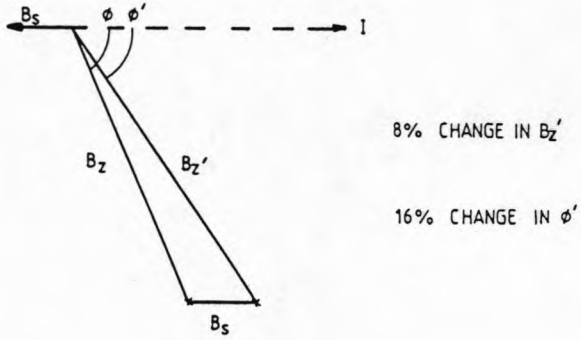

FIGURE 4·14. DISTORTING EFFECT OF OTHER MAGNETIC FIELDS

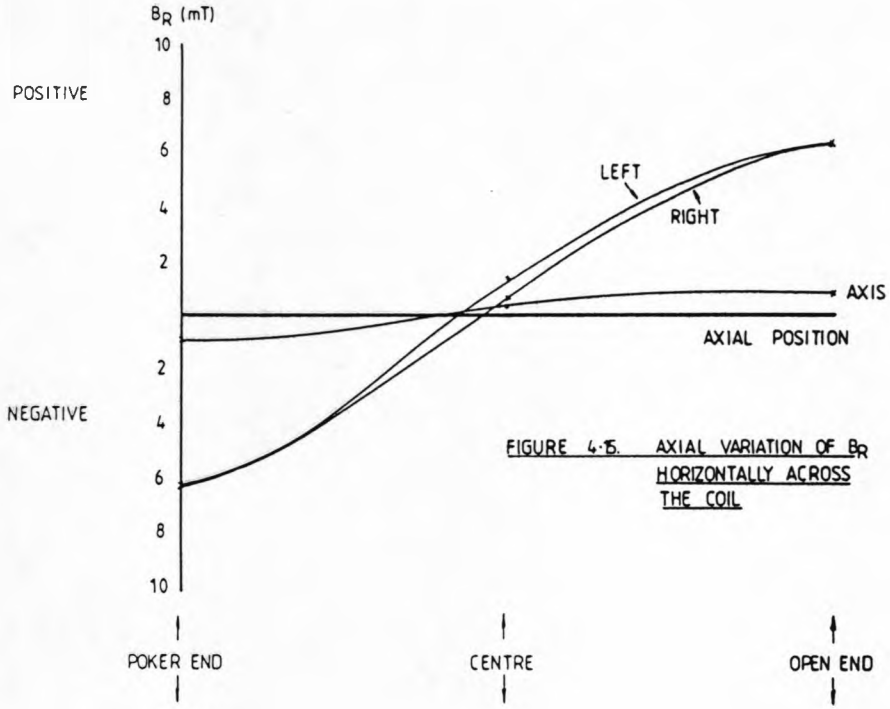

FIGURE 4·15. AXIAL VARIATION OF B_R HORIZONTALLY ACROSS THE COIL

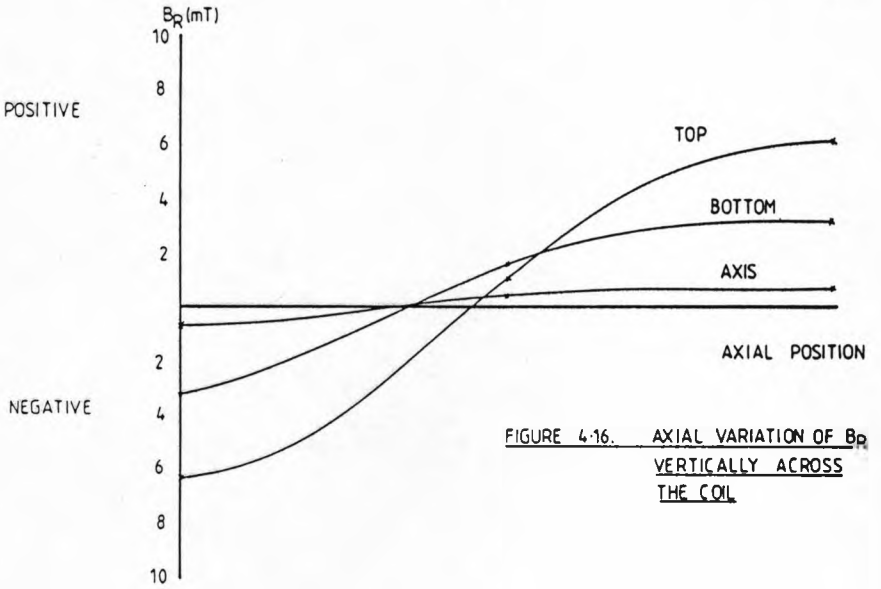

FIGURE 4·16. AXIAL VARIATION OF B_R VERTICALLY ACROSS THE COIL

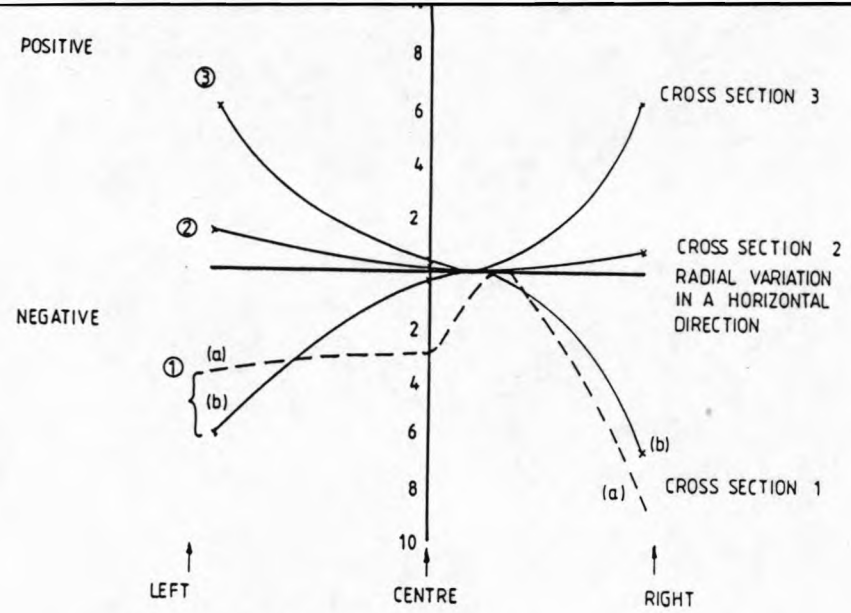

FIGURE 4·17. RADIAL VARIATION OF B_R FOR 3 AXIAL POSITIONS

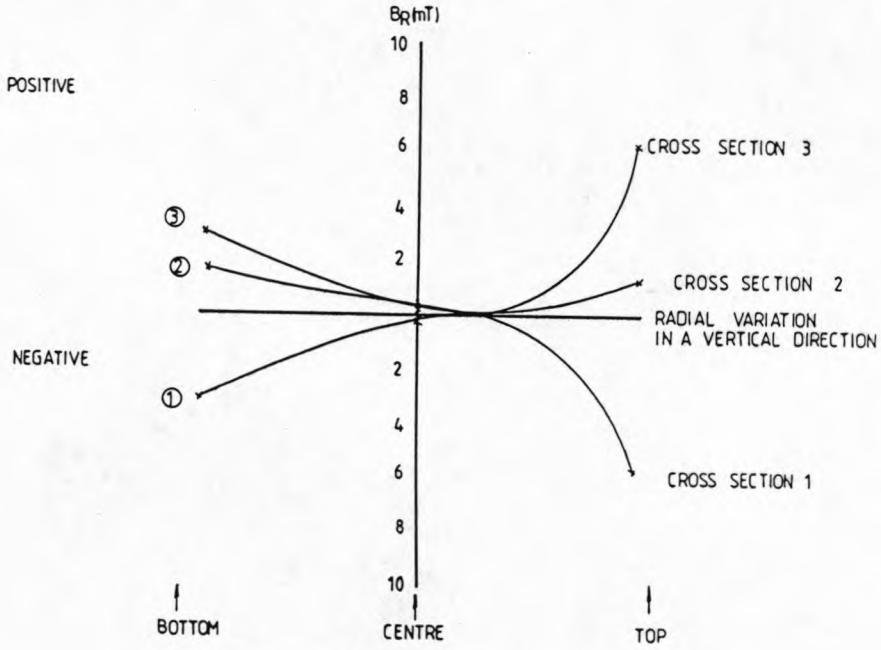

FIGURE 4·18. RADIAL VARIATION OF B_R FOR 3 AXIAL POSITIONS

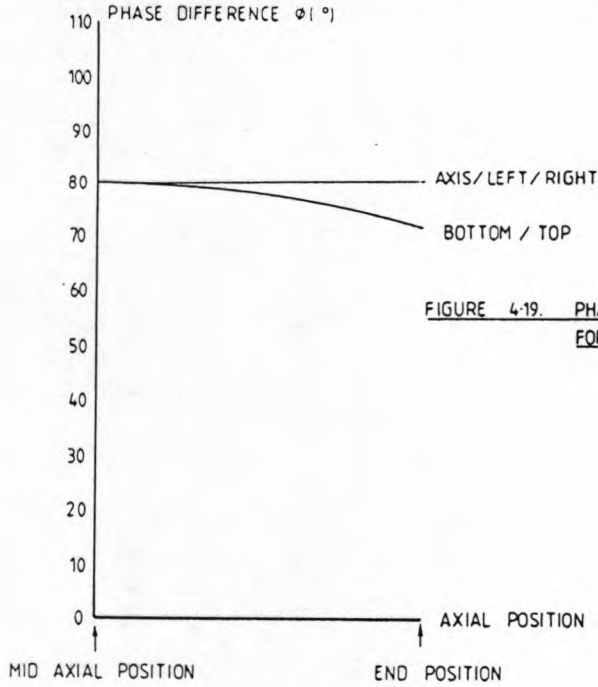

FIGURE 4·19. PHASE DIFFERENCE CHANGE FOR B_R WITH AXIAL POSITION

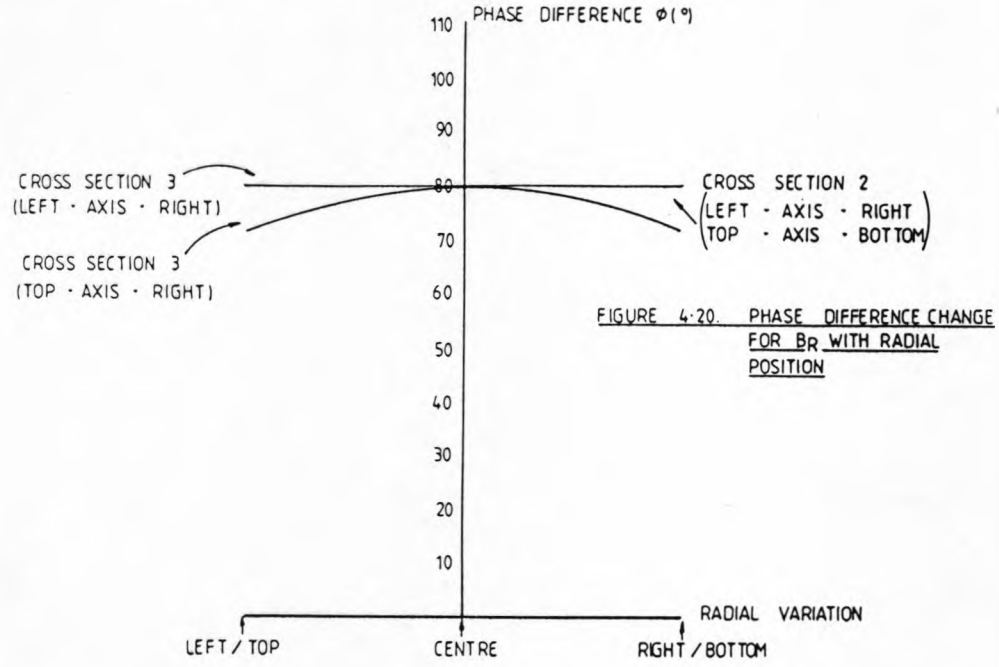

FIGURE 4·20. PHASE DIFFERENCE CHANGE FOR B_R WITH RADIAL POSITION

growth rate extends over approximately 3 cycles of the exciting current. The combined influence of these fields leads to the superposition of an exponential decay extending over 3 cycles upon a sinusoidal variation.

A further complication caused by this transient situation is that the time period for one half cycle of the magnetic flux varies over the first two half cycles because of assymetry. Figure 4.2 shows the first time period, t_1, for one half cycle to be 6.84ms and the second, t_2, is 4.2ms. Subtraction of the exponential component from the observed magnetic flux results in the quasi steady flux waveform B (Figure 4.2). Initially, this quasi stady magnetic field is negative but later passes through zero and increases positively to the first peak. Thus the complex magnetic flux waveform observed experimentally may be considered in terms of the two simpler waveforms. It is the superposition of these two simpler waveforms which leads to a phase difference which differs from $\pi/2$.

At all stations monitored a similar time response of magnetic flux was noted. The magnitude and phase difference of flux varied with location but the temporal trend was the same for all locations.

4.1.1.4 PRIMARY TURN EFFECT

Changing the number of turns on the copper former causes a corresponding change in the mmf produced by the primary winding $(IN)_1$. This in turn alters the magnitude of the eddy currents induced $(IN)_2$ in the core and results in a change in the overall magnetic field induced within the coil volume. The windings and copper core are analogous to a transformer with N_1 primary turns and a short circuited secondary. The mmfs $(IN)_1$ and $(IN)_2$ add vectorally for both the transformer analogy and the actual coil system. Figure (4.21) shows the effect of decreasing the number of primary turns experimentally. As expected the field decreases linearly. This decrease is true for both the axial field and the radial field components at all locations within the gap. The phase difference angle remains unaffected over most of the range until only two turns remain when the difference angle becomes sensitive to turn reduction, eventually increasing to 140° for less than one primary turn. Elsewhere in the cylindrical volume a similar trend could be observed. Provided that there are more than two primary turns on the coil the magnetic field can be increased substantially without affecting the phase difference angle. The magnetic field within the coil can

therefore be chosen for a specific phase difference angle simply by putting the required number of primary turns onto the copper former.

4.1.1.5 INTER-TURN INSULATION FAILURE

The consequences of insulation failure can have serious repercussions for the effectiveness of the circuit breaker. One of the main components of the ciruit breaker is the field generating coil. Any insulation failure will change the field inside the cylindrical gap to some degree.

The infuence of insulation failure is to introduce a source of a third mmf due to the formation of a number of short circuited turns. The summation of this mmf with the other two mmfs change the magnetic field strength and phase difference angle within the cylindrical gap. These mmfs interact differently depending upon the location from which the turns of insulation are removed. However, regardless of the location of the insulation failure there is an increase in the total amount of eddy current flow which reduces the overall magnetic field. The complexity of the interaction is manifest in the degree to which both the magnetic field and phase difference angles are affected.

Figure (4.22) shows that the reduction in the magnetic field is dependant upon the location from which the insulation is removed. The greatest reduction occurs if insulation is removed from the outer turns curve (3), rather than the inner turns curve (2). For example, experimental observations shown on Figure (4.22) indicated that for only 8 turns of insulation out of a possible 13 turns the magnetic field varies between 35 mT for insulation removed from the outer windings to 40 mT for insulation removed from the inner windings.

The phase difference angle is also affected by altering the number of turns of insulation. This angle increases irrespective of the location from which the insulation is removed. However, a greater increase is observed when insulation is removed from the inner windings. For the example shown on figure (4.22) and for 8 turns of insulation the change in the phase difference angle is from 78° for removal from the outer turns to 86° for the inner turns.

4.1.1.6 VARIATION OF MAGNETIC FIELD WITH CORE THICKNESS

Both the magnitude of the axial magnetic flux and the phase difference varies with changes in the core thickness. A thicker core reduces the axial flux and increases the phase angle (figure 4.23). There is a

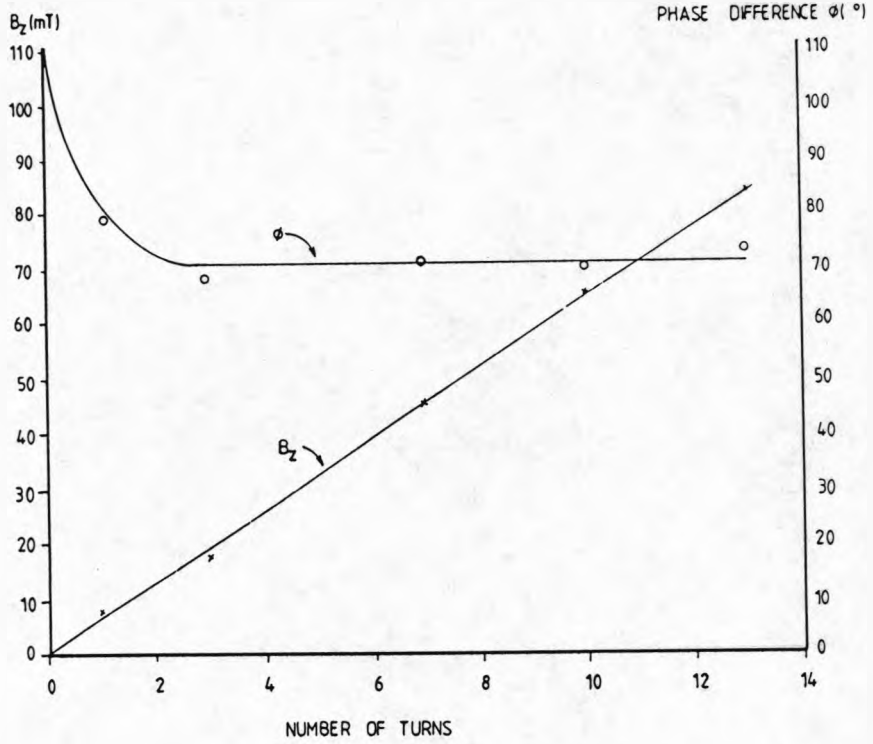

FIGURE 4·21. AXIAL FLUX AND PHASE DIFFERENCE VARIATION WITH THE NUMBER OF PRIMARY TURNS

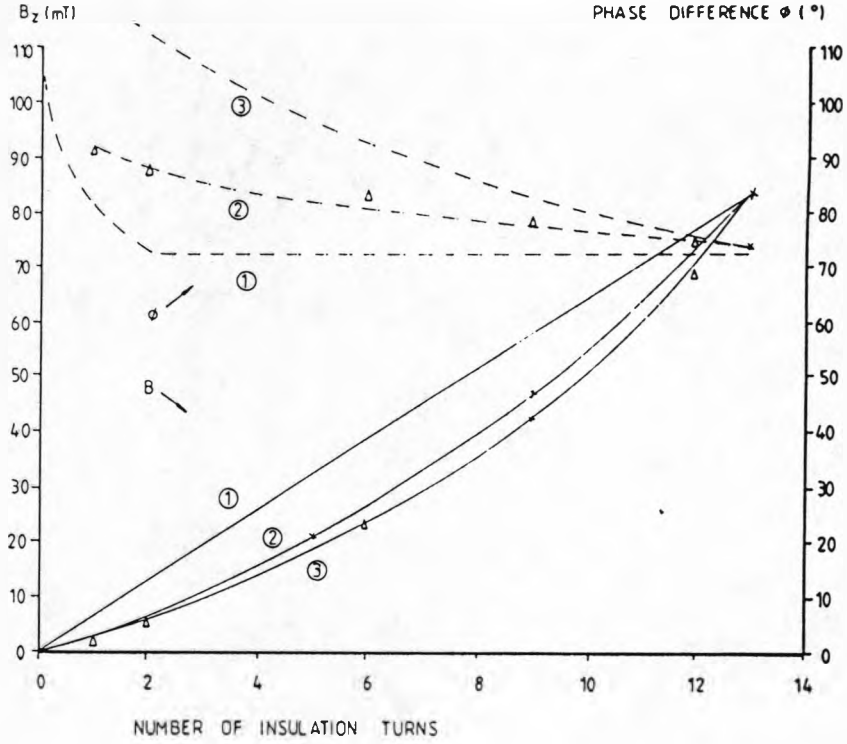

FULL INSULATION

REMOVED INSULATION FROM INNER TURNS

REMOVED INSULATION FROM OUTER TURNS

FIGURE 4·22. EFFECT OF INSULATION FAILURE

linear decrease in B accompanied by a linear increase in ϕ throughout the range investigated. For a three fold increase in the core thickness the axial field decrease by approximately half whilst the phase angle changes by one and a half times.

These changes reflect the effect of the shielding eddy currents in the copper core. Within a thicker copper core larger eddy currents can be induced for a given exciting current. The vector sum of the primary exciting current and the shielding eddy currents add vectorally, resulting in the overall flux pattern in the cylindrical gap.

4.1.1.7 PEAK CURRENT DEPENDENCE OF MAGNETIC FIELD.

To ensure that the generated peak magnetic field is linearly dependent upon the peak exciting current, the axial magnetic field at one station was recorded (figure 4.24). It shows that the axial magnetic flux is linearly dependent upon the exciting current in the current range of 0 to 6 kA. The phase difference angle is unaffected by the magnitude of the exciting current and remains constant at 49°. The field at other locations, including the radial field component showed similar trends.

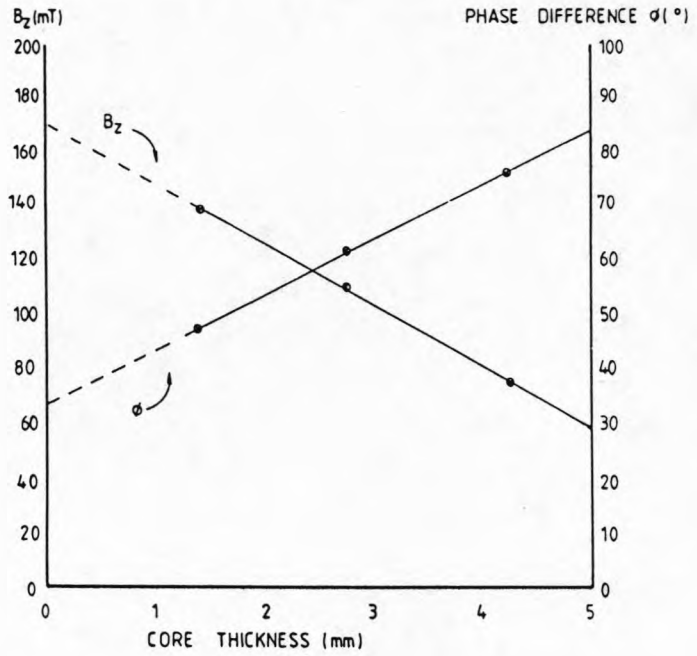

FIGURE 4·23. COPPER CORE THICKNESS

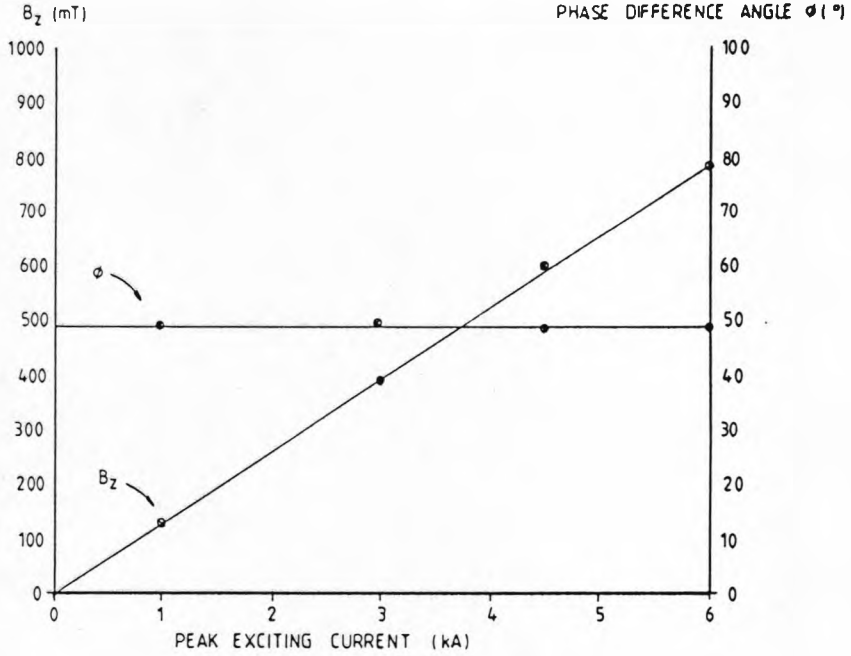

FIGURE 4·24 PEAK CURRENT EFFECT

4.1.2 ELECTRICAL BEHAVIOUR

During this peak current phase of arcing the electrical behaviour of the arc column is important. It is essential during this period to measure the arc current and arc voltage. For more information localised arc voltage measurement are useful especially in determining the local electric field strength and the degree of axial penetration of the arc column.

4.1.2.1 ARC CURRENT

Figure (4.26) shows two half cycles of arcing current. Both half cycles are sinusoidal in nature and there is a smooth commutation of current through the first current zero where the arc column has failed to extinguish.

Both the 20 mΩ and 1.038 mΩ current shunts give the same current waveform and the di/dt measured at the first current zero corresponds to $2\pi.f.I_{pk}$ ($f=110Hz$), where I_{pk} is the magnitude of the first current peak.

There was no evidence of the high value current shunt distorting the current waveform during the peak current and current zero regimes of arcing.

4.1.2.2 OVERALL ARC VOLTAGE

The arc voltage figure (4.26) for the first half cycle of arcing varies from 108 volts at the start to 252 volts towards the end of the half cycle but on average this voltage is 180 volts. For the second half cycle the voltage varies between 310 volts to 240 volts. On both the first and second half cycles there are many rapid voltage fluctuations. These are random and have a relatively slow rise to a voltage peak and then a sudden decrease to some nominal value. Towards the end of each half cycle there is a general voltage increase, resulting in an extinction voltage peak prior to current zero. There is both an increase in the average arc voltage and the number of voltage fluctuations as the peak current is increased or the magnetic field characteristic of the coil is increased.

4.1.2.3 LOCALISED ARC VOLTAGE

The localised probing of the arc voltage is depicted by figure (4.27) for a single voltage probe monitoring a 9 kA peak current force in a 35 mT/47° coil. The probe voltage recorded is not continuous because the arc sweeps past the probe wire every revolution and the arc plasma is only in contact with the probe during each incidence. This contact time is a function of the arcs diameter and the arcs velocity.

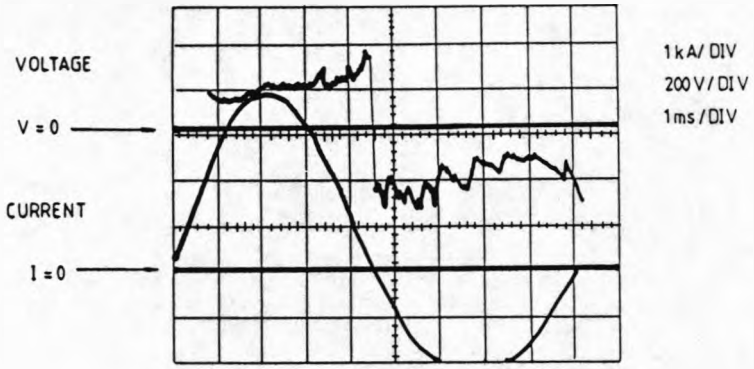

FIGURE 4·26. TYPICAL TWO HALF CYCLES OF ARCING

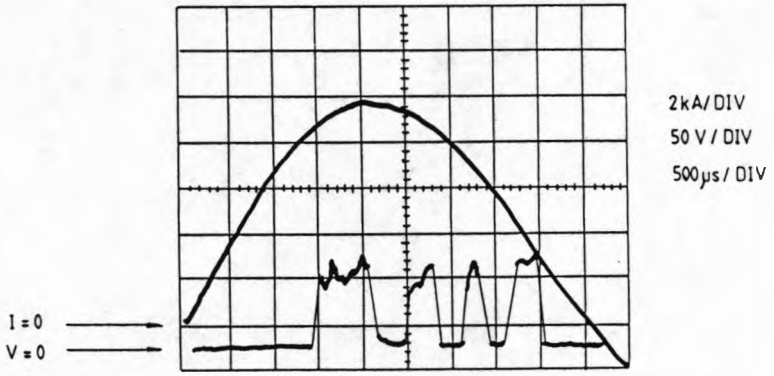

FIGURE 4·27. LOCALISED VOLTAGE MEASUREMENT USING ONE PROBE ROD

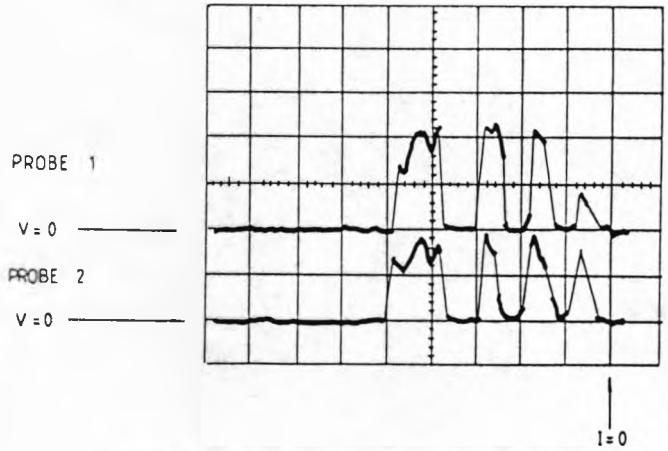

FIGURE 4·28. LOCALISED VOLTAGE MEASUREMENT USING TWO PROBE WIRES SEPARATED BY 0·7 cms.

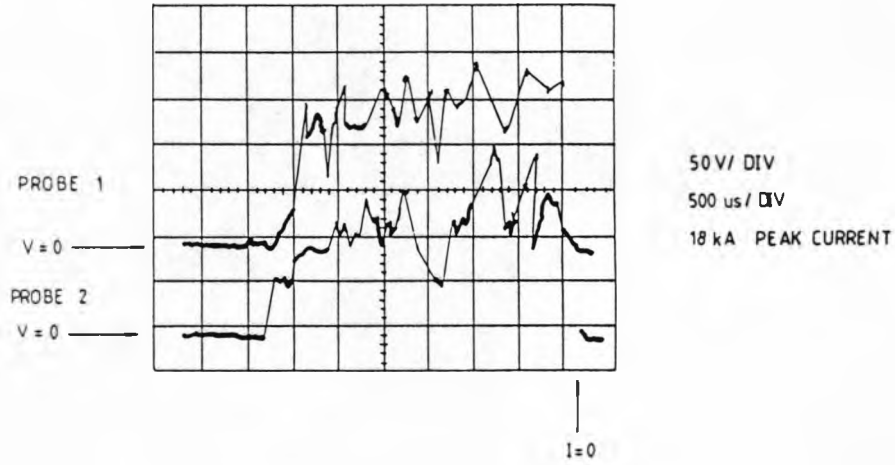

FIGURE 4·29. LOCALISED VOLTAGE MEASUREMENT

In figure (4.27) the arc rotates between four and five times during one half cycle. The maximum transient time of the arc across the probe is 600 μs for this particular condition and the minimum transit time is 300 μs.

Using two voltage probes separated by 0.7 cms the local electric field strength within the arc plasma can be evaluated. Figure (4.28) shows typical voltages recorded during this period for the same peak current and magnetic field conditions as for figure (4.27). There are the same number of revolutions as previously recorded but the time taken for the first revolution to begin is 500 μs longer this highlights the degree of shot-to-shot variation. Each voltage peak has a similar shape, persists for the same amount of time and occurs at the same point in time.

The local voltage measured by the two probe rods increases with increasing peak current and the number of rotations also increases during the half cycle. Figure (4.29) shows between 8 and 10 rotations for a 18 kA peak current but the generally higher voltage during most of the half cycle indicates that the arc has filled most of the arcing area.

4.1.2.4 AXIAL PENETRATION VOLTAGE PROBING

Discrete axial voltage probing of the coil volume showed that the arc penetrates the whole length of the coil volume. However, the degree of penetration is dependant upon the peak current and it is at peak current when maximum penetration occurs.

Figures (4.30 - 4.33) are probe measurements within the cylindrical gap. Probe 1 is positioned half way into this coil and probe 2 is situated at the coil exit opposite the poker electrode. Below 4.0 kA peak current the arc column does not even penetrate half way into the coil (figure 4.30). However, for a peak current of 9.7 kA the arc has penetrated at least half the axial length of the coil. This midway penetration occurs during the peak current phase of arcing and persists until current zero (figure 4.31) but this arc has not penetrated the full length of the arcing tube. A similar trend is observed for a 13 kA peak current arc; there was midway penetration of the arc but full penetration was not observed (figure 4.32). However, for an 18 kA peak current arc full penetration of the arcing tube was observed (figure 4.33). This occured during the peak current phase of the half cycle but unlike midway penetration which persisted until current zero full penetration ceased approximately 500 μs after peak current.

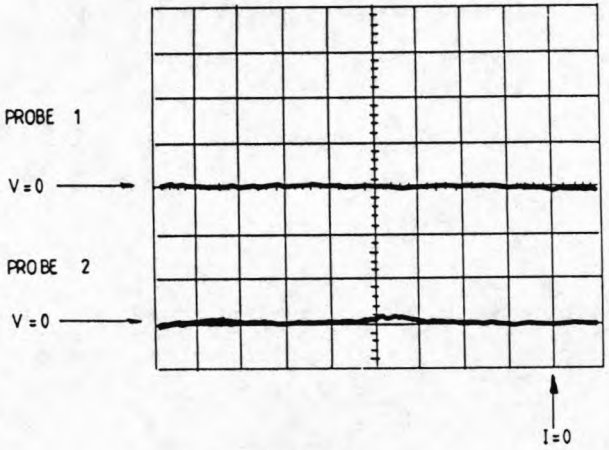

FIGURE 4·30. AXIAL PENETRATION PROBING

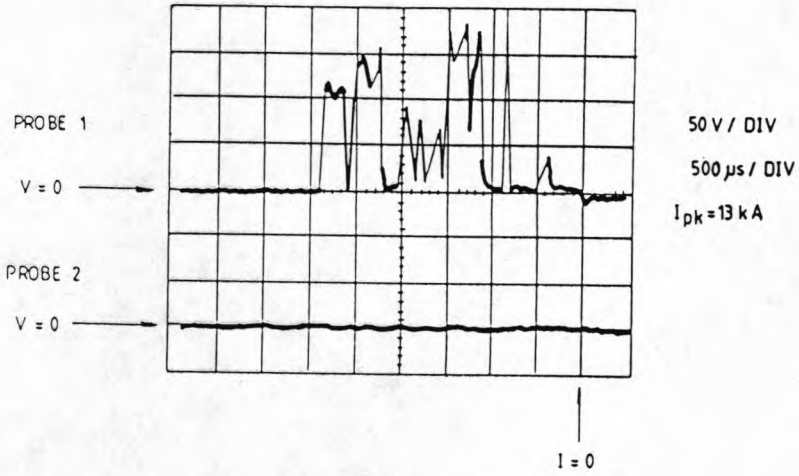

FIGURE 4·32. AXIAL PENETRATION PROBING

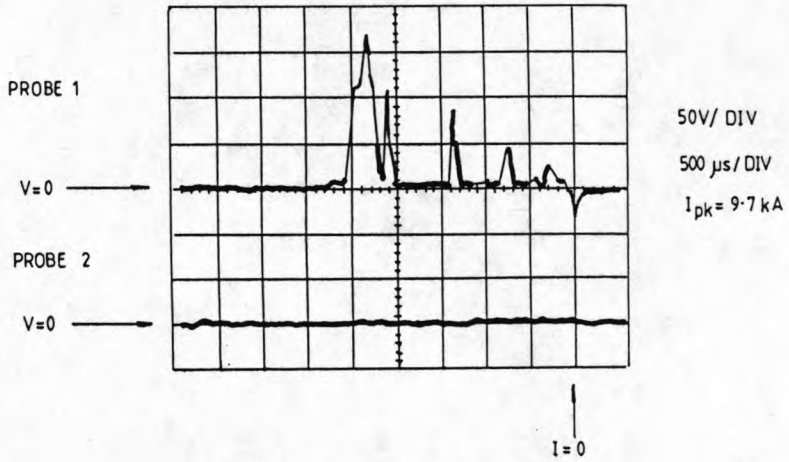

FIGURE 4·31. AXIAL PENETRATION PROBING

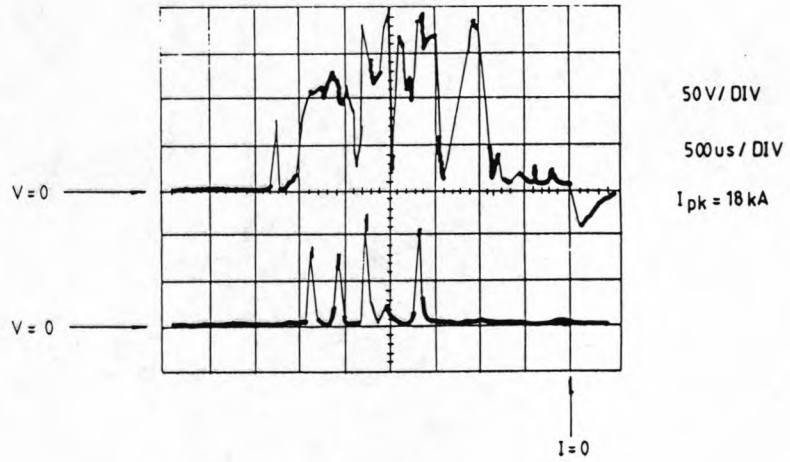

FIGURE 4·33. AXIAL PENETRATION PROBING

4.1.3 AERODYNAMIC EFFECTS

The transient pressure rise inside the test vessel was investigated for various peak currents and with a static pre-arcing pressure of 10 p.s.i gauge of sulphur hexaflouride (SF_6). Figure (4.34) shows a typical pressure transient within the test vessel for a 4.2 kA peak current arc and a 113 mT/kA 47° coil. Superimposed on a more gradual pressure rise are oscillations at frequencies of 1 kH_z and above, these are investigated in sections 4.1 3.3, 4.1 3.4. There is also an acoustic delay of about 1.75 ms between the beginning of arcing and the registering of a pressure rise due to the propagation of the pressure pulse through the sulphur hexaflouride medium.

The slightly negative change in pressure recorded during the first 1.8 ms of arcing (figure 4.34) is a pressure transient caused by the poker electrode moving from its fixed contact to its final resting position.

The average pressure rise increases to a maximum value which coincides with current zero. After arcing has ceased the pressure transient decreases and eventually disappears.

4.1.3.1 PRESSURE CHANGE AS A FUNCTION OF PEAK CURRENT

Several tests were performed at different peak current levels and for the 113 mT/kA; 47° coil, the averaged maximum pressure increase occuring at current zero, was noted (figure 4.35). An increase in the peak current causes a larger pressure transient. Over the peak current range investigated, 4.2 kA to 18 kA, the transient pressure rise varied linearly with peak current. The deviation from the average pressure rise caused by pressure oscillations also increases with the peak current (figure 4.35). The maximum average pressure increase observed was 0.34 of an atmosphere, approximately half the static pre-arcing pressure.

4.1.3.2 PRESSURE CHANGE WITH DIFFERENT MAGNETIC FIELD CHARACTERISTIC

The transient pressure rise during acring for a 35 mT/kA; 47° coil is similar to that shown by figure (4.36). The maximum averaged pressure rise occurs at current zero and there is the same linear dependence upon peak current. However, the change in pressure is generally smaller with the lower magnetic field producing coil.

The deviations from the average pressure rise generally show an increase in magnitude with increased peak current.

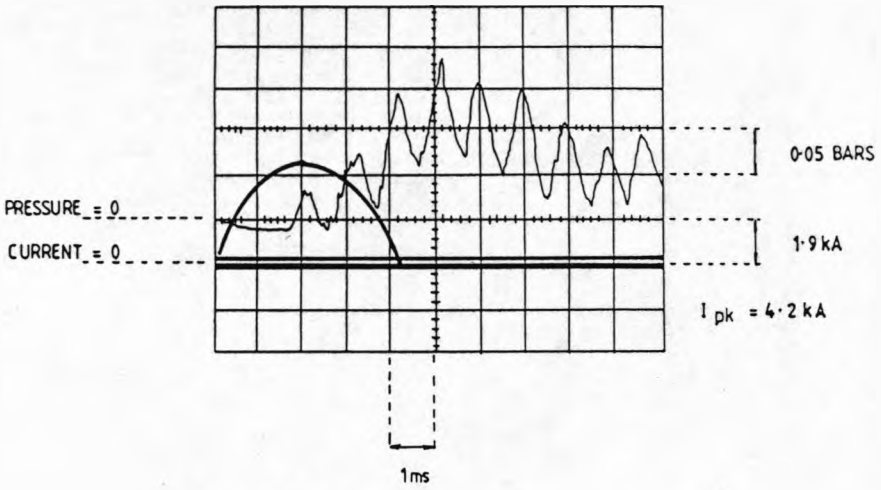

FIGURE 4·34. PRESSURE RISE DURING ARCING

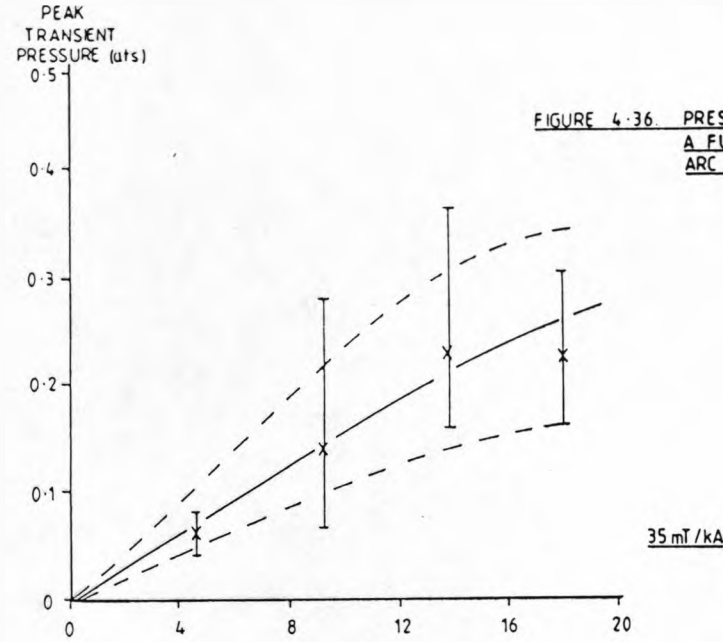

FIGURE 4·36. PRESSURE RISE AS A FUNCTION OF PEAK ARC CURRENT

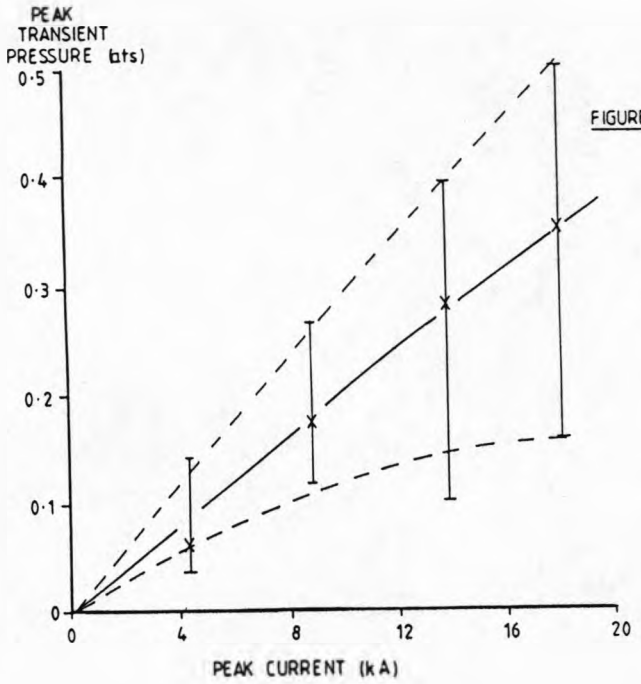

FIGURE 4·35. PRESSURE RISE AS A FUNCTION OF PEAK ARC CURRENT

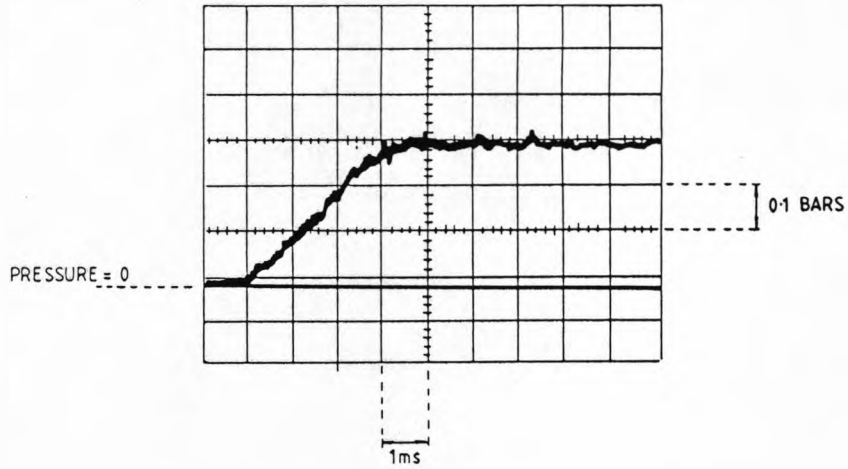

FIGURE 4·37. PRESSURE RISE DURING ARCING IN AIR

The maximum transient rise in pressure observed for this coil was 0.22 of an atmosphere which is approximately one third of the static pre-arcing pressure.

4.1.3.3 AERODYNAMIC INFLUENCE OF ENCLOSURE CHAMBER

Before investigating the aerodynamic effects of the enclosing chamber, the three main sources of noise namely electromagnetic, electrostatic and mechanical, were eliminated.

To determine conclusively that the oscillations observed earlier are a result of areodynamic factors, the SF_6 gas inside the breaker was replaced by air at a similar pressure. The overall pressure rise was 2.8 times greater than that for SF_6 and did not decay as rapidly (figure 4.37). There are oscillations superimposed upon this average rise whose frequency is higher than those for SF_6 and their amplitude only about one third.

To eliminate any influences exerted by the stainless steel interconnecting tube, the piezoelectric transducer was placed inside the chamber, now filled with SF_6. A similar pressure transient was observed as shown by figure (4.34).

This interconnecting tube had little effect upon the transient pressure rise. To investigate the transients further the lateral and longitudinal dimensions of the test chamber were reduced in turn. A lateral decrease caused the oscillations to increase in amplitude to 0.2 bars, the frequency remaining constant. A longitudinal reduction surpressed the oscillations at 1 kHz but promoted those of higher frequencies (figure 4.38). However the overall average pressure rise are similar in each case.

Thus the fact that the pressure oscillations are a characteristic of the enclosing chamber and the occupying medium, suggests that they are resonant in nature. Their peak to peak amplitude is of the same magnitude as the average pressure rise which in turn is only 32% of the static gauge pressure at maximum.

4.1.4 OPTICAL VIEW AT PEAK CURRENT

4.1.4.1 DYNAFAX HIGH SPEED PHOTOGRAPHY

A sequence of photographs showing two half cycles of arcing for a 8.7 kA peak current arc is presented on figure (4.39). Throughout one half cycle the arc diameter viewed in this plane generally increases toward peak current and decreases thereafter.

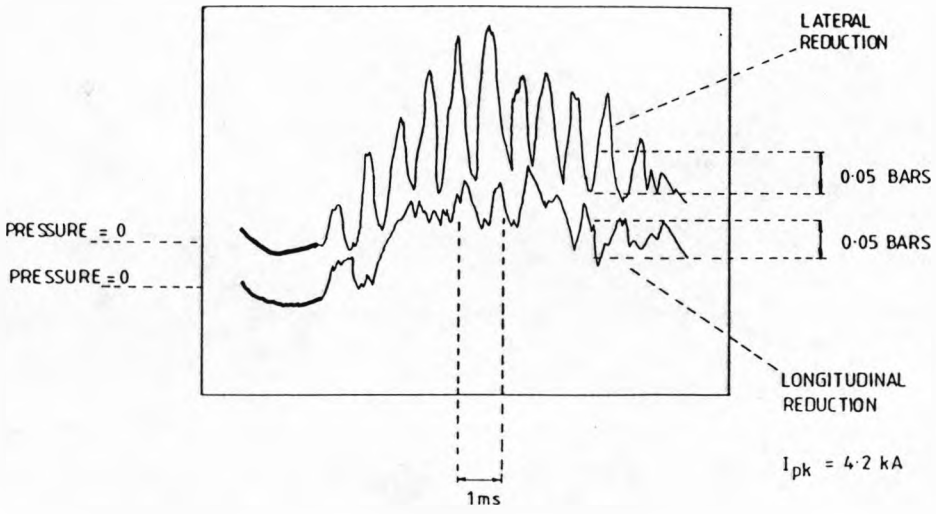

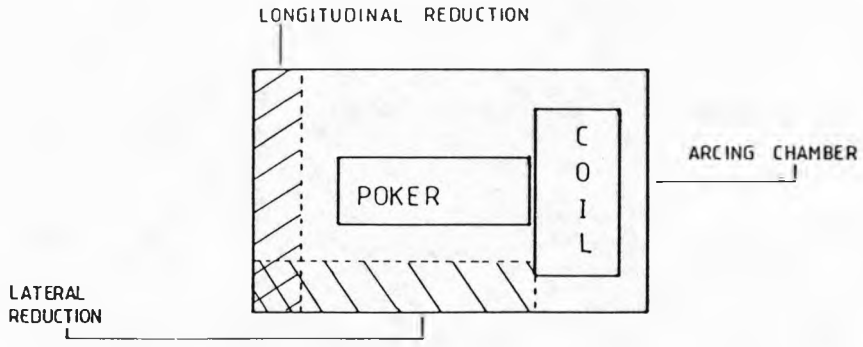

FIGURE 4·38. AERODYNAMIC RESONANCE

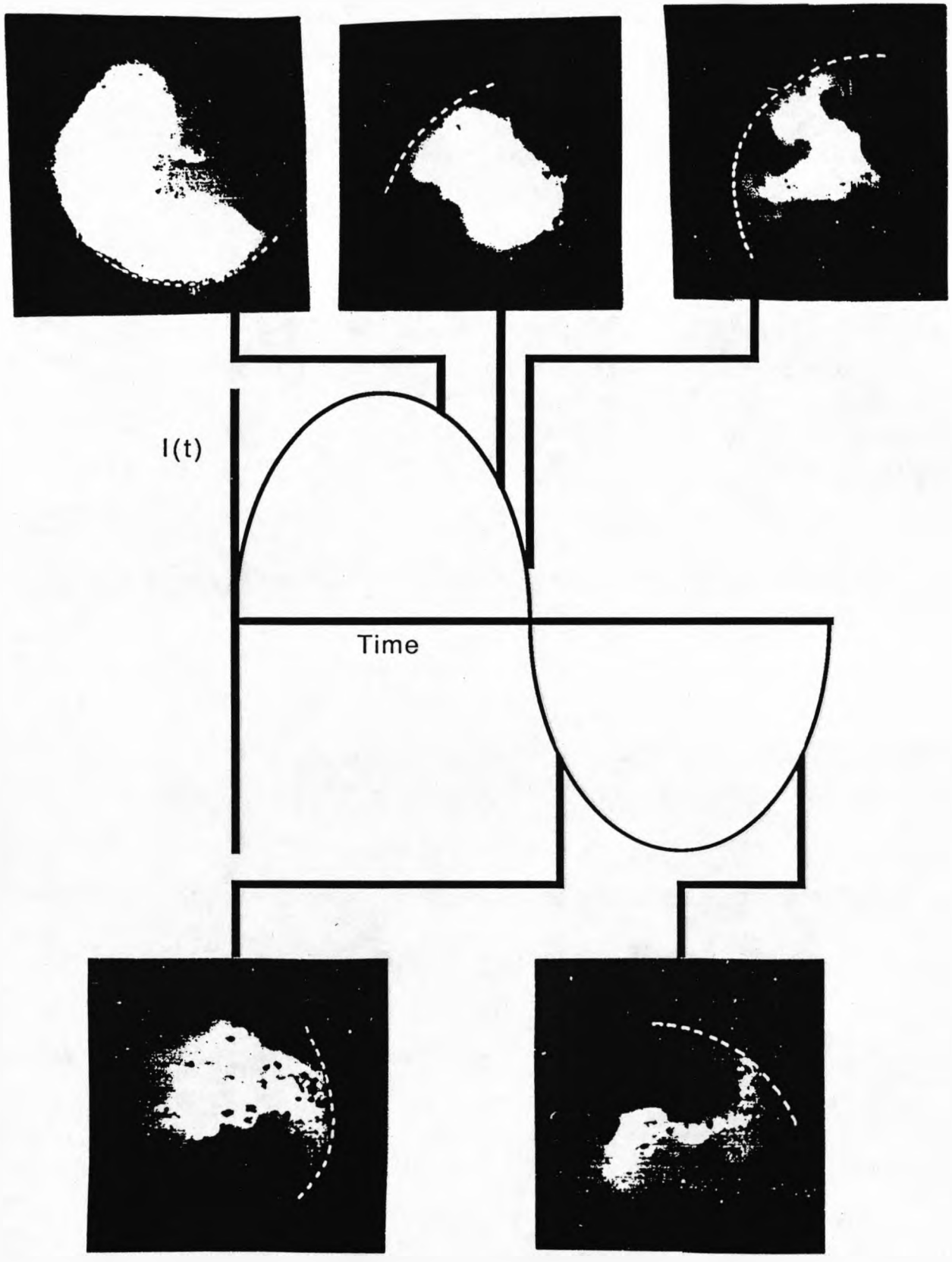

FIGURE 4.39. Arc Appearence

The arc does not move continuously but undergoes successive lengthening and shorting changes. During each lengthening process the arc plasma in the column moves predominently radial outwards to the cyclindrical electrode. Once the arc is in close proximity to this surface a new arc root is formed. The remaining length of the arc column between the new arcing site and the old one eventually decays. However the arc root attached to the centre electrode appears to be able to move with greater continuity. The arc motion is in the direction of the Lorentz's force.

A typical arc shape throughout the half cycle is that of an involute, the arc being bowed forward in the direction of travel. However occasionally the arc divides into two sections forming two different arc roots. This state did not persist and eventually one of the arc columns decayed.

The appearance of the arc column's boundary is of a rough and turbulent nature. Nevertheless, the arc column remains well defined.

A second half cycle of arcing is shown on figure (4.39). After current zero the arc begins to rotate in a direction opposite to that which occured during the first half cycle consistent with a reversal of the Lorentz driving force (figure 3.3).

A further reversal in rotation occurs later in the half cycle consistent with a delayed reversal of the principle axial magnetic field.

During both half cycles the time taken for each revolution within the coil, varies considerably. During the initial stages of arcing the arc movement is relatively slow and takes approximately 1.3 mS for one revolution but the second revolution occurs within only 0.5 mS. These values maybe used to give an apparent arc velocity and the manner in which velocity varies throughout both have cycles of arcing.

A similar arc appearance is recorded for various peak currents upto 18 kA. The arc column at these higher currents has a bigger diameter than those for lower arc currents. No significant change in the arc diameter could be observed for changes in either the magnetic field or phase difference angle for similar peak currents. Both the peak current, peak magnetic flux and phase difference affected the time taken for one arc revolution.

4.1.4.2 PHOTOMULTIPLIER/FIBRE OPTIC MONITORING

The number of arc rotations per half cycle has also been measured more directly using a photomultiplier viewing the arc space through an optical fibre.

Figures (4.40, 4.41) show typical results obtained with such a system from which the number of arc revolutions can be determined. For a 3.7 kA arc rotating in a 35 mT/KA, 47° magnetic field (figure 4.40), there are two revolutions during the first half cycle. The first occurs near to the peak current and the second starts approcimately 500 μs before current zero. There are other spikes at 1.1 ms, 2.8 ms and 3.1 ms which do not indicate a revolution but represent the arc's periphery wandering in and out of the field of view. Increasing the peak current to 18 kA for the same magnetic characteristic causes the arc column to rotate 10 times. The first revolution occurs within 1 ms after arcing has begun.

The distance between each successive peak and the width of each pulse is a measure of the arc velocity and the arc diameter respectively. For the low current case (figure 4.40) the arc is slow moving resulting in a long time to cross the viewing field (1.1 ms). For the high current arc this transit time at peak current is 0.2 ms even with a greater arc diameter.

Even at the higher current of 18 kA, the arc remains as a definite radial spoke as signified by the well defined peaks (figure 4.41). However the voltage zero time between each pulse diminishes towards peak current but later increasing as the current reduces to zero.

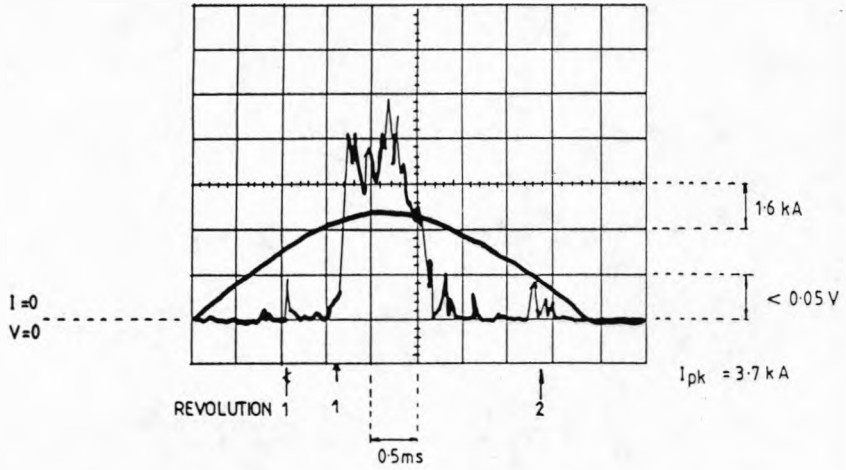

FIGURE 4·40. PHOTOMULTIPLIER/ FIBRE OPTIC MONITORING

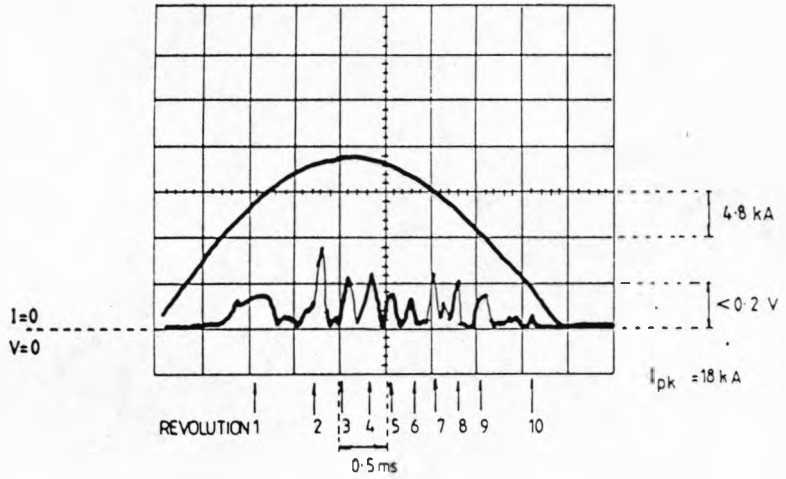

FIGURE 4·41. PHOTOMULTIPLIER/ FIBRE OPTIC MONITORING

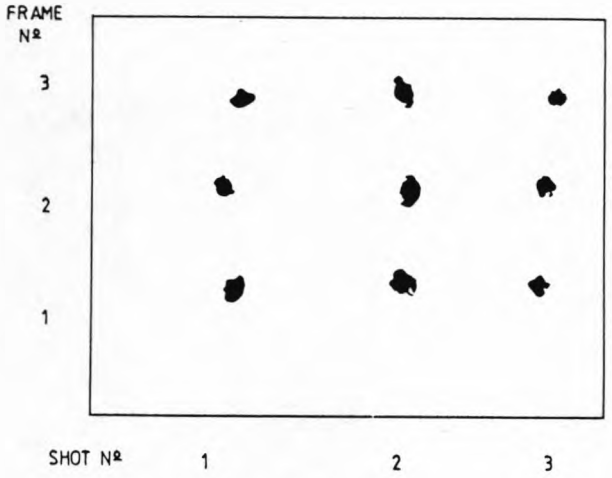

FIGURE 4·42. IMAGE CONVERTER IMAGE OF AN 18 kA PEAK CURRENT ARC

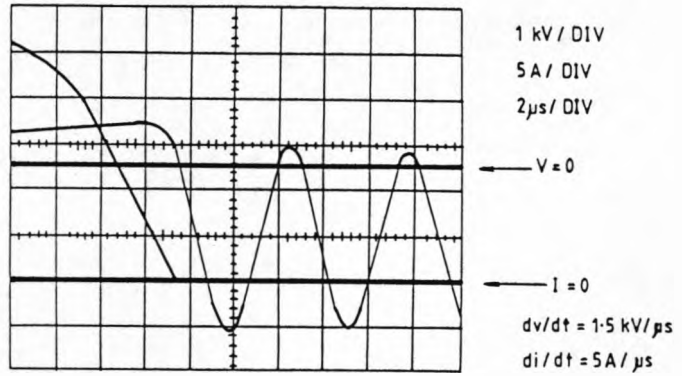

FIGURE 4·43. TYPICAL CURRENT ZERO RECORD

4.1.4.3 IMAGE CONVERTER PHOTOGRAPHY AT PEAK CURRENT

Conventional photography failed to resolve sufficiently the form of the arc column at high current levels on account of the exposure being long compared with the arc rotation rate. In an attempt to resolve this difficulty, short exposure photographs using an image convertor camera were taken for a peak current of 18 kA. These tests indicate that during this high current phase, the arc has a clear column form rather than a diffuse plasma occupying the whole cylindrical volume within the coil (figure 4.42).

The exposure times from the three frames of each of the three events was constant at 0.5 μs. For the first two events the frame separation is 110 μs for the first two frames and 115 μs for the second and third frames. The separation of frames for the third event is 22 μs.

4.2 CURRENT ZERO RESULTS

4.2.1 CURRENT ZERO ELECTRICAL BEHAVIOUR

A series of performance tests were performed on different coils which had various magnetic characteristics. The rate of change of current before current zero could be changed between 4A/ μs to 13A/ μs.

4.2.1.1 DETERMINATION OF di/dt AND dv/dt

Within the last few micro-seconds before current zero, the current decreases linearly to zero (figure 4.43). During the first part of this period, the arc voltage remains approximately constant at about 1 kV for this case (figure 4.43) before later, during the final micro-second, decaying to zero. The zero of both current and voltage arc coincident to within 0.2 μs.

The current zero di/dt is taken as the average value of the current ramp over the last three micro-seconds before current zero. This definition of di/dt is introduced in order to accommodate any destortion of the current range which may occur within one micro-second of current zero. Such a distortion is inherent because of the stray capacitance across the test breaker's terminal which becomes charged before current zero and discharges as the arc voltage collapses to zero (section 4.2.1.5). The projected current zero neglecting distortion and the actual current zero arc typically separated by 0.25 μs. The di/dt measured over the last 3 μs from figure (4.43) is 5A/ μs but measured over the last micro-second it is 2A/ μs clearly showing the degree of distortion.

The dv/dt is taken as the rate of change of arc voltage as it passes through zero.

The tangent to the voltage curve at v=o is 1.58 kV/ μs for the case shown on figure 4.43. This voltage transient is also affected by any stray capacitance across the test head terminals.

4.2.1.2 CLEARANCE OPERATION

Whether the arc reignites after current zero or extinguishes is determined by the relative rates at which the power input after current zero and the power dissipated during the same period change. Figure (4.44) shows a successfull clearance with no post arc current detectable. The arc current and voltage fall to zero and the natural restrike voltage applied after current zero rises to more than 2 kV in four micro-seconds. The previously ionised channel withstands this voltage. The sensitivity of the current measurement is such that a post arc current of at least 0.5 A could be detected. The di/dt, dv/dt are 6.8 A/ μs and 335 v/ μs respectively.

4.2.1.3 CLEARANCE WITH POST ARC CURRENT

If the input power and losses are nearly equal, the arc may briefly attempt to reignite after current zero before finally extinguishing. Such a behaviour is shown on figure (4.45). The di/dt and dv/dt are 5.6 A/μs and 525 V/ μs respectively. For approximately one micro-second after current zero there is no detactable

post arc current but after about two micro-seconds the amount of post arc current has slowly risen to ¼ A. The restrike voltage at this time is 1380 volts and the input power is 345 watts. Within the next 2.4 μs the arc current quickly increases to approximately 15 A and the total power input is then 23 kW. During the 2.4 μs the voltage reaches a peak within 1 μs and then decreases to 1530 volts at 2.4 μs. After this time the current decays to zero after 8 μs and the stressing voltage increases upto the capacitor bank voltage. The input power during this period decreases fairly quickly, falling to 9 kW, 7½ μs after current zero.

4.2.1.4 FAILURE OPERATION

If the input power exceeds the amount of dissipated power loss then the arc column reignites. Both figures (4.46, 4.47) show the current and voltage variations after current zero for failure conditions.

Figure (4.46) shows that for approcimately 1.4 μs after current zero there is no post arc current detectable. In the next 2 μs the current increases rapidly to 10A, and the power input has reached 14.7 kW. After a further 6 μs the current has increased to 18A and the power input is 25 kW. The arc current does not return to zero but increases, reflecting the fact that the arc has reignited. The di/dt before current zero is 4.3A/ μs and the initial dv/dt is 495 v/ μs.

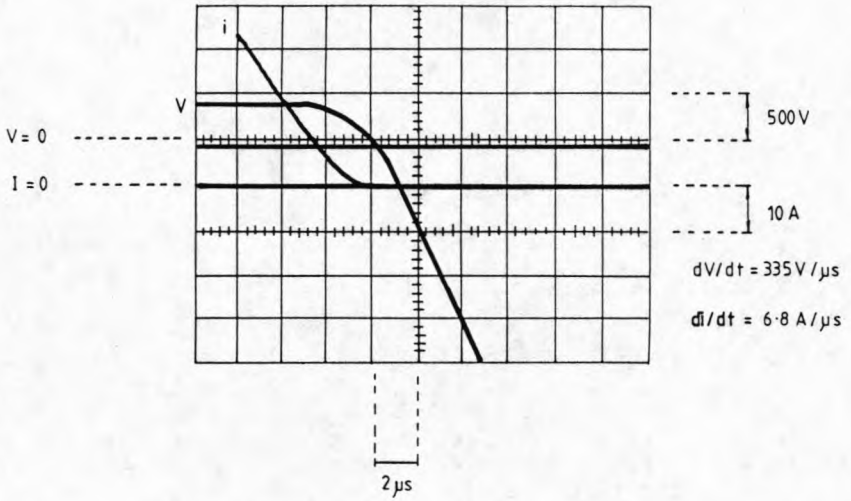

FIGURE 4·44. CLEARANCE OPERATION

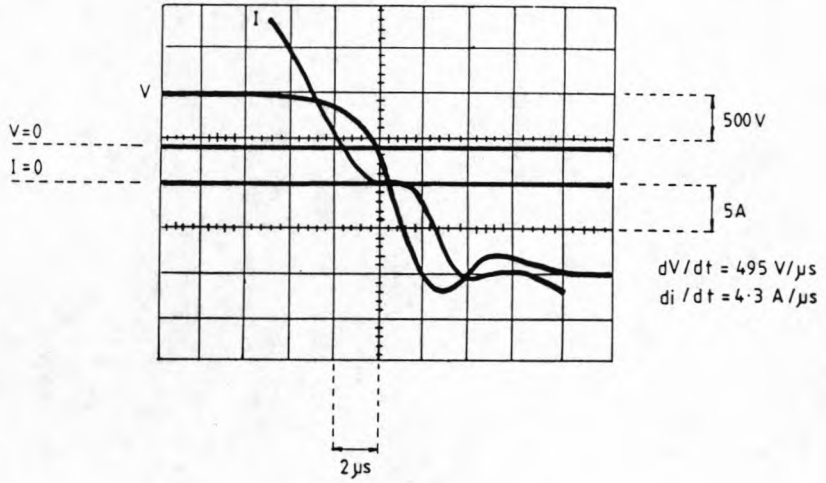

FIGURE 4·46. FAILURE

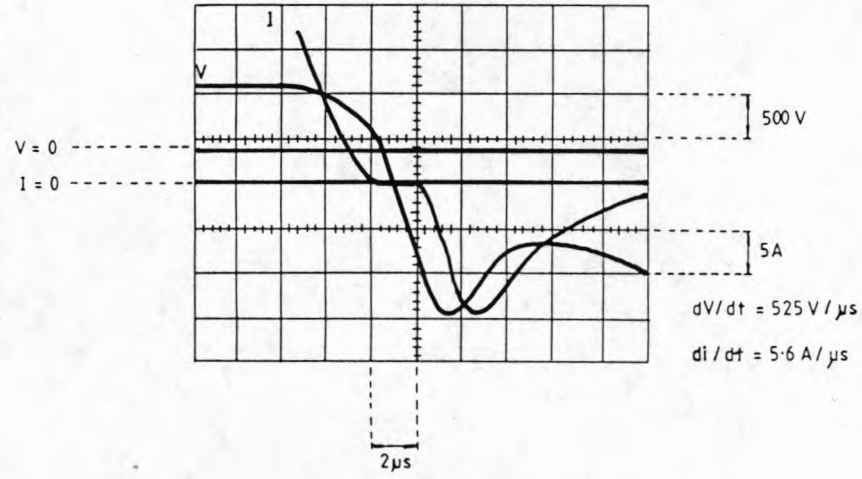

FIGURE 4·45. CLEARENCE WITH POST ARC CURRENT

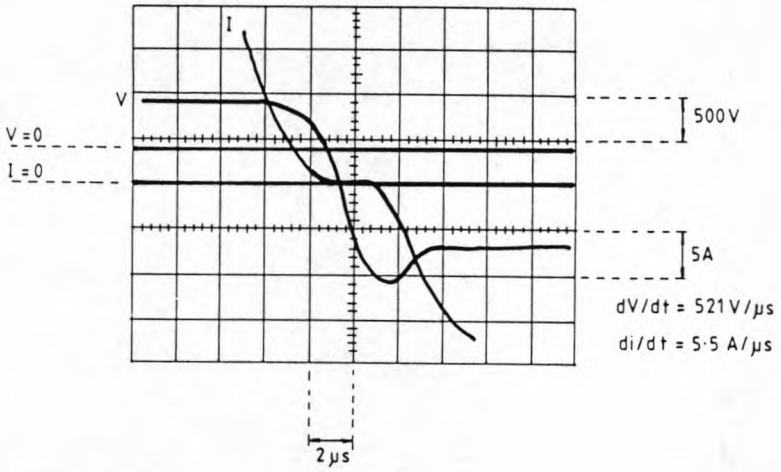

FIGURE 4·47. SEVERE FAILURE

Unlike the previous example of arc reignition where after current zero the current seems to hesitate for 4 μs before resuming its rise, figure (4.47) has no "current hesitation". After a delay of 1.4 μs, where no post arc current is detected, the arc current rises extremely rapidly, reaching 10A in 1.2 μs; the power input at this time is 15 kW. This is a severe failure. The di/dt and dv/dt are 5.5A/ μs and 521v/ μs respectively.

4.2.1.5 PARALLEL CAPACITANCE ACROSS THE TEST HEAD

To control the dv/dt following current zero without substantially changing the di/dt before current zero parallel capacitors were placed across the test head. To further reduce the rate of rise of voltage a 10~ resistor was placed in series with the capacitor.

The effect of this RC combination is two fold. The first reduces the dv/dt by controlling the discharge time of the inserted parallel network. The second causes distortion to the arc current during the last 1 μs before current zero. This distortion causes rounding of the previously linear current ramp, reducing the di/dt 1 μs before current zero. These effects are clearly shown by figure (4.48).

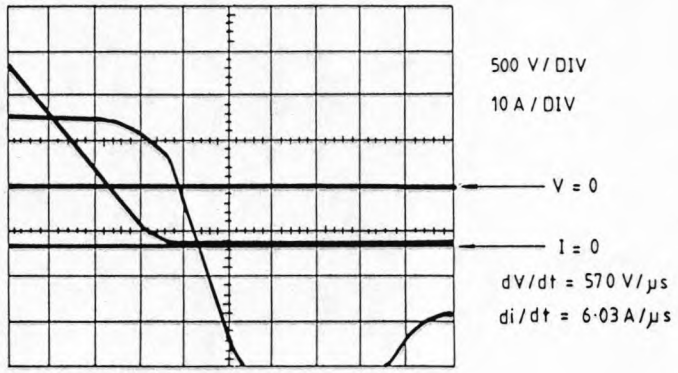

FIGURE 4·48. DISTORTION OF WAVEFORMS AT CURRENT ZERO BY PLACING PARALLEL CAPACITORS ACROSS THE TEST HEAD

4.2.1.6 THERMAL PERFORMANCE

The thermal performance for this circuit breaker was measured by studying the reignition at a series of di/dt values after one half cycle of arcing. If the circuit breaker withstood the imposed dv/dt after current zero then the dv/dt was increased until the critical performance boundary was determined. Oscillograms such as those in figures (4.44 - 4.47) were useful in determining the di/dt and dv/dt. A typical fail/clear performance graph is shown on figure (4.49). The magnetic characteristic of this coil is 55 mT/kA, 80° lag.

The failure operations are indicated by crosses and the clearences by circles. Generally when the arc reignites the dv/dt at current zero is lower than would otherwise be expected, that is the inherent dv/dt for the failure operation should be approximately 1.8 kV/ μs rather than the value of 670v/μs measured during reignition due to voltage regulation. Another problem associated with this type of performance testing is the statistical variation encountered. The critical performance boundary is defined by a series of experimental points at different di/dt's at which the dv/dt imposed after current is insufficient to cause reignition, but a slightly larger dv/dt will cause reignition.

The critical thermal performance boundary for this example given is shown on figure (4.49). The critical withstand voltage decreases with increasing di/dt.

Figure (4.50) compares the critical performance boundaries for a variety of field producing coils. Clearly performance improves with an increase in the magnitude of the field (compare B,C figure 4.50) also the gradient of the critical performance curve decreases as the magnetic field magnitude is lowered. A better performance is gained if the phase angle is 80° instead of 47° (compare D,E figure 4.50). All curves show a decrease in dv/dt for an increase in di/dt.

4.2.2. OPTICAL RESULTS

4.2.2.1. ARC APPEARENCE PRIOR TO CURRENT ZERO

The arc's appearence within the last 12 μs of current zero is complex and is variable from shot to shot. Two extreme examples are shown on figures (4.51I, 4.51II). These two arcs are photographed at the same point in time 7.2 μs prior to current zero and for identical di/dt and magnetic field conditions. The length of the arc column shown by figure (4.51I) is 18 cms measured in one plame and has a simuous appearence. The arc current of 21A is carried in some places by parallel arc channels. The luminous involuted spiral arc column

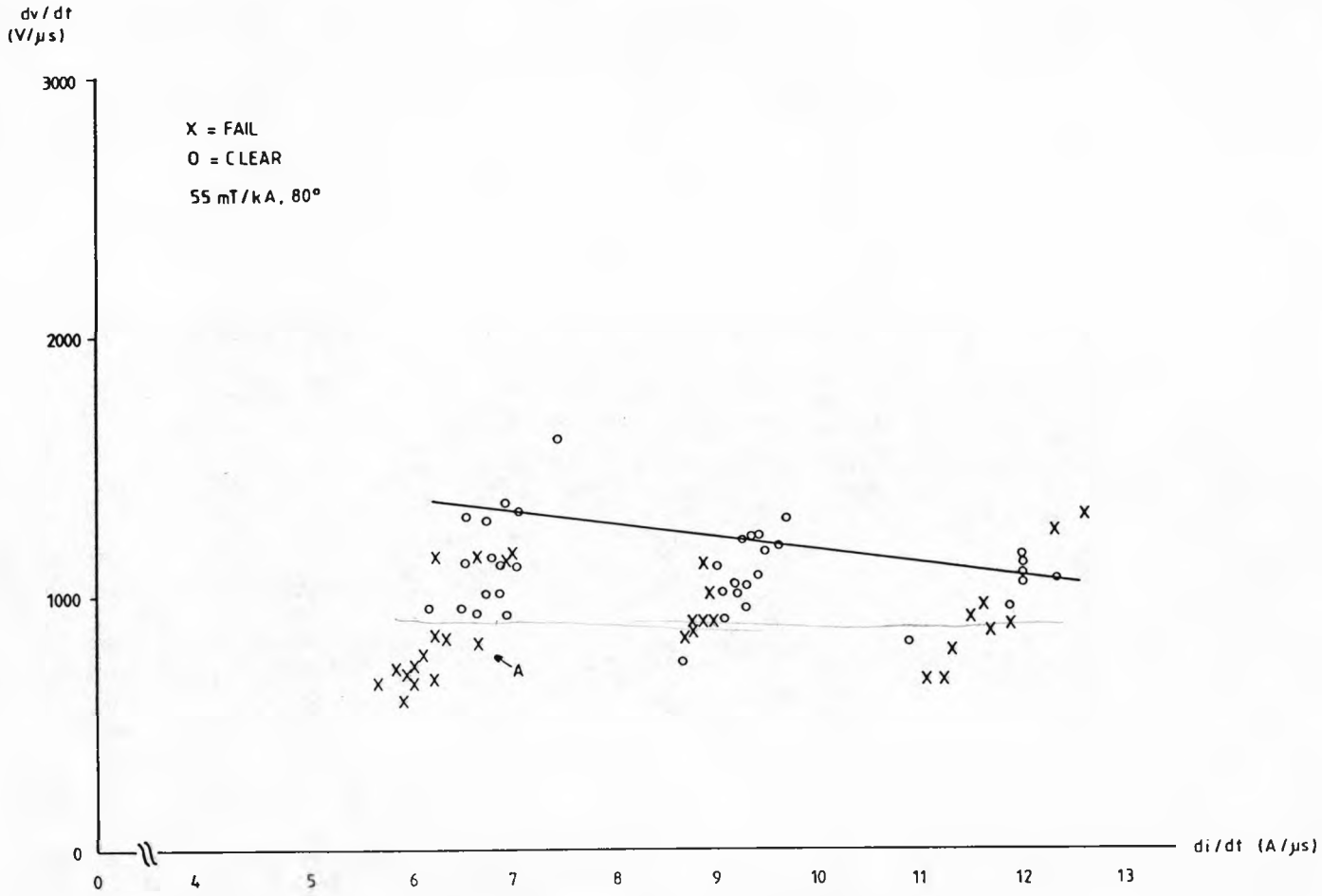

FIGURE 4·49. CRITICAL dv / dt , di / dt BOUNDARY

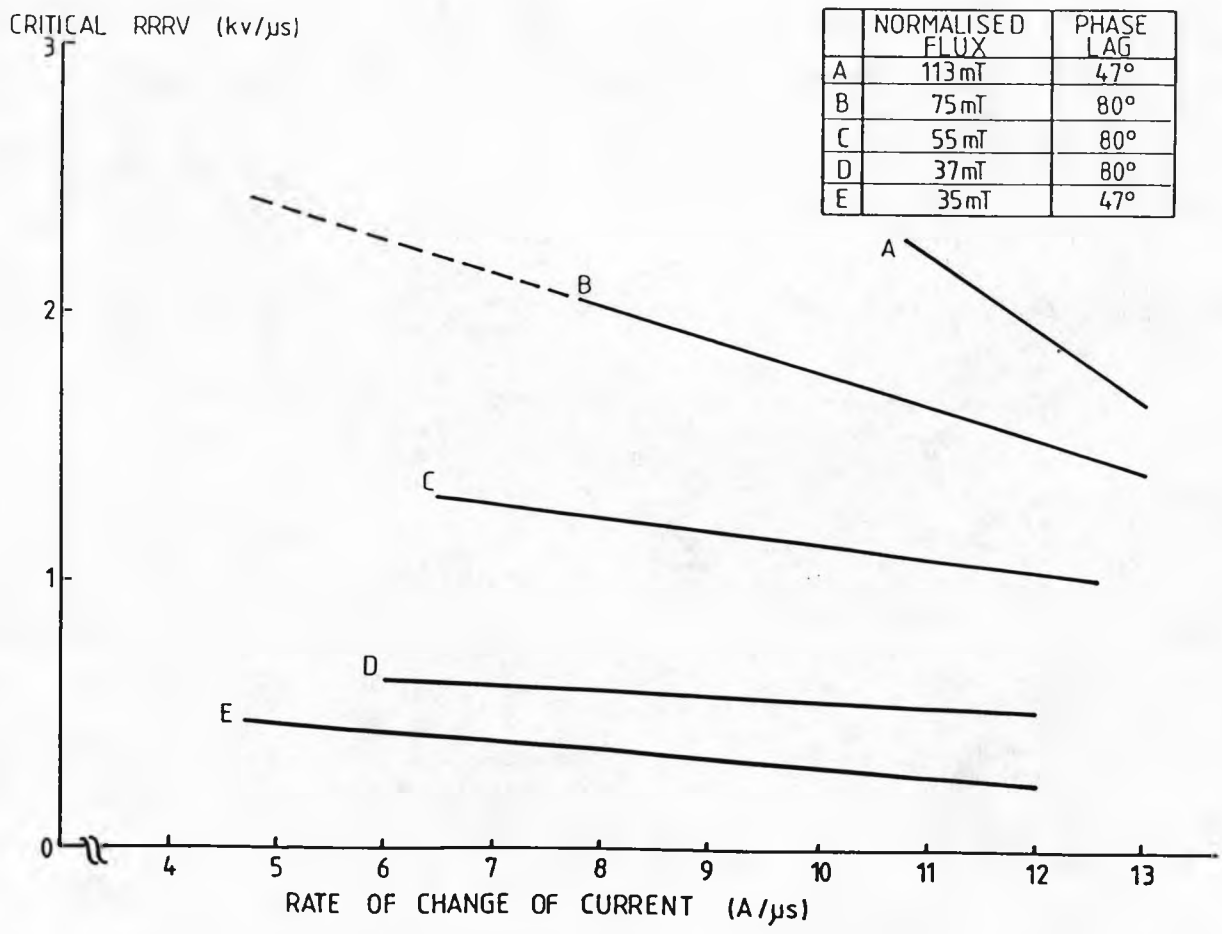

	NORMALISED FLUX	PHASE LAG
A	113 mT	47°
B	75 mT	80°
C	55 mT	80°
D	37 mT	80°
E	35 mT	47°

FIGURE 4·50. PERFORMANCE TRENDS

meanders a path from the centre electrode to the outer electrode the arc luminosity is very low and yet either side of this is a strongly luminous arc column and a bright arc root on the anode surface. On the next shot the arc is very differenct in appearence (figure 4.51II). Here the arc is relatively shorter in length, approximately 6 cms and the arc current of 21A is carried by a single arc channel. Again the arc channel varies in both luminosity and diameter. The arc is not spiralled as in the previous test but it is still an involute shape, bending in the direction of the Lorentz force.

A spectacular spiralled arc is shown by figure (4.51III). Although the peak current is nearly twice that for the previous two examples, the arc is similar in appearence. However the arc column has spiralled nearly 2½ times representing an arc length of 21 cms which is carrying 17A through a single arc channel, 3.4 μs prior to current zero.

4.2.2.2. DECAY OF ARC CHANNEL TOWARDS CURRENT ZERO

Three consecutive frames taken at 12, 8.6 and 5.3 μs before current zero are shown in figure (4.52). During this period the arc current decays from 35A to 15A. There is no detectable arc movement during this time but the arc column is rotating because the arc column

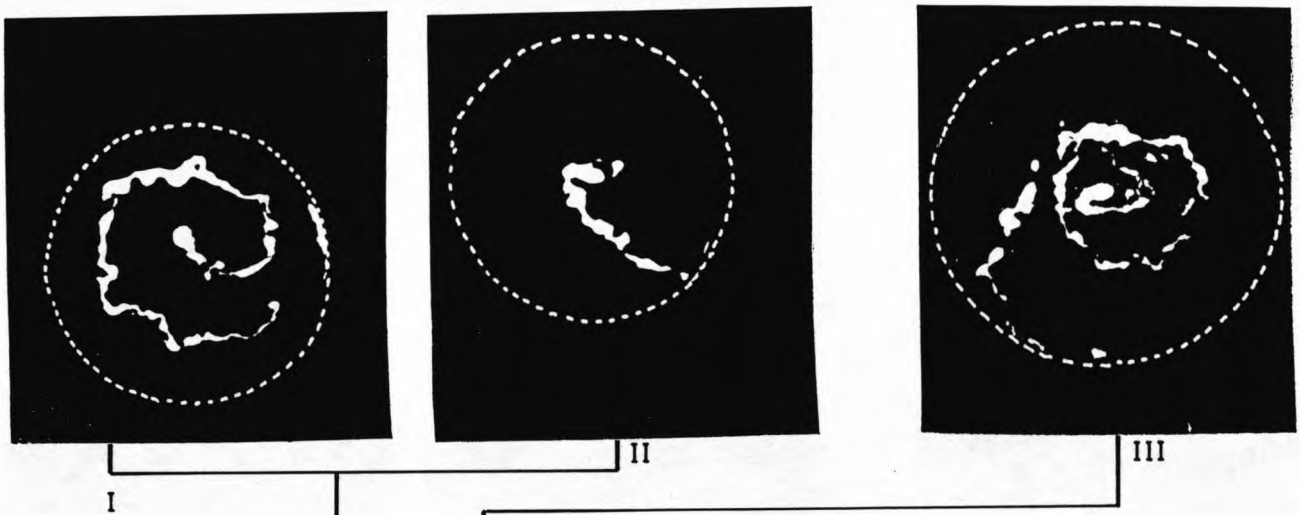

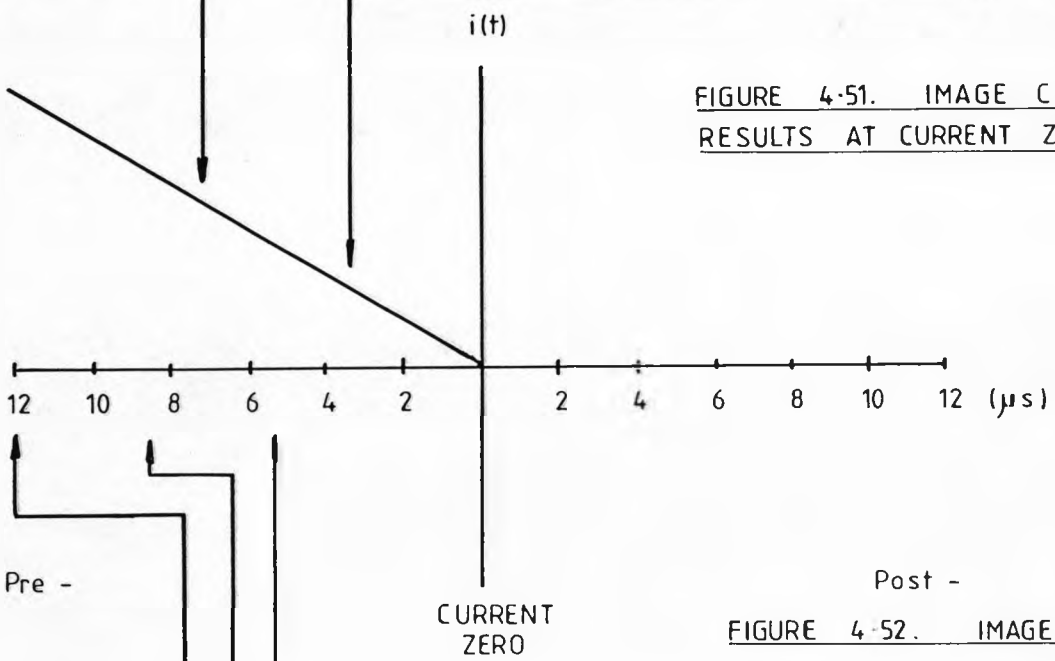

FIGURE 4-51. IMAGE CONVERTER RESULTS AT CURRENT ZERO

FIGURE 4-52. IMAGE CONVERTER RESULT

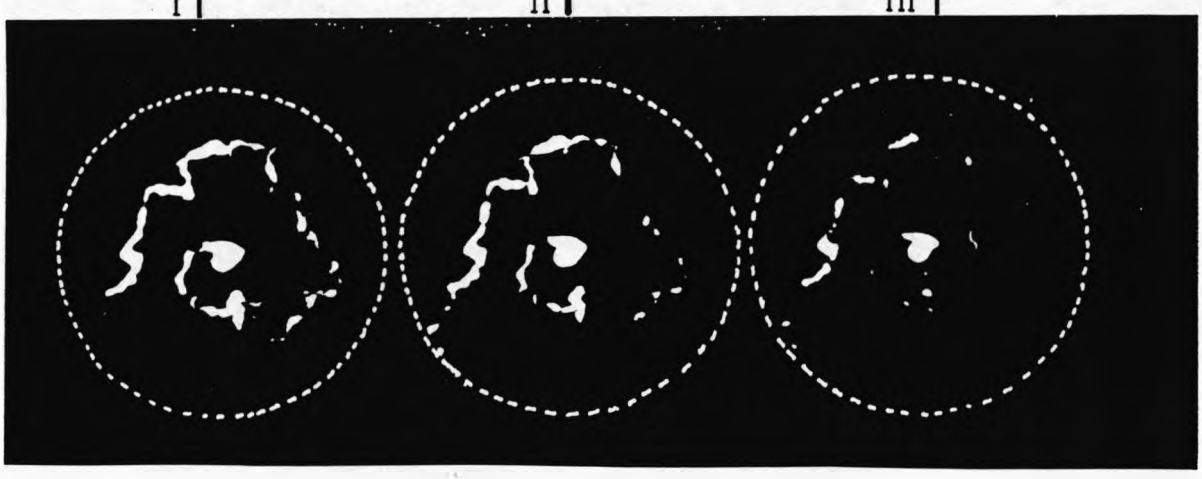

is an involute shape, spiralling just over one revolution.

The decay of the arc column is not uniform. Thinner parts of the arc channel lose their luminosity more rapidly than the wider parts of the arc column. The cathode spot on the poker electrode remains bright throughout each frame.

4.2.2.3. ARC REIGNITION

It is important to establish whether or not the arc will reignite along its old previously conducting channel or whether a new arcing channel is formed elsewhere. Figures (4.53, 4.54) shows arc reignitions for peak currents of 7.2 kA and 8.2 kA respectively. The arc column before current zero is as described above. It is clear that the second frame of figure (4.53) show that arc reignition occurs along the previously conducting arc channel, despite the considerable arc length. Arc reignition has occured within 3 μs of current zero and the arc's appearence is thin and sinuous. 6 μs later the arc still has a similar appearence but has grown in luminosity. However during the same time the more luminous areas prior to current zero still decrease in brilliance even though the arc column is conducting current again.

Another arc reignition process is shown on figure

(4.54). The arc column is shorter than for the previous example but reignition still takes place along the length of the arc column. However, reignition has not occurred within the first micro-second following current zero but it has definitely occurred within 9 μs after current zero.

In both of the previous figures there is no detectable arc movement in any direction. Since the arc current has commutated through zero the arc column experiences a reversal in the Lorentz force. The next section shows the arc column's response to this change.

4.2.2.4 REVERSED ARC ROTATION AFTER CURRENT ZERO (0-400 μS)

The arc column during the first 200 μs after current zero has become extremely twisted and it's shape is very complex. The series of frames showing 7.2 kA peak current are (figure 4.55) clearly demonstrates the complexity of the shape of the arc column during this period. The arc current is carried by a single channel. Approximately 300 μs after current zero the arc column is beginning to assume a more definite shape, rotating in the opposite direction to that recorded previously.

Figure (4.56) shows a further example where the arc column has completed its reversal and has a well

FIGURE 4·53. ARC REIGNITION

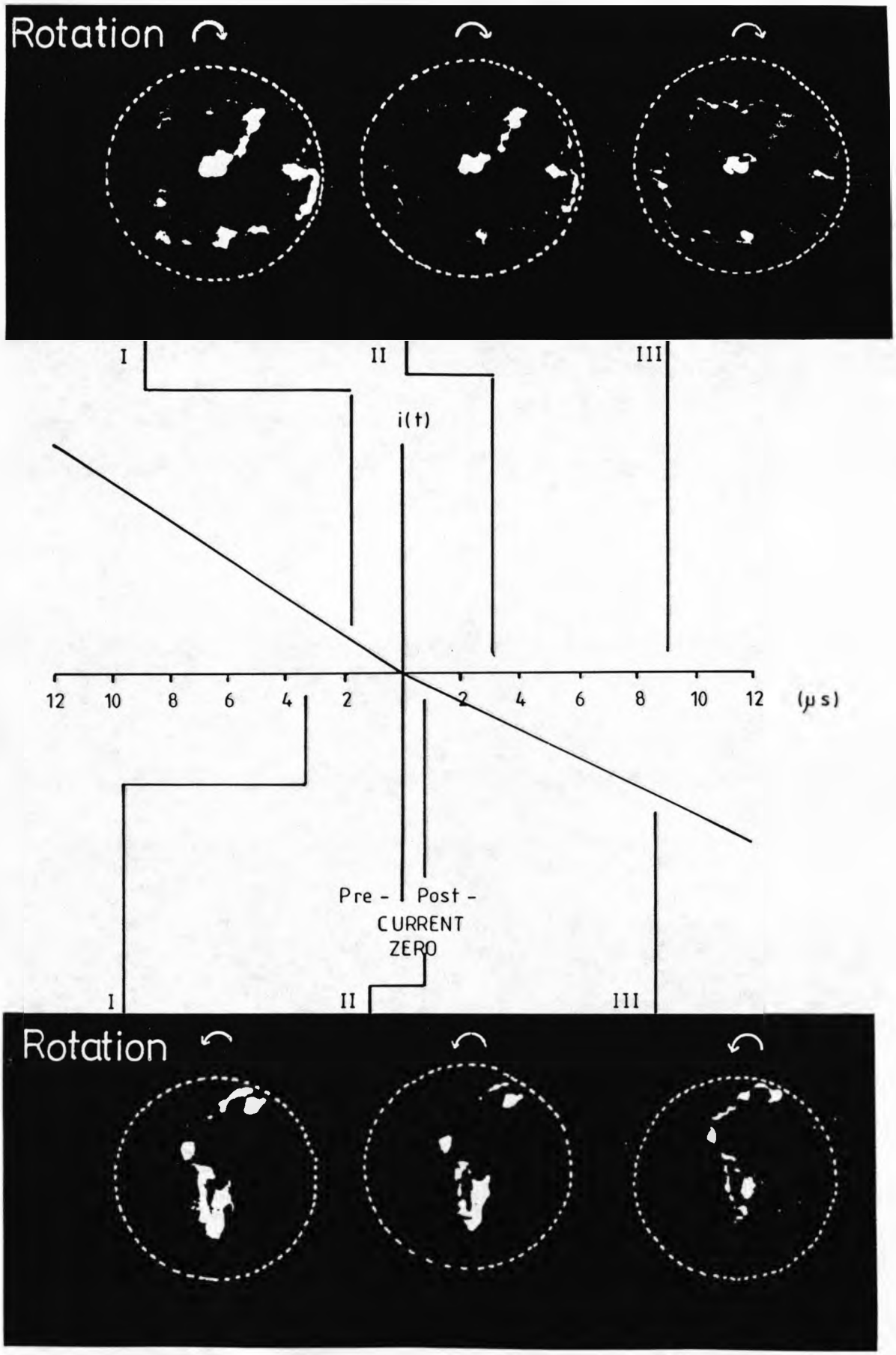

FIGURE 4·54. ARC REIGNITION

FIGURE 4·55. ARC REVERSAL

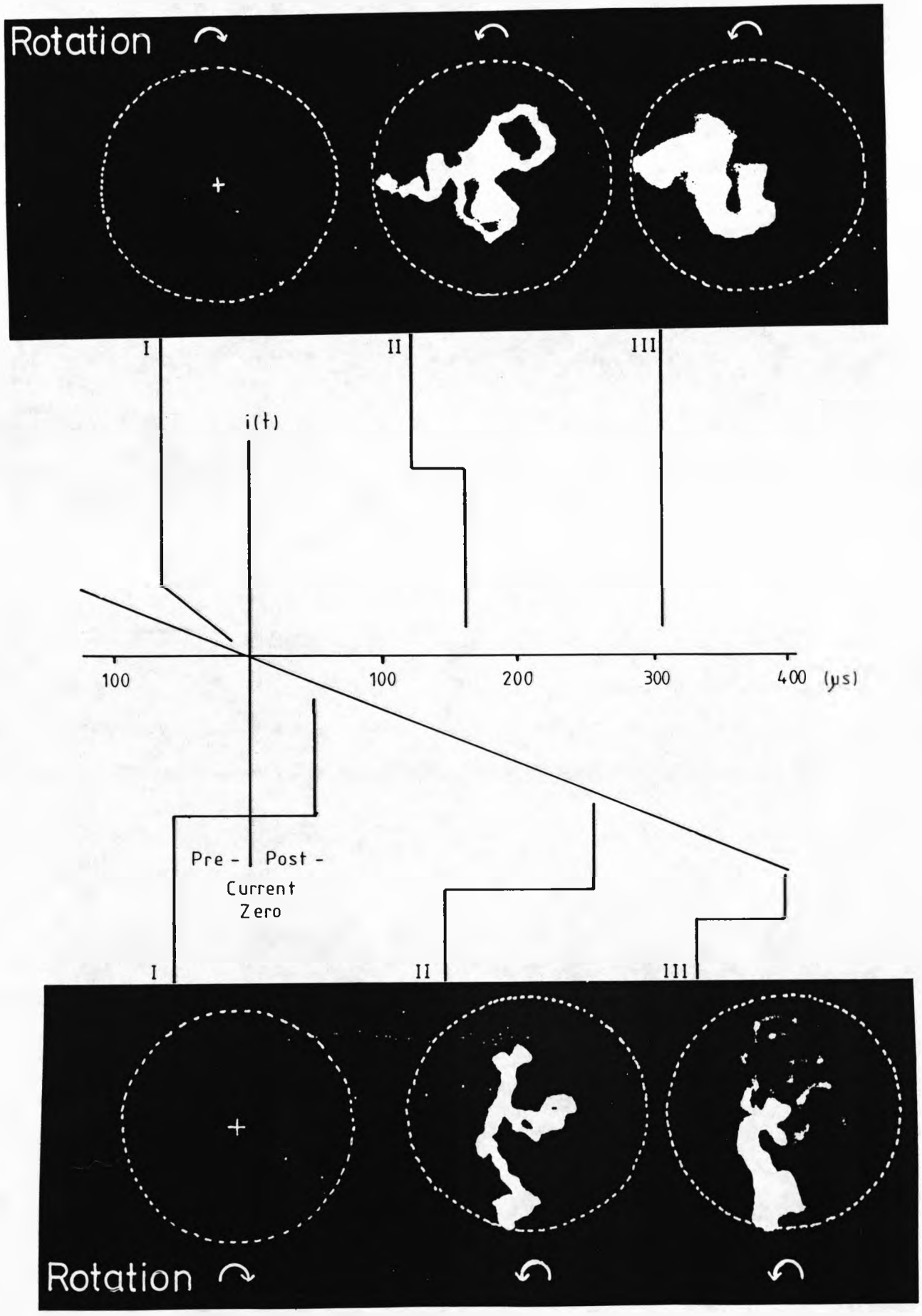

FIGURE 4·56. ARC REVERSAL

defined involute shape 400 μs after current commutation.

4.3. CONCLUSIONS

The magnetic field within the cyclindrical arcing volume can be resolved into two components, a radial and a dominant axial magnetic field. Both these fields are non-uniform within the arcing volume varying according to location. There is also an inherent phase lag between the exciting current and the transient magnetic field. The magnitude of the magnetic field is dependent upon the peak current, the number of primary turns with sufficient insulation and the copper core thickness. The phase lag angle is dependent upon the copper core thickness and whether adequate inter-turn insulation has been inserted.

The arc voltage during the peak current phase of arcing is not constant but shows rapid fluctuations during each half cycle of arcing. Localised voltage probing of the arc column showed that there were local disturbance within the arc plasma. The extent of axial penetration of the coil was established.

Over the peak current range investigated the pressure rise observed during arcing was small compared to the background pressure. However, this pressure rise was dependent upon both the peak current and magnetic

character of the arcing coil. Aerodynamic resonances occurred within the enclosing chamber.

Throughout one half cycle of arcing the arc column rotated in the direction determined by the Lorentz force and it's shape is that of an involute. The arc velocity varies throughout the arcing half cycle and is dependent upon both current and magnetic field. At the highest current investigated (18 kA) the arc, although very large in diameter, does not entirely fill the whole arcing volume.

The thermal performance curves for various magnetic conditions show degradation in performance, that is it's gradient differed according to the type of magnetic field conditions. A high magnetic field and a large phase difference increases the thermal performance of the circuit breaker.

Thermal reignition occurs along the previously conducting arc channel irrespective of the length of arc column. After reignition the appearence of the column is thin and sinuous. Once the arc current has reversed the Lorentz force acting upon the arc column also reverses and the arc column changes it's direction of motion within 400 μs of current zero.

5. DISCUSSION OF RESULTS

5.1. PEAK CURRENT PERIOD

During the peak current period the arc column is controlled by the magnetic field within the coil, the fault current, the phase difference angle, electrode effects and both the aerodynamic and thermodynamic properties of SF_6. To understand the complexities of this type of discharge under such conditions, it is necessary to evaluate each influence separately and determine the degree to which each factor controls the discharge.

5.1.1. MAGNETIC EFFECTS

Interaction between the arc current and the non-uniform magnetic field is difficult to ascertain unless both the arc current and magnetic field are considered separately.

5.1.1.1. AXIAL FIELD CONTROL

Interaction between the arc current and axial magnetic field is different when the arc column is an involute shape rather than a radial spoke. For an involute shaped arc column there are three component forces; an azimuthal or tangental force (F_θ) resulting from the interaction between radial current flow (i_r) an axial field (B_z) figure (5.1); an axial force (F_Z) produced

by the interaction between the azimuthal current flow (i_θ) and radial magnetic flux (B_R); and finally the third component is a radial force (F_R) produced by the interaction of an azimuthal current flow (i_θ) and an axial field (B_Z). If the arc column is a radial spoke then there would only be one component force, F_θ.

The axial magnetic field interaction with the arc current produces a Lorentz force per unit length of arc column which can be resolved into two components, azimuthal and radial. It is interesting to observe the change in this force acting upon an involute arc column along it's length. Near the inner rod elecrode where the arc current flows in a radial direction (76) there is only an azimuthal force. However, near to the surface of the cylindrical electrode this force is radial. Midway between these two positions the net force ($\underline{F}_C$) is a vector summation of two components ($\underline{F}_\theta + \underline{F}_R$). Thus an element of plasma is forced away from the centre electrode and onto the cylindrical copper electrode by F_C.

The non-uniformity of the axial magnetic field when interacting with the arc current causes a similar non-uniformity in the Lorentz force. The radial increase in B_Z is approximately 50% (section 4.1.1.2) from the coil axis to it's surface and this is reflected in the Lorentz force which also increases radially.

Consequently and element of plasma moving from the poker electrode to the outer electrode will be accelerated radially. From the end of the coil to the mid axial position, B_Z doubles. When arc penetration occurs there is a corresponding increase in the Lorentz force causing the arc column to accelerate. Too much penetration beyond the mid position where the axial field is smaller, causes deceleration, retarding the arc column.

The force governing movement of the arc column in a magnetic field is:

$$d\underline{F} = (\underline{I} \times \underline{B}).dl \qquad (5.1)$$

However, the movement of the arc column into the coil volume is not only governed by the interaction of the involute arc column with B_Z but also by the axial inclination of the arc to the field resulting in the force on an element of arc being,

$$dF_c = \left[(\underline{i}_r \times \underline{B}_z) + (\underline{i}_\theta \times \underline{B}_z)\right] dl \qquad (5.2)$$

Both the axial field and arc current are functions of time. The resulting change in the Lorentz force for any arbitary element of arc plasma is shown on figure (5.3) provided that the angle of inclination between the arc current and axial field remains the same throughout the half cycle. During this period the Lorentz force increases sinusoidally to a maximum at a

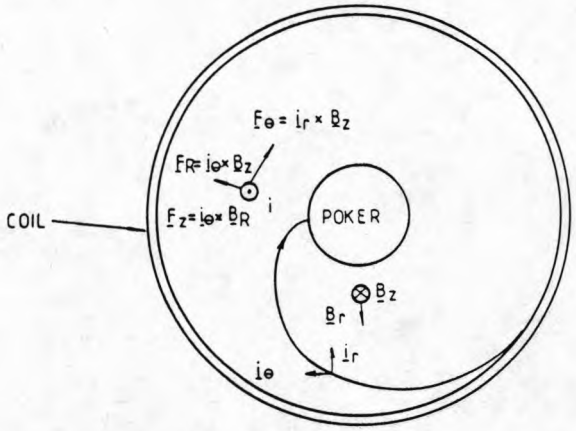

FIGURE 5·1. COMPONENTS OF LORENTZ FORCE ACTING ON AN INVOLUTE ARC.

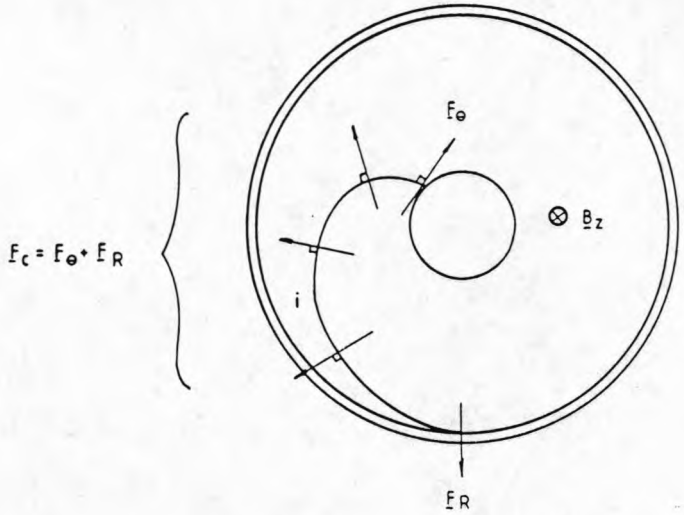

FIGURE 5·2. ELEMENTAL FORCE

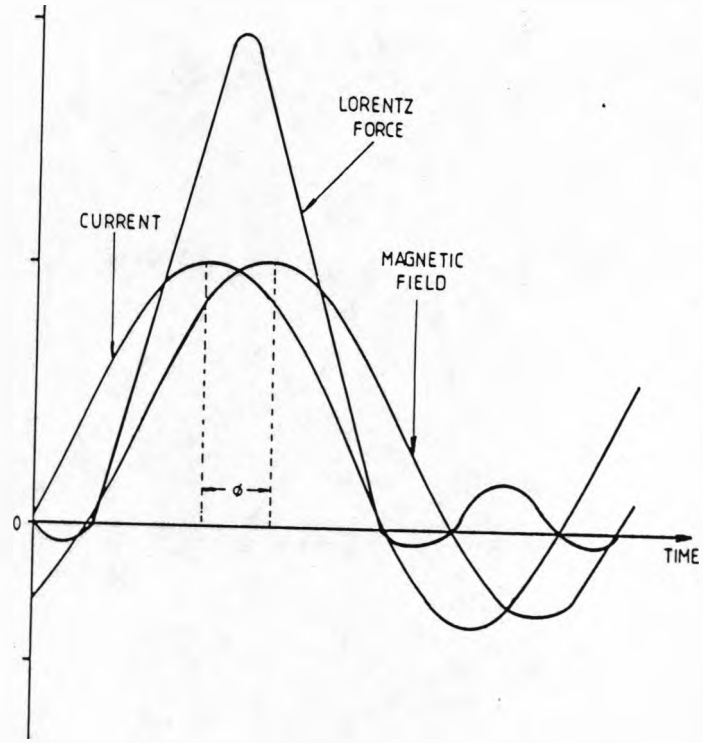

FIGURE 5·3. TIME VARIATION OF LORENTZ FORCE

time midway between the peaks of the arc current and the magnetic flux. After this peak it then decreases to zero at current zero. This implies that during arcing the arc plasma will be subjected first to an increasing Lorentz force followed by a decreasing Lorentz force so causing acceleration and deceleration respectively of the arc plasma element. The magnitude of this force is controlled by three factors, the arc current, the magnetic field and the phase difference angle ϕ. The latter will be discussed in section (5.1.1.3). An increase in either peak current or peak magnetic field would cause a proportional increase in the Lorentz force during the whole arcing period. Reversing the current flow or the magnetic field cause the Lorentz force to reverse. If both current and field change direction then the net effect upon the arc column is uncanged. Figure (5.3) show these changes in the Lorentz force as a function of time. The duration of the negative Lorentz force is controlled by the phase difference angle and it's magnitude by the instantaneous value of current and field. Also shown is a general overall reduction in the peak magnitude of the Lorentz force from half cycle to half cycle because of the transient decay in both the arc current and magnetic field which occurs during the capacitor bank discharge used in the present experiment.

5.1.1.2. RADIAL FIELD CONTROL

The interaction between the radial magnetic field and the arc current produces an axial force (figure 5.1). This force is directed into the cylindrical volume enclosed by the coil. Even if the arc column penetrates to the other end of the coil the radial field interaction with the arc current would produce an axial force which again has a direction into the coil. This apparent reversal in direction from one end of the coil to the other is caused by the change in the direction of radial flux component over that length. At the mid axial point along the length of the coil the radial component is zero and therefore is the axial force.

The arc column under the influence of this axial force only is therefore directed into the mid way point of the cylindrical electrode and would remain there in a magnetic trap. In practise this does not happen because of other magnetic effects which are considered later.

The radial variation of this axial Lorentz force is similar to the variation of B_R. It is a maximum near to the surface of the cylindrical electrode and zero on the axis. This radial variation only changes the magnitude of the force and not it's direction because

B_R and I maintain their respective orientations. The greatest axial force exserted upon the arc column will be at the end of the coil, near the surface of the cylindrical electrode.

It is interesting to note that when the arc penetrates into the coil there is an axial components of current. This component interacts with the radial field producing an azimuthal Lorentz force which is in opposition to the main azimuthal force ($\underline{i}_r \times \underline{B}_Z$). This retarding force is a maximum where the main force is a minimum, near to the surface of the cylindrical contact. The net force here may be in the reverse direction but it's effect would be masked by the electrode effects. Closer to the axis of the coil the influence of this force deminishes whilst ($\underline{i}_r \times \underline{B}_Z$) increases.

As well as a spatial variation in B_R there is also a time dependent change similar to that for the axial field. The Lorentz forces $(\underline{i}_\theta \times \underline{B}_R)$ and $(\underline{i}_z \times \underline{B}_R)$ will vary with time causing maximum axial penetration and azimuthal retardation respectively at a point in time midway between the peak of the current and radial flux.

5.1.1.3. CHANGE IN LORENTZ FORCE WITH THE PHASE DIFFERENCE ANGLE (Φ)

The time at which the Lorentz force is a maximum is

controlled by the phase difference angle. One inherent disadvantage of increasing ϕ is that there is an accompanying decrease in ($\underline{i} \times \underline{B}$) (figure 5.4) although I_{pk} and B_{pk} remain the same. In practise there is an additional effect which caused a further decrease in B as ϕ is increased. This is associated with the methods of producing the phase delay which are by making the coil yoke thicker (figure 4.23) or increasing the electrical conductivity of the yoke (85). However such changes also produce a reduction in the field strength because of increased shielding effects. The Lorentz force is therefore reduced by two effects, i.e. increasing ϕ and increased shielding.

The time at which the Lorentz force reaches a maximum moves closer to current zero as ϕ is increased. Correspondingly the arc velocity also reaches a maximum at a similar instant as will the forced convection losses. An advantage of a large ϕ is that the magnetic field at current zero remains high (figure 5.4) and hence the rate of change of Lorentz force during the current zero period is constant for large phase angles close to 90°.

The magnitude of ($i \times B$) is greater than for similar conditions of small ϕ's. The implication of this greater Lorentz force during the current zero period is that the velocity of the arc column will be maintained

more than for small values of ϕ.

5.1.1.4 DISTORTION OF MAGNETIC FIELD DUE TO CURRENT FLOW THROUGH THE POKER AND TEMPORARY MAKING STRAP.

To measure this magnetic field inside the coil without an arc present a temporary shorting is used is discussed in the previous chapter. The magnitude of the magnetic field generated by current flowing through the poker electrode and temporary making strap can be calculated using the volume integral of the Biot-Savart law (See Appendix 1, equation A1). These resulting fields are perpendicular to each other. Current flowing through the poker electrode gives rise to an azimuthal field which is a maximum at the surface of this electrode (9.8 mT/kA) but quickly diminishes both axially and radially to less than 0.6 mT/kA at a 6 cms axial position and 2.5 mT/kA at 3.5 cms radial position (figure 5.5).

Current flowing through the temporary copper strap gives rise to a field which would change both the axial and radial field components produced by the coil system but it's affect will vary from location to location. The location greatly affected is near to the copper strap. This field quickly diminishes to less than 4 mT/kA at the mid-axial position (figure 5.6).

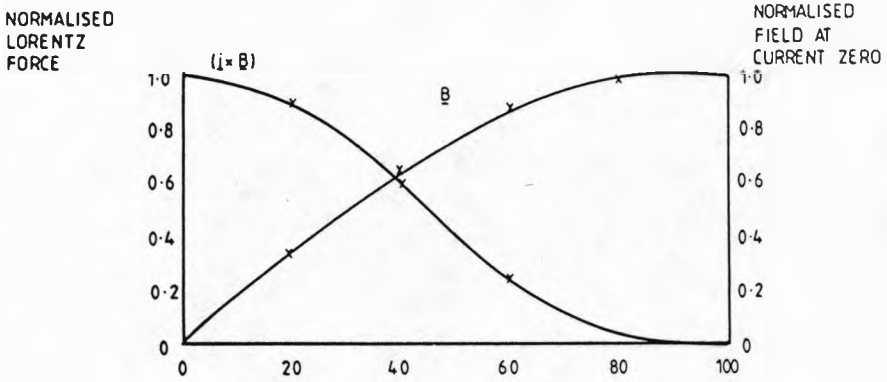

FIGURE 5·4. NORMALISED LORENTZ FORCE

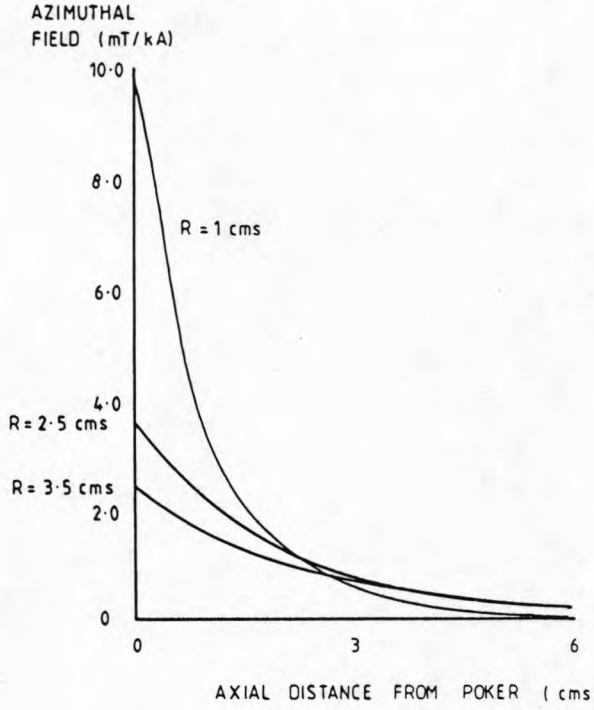

FIGURE 5·5. VARIATION OF AZIMUTHAL FIELD

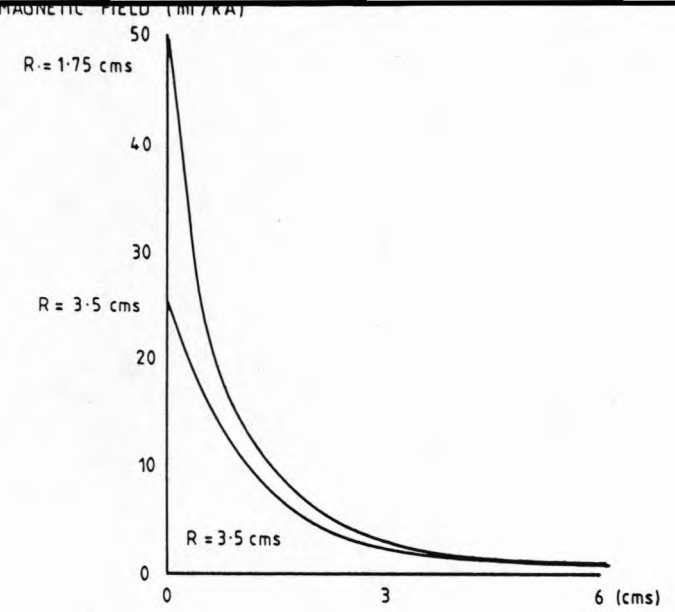

FIGURE 5·6. FIELD GENERATED BY MAKING CONTACT

Both the additional fields add vectorially with the main field causing distortion of the axial and severe distortion of the radial fields. The greatest distortion occurs where these fields are largest at the poker end of the coil but rapidly diminish over a short distance.

5.1.1.5 MAGNETIC INSTABILITITES

Arcs in magnetic fields are inherently unstable and for the present investigation the imposed magnetic field is relatively large. Schrade (77) investigated the stability of an arbitrary shaped arc with finite cross-sectional area whose dimensions are known. In section (2.4.6) his governing equation of stability is quoted in equation (2.4.4) as

$$1 + \beta - 2\lambda^2 - 2\cos^2\alpha \quad \begin{cases} > & \text{Stable} \\ = 0 & \text{indifferent} \\ < & \text{unstable} \end{cases} \qquad (5.3)$$

There are simplifications introduced into Schrade's analysis but it is applicable for any arbitrary shaped arc column with a known finite arc radius. If the arc radius is known then this eliminates the need for any energy considerations avoiding a knowledge of complex energy dissipation mechanisms and local temperature profiles. Consequently only the momentum transport from the current carrying arc column to the

non-conducting gas needs to be considered which leads to the stability criterion (equation 2.4.4).

A disturbance in the arc column will either grow or decay, so constitutuing unstable or stable behaviour respectively. The direction of most likely instability is axially into or out of the coil volume, however because the arc column is already inclined into the coil by the action of the radial field the instabilities promoting further the growth of penetration beyond the mid coil point (despite the reversed radial field in this region).

Further development of Schrade's analysis is essential before determining the stability boundary for the present set of arcing conditions.

In equation (5.3) β is the ratio of the average static pressure to magnetic pressure,

$$\beta = \frac{P}{B^2/2\mu} \qquad (5.4)$$

Where; P = average static pressure (N/m^2)

B = external magnetic field (T)

μ = permeability (H/m)

λ (equation 5.3) is the ratio of average self-magnetic field to the applied magnetic field,

$$\lambda = \frac{\mu I}{2\pi RB} \qquad (5.5)$$

Where, I = arc current (A)

R = arc radius (m)

Equation (2.4.4) is modified after sustitution of equations (5.4) and (5.5),

$$1 + \frac{P}{B^2/2\mu} - 2\left[\frac{\mu I}{2\pi RB}\right]^2 - 2\cos^2\alpha \begin{cases} > \\ = \\ < \end{cases} \begin{matrix} \text{Stable} \\ 0 \text{ indifferent} \\ \text{unstable} \end{matrix} \qquad (5.6)$$

Throughout the half cycle of arcing the arc radius varies in approximate sympathy with the current. Thus the current density can be assumed constant during the major part of the half cycle excluding the current zero period (figure 5.7) and also as the peak current increases. Introducing current density into equation (5.6) an expression for the critical stable magnetic field is obtained as a function of current density, arc current, static pressure and the azimuthal angle (α) between the applied field and the radius of curvature vector of the local disturbance. If this latter angle is 0 or π then

$$B^2 = 2\mu P - \frac{\mu^2 J I}{2\pi} \qquad (5.7)$$

Where B is the critical magnetic field boundary as a function of the other parameters. The critical stability boundaries for two static pressures (0 psi and 10 psi guage) arc shown on figure (5.8i).

For currents less than 100kA, arc instabilities are

dominated by the external magnetic field rather than self magnetic effects. The magnitude of this external magnetic field varies depending upon the background static pressure but for 0psi pressure a magnetic field greater than 500 mT would cause arc column instability, for a larger static pressure of 10 psi this critical magnetic field is 700 mT. For arc currents in excess of about 100 kA self magnetic effects may cause instabilities. The exact shape of the boundary is controlled by three factors, the static pressure, arc current density and arc current. To some extent the current density is not independent of the background pressure as an increase in pressure would cause a greater constriction of the arc column so increasing the current density. The stability theory as derived by schrade (77) appears to be only rigourously applicable to quasi stationary arc columns but it seems reasonable to assume that it should apply during the major part of the arcing half cycle. The steady state restriction maybe traced back to the non-time dependent form of the momentum equation.

$$RC_D\rho_\infty U_\infty^2 \left[\frac{\underline{U}_\infty}{U_\infty}\right] = \underline{I} \times \underline{B} \qquad (5.8)$$

C_D = drag coefficient

R = arc radius

ρ_∞ = density of imposed flow

U = incoming flow velocity

If the arc column moves in the Lorentzian direction because the drag force is insufficient to maintain equality then a further term should be added to equation (5.8) which is a rate of change of momentum per unit length thereby transforming equation (5.8) into the form,

$$\frac{\delta}{\delta t}\left[M U_\infty \left(\frac{\underline{U}_\infty}{U_\infty}\right)\right] = \underline{I} \times \underline{B} - R C_D \rho_\infty U_\infty^2 \left(\frac{\underline{U}_\infty}{U_\infty}\right) \qquad (5.9)$$

Where M *= mass of the plasma forming the arc column*

Schrade's definition of this extra term is given in his papers (77,86) as δM *where* M *is the momentum per unit time per unit length of arc column. The change in momentum per unit time,* δM *is equivalent to the added term appearing in equation (5.9). Schrade in his stability derviation considers* δM *and has implied that his stability equation is not only for a steady state arc but also for the transient case and therefore can be applied to a rotating arc column.*

The translational velocity of the arc column can also be transformed from being the incoming gas velocity to the velocity of the arc column relative to the surrounding gas simply by changing the frame of reference.

The stability equation is further generalised by considering the arc column as a current carrying, gaseous channel whose axis assumes any configuration in a three dimensional space.

The stability criteria divised by Schrade has an application to other arc configurations and move interesting to a transient condition of arcing. Using equation (5.6) the stability of the rotary arc column can be examined in that direction of greatest instability.

Two specific cases are shown on figure (5.8i) for a peak current of 9 kA, peak magnetic flux of 1T and phase difference angles of 47° and 80°. For the first case of ϕ = 47° (label A) the arc column is initially stable until just before the peak current when the magnetic field becomes greater than 700 mT. At this stage any kink which forms in the arc column would be unstable and will grow in the axial direction. Arc column stability is re-established not by the reducing arc current but by a decrease in the applied magnetic field below 700 mT. In this case stability is re-established some 2 ms before current zero.
To highlight the effect of the phase difference between B and I, case B is for an 80° phase lag of magnetic field. At the beginning of the half cycle the arc column is unstable due to the magnetic field but

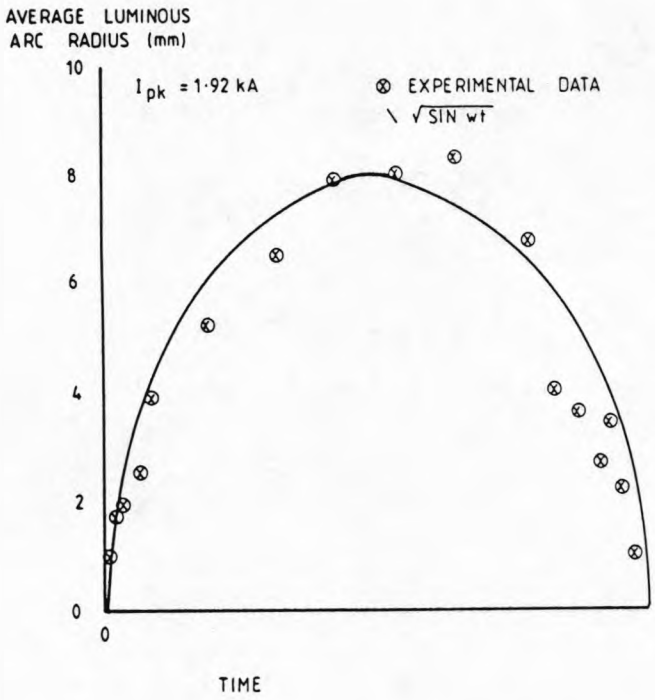

FIGURE 5·7. LUMINOUS ARC AREA

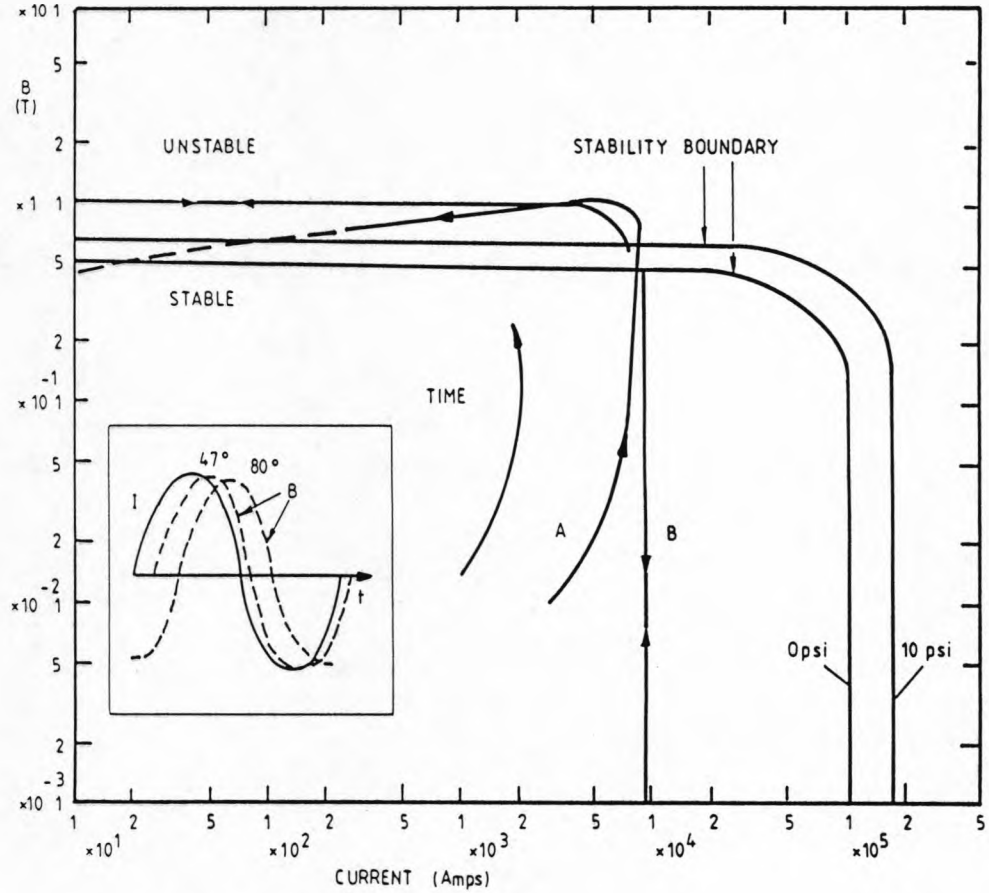

Ⓐ I_{pk} = 9kA ; B_{pk} = 1T; ϕ = 47°

Ⓑ " ; " ; ϕ = 80°

FIGURE 5·8i. STABILITY BOUNDARIES

becomes stable during the peak current period. However the column again becomes unstable towards the current zero period.

The magnitude of the applied magnetic field and the phase difference angle controls the time at which instability occurs. B determines whether instability occurs during the half cycle of arcing. ϕ controls the time at which this occurs, a small phase difference angle will cause the instability to occur near to the peak current, a large ϕ promotes arc instabilities at those times when the arc current is small, that is at the beginning and end of the half cycle of arcing.

It is interesting to examine the direction in which instability would occur. The two most susceptible directions are axial penetration into the cylindrical arcing volumne and axial ejection from the coil volume. The mechanisms responsible for producing the original kink in the arc column are flow turbulence and the axial Lorentz force arising from current interaction with B_R.

Kinks formed by flow turbulence are likely to occur randomly because of the passage of the arc through the surrounding gas generating large random turbulent vortices. Both favoured directions have a similar

probability of disturbance and the arc column can be equally injected or ejected. However, experimental evidence shows that arc movement into the coil volume is dominant.

The controlling mechanism which initiates arc column injection into the arcing coil volume is the interaction of the radial field with the arc current. This is a maximum at the same period in time for which the arc column experiences maximum instability.

Experimentally (figures 4.31 - 4.33) penetration occurs during the peak current period for the case of a 47° phase difference angle. As expected an increase in B causes an earlier onset of instability and the duration is extended perisisting down towards current zero. A larger magnetic field causes a stronger instability which is manifest as a further axial penetration into the arcing volume as seen experimentally. Figure (5.8 ii) compares experimental test information for axial penetration with that derived from equation (5.6). Both the experimental and theoretical values for midway penetration agree very well. The time of the onset of instability increases as the magnetic field is reduced, and there is a critical magnetic field below which magnetic instabilities will not occur.

5.1.2. ARC MOVEMENT AND CONTROL

The importance of those parameters controlling the arc's velocity and arc shape are identified from experimental results of one half cycle of sinusoidal arcing current.

5.1.2.1 ARC VELOCITY

During one half cycle of arcing the arc's velocity varies considerably. At the beginning of the half cycle the velocity of the arc column is zero but quickly rises with the increasing arc current and applied magnetic field. Figures (5.9) and (5.10) show two different cases for an 80° and a 47° phase difference angle respectively. Although there is a difference in both the magnitude of the peak current and the magnitude of the peak magnetic flux each is representative of the trend of arc velocity for each phase difference.

An increase in Lorentz force causes the arc column to accelerate to a maximum velocity occuring not at the instant of maximum driving force but nearer that instant at which the magnetic field is a maximum. This occurs at a time of 4.3 mS for ϕ = 80° and 3.4 mS for ϕ = 47° (figures 5.9, 5.10). This superficially curious result whereby the arc column continues to accelerate

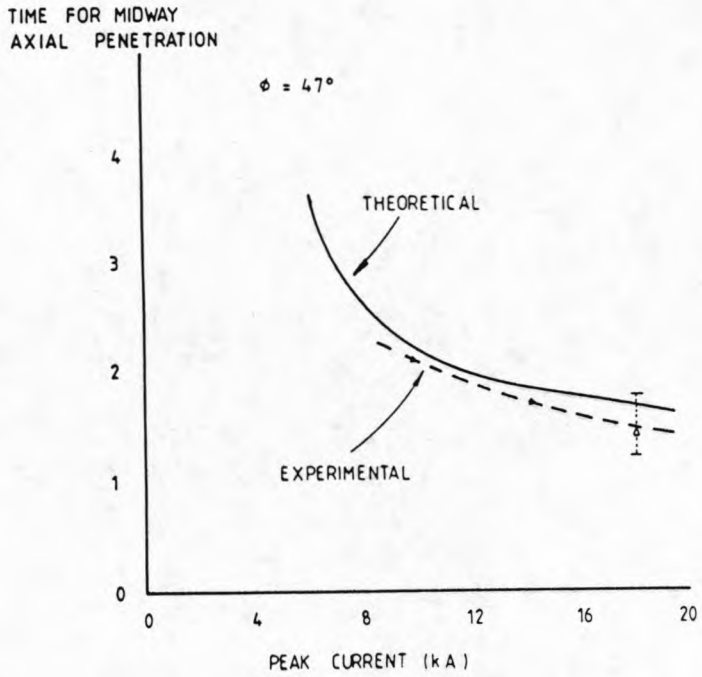

FIGURE 5·8 ii. MIDWAY PENETRATION

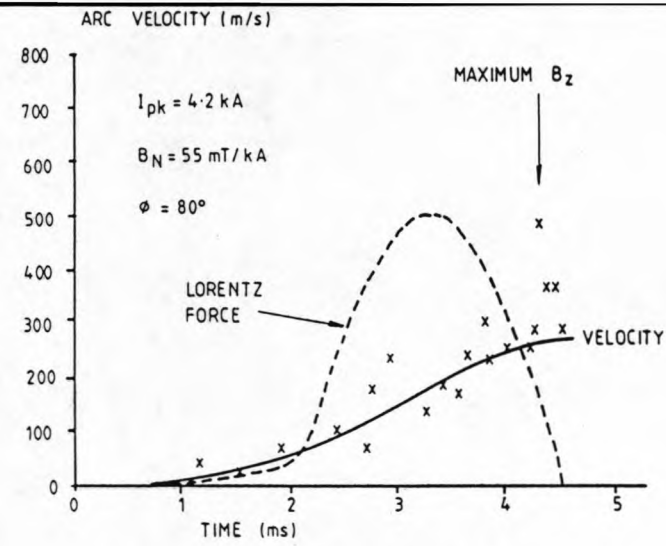

FIGURE 5·9. ARC VELOCITY FOR 80°

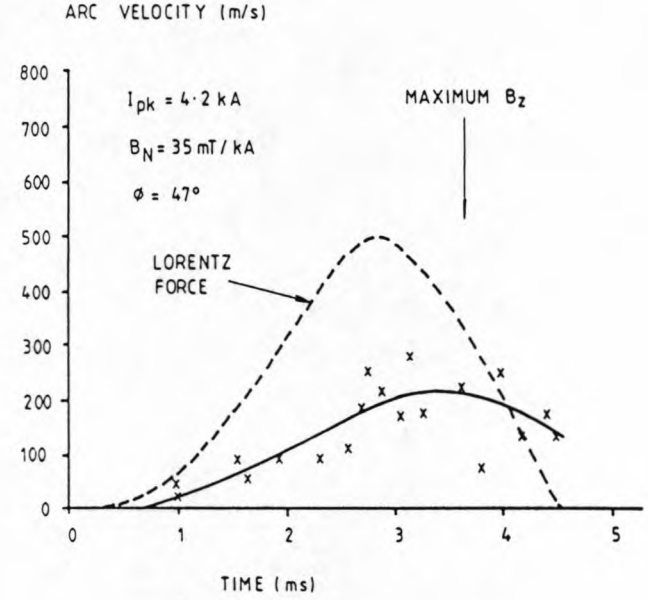

FIGURE 5·10. ARC VELOCITY FOR 47°

despite the Lorentz driving force decreasing, is explicable with equation (5.9).

Modifying this equation and eliminating the vector co-ordinates (by assuming mutual orthagonal fields), results in

$$\frac{\delta U}{\delta t} = \frac{iB}{\bar{\rho}A} - \frac{RC_D\rho_\infty U^2}{\bar{\rho}A} - \frac{U}{\bar{\rho}A}\frac{\delta M}{\delta t} \qquad (5.10)$$

"Lorentz" "drag" "mass change"

Where $M = \rho A$ *(per unit length)*

$\bar{\rho}$ = *plasma density*

A = *arc area.*

and where i, B, $\bar{\rho}$, A, R, ρ_∞, M *vary with time.*

The important modification is to the Lorentz force where i/A can be replaced by the current density (J). This is approximately constant during the high current period of arcing (47). Although there is a small pressure increase during arcing (4.1.3) the parameter is approximately constant and the plasma temperature remains practically constant during the same period (47, 48). The remaining parameter in the Lorentz force B, therefore must govern the driving force which consequently will be a maximum when B is a maximum.

The other two terms of equation (5.10) are both functions of arc velocity. The first is the "drag"

force which is also dependent upon arc dimensions, gas density and plasma density. During the quasi-steady phase R, C_D, $\bar{\rho}$, ρ_∞ change very little; however U^2 may change significantly. U^2 is a stabilising feedback term which increases the drag force resulting in $\delta U/\delta t$ becoming zero for a given set of external driving conditions and plasma conditions. If $\delta U/\delta t$ is positive then the arc velocity would increase because of the dominance of the Lorentian term.

The third term is the "mass change" term. The rate of change of mass that this term represents is small during the peak current period of arcing but can become more significant towards current zero. But towards the current zero period there are two opposite effects; one is the decrease in arc temperature making $\delta\bar{\rho}/\delta t$ positive; the second is the arc area decrease making $\delta A/\delta t$ negative. The effect of these two factors reduces the importance of $\delta M/\delta t$ not only during the peak current period of arcing but also down to within micro-seconds of current zero.

Essentially the rate of change of velocity is governed by the difference between the Lorentz and drag forces.

The maximum arc velocity occurs when the difference between the two forces is zero which is when the rate of change of B is zero (i.e. a quasi-steady field),

that is when B is a maximum. Figures (5.9), (5.10) show this effect. An increasing b field accelerates the arc whilst a decreasing B field causes deceleration of the arc.

5.1.2.2 MAGNETIC CONTROL OF MAXIMUM ARC VELOCITY

Another effect of the magnetic field is shown by the analysis of the high speed photographic results shown by figures (5.11, 5.12). These graphs show the change in maximum arc velocity against maximum normalised flux density for two phase difference angles 47° and 80° but for the same peak-current. The trends are similar for each, despite a larger flux density causing a higher arc velocity.

Empirical analysis of these results allows the maximum arc velocity to be related to the maximum normalised magnetic field (B_N).

For the case of an 80° phase difference this empirical relationship is described as

$$U_{max}^{2.13} = 5.68X10^{6}B_N - 155X10^{3} \qquad (5.11)$$

For the case of a 47° phase difference the empirical formula is;

$$U_{max}^{2.0} = 4.1X10^{6}B_N - 104X10^{3} \qquad (5.12)$$

These empirical relationships together with experimental results are shown on figures (5.11, 5.12).

5.1.2.3 ARC COLUMN ROTATION THROUGH IT'S OWN HOT WAKE

The evidence for the rotation of the arc through its own wake is reported by Kopainsky and Schrade (73). Their results derived from Schlieren photography of a rotating arc in sulphur hexaflouride indicate that the decay of the arc's wake by turbulence and thermal conductivity occurs only slowly (>> 10 mS). Furthermore this experimental study proves that the wake contour changes only slightly during one arc revolution (~ 1 mS).

This experimental conclusion is consistent with an approximate thermal conduction model of the arc wake. The geometry of the model is shown on figure (5.13). The arc column is represented by a circular cylinder and the wake by a uniform volume behind the arc. The thermal power dissipation from the arc wake is assumed solely due to thermal conduction in the x direction (figure 5.13). The temperatures decay is governed by

$$\frac{1}{\lambda_p}\frac{\delta T}{\delta t} = \frac{\delta^2 T}{\delta \lambda^2} \qquad (5.14)$$

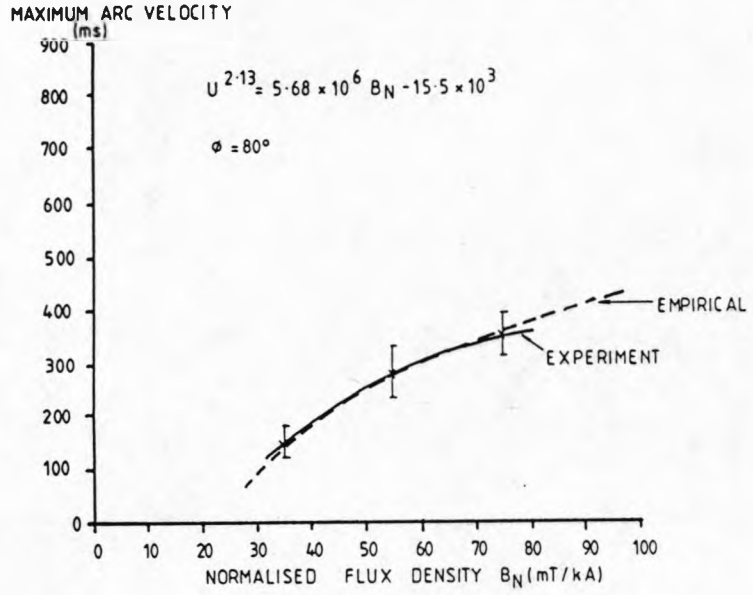

FIGURE 5·11. MAXIMUM ARC VELOCITY FOR 80°

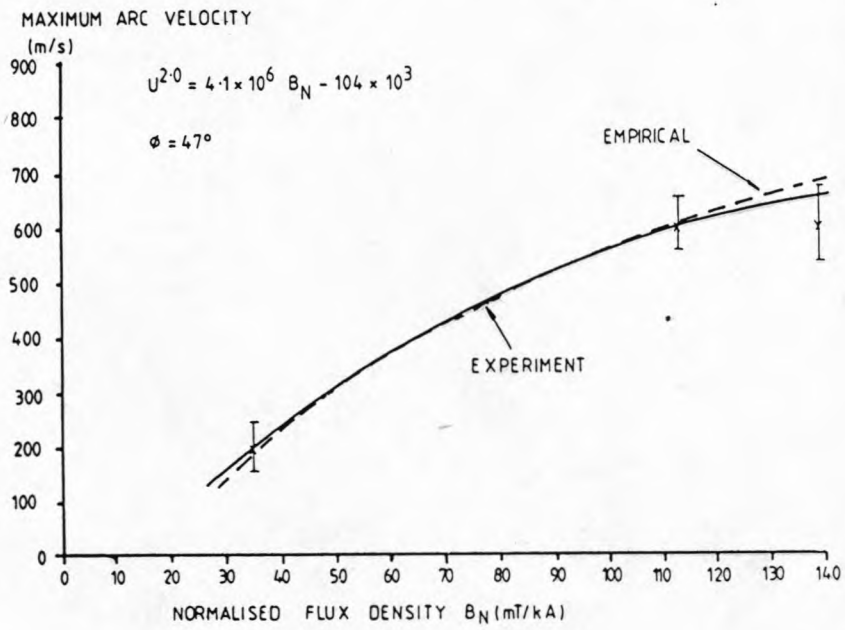

FIGURE 5·12. MAXIMUM ARC VELOCITY FOR 47°

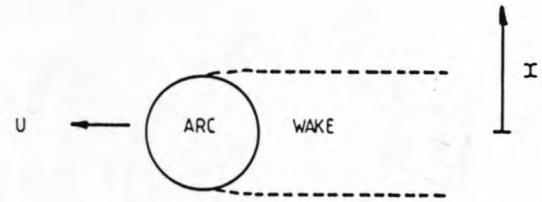

FIGURE 5·13. ARC WAKE SCHEMATIC

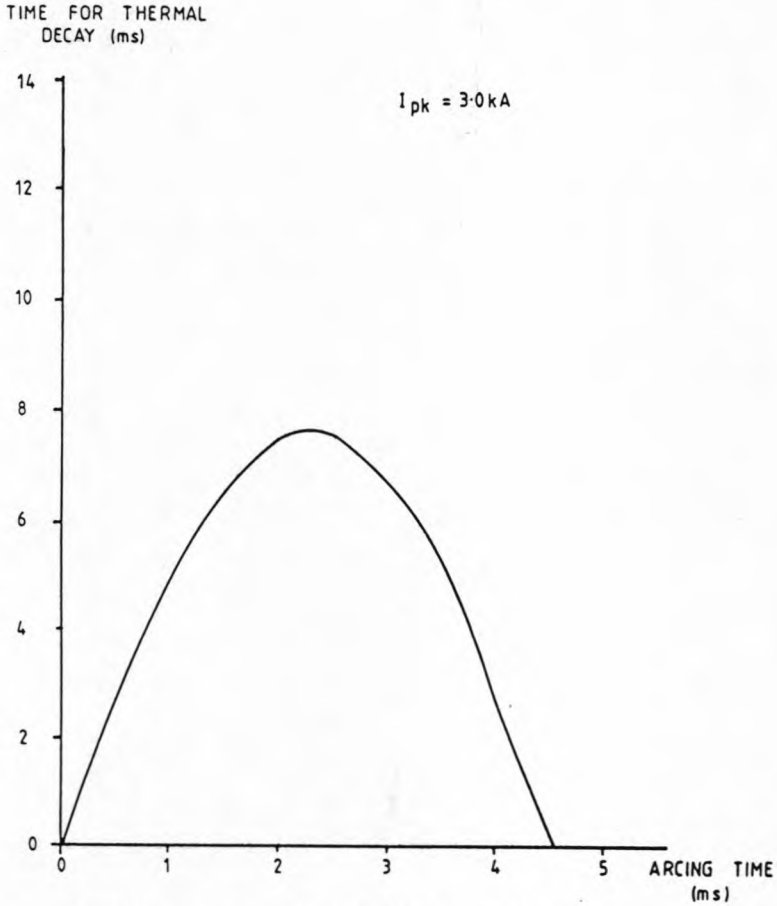

FIGURE 5·14. THEORETICAL THERMAL DECAY

The solution is given by;

$$\frac{T}{T_o} = \frac{1}{2}\left[\operatorname{erf}\left[\frac{R - X}{2\sqrt{\lambda_p t}}\right] + \operatorname{erf}\left[\frac{R + X}{2\sqrt{\lambda_p t}}\right] \right] \qquad (5.15)$$

λ_p = average thermal diffusivity

R = arc radius

T_O = wake temperature before thermal decay

T = wake temperature after thermal decay

x = radial distance

t = time for thermal decay from T to T_O

Information reported by Kopainsky and Schade (73,74) allows extreme values of thermal diffusiuity to be estimated. This information relates to the temperature decay which during one revolution of the arc which is limited to 100°K (from 2000°K (74) to 1900°K). This leads to a value of λ_p of 1.58×10^{-4} m^2/s (Appendix 2). As a result a thermal decay time (the time taken for the wake temperature to decay to 1900°K) may be determined. The results of such calculations at each instant during an half cycle (peak current 3KA) are shown on figure (5.14). The maximum decay time occurs at peak current when the arc's radius is a maximum. This time is 13 ms for a 3kA arc. The arc column will rotate in its own wake after one revolution provided that the time taken for the second and subsequent

revolutions (t) is less than the thermal time constant ie,

$$\frac{R^2}{\lambda} >> t \qquad (5.16)$$

Experiment shows that the observed times between successive revolutions after one complete revolution is much less than the thermal time constant.

The above analysis does not include the effects of turbulent mixing of heated gas with the surrounding cooler gas. This would of course reduce the dissipation time and lead to a more uniformly heated gas volume.

5.1.2.4 ARC CURRENT CONTROL OF ARC VELOCITY

The influence of the arc current upon the rotational velocity is shown on figure (5.15) which compares experimental results (full curves) for the maximum recorded arc velocity as a function of peak current and peak magnetic flux as well as the empirical trend as a function of peak magnetic flux only (equations 5.11, 5.12 dashed curves). These results show reasonable agreement between empircism and experiment at lower peak currents ($\leq$14kA) but with increasing departures at the higher currents. They also suggest that the effect of phase angle is somewhat exagerated at the higher

peak currents by the empirical description. It may however be more meaningful to interpret these changes in terms of arc velocity rather than peak current in which case the deviations occur at higher velocities. It is possible that this trend may be associated with changes in the arc column aerodynamic structure as well as the thermodynamic properties of the surrounding gas which occur at high rational velocities.

5.1.2.5 ARC SHAPE

The arc shape was briefly mentioned in section (2.4.5). The formula derived from some broad assumptions describes the arc's shape as a function of distance from the inner electrode and a constant which is the ratio of arc velocity perpendicular to the arc and the angular velocity of the arc column.

Although the analysis reported by Adams (76) is applicable to steady state arcing, this may be extended to the transient situation of the present investigation. This extension simply involves modifying the constant C (equation 2.43) to represent the same ratio of arc velocity (U) to angular arc velocity (W).

$$C = \frac{U}{W} \qquad (5.17)$$

Instead of calculating the arc velocity from the steady state equation it is determined from the transient equation describing the arc's velocity (equation 5.10). Examination of this equation shows that there is no analytical solution but that the arc velocity may be calculated by an iterative process.

Neglecting electrode effects, other Lorentzian forces and stability factors the arc will rotate in the anular gap with the same shape as that specified by Adams (equation 2.42). In other words the arc shape is independant of arc velocity but is dependant upon the distance from the centre of the inner electrode to the element of plasma under consideration.

However, if there is a radial variation of the axial magnetic flux; then a non-uniform Lorentz force is produced along the arc column and results in a varying velocity of each arc segment along its length. This results in the constant C in equation (5.17) becoming radially dependent.

Equation (2.42) is therefore modified viz

$$\theta = \left[\frac{r^2}{C^2(r)} - 1\right]^{1/2} - \cos^{-1}\left[\frac{C(r)}{r}\right] \qquad (5.18)$$

Where $C(r) = \frac{u(r)}{\omega}$ (5.19)

A radial increase in B_z is accompanied by a radial increase in the velocity of each element. The overall effect upon the shape of the arc column is to make it more radial in shape. Some typical shapes corresponding to a range of radial nonuniformities of the axial magnetic field configurations are shown on figure (5.16). Comparison between a 10% radial increase in magnetic field, a uniform field and a 50% radial decrease in field is shown on this diagram, with the arc becoming progressively more involute and longer. An average arc shape from experimental observation with no axial penetration is also shown on figure (5.16). There is a considerable difference between the experimental arc shape and the nearest calculated shape, (+10% shape). This is believed to be due to the influence of electrode effects which promote distortion in length close to the electrode (with a uniform magnetic field and polished electrodes Adams found that his theory predicts correctly the arc shape).

5.1.3 ELECTRICAL INFLUENCES

During the peak current period of arcing the arc voltage exhibits some transient variations. Some phenomena which may give rise to these changes arc considered overleaf.

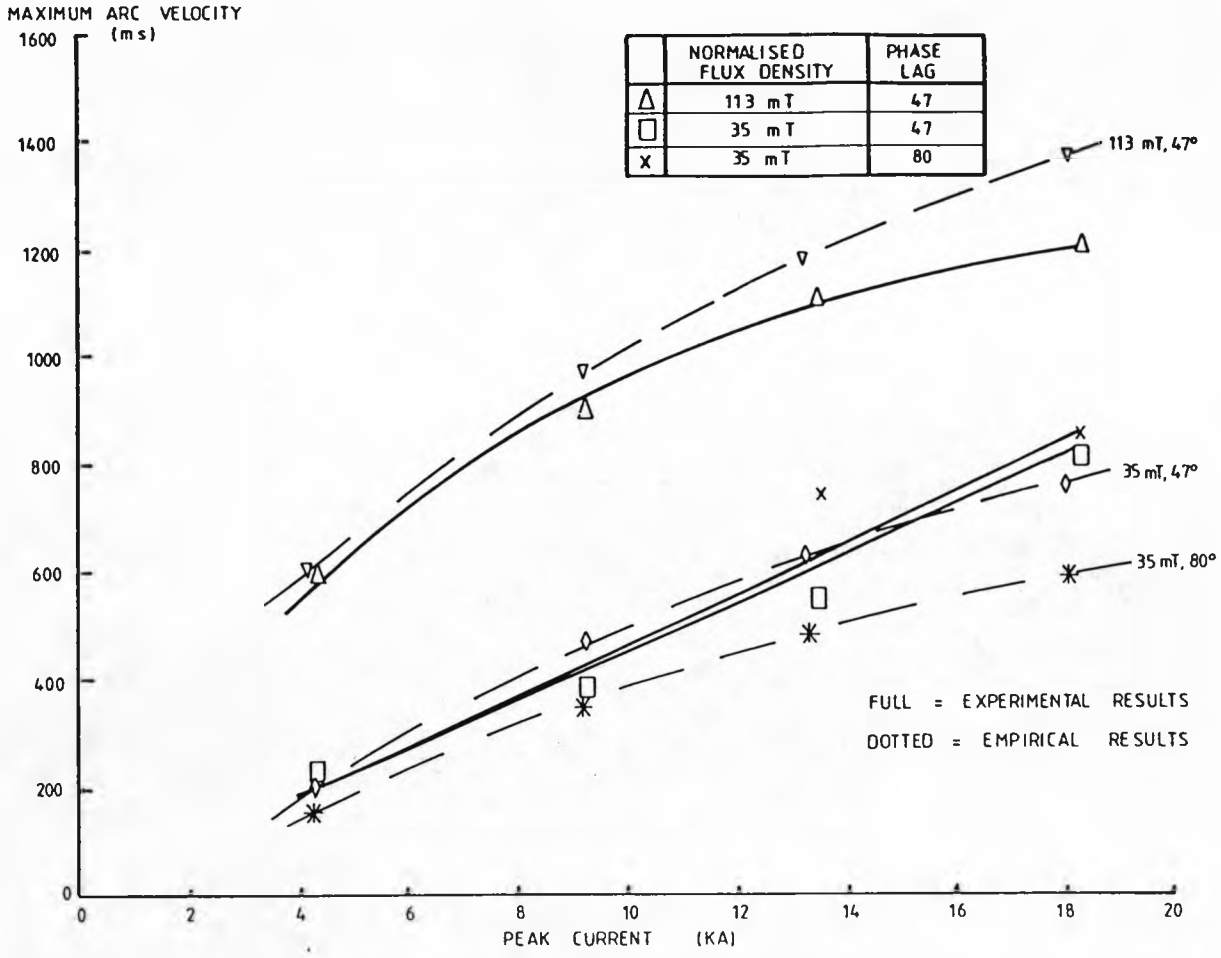

FIGURE 5·15. MAXIMUM ARC VELOCITY AGAINST PEAK CURRENT

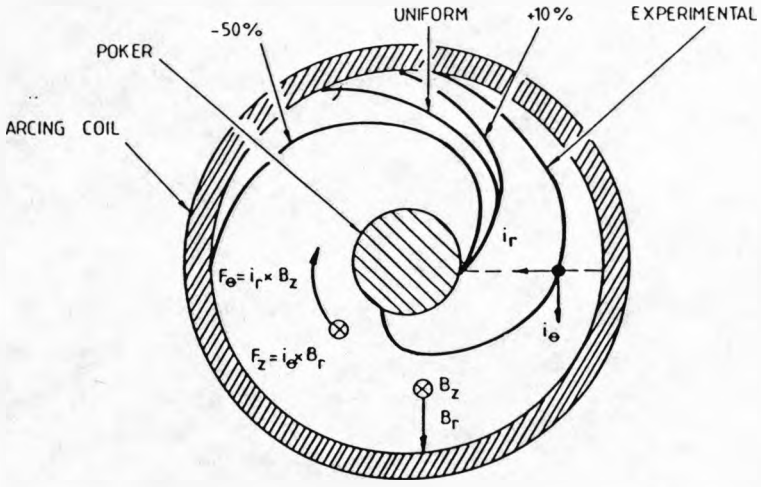

FIGURE 5·16. ARC LENGTH VARIATION

5.1.3.1 ARC VOLTAGE AND ARC LENGTH CORRELATION

A typical example of corresponding changes in arc length and voltage are shown in figure (5.17) for a 3kA peak current arc with a magnetic field characteristic of 35mT/kA, 47° phase lag. Both parameters clearly exhibit the same general rise during the half cycle of current and superimposed upon this are rapid fluctuations. These fluctuations correlate well with each other, so implying that to a first approximation the electric field strength remains constant. For this particular case the electric filed strength is 2.67kV/m.

At higher peak currents the frequency of these rapid fluctuations increases but the average length of the arc reduces to typically one third. Simultaneously the mean arc voltage increases by 15% (figure 5.18). These two changes taken together imply that the electric filed strength increases to 3.8kV/m for this particular condition. This third for the electric field variation may be qualified in terms of an average electric field at peak current: peak current characteristic with magnetic field strength as parameter (figure 5.19). These results indicate that the power dissipated in the arc (EI) increases with peak current and increasing

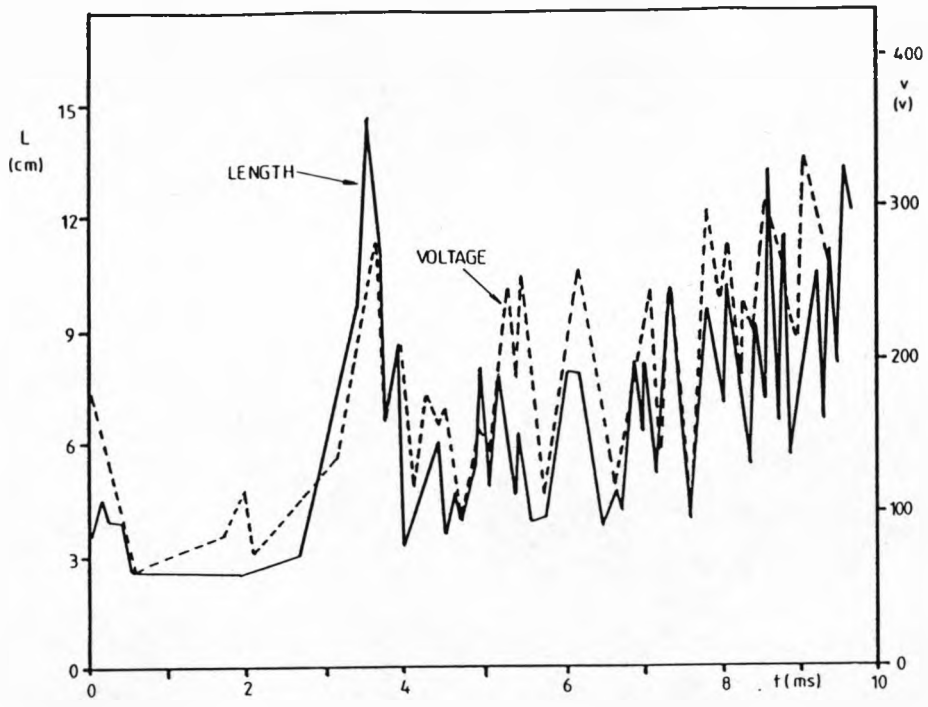

FIGURE 5.17 ARC LENGTH / ARC VOLTAGE VARIATION

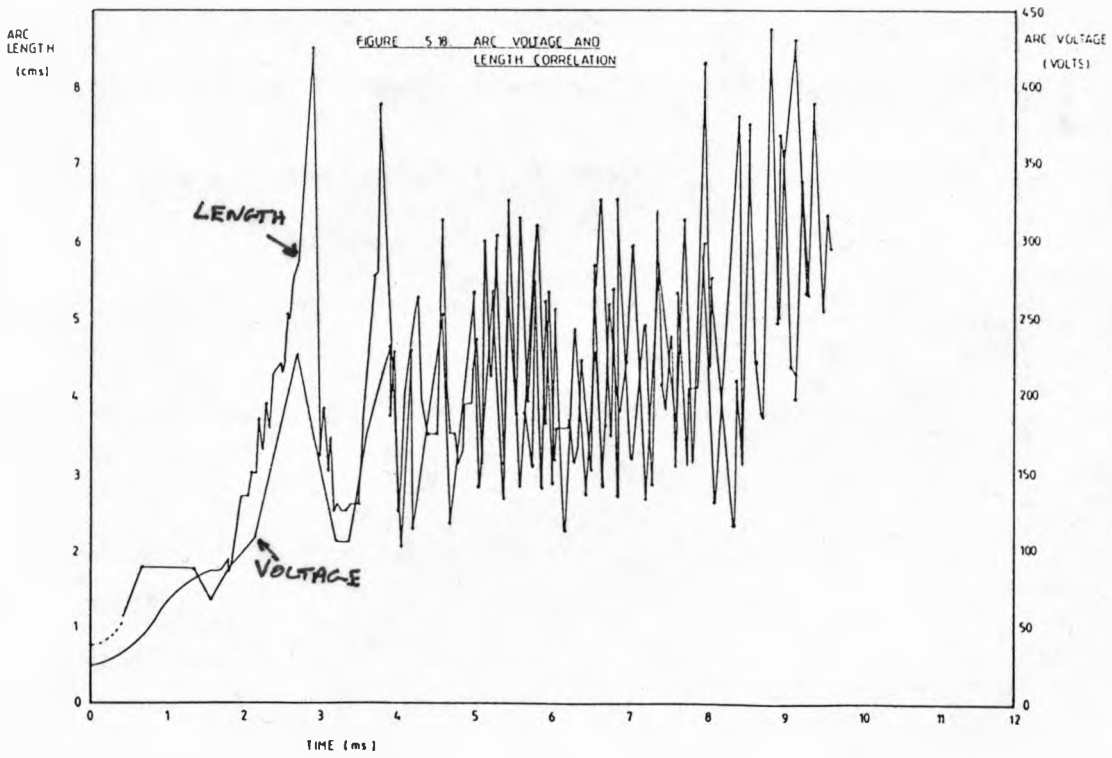

magnetic flux density. Both these changes reflect the effects of an increased arc velocity as indicated on figure (5.15). The accompaning shortening of the arc length and the greater forced convection produces the gradual rise in the mean electric field strength.

An approximate quantitative indication of the effect of velocity upon the convective losses is given by the fact that for a given peak current (e.g. 9kA) a 250V/m difference exists in the electric field strength for the two driving magnetic fileds and this corresponds to a doubling of the arc velocity figure (5.15).

5.1.3.2 MAGNETIC FIELD INDUCED EMF IN THE ARC

The emf induced in a conductor rotating in a time varying and spatial magnetic field is given by

$$E_{ind} = \oint (\underline{U} \times \underline{B}) \cdot d\underline{l} - \int_S \frac{\delta \underline{B}}{\delta t} \cdot d\underline{s} \qquad (5.20)$$

The physical representation of the two terms on the right hand side of this equation are induction by motion only (motional induction) and induction by a temporal change in the magnetic field (transformer induction). Both these induced emfs are present for the rotary arc configuration and their effects need to be examined separately.

The rotional induction produces an emf when the arc column "cuts" lines of magnetic flux. Because of the predominate rotary motion of the arc column and the relatively small radial variation of the dominant axial field the amount of flux "cut" by the arc is small. An estimate of the maximum value of this emf may be made from the maximum spatial variation of the magnetic flux and maximum arc velocity. Thus an arc column moving with a velocity of 1200m/s in a magnetic flux of 240mT will induce an emf of 0.29kV/m which is only one tenth of the magnitude of the measured electric field. Furthermore since the direction of this emf is orthogonal to both B and U it opposes the driving emf (figure 5.20).

The second term representing transformer induction is dependant upon the rate of change of the magnetic field. Consequently this effect would be negligible during the peak current period but could be significant during the initial rise or final decay of the flux towards current zero.

The temporal change of the magnetic field will induce an emf in the arc column in opposition to the Ohmic electric field. The loop involved in this type of induction is defined by the moveable contact (poker), the arc column and the cylindrical coil electrode.

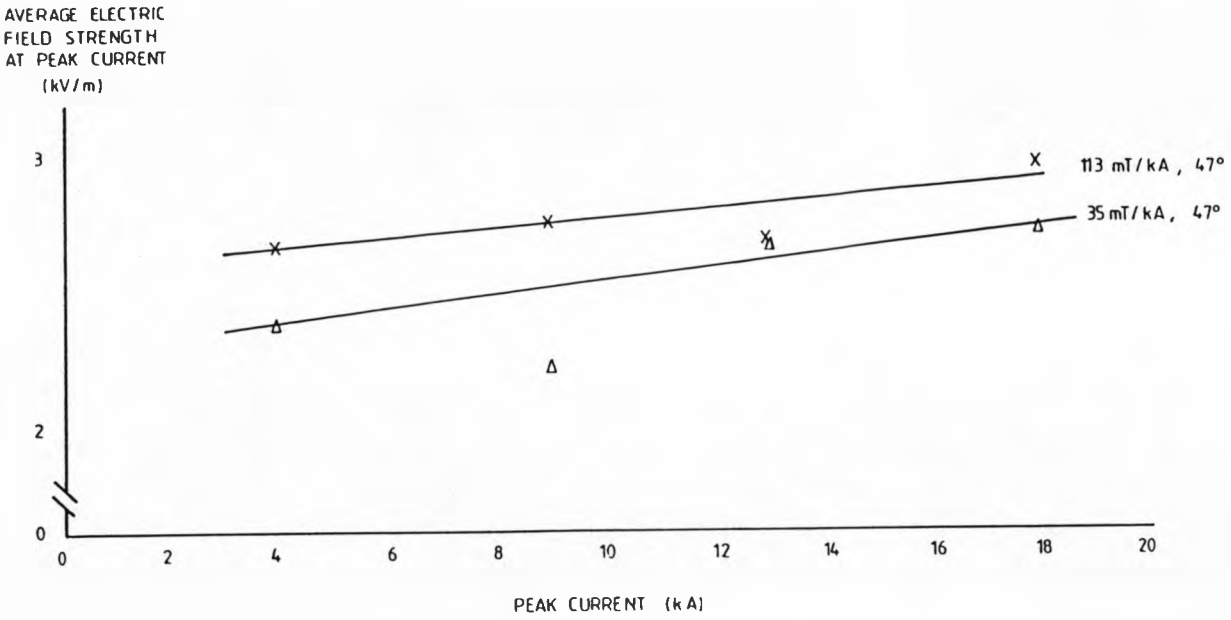

FIGURE 5·19 ELECTRIC FIELD STRENGTH AT PEAK CURRENT FOR VARIOUS PEAK CURRENTS

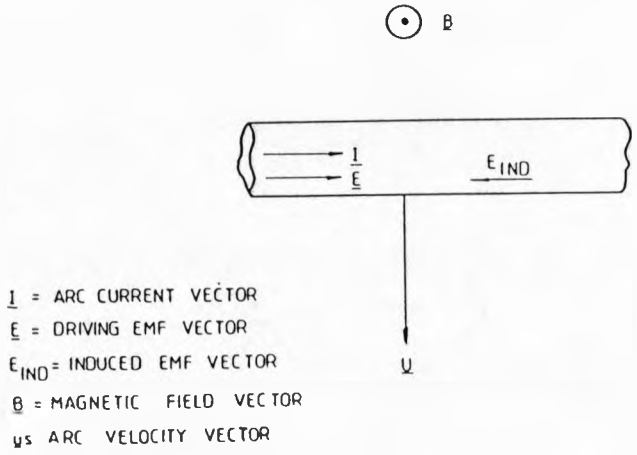

$\underline{I}$ = ARC CURRENT VECTOR
$\underline{E}$ = DRIVING EMF VECTOR
E_{IND} = INDUCED EMF VECTOR
$\underline{B}$ = MAGNETIC FIELD VECTOR
$\underline{v}_s$ ARC VELOCITY VECTOR

FIGURE 5.20 INDUCED ELECTRIC FIELD

Because of the arc's motion this loop is not uniquely defined so that the magnitude of the induced emf depends upon the arc position. This is apparent from figure (5.22) which indicates that there would be no net emf induced at positions U and W because of the opposite and equal emfs induced in the two loops defined by YWXU and YWVU. Maximum emf is induced when the arc column is at positions V and X and is given by the second term of equation (5.20).

$$E_{ind} = - \int_s \frac{\delta \underline{B}}{\delta t} \cdot d\underline{s} \qquad (5.21)$$

For the relevant experimental conditions the maximum emf is 0.91 V/m which is several orders of magnitude lower than the Ohmic electric field which is itself greater close to current zero than during the peak current period (compare figures 5.19 and 5.21).

5.1.3.3 ARC COLUMN INDUCTANCE AND INDUCTIVE VOLT DROP

During rotation the arc column can circumvent the outer coil surface more than once. If two turns of arc column exist within the arcing volumne then the arc column will itself have inductance. This may produce an emf which would be a maximum for high di/dt which occurs during the approach to current zero.

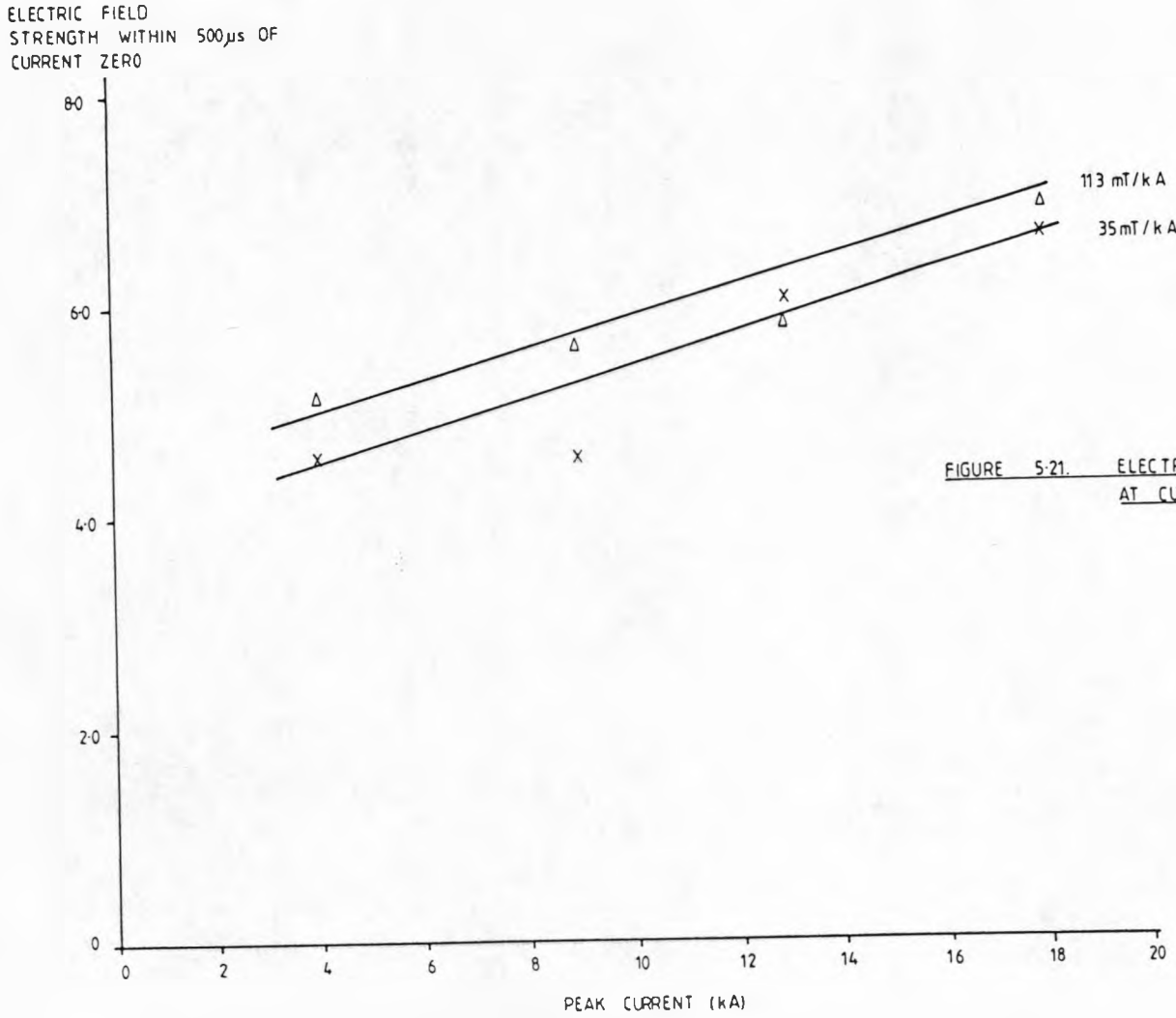

FIGURE 5·21. ELECTRIC FIELD STRENGTH AT CURRENT ZERO

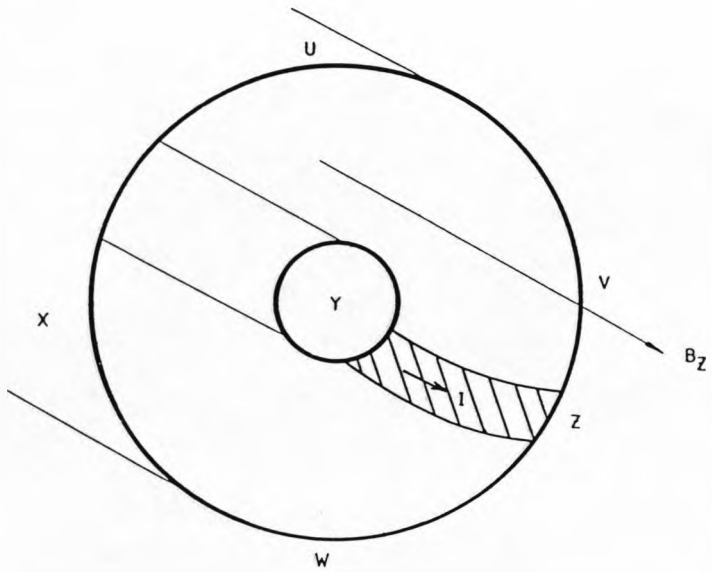

FIGURE 5.22. INDUCTION LOOP

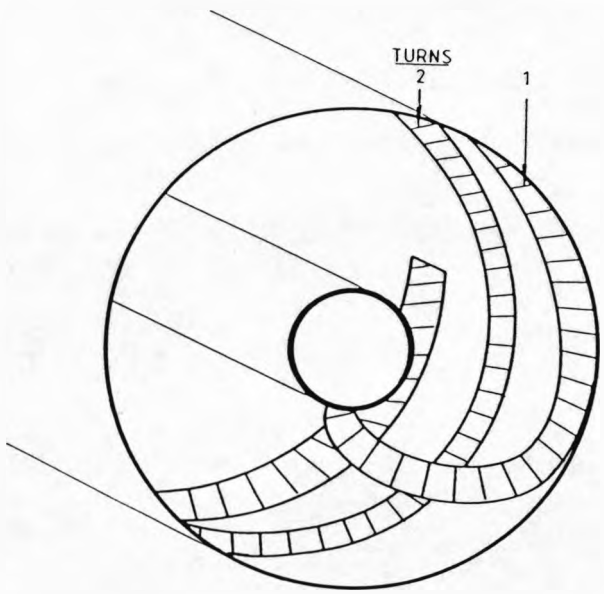

FIGURE 5.23. ARC INDUCTANCE

The inductance of the arc column depends upon its shape the number of turns and the self magnetic field generated. To simplify matters the arc is assumed to lie near the surface of the outer electrode and to have two turns separated by a small distance. The magnetic field generated by these turns is similar to that of a short solenoid, i.e.

$$B = \frac{\mu N I}{\sqrt{4R^2 + l^2}} \qquad (5.22)$$

Where μ = permeability of the medium (H/m)
N = number of arc turns
I = arc current (Amps)
R = radius of circle ascribed by arc (m)
l = separation of two turns (m)

Figure (5.23) shows a shematic of the geometery. The total flux linkage (Λ) of these two turns is,

$$\Lambda = \frac{\mu N^2 I A}{\sqrt{4R^2 + l^2}} \qquad (5.23)$$

So that the inductance of these turns becomes,

$$L = \frac{\mu N^2 A}{\sqrt{4R^2 + l^2}} \qquad (5.24)$$

The maximum effect of the induced voltage will occur close to current zero when both the rate of change of arc current is large and the inductance of the arc column is a maximum.

For an arc cross-sectional area of 3.14×10^{-6} m^2, inter-turn separation of 2mm and two turns of arc column, the inductance is 5.6nH. As a result for the most severe di/dt, the inductive volt drop would only be aproximately 0.07 volts maximum for two arc loops. For four loops of arc column the inductance increases to 10nH with an equivalent volt drop of 0.12 volts.

These induced voltages are negligible in comparison with the purely Ohmic voltage drop of the arc column.

5.2 CURRENT ZERO PERIOD

5.2.1 PRE-CURRENT ZERO CONDUCTANCE DECAY

5.2.1.1 SHOT-TO-SHOT VARIATION OF ARC CONDUCTANCE

Experimental results for the arc's conductance during the last 3μs of the pre-current zero period for fixed length arc columns, (whether they are free burning or have enforced gas flows) show a statistical variation (87). Having an arc which also has a statistical variation in length considerably complicates the determination of the magnitude of the arc's conductance prior to current zero. This is demonstrated by figure (5.24). The arc conductance shown is for four separate tests with the same operating conditions. Each test shows the same trend demonstrating a linear decay of the arc's conductance towards current zero which is similar to that for fixed length arc's. However, the

amount of scatter in the results represents both the statistical variation in the arc's thermal and aerodynamic structure and the statistical variation in the arc's length.

Before making any comparison of the arc's conductance between similar or dissimilar experimenal conditions the effect of arc length must clearly be eliminated. This may be achieved through a normalisation procedure.

5.2.1.2 NORMALISED ARC CONDUCTANCE

The normalising procedure must satisfy two criteria which are that it should take account of the arc's length and that this length should not change during the last 10us before current zero.

In section (5.1.3.1) a relationship between the arc's voltage and length was concluded and a direct correlation between arc voltage and length demonstrated (figures 5.17, 5.18). Image convertor photographs of the arc channel show that the arc length does not change during the 10us prior to current zero so that the second condition is satisfied.

The method proposed for normalising the arc conductance curves is to choose a particular length of arc column which corresponds to an arc voltage close to current zero. The point at which this voltage is measured must

be within 10 μs of current zero and the rate of change of voltage (dv/dt) should be zero.

The result of normalising the arc's conductance is apparent from a comparison of figures (5.24) and (5.25). The un-normalised results for a given di/dt (11A/μs) show a large variation from test to test (figure 5.24). Following normalisation the difference between the separate tests reduces as shown on figure (5.25). Also shown on this figure is the conductance variation for a di/dt of 6.1A/μs.

Clearly the normalisation procedure reduces the test to test variation so that behaviour under different operating conditions becomes distinguishable.

5.2.1.3 NORMALISED ARC CONDUCTANCE VARIATION FOR DIFFERENT dI/dT.

Figures (5.26) shows the normalised variation during the approach to current zero for di/dt values of 5.9A/μs, 7.5A/μs and 11.5A/μs (constant peak magnetic field of 610 mT and an 80° phase difference angle). These results show that the conductance and conductance decay rates both increase with di/dt.

Further analysis of these results may be considered in terms of the Mayr theory for which a knowledge of the normalised power input is required as a function of this

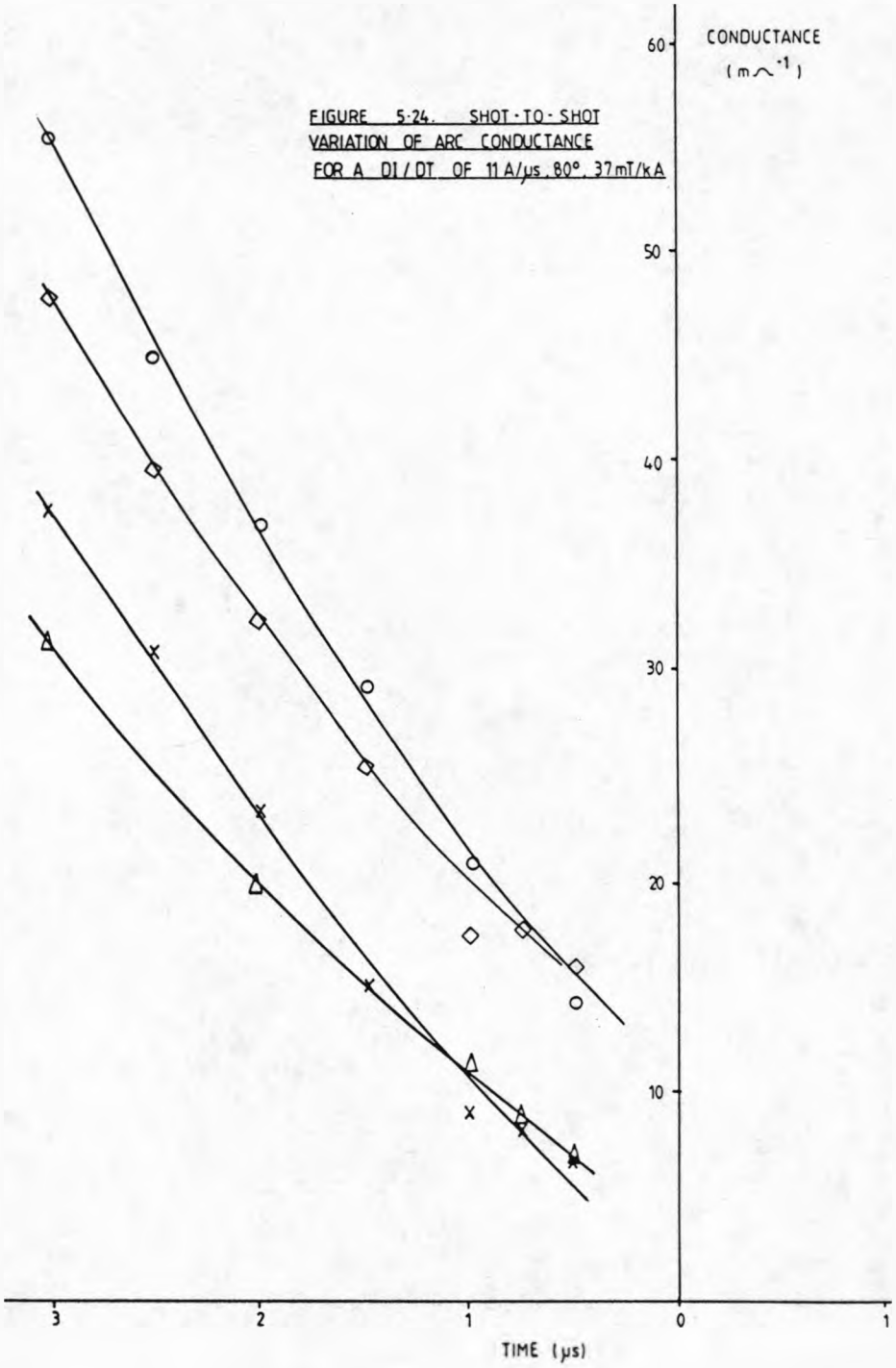

FIGURE 5·24. SHOT-TO-SHOT VARIATION OF ARC CONDUCTANCE FOR A DI/DT OF 11 A/μs, 80°, 37 mT/kA

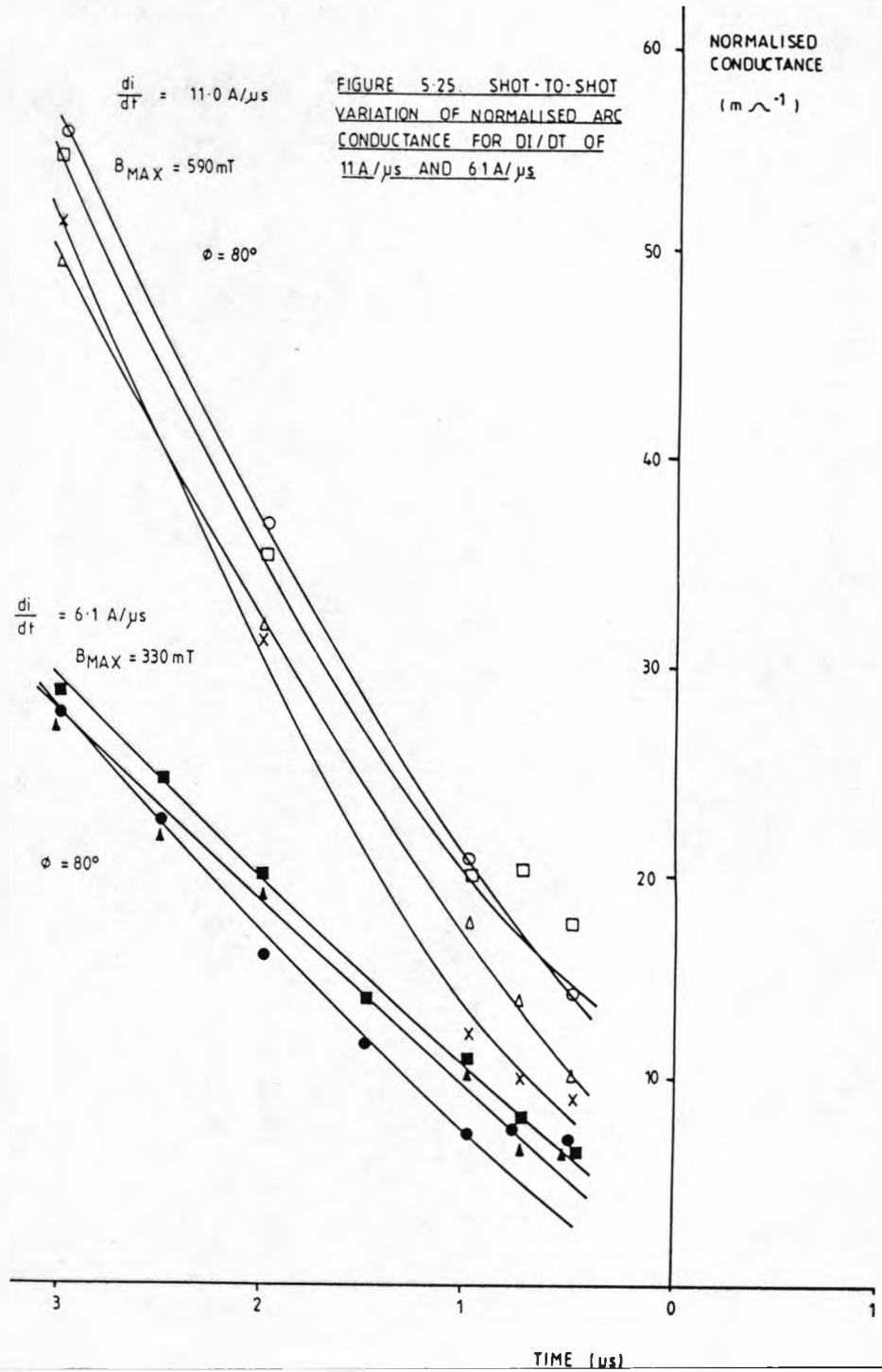

FIGURE 5·25. SHOT-TO-SHOT VARIATION OF NORMALISED ARC CONDUCTANCE FOR DI/DT OF 11 A/μs AND 6·1 A/μs

parameter,

$$\frac{1}{G}\frac{dG}{dt} \qquad (5.25)$$

Figure (5.27) shows the results of figure (5.26) plotted in this manner. These results show that results for different di/dt fall onto a unique characteristic and that the parameter in equation (5.25) increases as the power input decreases. The characteristic may also be used to estimate the arc time constant as the inverse of the intercept of the tangent with the vertical axis. This interpretation is consistent with the Mayr arc equation,

$$\frac{1}{G}\frac{dG}{dt} = \frac{1}{\tau}\left[\frac{VI}{N_o} - 1\right] \qquad (5.26)$$

τ = time constant, V = normalised arc voltage, I = arc current, No = rate of energy loss per unit length.

The result of this procedure is a set of curves describing the thermal time constant as a function of time (figure 5.28). This curves decay linearly towards current zero with a residual time constant at current zero. These results show that the time constant increases with di/dt.

The implication of these results is that the arc recovery is independent of arc length and that therefore the thermal performances of the interrupter is also

FIGURE 5·26. NORMALISED CONDUCTANCE FOR VARIOUS di/dt's AND CONSTANT FLUX DENSITY OF 610 mT

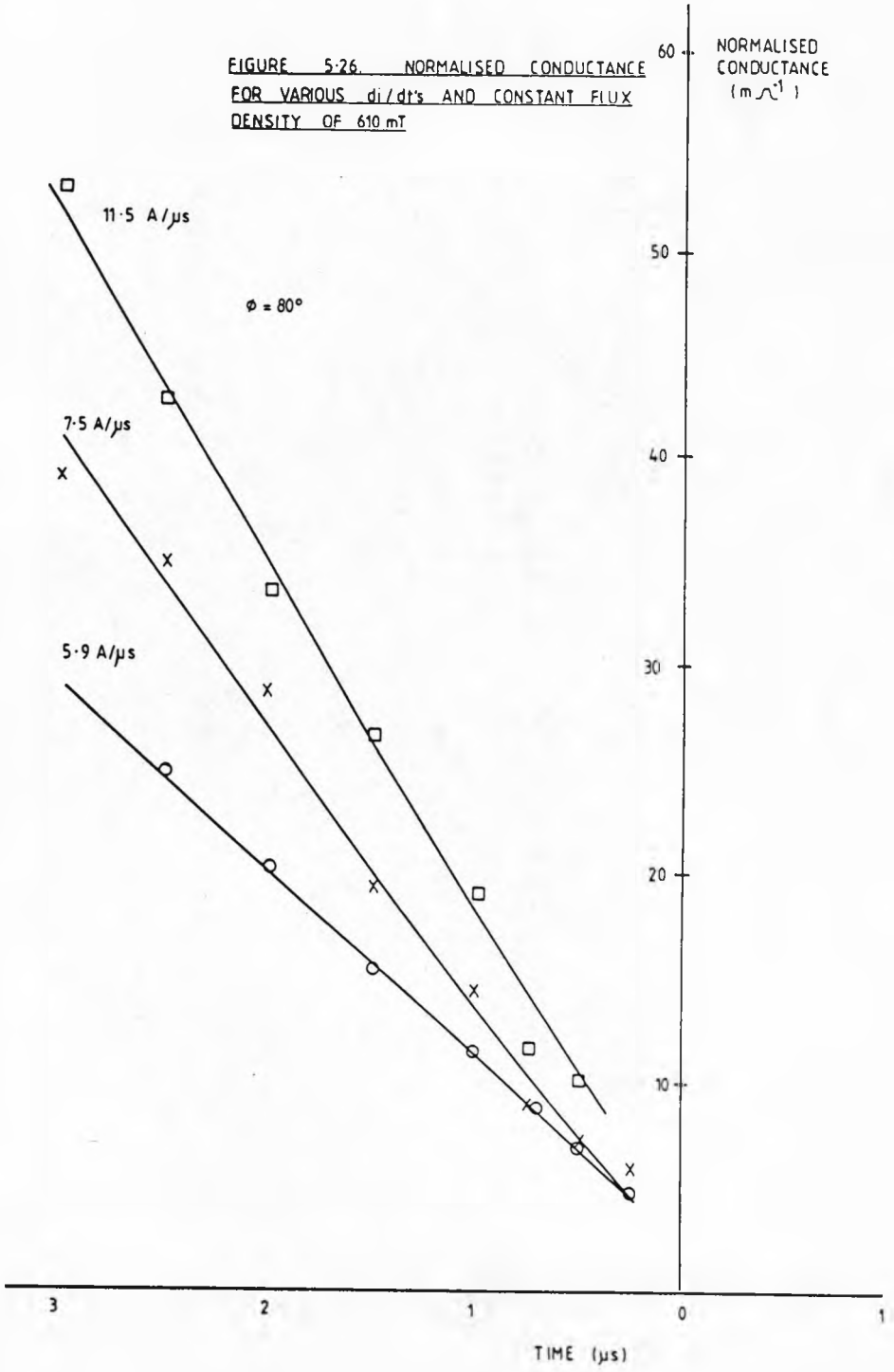

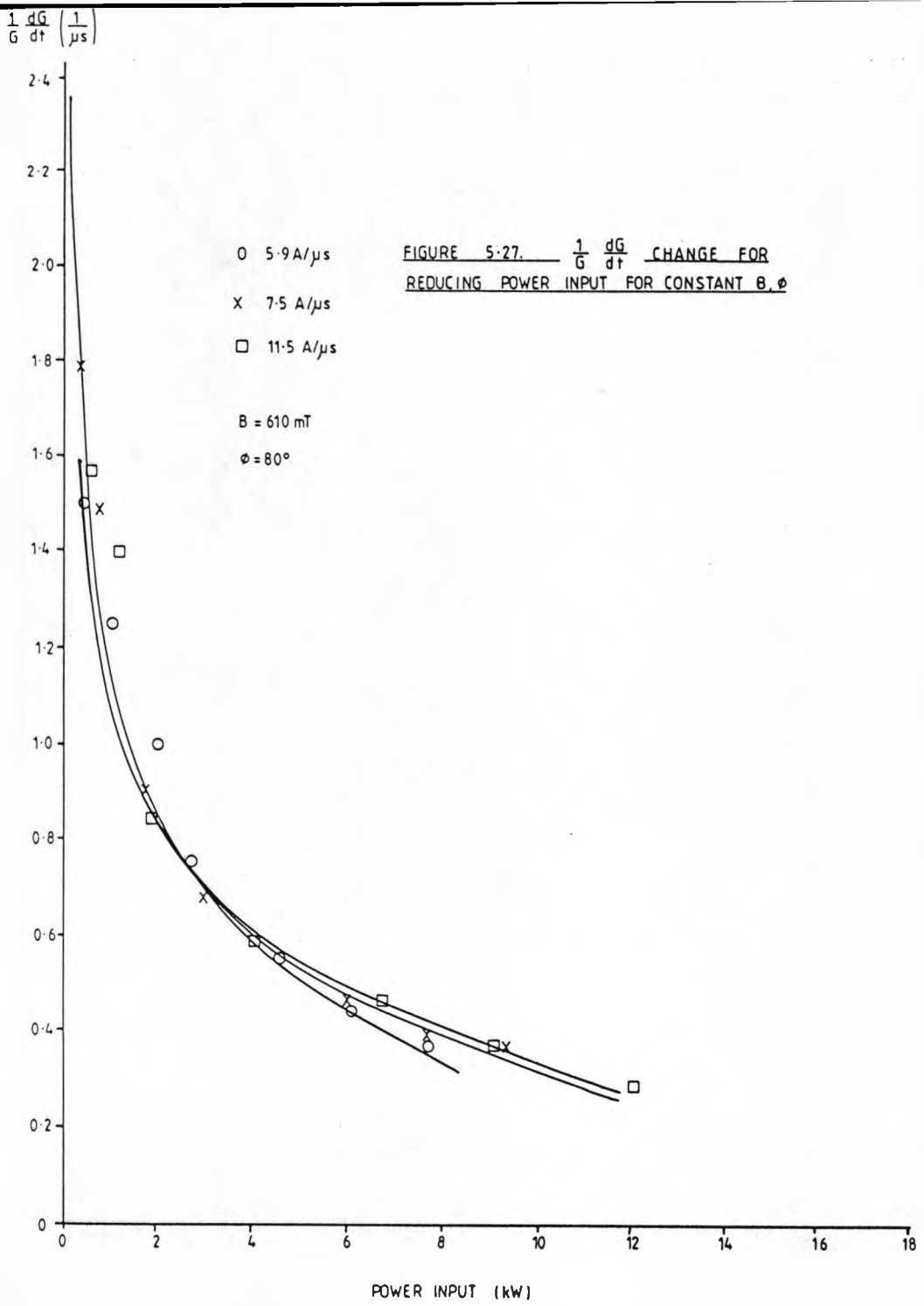

FIGURE 5·27. $\frac{1}{G}\frac{dG}{dt}$ CHANGE FOR REDUCING POWER INPUT FOR CONSTANT B, φ

independent of arc length.

5.2.1.4 NORMALISED ARC CONDUCTANCE VARIATION FOR DIFFERENT MAGNETIC FIELD STRENGTHS.

The conductance variation towards current zero for the same di/dt and phase difference angle but various normalised magnetic field is shown of figure (5.29). There are three cases shown corresponding to peak magnetic fields of 410 mT, 597 mT and 830 mT. All curves decay linearly towards current zero but the conductance at a given instant increases as the magnetic field strength decreases. This behaviour is consistant with the greater power dissipation due to the higher velocities produced by the high magnetic fields.

The 1/G(dG/dt): VI characteristics show a dependence upon the magnetic flux density as given of figure (5.30). The corresponding Mayr time constants derived from these results (figure 5.31) reduce linearly towards current zero. Although their magnitudes differ the rate of change of decay of the Mayr time constant is approximately the same for all cases. However the most interesting point about these curves is that an increase magnetic field reduces the Mayr time constant. For example one microsecond before current zero the time constant for the lowest magnetic field is 1.3 μs and for the greatest 0.46 μs. This variation is probably caused

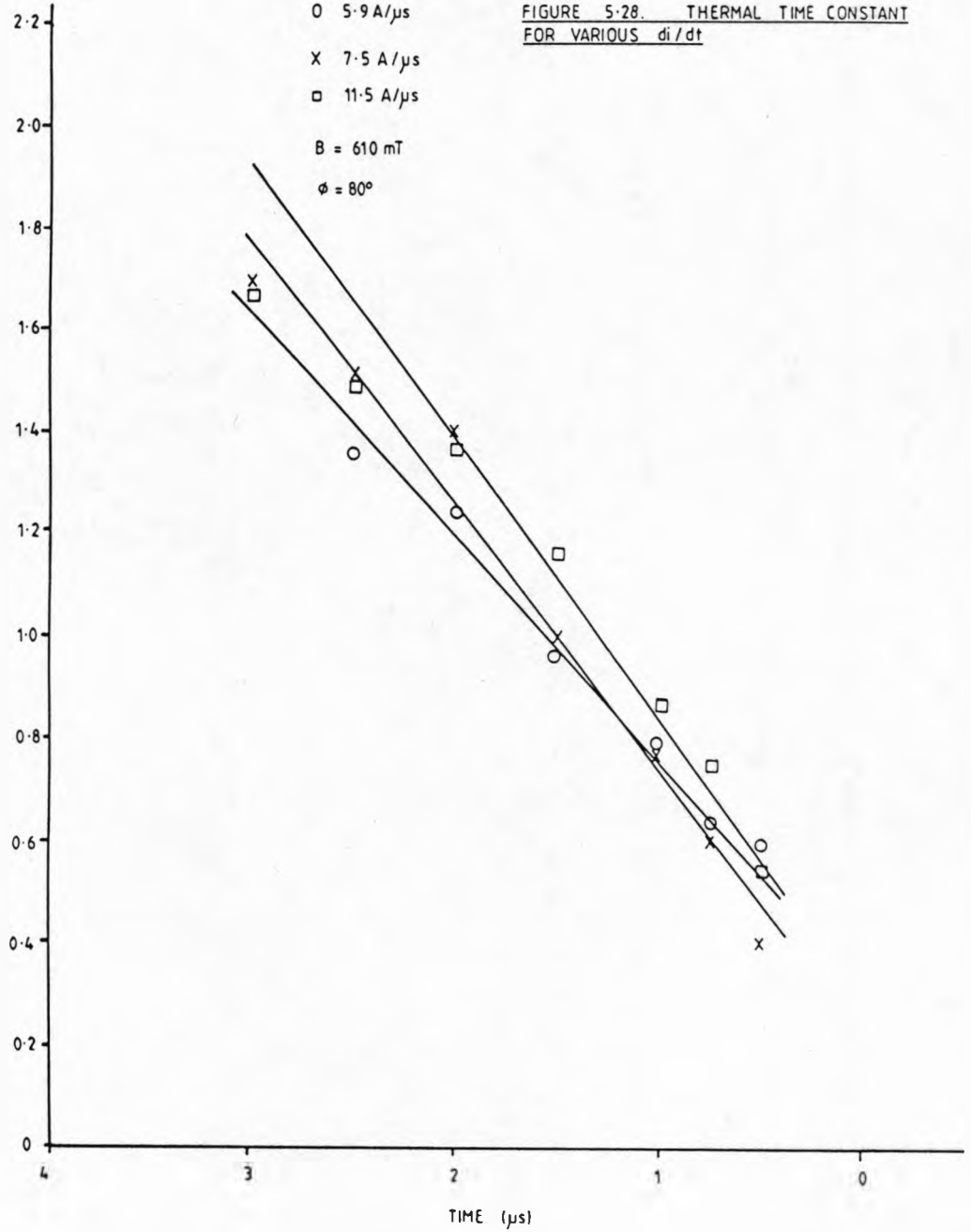

FIGURE 5·28. THERMAL TIME CONSTANT FOR VARIOUS di/dt

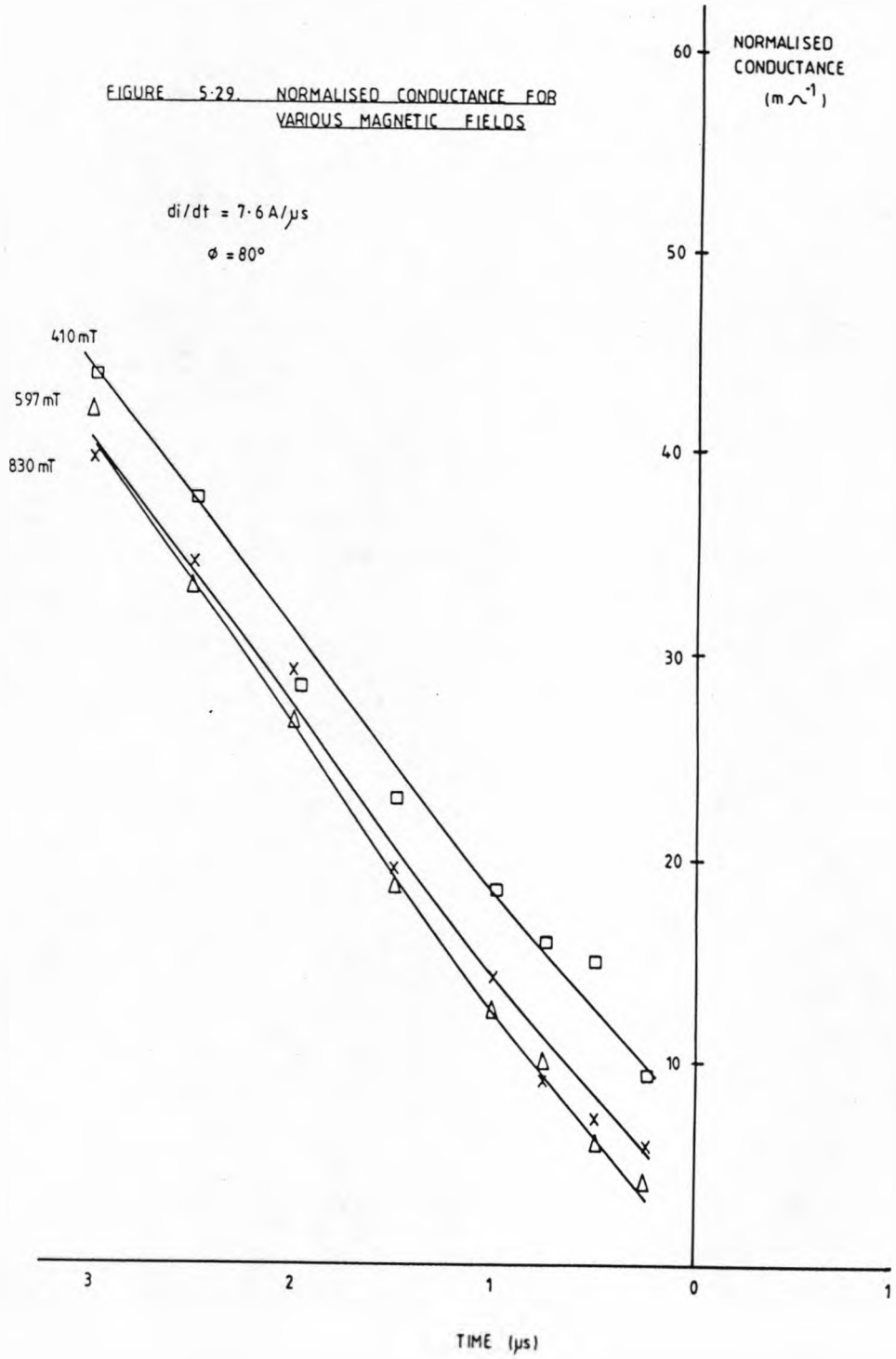

FIGURE 5·29. NORMALISED CONDUCTANCE FOR VARIOUS MAGNETIC FIELDS

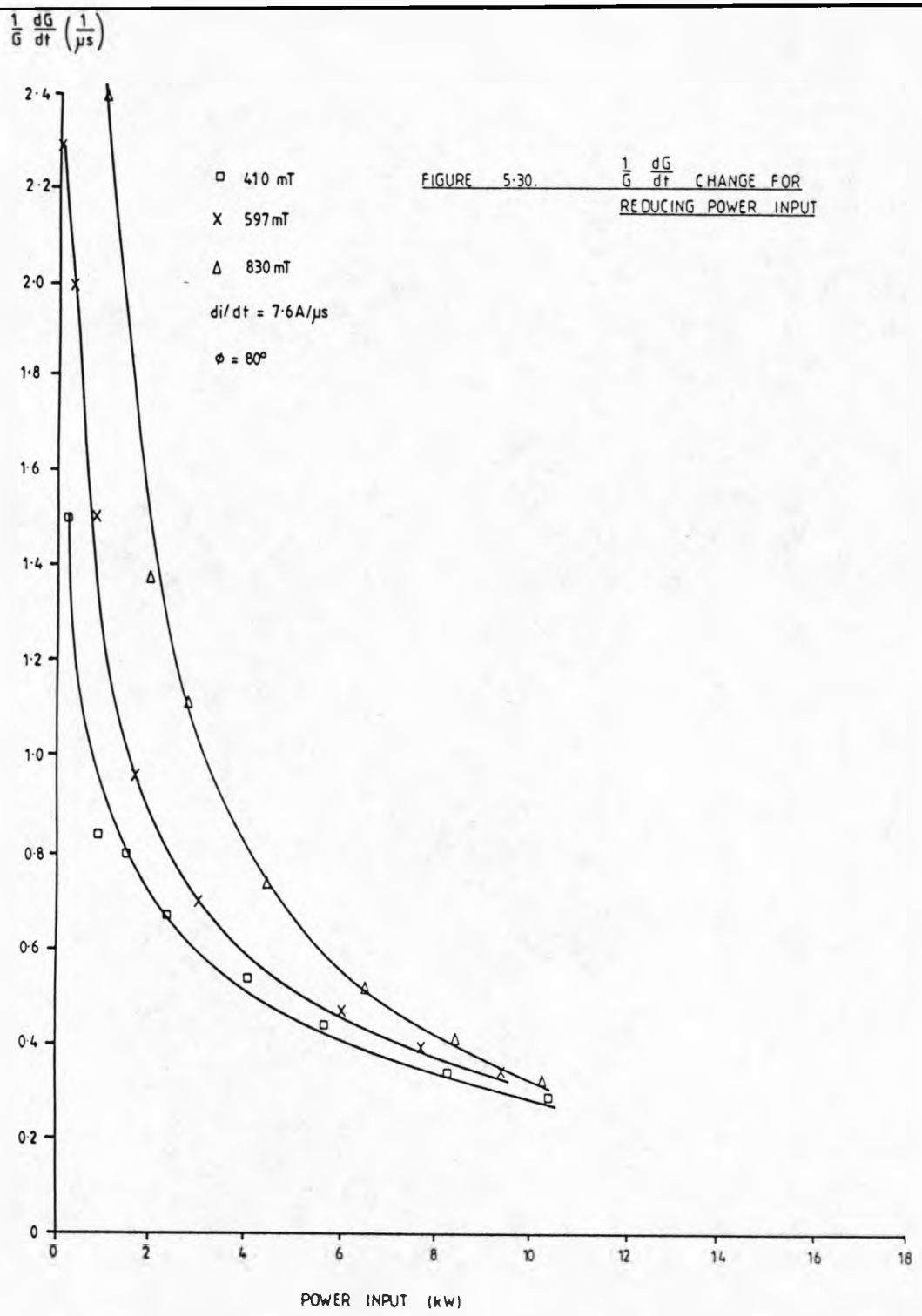

FIGURE 5·30. $\frac{1}{G}\frac{dG}{dt}$ CHANGE FOR REDUCING POWER INPUT

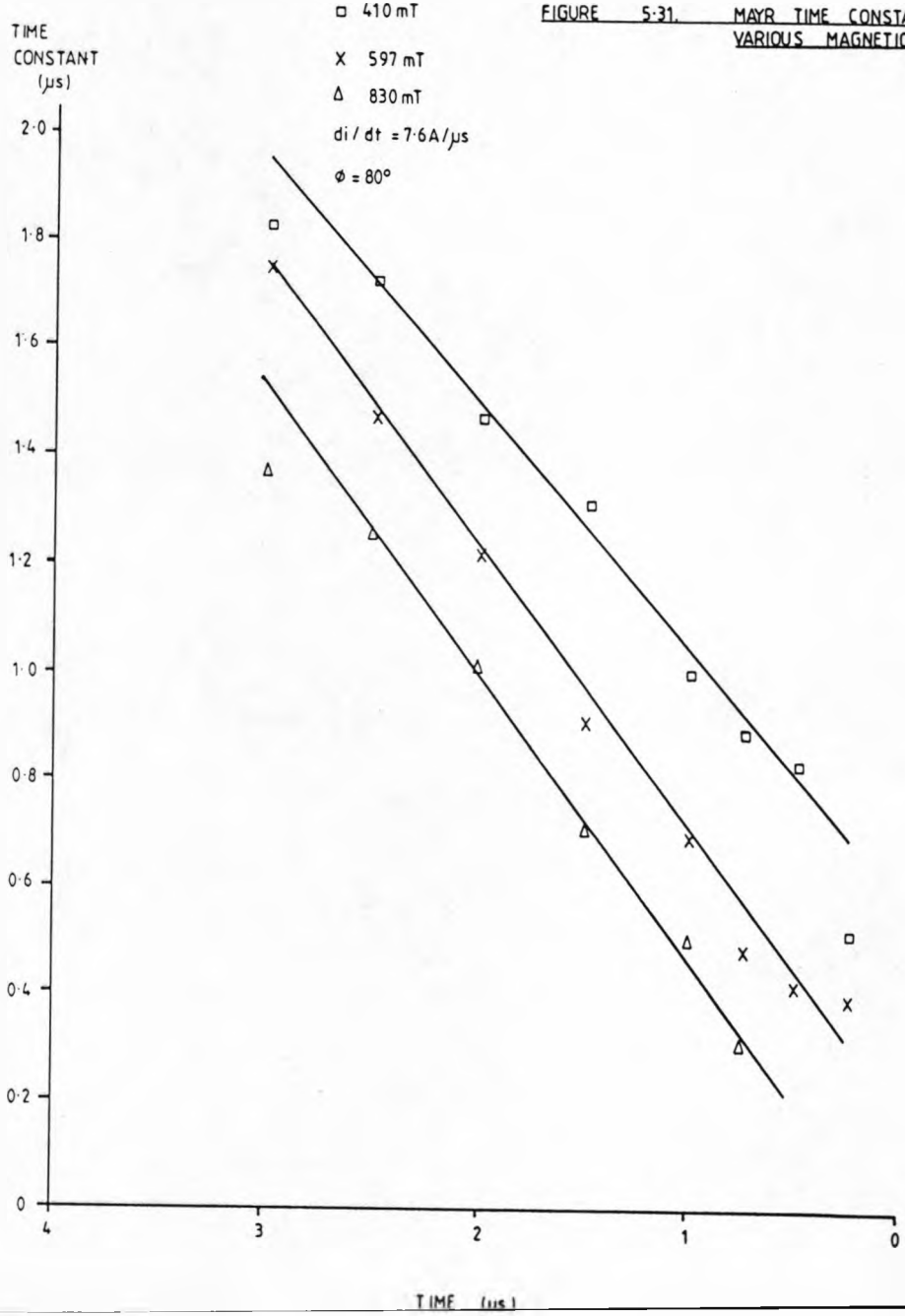

FIGURE 5·31. MAYR TIME CONSTANT FOR VARIOUS MAGNETIC FIELDS

by differences in the thermal structure of the arc column caused by the decrease in stored energy by the increased convection losses.

5.2.1.5 NORMALISED ARC CONDUCTANCE VARIATION FOR DIFFERENT PHASE ANGLES.

Conductance decay results for different phase angles, magnetic fields and di/dt values are shown on figure (5.32 - 5.37). Figure (5.32) shows a comparison between the effect of two phase angles (47° and 80°) for a di/dt of 5.2A/μs. The arc conductance decay is linear for both phase angles, the two curves having the same gradient. The difference between the results for the two phase angles in too small to allow distinct conclusions to be drawn.

The 1/G(dG/dt): Power characteristic derived from these results are shown on figure 5.33, the 1/G (dG/dt) values for a phase angle of 47° being greater than for the 80° case. The corresponding changes in the Mayr time constant during the current zero period are shown on figure (5.34). The results for the higher phase lag are greater than for the lower, but this difference diminishes towards current zero.

Similar trends for the three characteristics (G:t; 1/G (dG/dt): VI; τ:t) occur for a higher di/dt of 7.6A/μs (figures 5.35 - 5.37). However the Mayr time constant

has a slower rate of decay than that for the lower di/dt (figure 5.34) resulting in an overall larger time constant at current zero for the higher di/dt.

5.2.1.6 COMPARISON OF NORMALISED ARC CONDUCTANCE FOR ARC EXTINCTION AND ARC REIGNITION CONDITIONS.

Small changes in the arc's conductance near to or at current zero can cause the arc column to reignite after current for a given rrrv. Figure (5.38) show two results of identical arcing conditions, for one test the arc column reignited after current zero whilst for the other the arc extinguished. The difference in the arc's conductance is not large and could be attributed to test-to-test variation. However although these arc columns have similar (although not identical) conductances they may well have different cross-sectional areas and/or temperatures.

The 1/G (dG/dt) characteristics are similar for both arc's (figure 5.39) increasing with the decrease in power input. Consequently, the Mayr time constants for both cases are also similar but not identical. The time constant for this arc which reignited is larger than for the clearance case.

FIGURE 5·32. NORMALISED CONDUCTANCE FOR DIFFERENT PHASE ANGLES

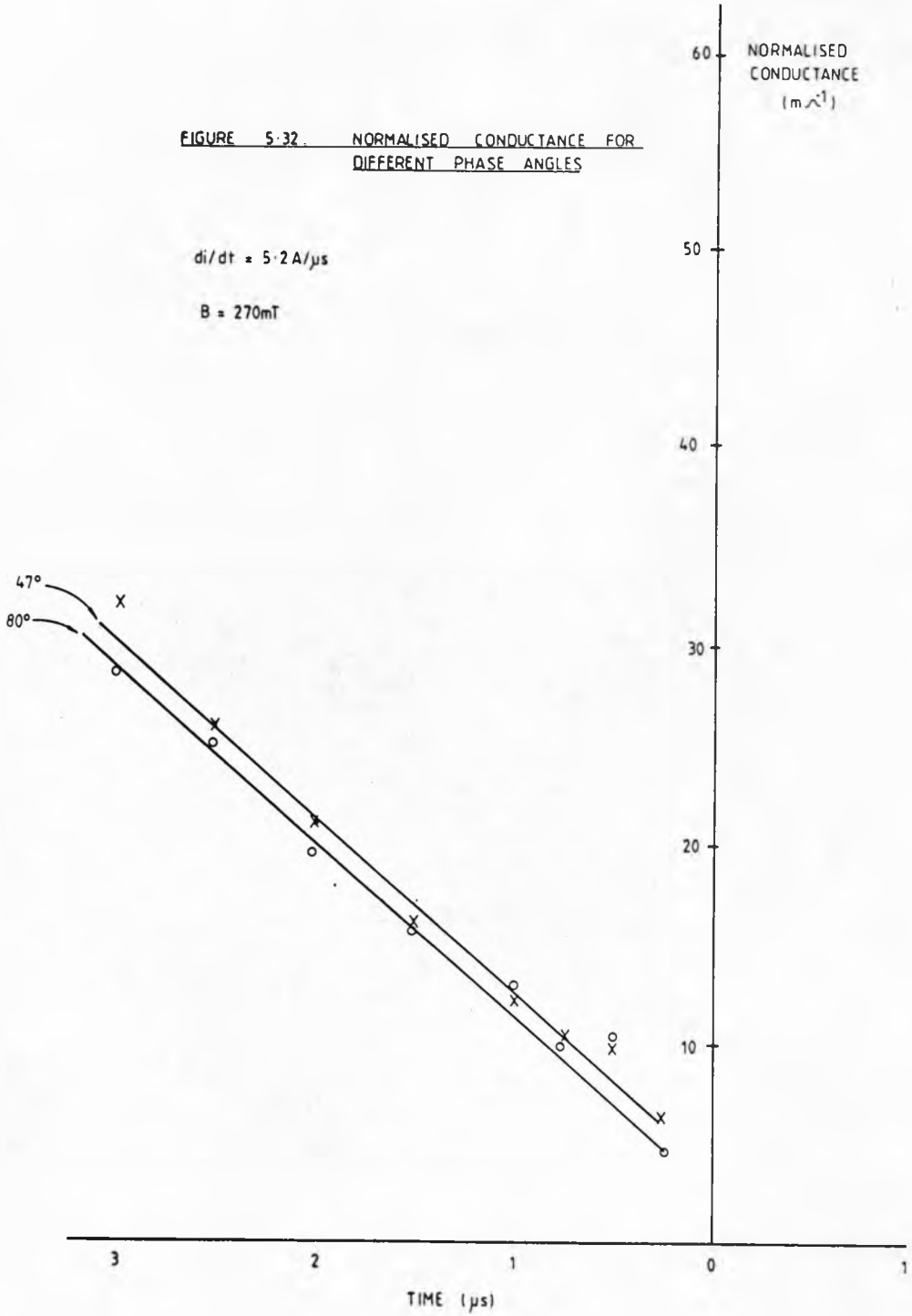

FIGURE 5·33. $\frac{1}{G}\frac{dG}{dt}$ VARIATION FOR REDUCING INPUT POWER FOR DIFFERENT PHASE ANGLES

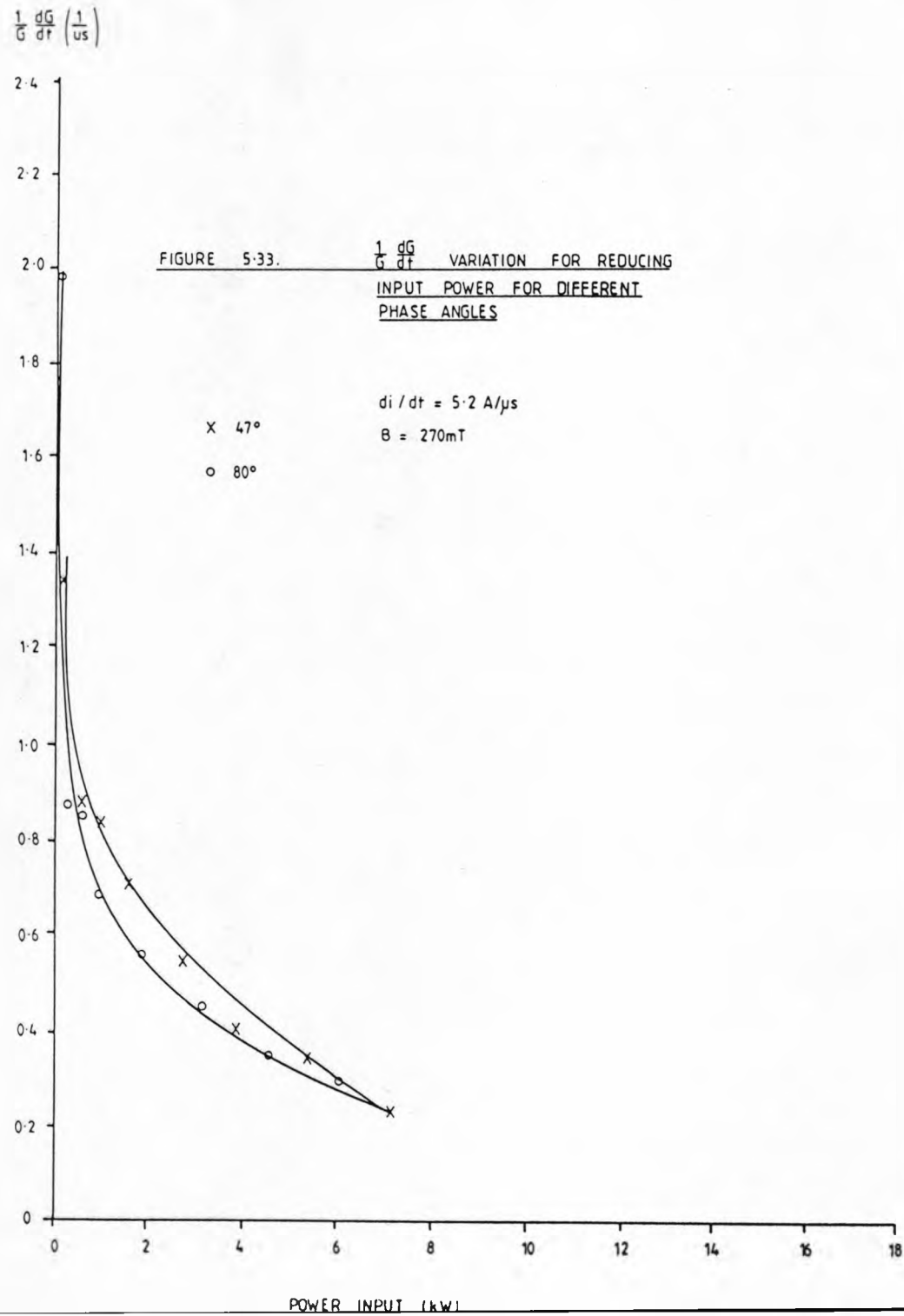

X 47°

o 80°

FIGURE 5·34. THERMAL TIME CONSTANT FOR DIFFERENT PHASE ANGLES

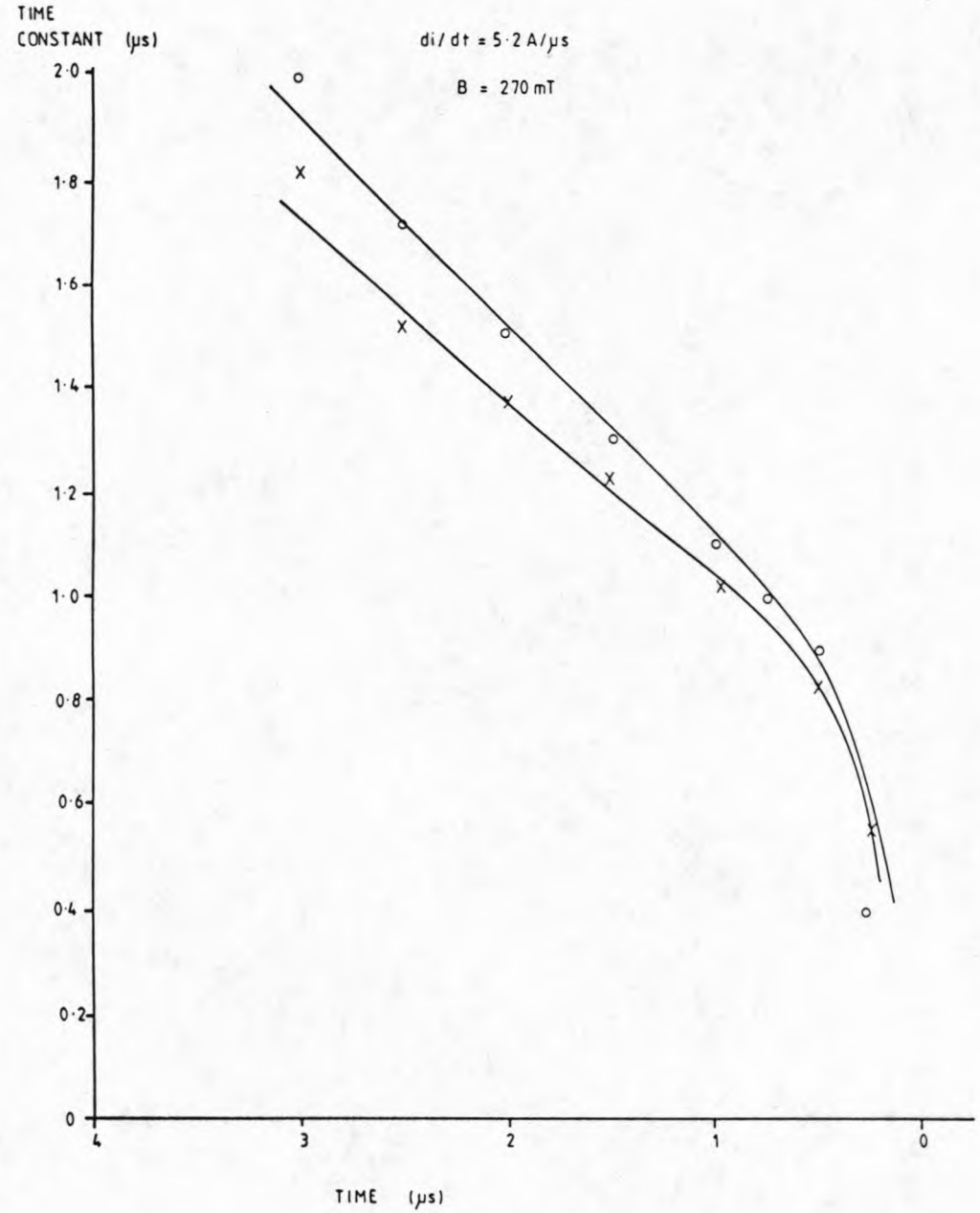

FIGURE 5·35. NORMALISED CONDUCTANCE FOR DIFFERENT PHASE ANGLES

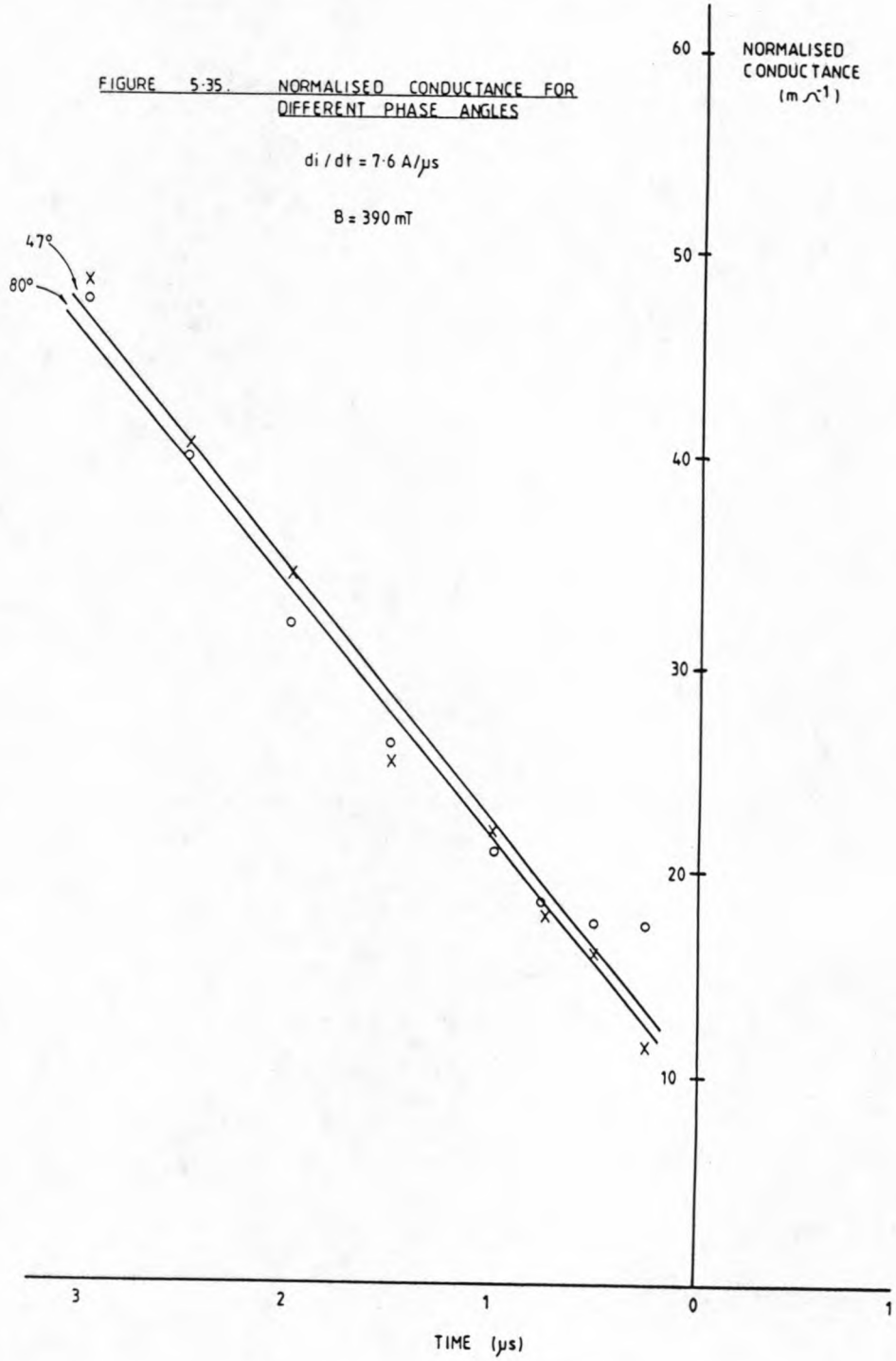

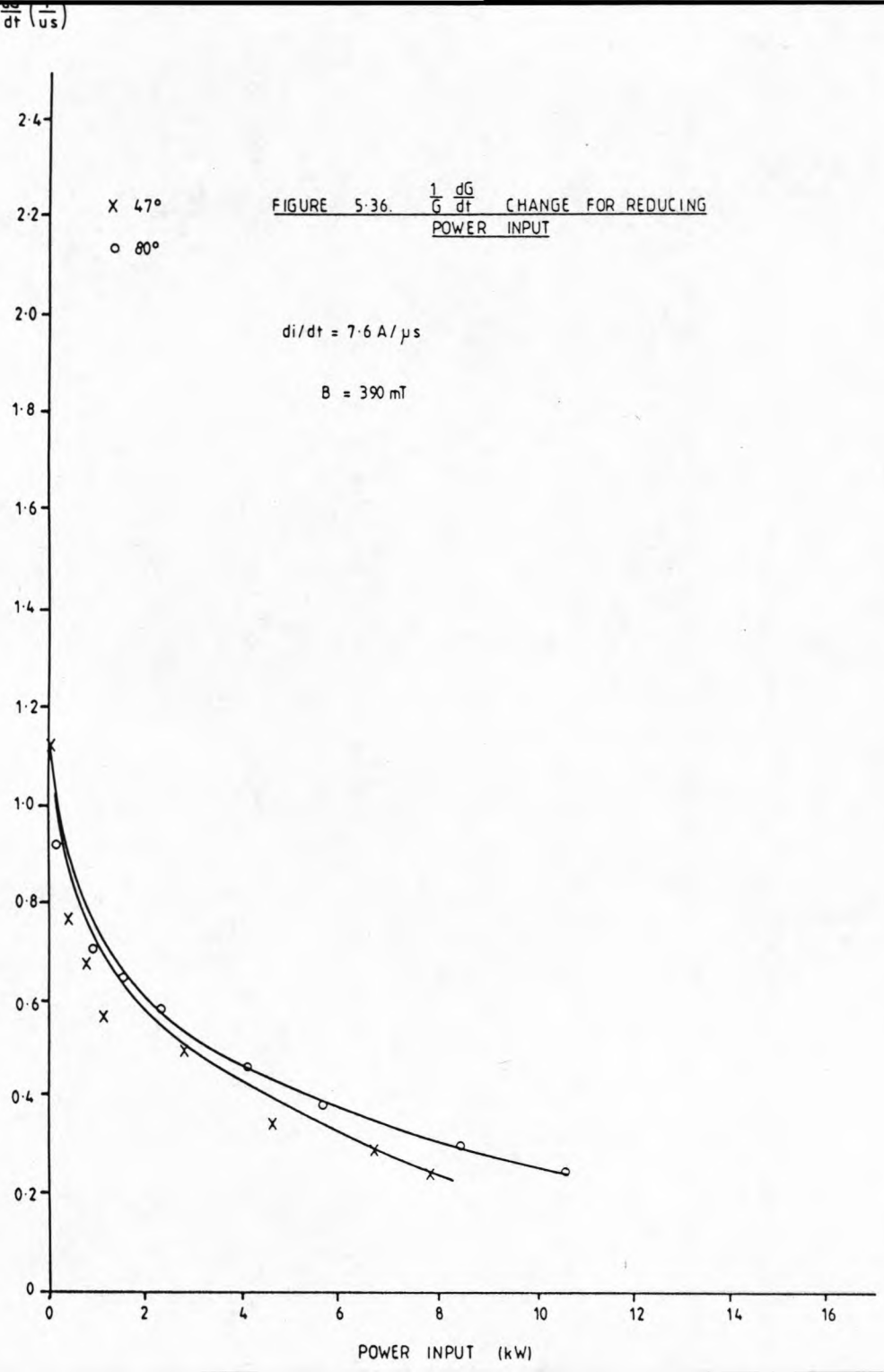

FIGURE 5·36. $\frac{1}{G}\frac{dG}{dt}$ CHANGE FOR REDUCING POWER INPUT

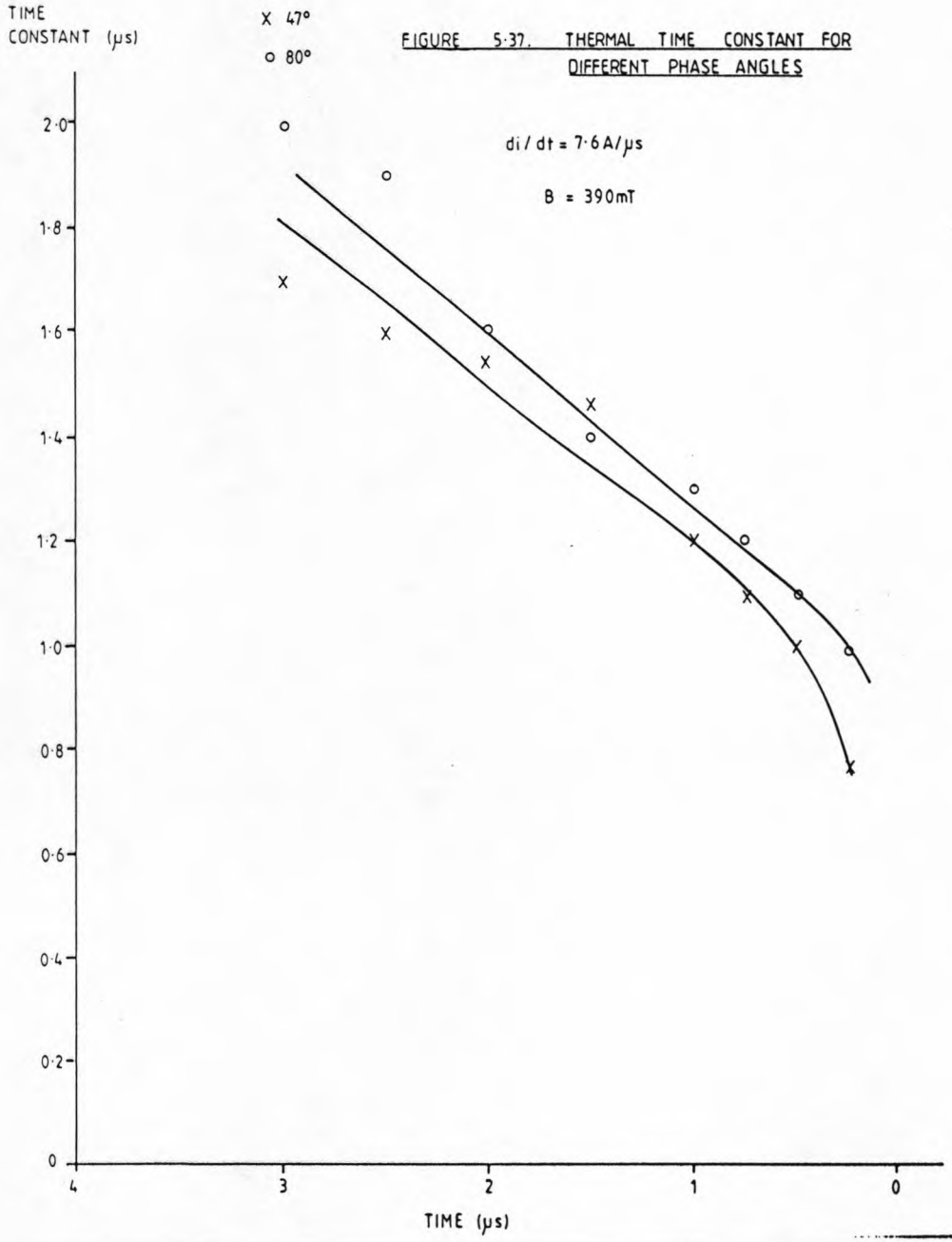

FIGURE 5·37. THERMAL TIME CONSTANT FOR DIFFERENT PHASE ANGLES

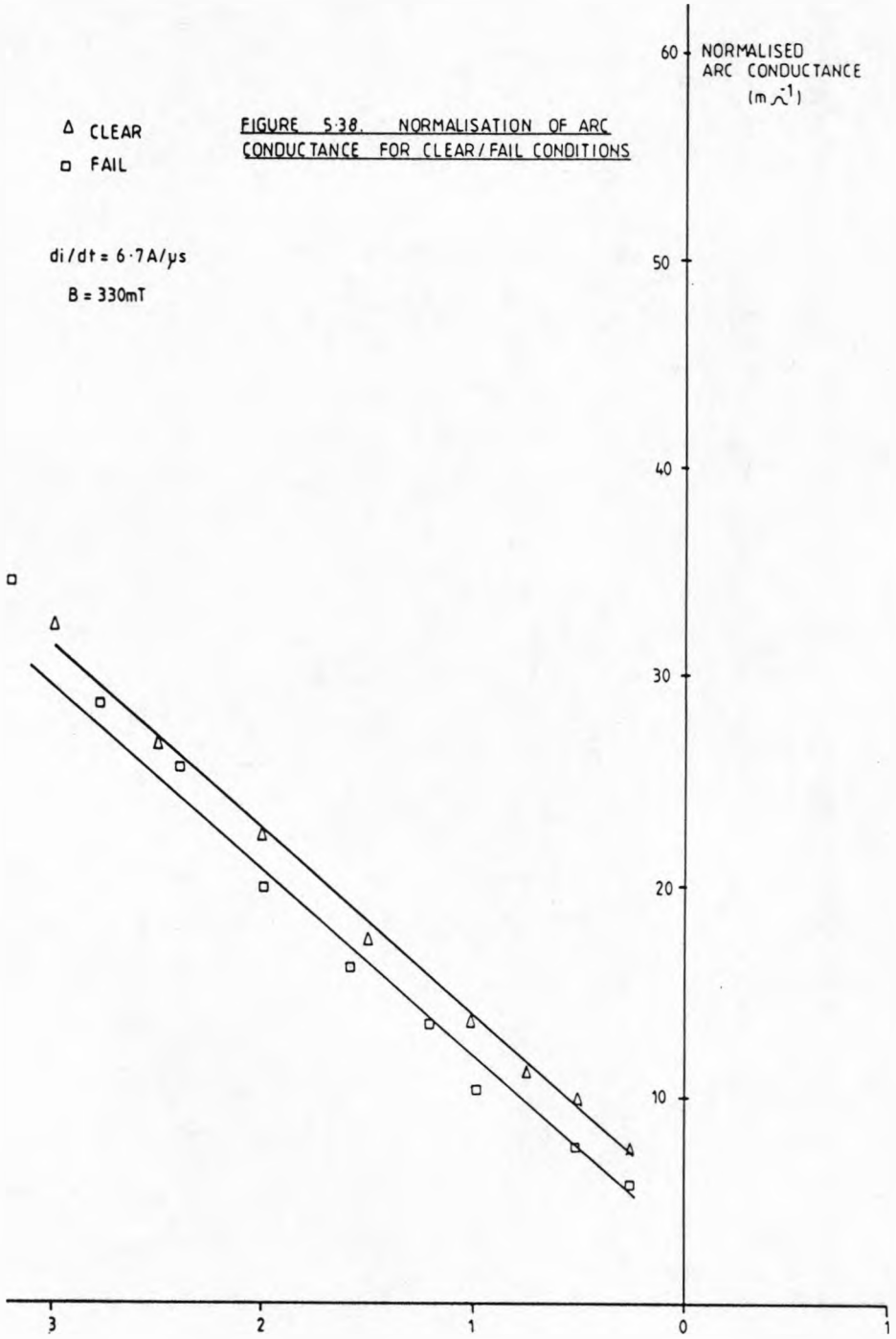

FIGURE 5·38. NORMALISATION OF ARC CONDUCTANCE FOR CLEAR/FAIL CONDITIONS

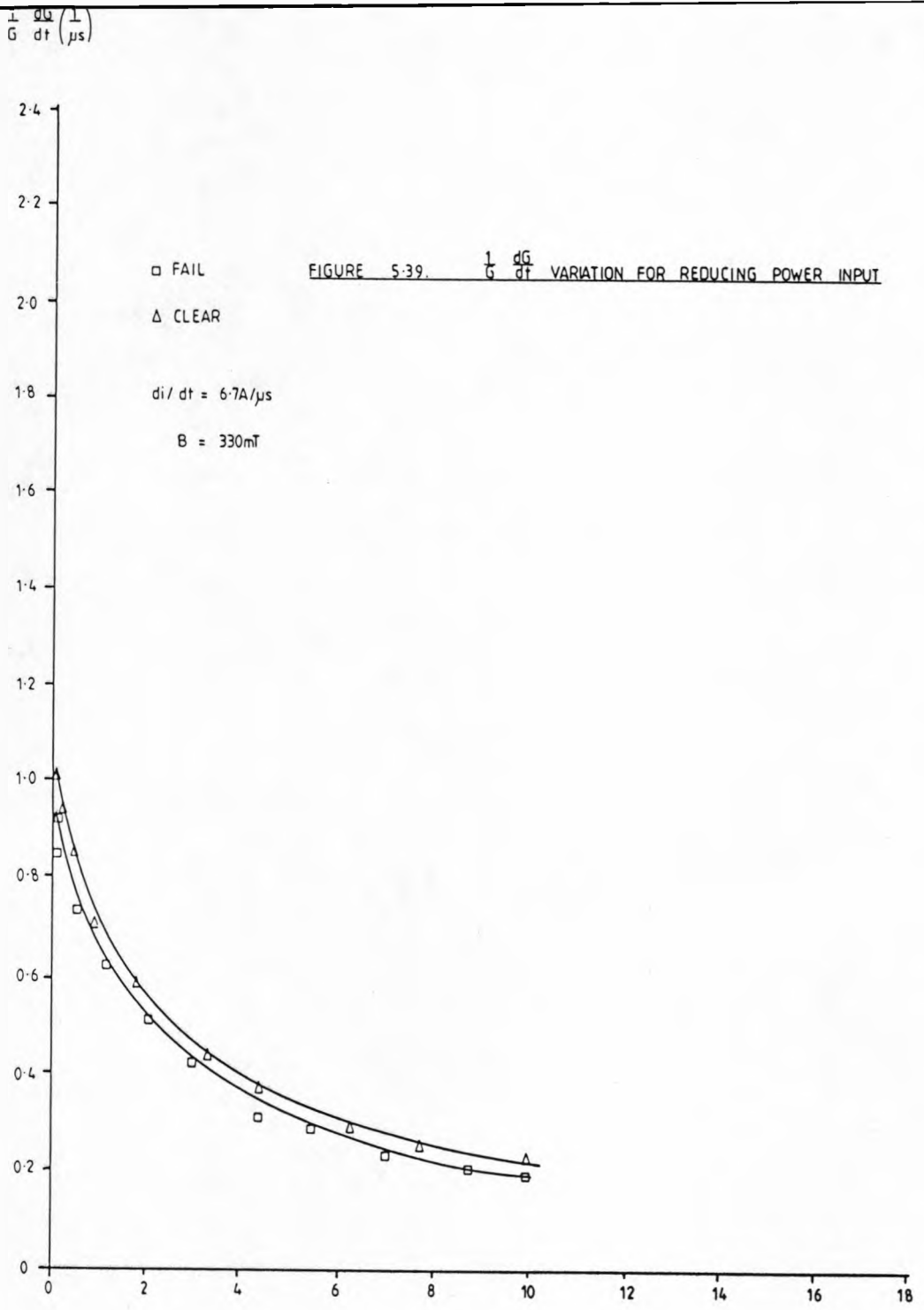

FIGURE 5·39. $\frac{1}{G}\frac{dG}{dt}$ VARIATION FOR REDUCING POWER INPUT

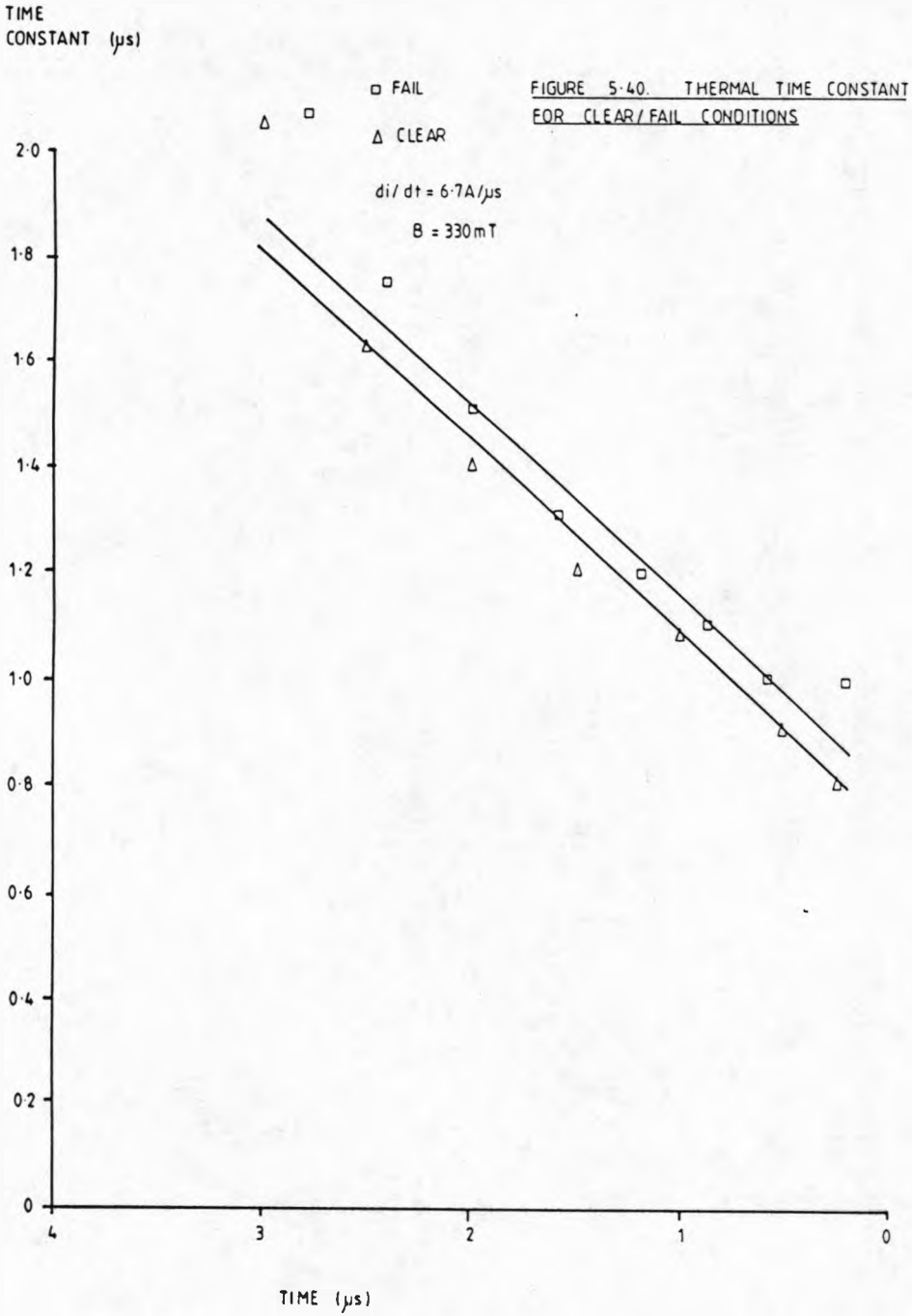

FIGURE 5·40. THERMAL TIME CONSTANT FOR CLEAR/FAIL CONDITIONS

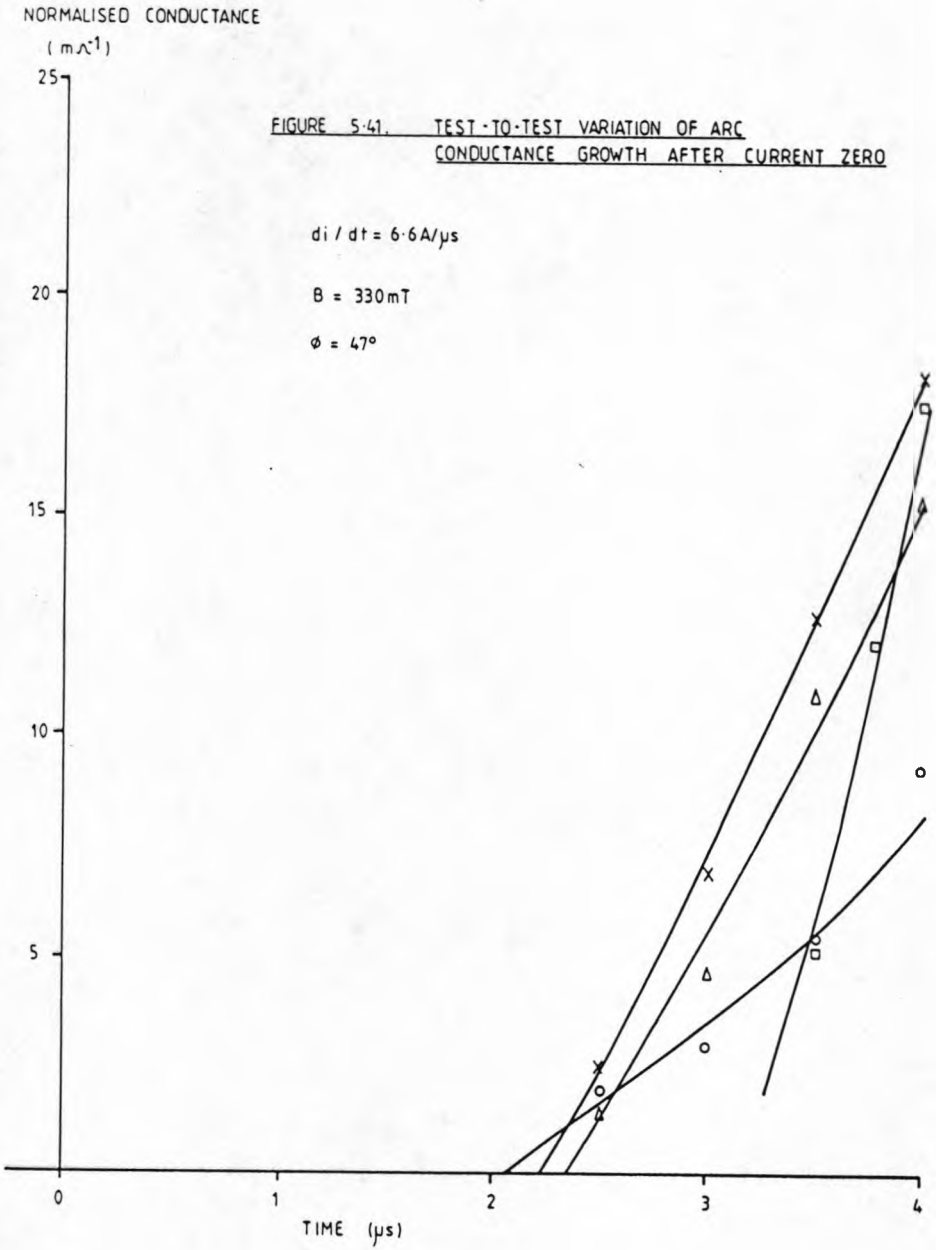

FIGURE 5·41. TEST-TO-TEST VARIATION OF ARC CONDUCTANCE GROWTH AFTER CURRENT ZERO

5.2.1.7 GROWTH OF ARC CONDUCTANCE DURING THE REINGNITION PERIOD

The conductance rises rapidly after arc reignition (figure 5.41). Each case shown is for the same conditions. The arc's conductance during the first two microseconds after current zero could not be detected. Subsequently the conductance increases rapidy leading to reignition within four microseconds following current zero which is consistent with thermal reignition trends.

5.2.2 THERMAL PERFORMANCE CHARACTERISTICS

5.2.2.1 INTERPRETATION OF THE DV/DT: DI/DT CHARACTERISTICS

The traditional manner of presenting the thermal performance characteristic for axial flow symmetric arcs is used for presenting similar results for the non-symmetric rotating arc column (figure 4.50). But for the latter case changing the di/dt for each coil also changes the magnetic field strength proportionally. Of course this increase in the magnetic field represents a change in an important arc controlling parameter. To isolate these two effects, lines of constant magnetic flux are drawn onto figure (4.50) as shown on figure (5.42), only the flux line representing 442 mT is shown. The point of intersection of a constant magnetic flux curve and a thermal performance curve gives a set of

uniquely defined values of dv/dt and di/dt. These values can be plotted onto a graph which is of dv/dt: di/dt for constant magnetic flux densities and one phase difference angle.

The results of this recasting is shown on figure (5.43). As expected the thermal performance degrades as di/dt increases. For a given phase difference angle (for example 80° phase lag) the performance curves are parallel for various magnetic flux density values. For all cases the d^2v/dt^2 is zero for each curve. A larger magnetic flux density promotes a better rrrv value for a given di/dt.

The influence of the phase difference angle is more readily shown through a comparison of curves "C" and "D". Curve "C" represents the thermal performance of an arc column in a magnetic flux density of 605 mT, a phase difference angle of 47°, curve "D" is for a magnetic flux density of 535 mT and a phase difference angle of 80°. Although condition D is for a smaller magnetic field the thermal performance over this range investigated is much better. A larger phase angle improves the withstand voltage of the arc column after current zero for a given di/dt, particularly at higher values of di/dt.

Another difference between curves "C" and "D" is that

the gradient of each is different. The smaller phase difference curve has a steeper gradient, so that the thermal performance degrades much more severely than for a higher phase angle.

The form of the thermal performance curve is related to the thermal condition of the arc column at current zero which in turn depends upon the conditioning of the column during the whole of the arcing cycle by the magnetic filed both in terms of it's magnitude and phase. These factors are discussed later.

5.2.2.2 EMPIRICAL ANALYSIS OF PERFORMANCE CHARACTERISTICS

The recent results shown on figure (5.43) allow some empirical relationships to be established which should be useful for future design considerations.

The performance characteristic is of the form,

$$\left.\frac{dv}{dt}\right|_{crit} = KB^{a}\left(\frac{di}{dt}\right)^{-b} \qquad (5.27)$$

where the indices a,b and the constant of proportionality k are all functions of the phase angle (ϕ). For a 47° phase difference angle these values are 2.3, 2.5 and 3.9 x 10^{26} respectively and for the larger 80° phase lag 1.8, 2.0 and 1.7 x 10^{17} respectively (k has units of V/AT).

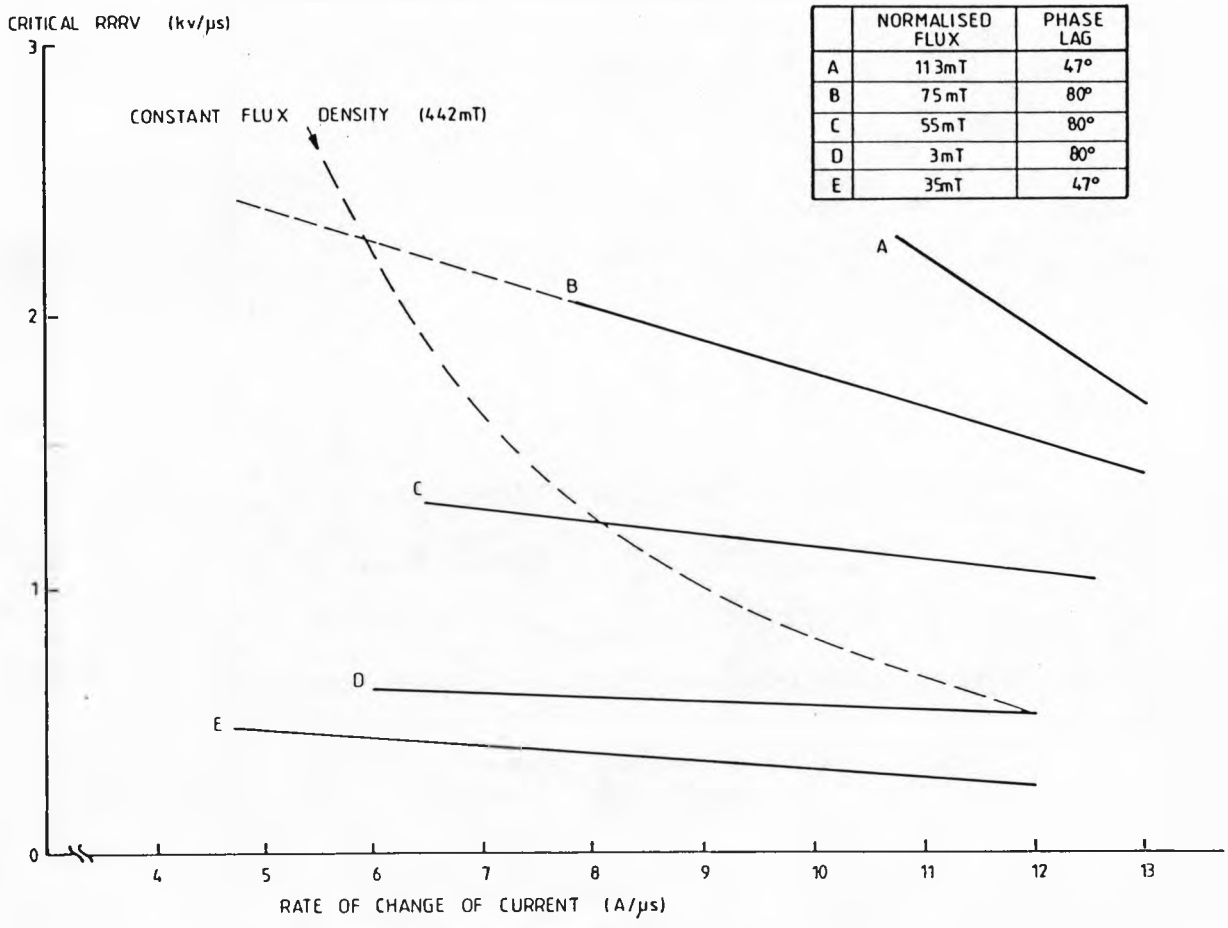

	NORMALISED FLUX	PHASE LAG
A	113mT	47°
B	75mT	80°
C	55mT	80°
D	3mT	80°
E	35mT	47°

FIGURE 5.42 CONSTANT MAGNETIC FLUX CURVE

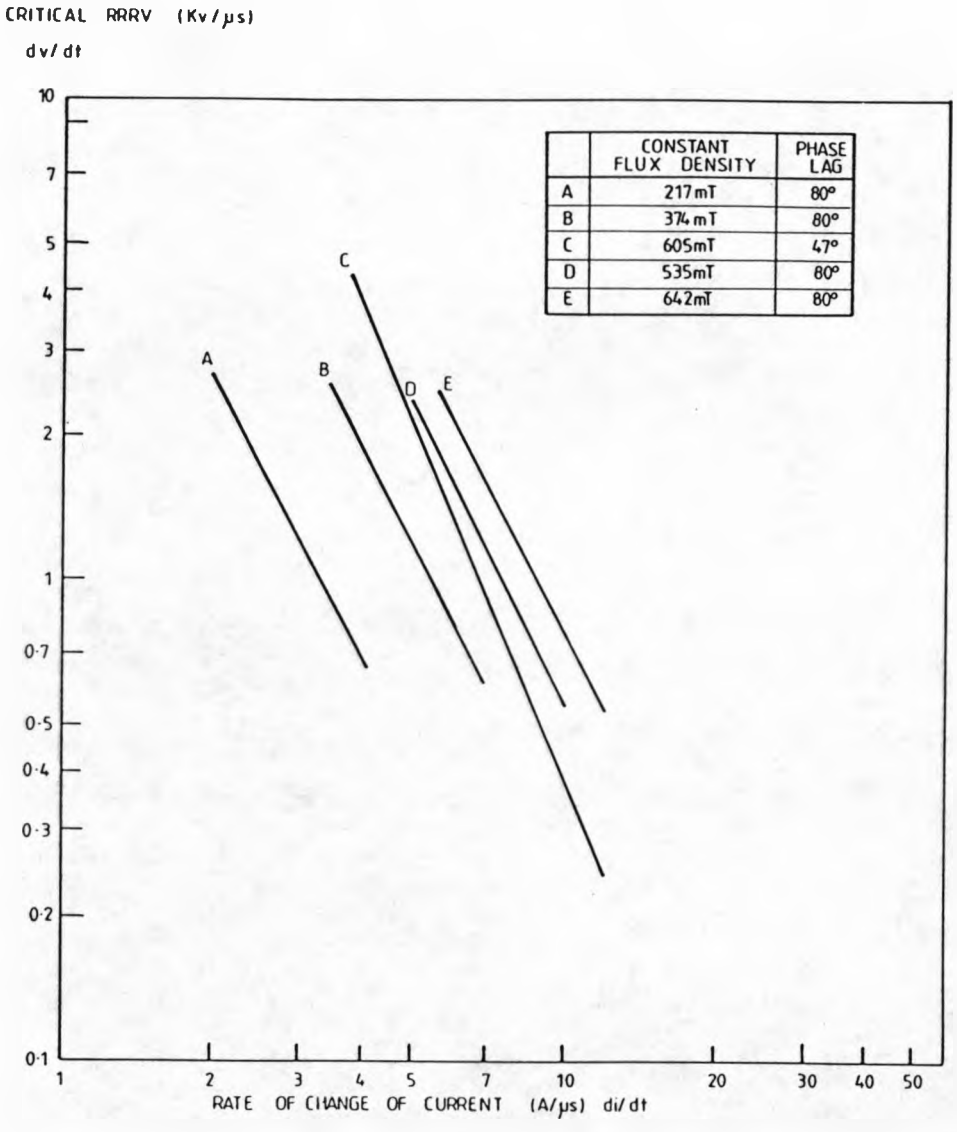

FIGURE 5·43 RECAST THERMAL PEFORMANCE CHARACTERISTIC

It is interesting to note that the indices of the di/dt is different for each phase difference angle reflecting the various gradients of performance. This phenomena is an end product of the delay in the arc's velocity and the delay in the forced convection losses. The power to which the magnetic field is raised is also altered by the change in the phase difference angle, this decreases with an increase in phase difference angle. The effect of magnetic field is to increase the magnitude of the critical dv/dt. The constant K is reduced by the increase in phase difference angle.

5.2.2.3 PARAMETERS CONTROLLING THE PERFORMANCE

The arc properties at current zero is governed by the conditioning produced during the previous half cycle of current. This conditioning is most conveniently monitored in terms of those parameters which are easily measured (I,B,U,rrrv, arc length etc). Although the influence of those parameters upon the thermal structure and electrically conducting area of the arc column is difficult to assess for this particular case information from other experimental investigations can be used to provide a better understanding.

The similarity between the trends in the parameters which control the arc's velocity, rrrv, Mayr time constant and arc conductance is self consistent and

correct from an arc physics point of view. It is clearly advantageous to have the minimum possible energy storage in the arc column at current zero. This storage of thermal energy may occur either as an increase in the arc's temperature or as an enlargement of the arc's area.

In the rotating arc the energy loss is strongly influenced by the arc's velocity u(t). This is a maximum after peak current because the Lorentz force and the already decaying area of the arc column reducing the retarding drag force. The strongest external influence upon u(t) is provided by the magnetic field B(t). The evidence of figures (5.34, 5.11, 5.12) indicates that for a fixed peak velocity the thermal performance improves as the instant of peak velocity moves nearer to current zero over the range monitored. For similar magnetic fields and rates of change of current, the performance is better for the larger phase angle, despite the maximum arc velocity being less and the conductances before current zero being similar.

It is believed that this behaviour is due to different arc column structures produced by the different convective influences.

5.3.2 CONCLUSION

A number of features need to be considered before

attempting to interpret the results reported above. These include the complex interaction between the spatial and temporal variations in the magnetic field and the possible orientations of the arc column. As a result a highly complex set of Lorentian forces are produced which continually change with the arc's orientation.

It has been shown that the arc column moves rotationally and axially into the coil. The depth of penetration is governed by both magnetic trap considerations as well as electromagnetically induced instabilities.

The velocity with which the arc column moves is governed by many factors which include the magnitude and phase of the magnetic field, the gas density and to a lesser extent the arc current. The extent to which this velocity controls and finally conditions the arc column is reflected in conductance variation prior to current zero and in the Mayr time constant during the current zero period.

These parameters are highlighted in the empirical description of the thermal performance of the arc column. The most influential of these parameters is the magnetic field.

In order to give a deeper appreciation of the interrupter behaviour, a theoretical assessment of the arc column is undertaken in the next chapter. This

constitutes a computer aided design package which examines the influence of the above factors upon the arc's velocity and ultimately it thermal performance characteristic.

6. COMPUTER AIDED MODELLING

The degree of complexity introduced into a theoretical description of an arc column with a finite radius of curvature makes the solution of energy and momentum equations difficult if not impossible from a purely theoretical treatment. To obtain reasonable solutions to such equations and an estimate of the arcs behaviour recourse is made to a mixture of detailed theoretical analysis and approximate empirical formulation.

An approximate solution of the arc column's behaviour for a set of input conditions should be able to predict the arc column area, temperature, velocity, electricial conductance and electric field with some reasonable accuracy.

The overall ideal design package is shown on figure (6.1). It consists of three sub-groups which deal with field related computations, arc modelling and circuit influences which subsequently lead to a description of the interrupter's performance. These three sub-groups can be further sub-divided. For instance, the field calculations can be sub-divided into three groups concerned with aerodynamic, magnetic and electrical influences (figure 6.2). The aerodynamic and thermal fields are used to predict pressure transients and gas flows produced by the arcing. Experimental results have

shown that over the current range investigated such pressure transients are small so that to a first approximation they may be neglected. The second section concerns the magnetic field calculations and the distribution of the magnetic flux within the arcing volume. Such calculations were made by Chen and Turner (85) for the present arcing environment. At present only an approximate model with an average magnetic field (no spatial variation) is considered as a simulation of the true situation within the arcing coil. The third section deals with both the electric field associated with the arc during arcing and also system induced field distribution following arcing and the subsequent likelyhood of dielectric breakdown. The case of dielectric breakdown studies was outside the scope of the present investigation. Consideration also needs to be given to the mechanical strength requirements for the field producing coil when subjected to the compressive action of the self produced field. Field calculations (e.g. Chen and Turner (85)) consider the shielding effect of the annular arc contact (which also acts as the yoke); the eddy current flow in this contact and the delay in field growth and produced by these eddy currents. Consideration also needs to be given to geometric and material influences.

The second sub-group that of the computational package

deals with aspects of the arc modelling (figure 6.3). The modelling involves calculating the velocity of the various arc plasma elements, the geometric shape of the arc plasma column, the stability of the arc column, the energy conservation in the arcing environment, the response of the arc column to network stimulii and particularly it's thermal recovery behaviour. A series of such calculations allows the conventional Rate of Rise of Recovery voltage: current decay rate characteristic to be determined. Since the estimates of arc velocity and arc shape are closely related they are more conveniently treated together.

As discussed earlier the arc column rotates with a fixed annular velocity having a finite radius of curvature therefore with individual plasma column element having identical velocities. However, disturbing influences may be produced by electrode phenomena which for instance may produce arc elongation. Since these electrode regions form only a small fraction of the arcs length, losses associated with this region are neglected in the present approximate model (31,33,34,36). Furthermore experimental verification of the uniform nature of the arc column as provided by the correlation between the arc length and voltage as well as the fact that all elements of the arc column have identical velocities allows the modelling to be made per unit length of the

arc column.

At this approximate level of modelling arc instabilities are ignored, since the inward movement of the arc column relative to it's major velocity component is small and consequently the convected loss attributable is neglected. Although such instabilities elongates the arc column the correlation between arc length and voltage is not violated.

The equations governing the behaviour of the arc column are formulated in the following sections. These will describe the arc column during the peak current phase of arcing and the current zero period. The thermal reignition behaviour after current zero is also investigated.

The third modelling sub-group deals with the interactions with the external circuit (figure 6.4). The phase shift between the coil exciting current (i) and the resulting field is important when considering the momentum conservation equations. The problem of multiple loop arcing where two or more loops of arc exist in the coil volume to produce additional current carrying turns has been over come by considering a representative length of arc column and the induced voltage from such multiple loops can be shown to be negligible (section 5.1.3.3.).

COMPUTER AIDED DESIGN PACKAGE FOR ROTARY ARC INTERRUPTER

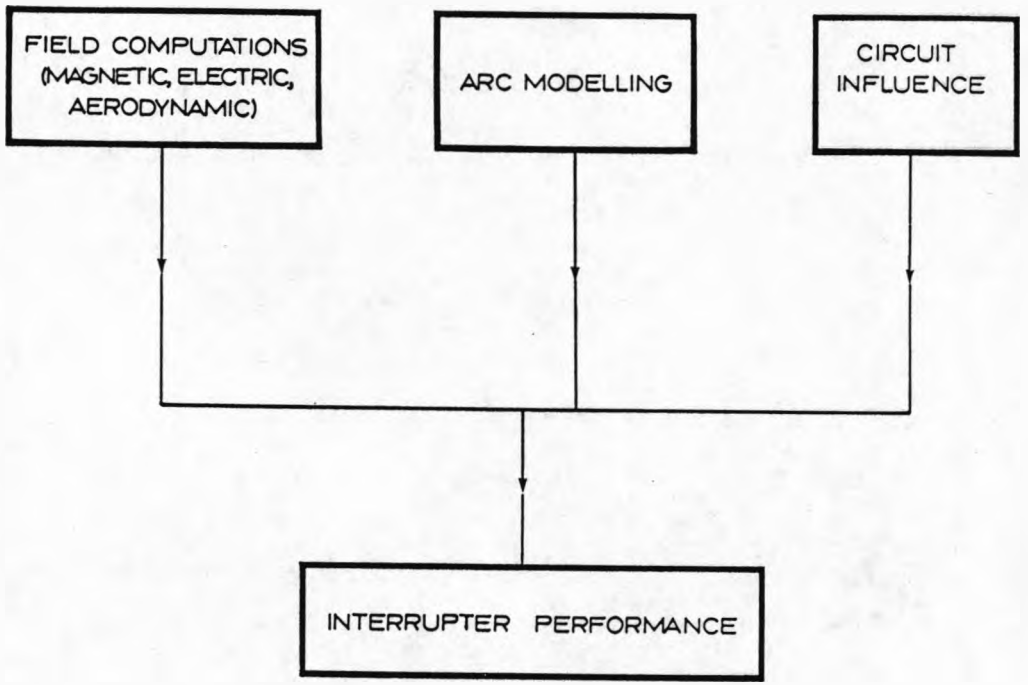

FIGURE 6·1. DESIGN PACKAGE

FIELD CALCULATIONS

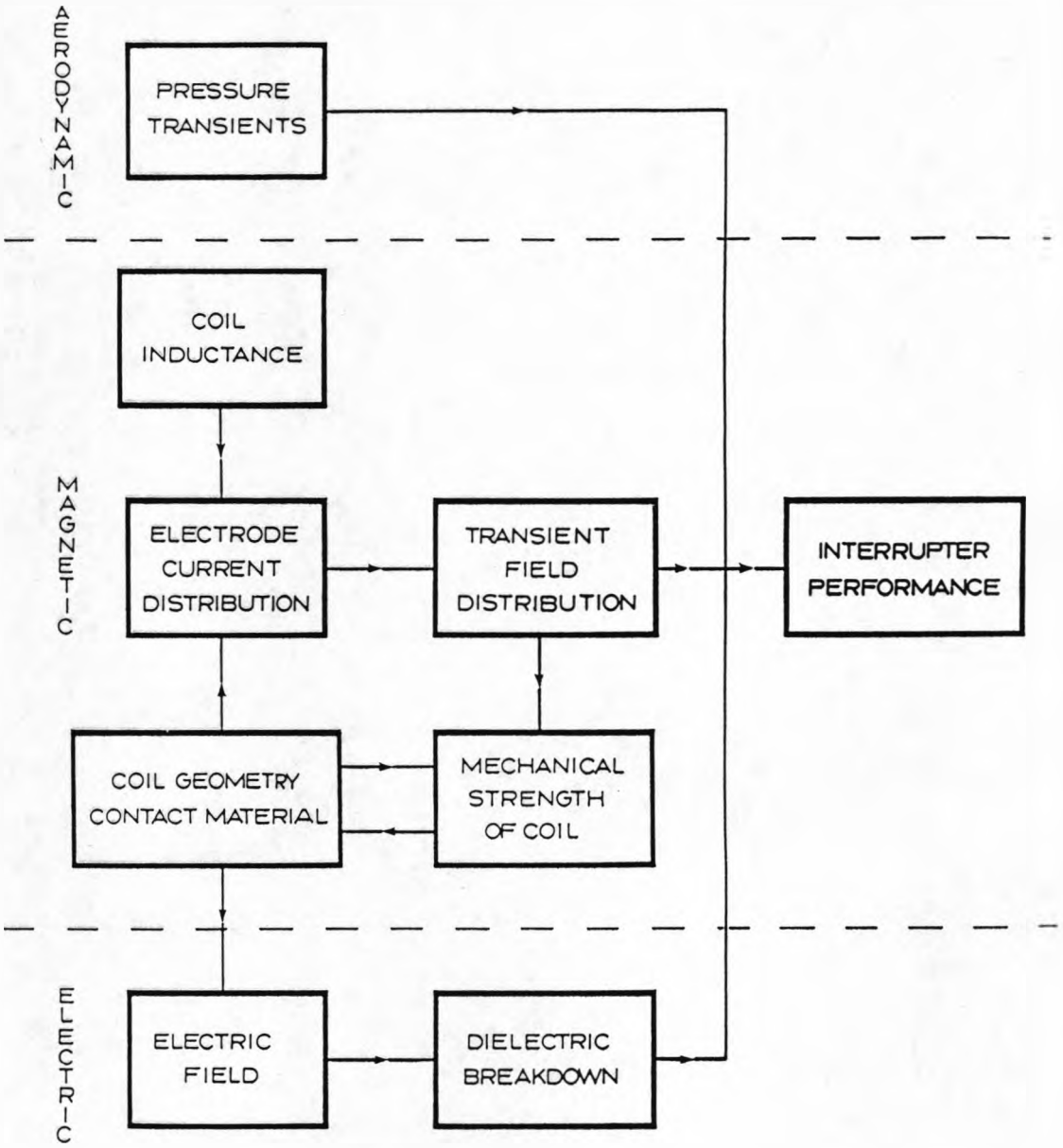

FIGURE 6·2 FIELD CALCULATIONS

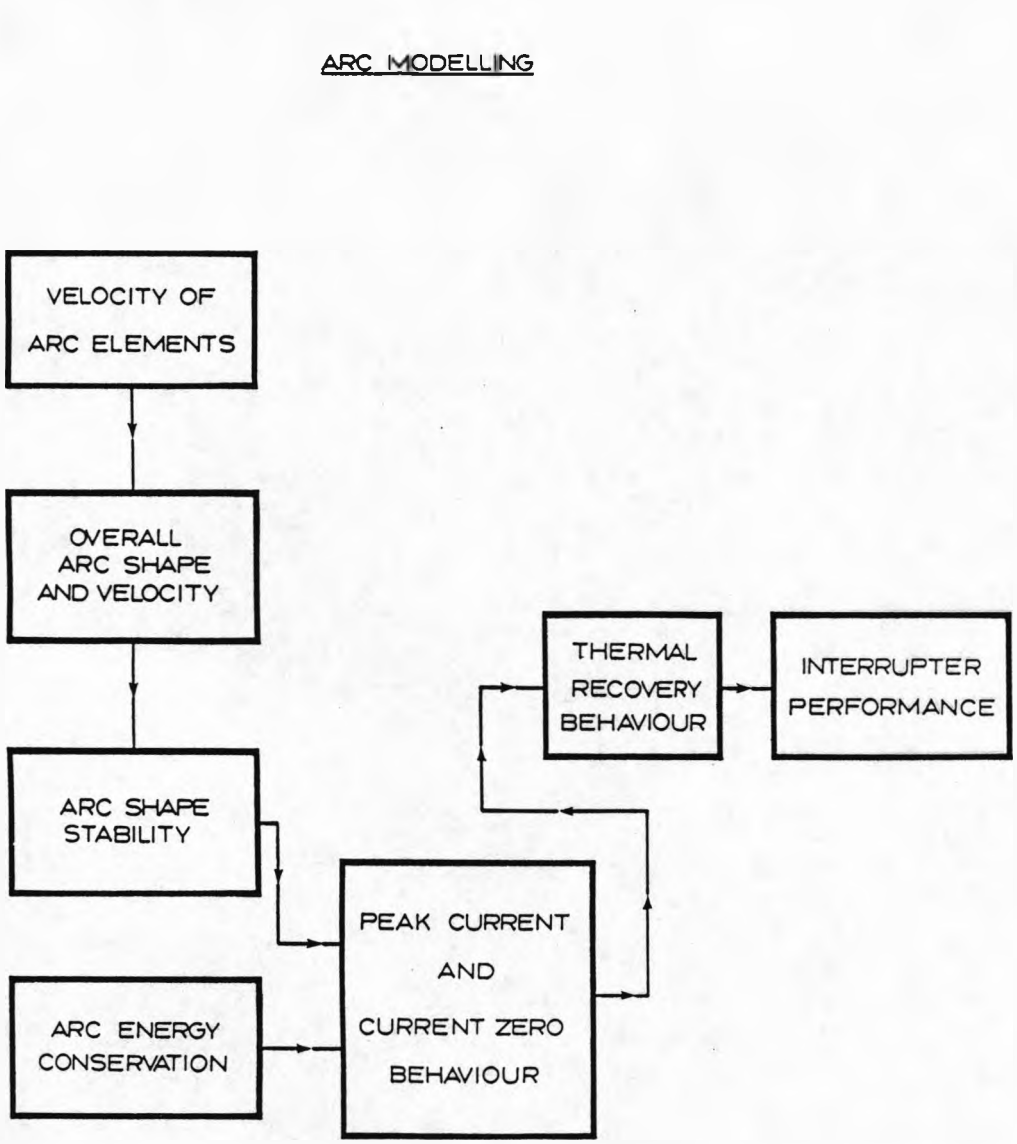

FIGURE 6·3. ARC MODELLING

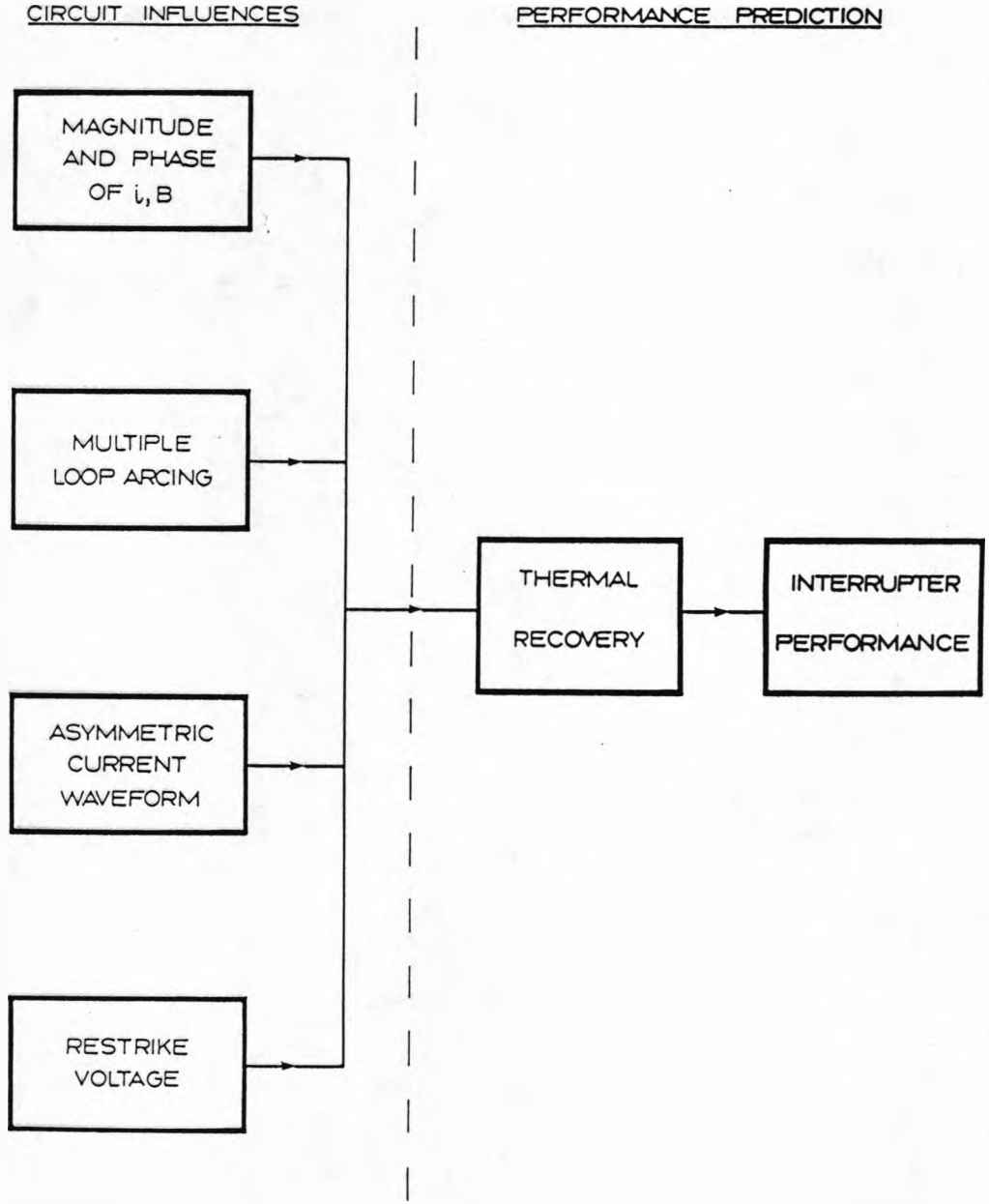

FIGURE 6·4. CIRCUIT INFLUENCES

The third section considers the asymmetric fault currents whereby a D.C. component is superimpsed upon the alternating current component so leading to alternate major and minor half cycles of current. Finally the modelling of the restrike voltage produced by the power circuit needs to be incorporated for performance predictions.

These sections can be brought together in a computer package to highlight the effects on thermal performance of charging one or more parameters. Since the crucial focus of this computer package is probably the arc modelling with its diversity of requirements particular attention is given to this aspect in what follows.

6.1 PEAK CURRENT ARC MODEL

6.1.1 SIMPLIFIED ARC MODEL

Major problems in realising a model of the magnetically rotated arc arise from the increased number of variables compared with for instance stationary axisymmetic arcs and also the reduced amount of experimental information which is available for such non-axisymmetric arcs. The first requirement is therefore to reduce the number of variables by attempting to eliminate the spatial variations and replacing them with averaged quantities. This approach may be applied by considering two spatial zones. The first zone is within the arc column itself

where the arc current is conducted, where temperatures and conductivity are high and gas density low. The other zones represent the cooler ambient region through which the arc rotates, where temperatures are low, the conductivity negligible, the gas density relatively high, no current is conducted through this region.

A major difficulty with this two zone type of model is the absence of a boundary layer region between the two zones which determines the transfer of energy from one zone to the other. Such a boundary region represents a transition between a highly conducting arc region to a non conducting ambient region. Consequently, it is essential to utilise a three zone method to describe a rotating arc column. This is the approach used here.

Each zone can be described by a set of energy, balance equations, ohms law, radiation and momentum conservation equations. However, each zone is dependent upon the other two reflecting the complex interaction between the arc and the ambient gas. Because of this interaction and lack of experimental information it is impossible to calculate precisely all the parameters needed to construct a complete picture fo the arc's behaviour. Where possible empirical descriptions derived from experimental results presented here and also by other authors has been used to add extra detail to the arc model. The assumptions used in each region

together with the empirical laws are now discussed in relation to each region.

6.1.1.1. ARC CORE REGION

The arc core refers to the highly conducting region which carriers the arc current and is therefore subjected to ohmic heating as a power input phenomena which can increase the internal energy of the gas. The power input is balanced by power losses.

The radiation loss is the gross loss (without absorption) by the surrounding gas but may be estimated empirically from a knowledge of the theoretical radiative properties such as those published by Lowke (89). Such theoretical values refer to the pure plasma and do not include contamination caused for instance by the injection of copper vapour from the electrodes into the arc's core. For the high current conditions the rotary arc investigated is contaminated by copper vapour which is present within the arcing chamber as indicated by deposits of copper metal found on the inspection window after one half cycle of high current arcing. Thus to obtain a more realistic value of the emission coefficient for the prevailing high current arcing conditions adjustment needs to be made to the pure SF_6 values given by Lowke. The adjustment factor can be calculated from the core energy balance equation and

experimental information about temperature and pressure for axial flow arc's with copper contamination (48). The magnitude of the new emission coefficient for copper contaminated SF_6 is found to be twice that for pure SF_6. This new estimate can be used for the high peak current modelling.

The other important loss from the arc is by thermal conduction. In general it is difficult experimentally to identify separately this loss from other loss mechanisms. However an order of magnitude estimate of this loss may be made using results obtained for wall stabilised arc columns where the dominant loss is known to be by thermal conduction. Freeman (90) has investigated the transient behaviour of such cylindrical arc columns, resulting in a theorectical description of the conduction loss for particular cases.

The thermal conduction term in cylindrical co-ordinates may be written as the sum of two terms

$$\frac{k}{r}\frac{dT}{dr} \qquad (6.1)$$

and

$$k\frac{d^2T}{dr^2} \qquad (6.2)$$

Where the thermal conduction coefficient (k) is choosen to be an averaged value across the entire arc column.

These two terms which are derived from the overal thermal conduction term represent losses which are dependent upon the temperature profile but differ from each other because (6.1) represents a loss which is a function of the gradient of the temperature profile whilst (6.2) is a function of the rate of change of this gradient.

To position these two terms into the energy balance equations, there influence on a particular region has to be assessed. This is done by assuming a triangular temperature profile for the arc and choosing a position of maximum temperature (on the axis) (6.2) would dominate because (dT/dr = 0). Therefore (6.2) can be assigned to the energy balance equation describing the core region and (6.1) assigned to the energy balance equation describing the boundary region because $d^2T/dr^2 = 0$

In general the radial temperature profile in the arc column may assume any one of a complex distribution particularly for the rotary arc case it is nonetheless interesting to consider the case of a representative profile in order to establish typical values for the thermal conduction loss. A reasonable but nonetheless mathematically tractable temperature profile is the parabola.

$$T(r) = T - \frac{\Delta T r^2}{r_o^2} \qquad (6.3)$$

The first differential gives

$$\frac{dT}{dr} = - \frac{2r\Delta T}{r_o^2} \qquad (6.4)$$

and a second differentiation gives

$$\frac{d^2T}{dr^2} = - \frac{2\Delta T}{r_o^2} \qquad (6.5)$$

Note that the first term increases with arc radius from zero at the arc axis whilst the second remains constant. This then provides an approximate estimate of the magnitude of the thermal conduction terms when taken in conjuction with (6.1 and 6.2).

In addition to the radiative and conduction losses consideration also needs to be given to convective losses as well as energy storage due to themal capacity. At this level of approximation being considered the convective losses within the arc core are neglected (but are included in the boundary region; section (6.1.1.2). The stored energy may be expressed in terms of the enthalpy of the plasma and its rate of change determine whether it contributes as a power loss or input.

An appropriate time dependant energy conservation may then be written for the arc core and assuming radially invariant plasma properties as:

STORED = OHMIC - GROSS - CORE

ENERGY HEATING RADIATION CONDUCTION

$$\rho A \frac{\delta h}{\delta t} = \left\{ \frac{I^2}{\sigma A} \right\} - \varepsilon A - \frac{2 \Delta T k}{r_o^2} \qquad (6.6)$$

Where;

ρ = average mass density

A = average arc area

σ = average electrical conductivity

h = average enthalpy

I = arc current

ε = average emission coefficent

T = core/Boundary temperature differences

It should be noted that the radiation loss dominates over the conduction loss within the arc core so that the approximate nature of the conduction term may be tolerated without serious error.

6.1.1.2 BOUNDARY REGION

The boundary region is taken to represent the transition between the electrically conducting arc core and the non conducting ambient region. Losses from the arc core appear as power inputs into the boundary region. In the case of radiative transfer part of the radiative power is transmitted unimpeded across the boundary region whereas the remainder is absorbed and then ultimately dissipated by convection, boundary conduction and the

heating of any mass entrained. Thermal conduction losses from the core are also dissipated in a similar way. Any imbalance is stored as thermal energy, which is manifest as a change in arc area.

The net radiative loss across this boundary region may be described empirically using the laws derived experimentally by Strauchan et al (93). It is proposed to apply these empirical laws for the radiative power loss to the rotary arc case in order to further simplify the modelling.

The radiation loss may then be written as a fraction of the electrical power input ($I^2R = I^2/\sigma A$);

$$\text{Radiation loss} = \frac{\alpha I^2}{\sigma A} \qquad (6.7)$$

where experiment indicates that $\alpha = 0.2 - 0.4$

The effect of convection although neglected in the arc core makes a major contribution to the overall losses and in the present model is incorporated in the description of the boundary region. The convection term is modelled using the Nusselt number which gives

$$\text{Convection loss} = \text{Nuk}\pi\Delta T \qquad (6.8)$$

Nu = Nussett number

k = thermal conductivity

ΔT = temperature difference between the boundary and the ambient region.

The Nussett number may in turn be related to the Reynolds number (Re) using experimental results obtained for a rotating arc column is mutually orthoganol magnetic and flow fields (92). This relationship is

$$Nu = 0.2\ Re \qquad (6.9)$$

The Reynolds number is in turn related to the gas properties according to

$$Re = \frac{2\bar{\rho}UA^{1/2}}{\mu\pi^{1/2}} \qquad (6.10)$$

$\bar{\rho}$ = average mass density of the incoming flow,

u = flow velocity

A = arc area

μ = average viscosity coefficient of the flowing gas

The energy loss per unit length of arc column due to convection may then be written.

$$Q_{conv} = \frac{0.4\pi^{1/2}A^{1/2}k\bar{\rho}U\Delta T}{\mu} \qquad (6.11)$$

So that the loss of energy due to convection can be estimated from known parameters and properties of the arc and SF_6. But this empirical loss also represents conduction losses when the arc column is moving. When the arc velocity is zero this hidden conduction in this empirical term also dissappears. Provision has to be made to assess the magnitudes of this empirical convection loss term and the following thermal

conduction term and then ommitting one term when the other dominates.

Thermal conduction across the boundary region is believed to be an important parameter. Consistent with the approximate modelling being proposed this conduction loss has been described using results derived by other authors (90).

As already indicated the conduction loss is rigorously given by (Freeman and Jones 90).

$$Q_{cond} = \int_0^{R_c} \frac{1}{r}\frac{\delta}{\delta r}\left(kr\frac{\delta T}{\delta r}\right)2\pi r\,\delta r \qquad (6.12)$$

Rc = boundary radius.

To reduce the complexity of equation (6.12) the conduction term can be rewritten in terms of the heat flux potential (S) yielding

$$Q_{cond} = 2\pi^{1/2}A^{1/2}\left.\frac{\delta S}{\delta r}\right|_{R_c} \qquad (6.13)$$

Rc = Arc boundary

S = heat flux potential = $\int_0^T k\,dT$

For a wall stabilised arc Freeman and Jones (90)

$$S = S_1 + (S_0 - S_1)J_0\left(\frac{\beta x}{x_1}\right) \qquad (6.14)$$

x = normalised radius (r/Rw)

S_0 = value of s when $\sigma = 0$

$x_1 = r_1/Rw$

Differentiating (6.14) denormalising and substituting into (6.13) the expression for the loss due to thermal conduction becomes

$$Q_{cond} = 2(S_0 - S_1)\beta J_1(\beta)\pi \qquad (6.15)$$

β = the first Bessel zero

Equation (6.15) represent the magnitude of the thermal conduction at the arc's boundary. In the same way as equation 6.5 was used to describe the approximate thermal conduction in the arc core equation (6.15) is used to describe the approximate conduction across the boundary region.

The variation of the temperature due to excess energy input in the core also effects the boundary region since the temperature increase causes a mass density variation within the column. This term is given by;

$$Ah\frac{\delta\rho}{\delta t} \qquad (6.16)$$

This term represents a mass transport across the boundary region due to a temperature variation alone and does not include any convective induced effects.

It remains to consider the effect upon the energy storage of changes in the arc column area. Arc column expansion occurs into the cooler surrounding gas and

energy is expanded in this heating which can be written as

$$\rho(h - h_1)\frac{\delta A}{\delta t} \qquad (6.17)$$

The processes discussed above as represented by the terms (6.7 to 6.17) may be assembled to form the boundary region energy balance equation.

$$\rho(h - h_1)\frac{\delta A}{\delta t} = \varepsilon A - Ah\frac{\delta \rho}{\delta t} - \frac{\alpha I^2}{\sigma A} - 2(S_0 - S_1)\beta J_1(\beta)\pi - \frac{0.4\pi^{1/2}A^{1/2}k\bar{\rho}U\Delta T}{\mu} \qquad (6.18)$$

All quantities in (6.18) are known or can easily be calculated.

6.1.1.3 CORE/BOUNDARY EQUATIONS

Whereas equations (6.6) represents the power conservation within the arc core equation, (6.18) represents the power conservation within the boundary region. The overall power balance is therefore represented by the algebraic sums of the terms in these two equations, ie.

$$\frac{\delta(\rho Ah)}{\delta t} = \frac{I^2}{\sigma A} - \frac{\alpha I^2}{\sigma A} - \text{Conduction} - \text{Convection} + \rho h_1\frac{\delta A}{\delta t} \qquad (6.19)$$

Where conduction is defined by equations (6.2, 6.5 and 6.15) and convection is defined by equation (6.11).

The computer package involves the simultaneous solution of equation (6.6) and (6.18) to represent the overall arc column behaviour.

6.1.1.4 ARC VELOCITY EQUATION

In order to achieve this solution it is necessary to relate the rotational velocity of the arc column to the driving and retarding forces through the momentum conservation equation as embodied in equation (5.10) of section (5.1.2).

$$\frac{\delta U}{\delta t} = \frac{iB}{\bar{\rho}A} - \frac{RC_D\rho_\infty U^2}{\bar{\rho}A} - \frac{U}{\bar{\rho}A}\frac{\delta M}{\delta t} \qquad (6.20)$$

The parameter ρ_∞ in equation (6.20) which represents the mass density of the gas through which the arc column rotates needs to be specified. In section (5.1.2.3) it was established that the arc column may rotate through its own wake after only one revolution within the driving coil and that the maximum temperature of this gas would be 1900°k (86). Of course the temperature of the gas through which the arc rotates initially is ambient (300°k). The ensuing temperature and mass density variation may be modelled by allowing them to change exponentially so that after one approximate arc revolution the gas temperature is 1900°k as well as a change in mass density.

The value of the drag coefficient which also appears in equation (6.20) is between 1.5 - 1.7 (86) for a rotating arc and remains constant throughout the half cycle of arcing. The other parameters in equation (6.20) are determined by the external circuit or by the energy balance equations (6.16, 6.17).

6.1.1.5 BASIC MODEL

There are three main equations describing the arcs behaviour, these are the core and boundary energy conservation equations and a momentum conservation equation. The model neglects any arc length variation and assumes that there is no axial variation in the arcs properties. Electrode effects have been nelgected.

The model gives no details of the arc's thermal structure but only provides information about the average values of relevant parameters such as arc area and temperature. Expensive use is made of empirical relationships derived from the results of other workers.

6.1.2. PROPOSED SOLUTION METHOD FOR THE ARC EQUATIONS

The set of differential equations describing the arc's behaviour need to be solved simultaneously. The procedure is first used to satisfy the differential equations at a starting point before incrementing the time by one interval. Initial input conditions

therefore need to be defined.

6.1.2.1 INITIAL CONDITIONS

At a time equal to 25 μs which is taken as the initial time, a set of starting values are choosen for arc temperature, area, $\delta\rho/\delta t$ and $\delta A/\delta t$. The set of equations (6.6, 6.18, 6.20) are subjected to a mathematical relaxation routine for n iterations until the previous values for temperature, area etc are within a specified error margin with the next set of relaxation solutions. When this specified error margin is satisfied this is taken to represent the set of starting conditions for the simulated half cycle of arcing.

6.1.2.2. TEMPORAL SOLUTION

A forth order Runge-Kutta method is used to calculate a set of values for the arc at the next time interval. To eliminate error due to size of the time interval a relaxation routine is used at the end of each interval to adjust the values calculated until successive relaxation values are within the specified error. This procedure continues throughout the arcing half cycle until current zero.

6.1.2.3 COMPUTER ANALYSIS

The number of relaxation iterations and Runge-Kutta time intervals required make the entire calculation

labourous. An IBM 4341 and an IBM 3083 main frame computers were therefore used to these equations by the above method.

Figure (6.5) shows the flow chart for the computer aided analysis. The computer program is constructed in a "Top Down" method. Subroutines for various calculations are called from the main program. This method makes the program flexible so that it may be easily extended or amended as future developments demand.

The use of relaxation routines make the differential equations relatively insensitive to the size of the time interval provided it is smaller than the greatest rate of change of the arc's parameters. For this particular investigate the time interval is choosen to be 0.5 us. To further ensure the stability of the differential equations for this particular time interval a stringent error margin is imposed in the relaxation routines of better than 1 part in a million.

The up dating of temperature dependent quatities such as density, thermal conductivity etc, is controlled by a subroutine which can extrapolation the required value between to data points in the data file derived from (89, 94).

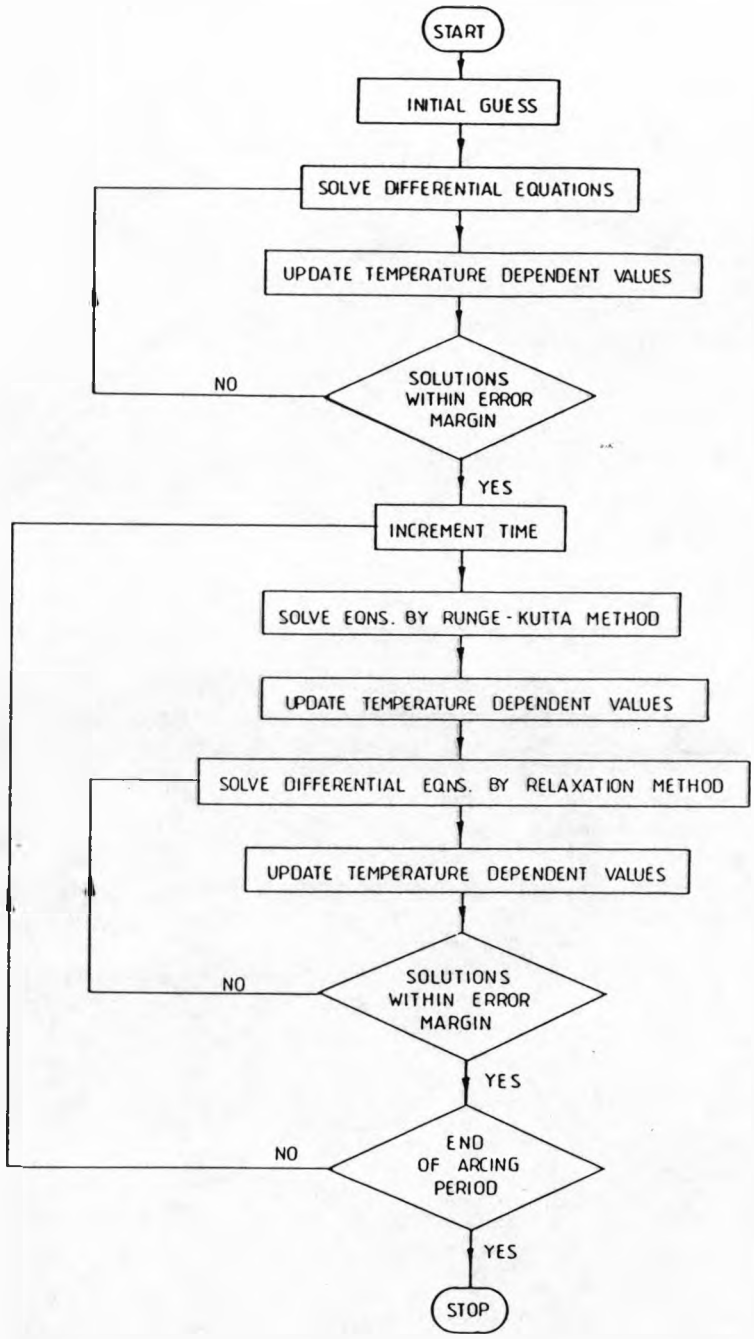

FIGURE 6.5. FLOW CHART FOR COMPUTER SOLUTION UPTO CURRENT ZERO

6.1.3 RESULTS OF COMPUTER SIMULATION

The input condition for which the arc equations are satisfied must encompass at least the same range over which the arc column was investigated. Several input values are chosen for the arc current, the magnetic field strength and phase difference angle. The input values were changed over the following ranges; the peak arc current was set to either 3kA or 18kA; the normalised magnetic flux density was either 47° or 80°. The choice of these values coincides with those used for the experimental investigations. The results for an 80° phase difference angle are presented in detail for illustrative purposes.

6.1.3.1 LOW PEAK CURRENT ARC SIMULATION

6.1.3.1.1 80° PHASE DIFFERENCE

Low peak current conditions refer to a 3 kA peak sinusoidal current. Figures (6.6, 6.7), show the results of this simulation for a normalised magnetic field of 35 mT/kA and an 80° phase difference angle. Figure (6.6) clearly shows the change in the arc's temperature, area and conductance over one half cycle of sinusoidal current.

During the first 200 μs of arcing the temperature of the arc rises rapidly from below 10,000°k to 13,000°k and

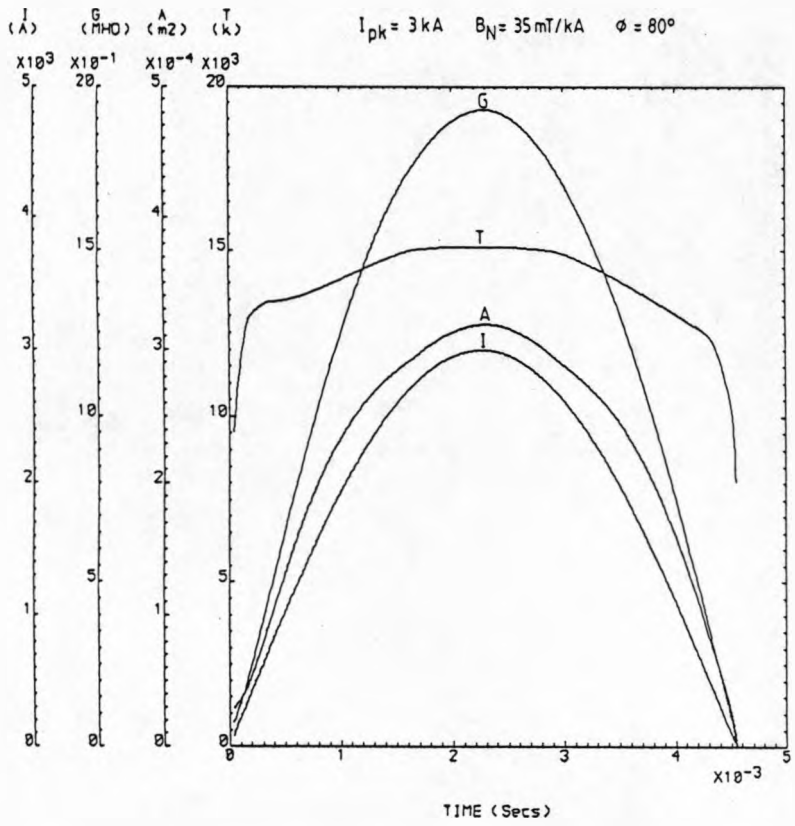

FIGURE 6:6 PEAK CURRENT RESULTS SHOWING ARC TEMPERATURE, AREA AND CONDUCTANCE VARIATION

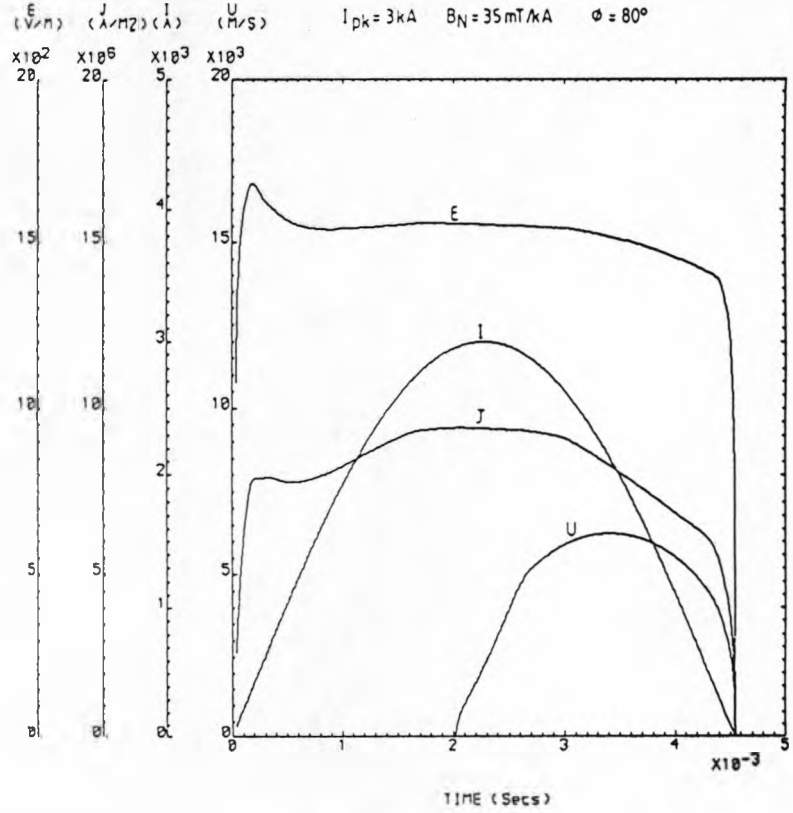

FIGURE 6 7 PEAK CURRENT RESULTS SHOWING ARC VELOCITY, CURRENT DENSITY AND ELECTRIC FIELD VARIATION

subsequently rises less steeply reaching a maximum of 15,000°k at peak current. During the peak current regime the temperature variation is slight. This rise in temperature reflects the increase in stored energy within the arc due to the imbalance between ohmic input and power losses.

After peak current the arc temperature begins to decrease moderately until 250 μs before current zero when there is a more rapid decrease. This reflects a substantial loss of stored energy from the arc column which is increased as current zero approaches.

Apart from these variations at the beginning and end of the half cycle, the arc temperature is relatively insensitive to the change in instantaneous current (therefore power input) throughout the remainder of the arcing period.

The arc's area changes in sympathy with the current although it is not a true sinusoid. The maximum area of 3.20×10^{-4} m^2 *occurs at peak current consistant with experimental observation. The increase and subsequent decrease in area shows the rise and fall in the level of stored energy within the arc column.*

The electrical conductance of the arc per unit length changes in sympathy with the input current and is a sinusoid with a peak value of 1.85 mho/M at peak current.

The arc conductance changes are of course consequent upon both the arc temperature and area variations.

Figure (6.7) presents results for the arc's velocity, current density and electric field over the half cycle of arcing.

The arc velocity is of course zero until the magnetic field has increased sufficiently to cause acceleration. Once the arc begins to move it accelerates rapidly upto a maximum of 150 m/s which occurs at 3.4 ms during the arcing cycle. This maximum velocity occurs between the Lorentz maximum and the magnetic flux maximum. Subsequently the arc's velocity rapidly decreases with the onset of current zero.

The current density reflects the deviation of the arc's area away from a true sinusoid. During the first 200 μs of arcing the current density rises rapidly to 8.9×10^6 A/M^2, after which the increase is less rapid and the current density reaches a maximum of 9.4×10^6 A/M^2 at peak current. Following peak current the current density decreases more rapidly and has a smaller value than for the same value of instantaneous current prior to peak current. This difference is due to the extra convection losses caused by the arc's movement. 200 μs before current zero there is a rapid fall in current density similar to the rapid rise within the first 200

μs of arcing.

The electric field during most of the half cycle is approximately constant at an average of 1500 v/m. However there are rapid rises at the beginning and at the end of the arcing cycle. During the initial increase the electric field reaches a maximum of 1680v/m at a time of 200 μs, but then this decreases to the approximately constant value.

The second rapid change in the electric field occurs during the last 200 μs of arcing. The electric field decays from 1500 to 0v/m within this period. These rapid chages are a result of the highly transient nature of the arc at these times.

Increasing the magnetic flux density from 35mT/kA to 55mT/kA does not cause a substantial change in the arc's electrical behaviour as shown by figures (6.8, 6.9). The transient nature of both arc column is similar and only the magnitudes alter by a small amount. The arc temperature has increased to 15,100°k, the arc area has decreased to 3.17×10^{-4} m^2, the conductance reflects these changes and reduce to 1.82 mho/m, the current density rises to $9.46A/M^2$ at peak current, the electric field is approximately the same its average value changing by 200 v/m and the arc's velocity increases to 190 m/s.

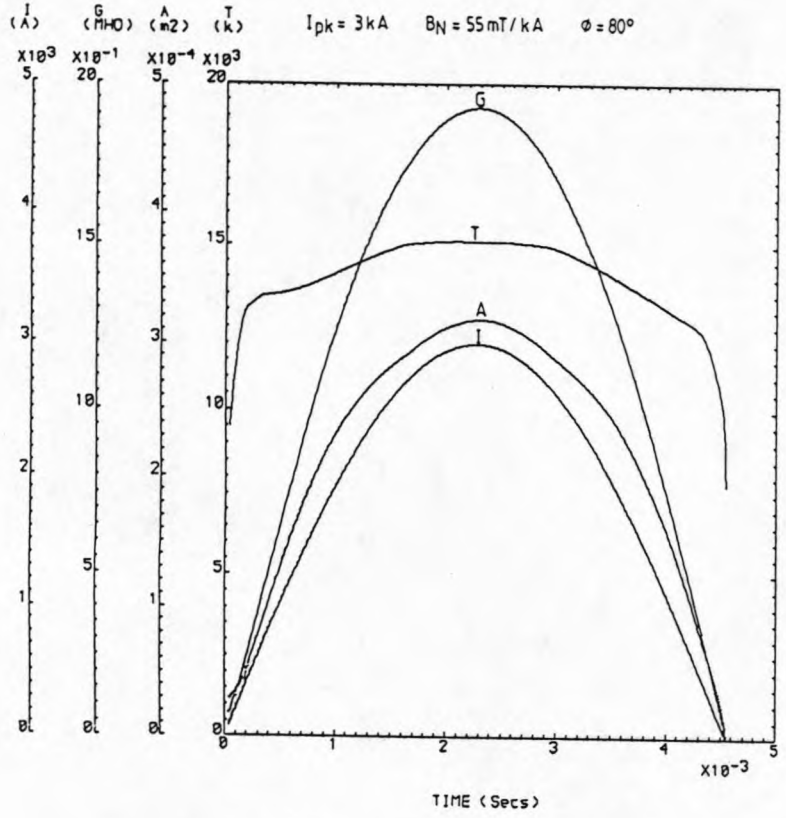

FIGURE 6·8. SIMULATED PEAK CURRENT RESULTS FOR THE ARC TEMPERATURE, AREA AND CONDUCTANCE

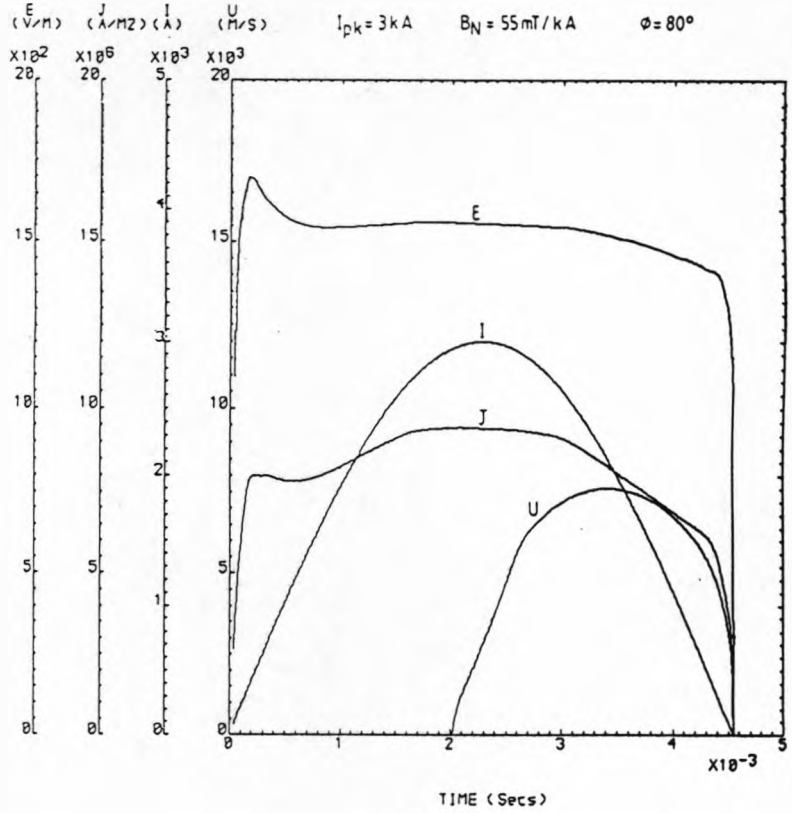

FIGURE 6·9. COMPUTER SIMULATION OF ARC VELOCITY, CURRENT DENSITY AND ELECTRIC FIELD

Increasing the magnetic field further produces a similar additional changes in the above quantities figures (6.10 and 6.11). These changes are summarised on figures (6.12, 6.13). Doubling the magnetic field increases the arc's velocity from 150 m/s to 220 m/s but the arc's temperature, area, conductance, electric field and current density change very little.

6.1.3.1.2 47° PHASE DIFFERENCE SIMULATION

Figures (6.14 and 6.15) are results obtained for a 3 kA peak current arc rotating in a 113 mT/kA normalised magnetic field with a 47° phase difference angle. There is no significant change in any of the arc parameters except the arc velocity. This has increased substantially to 318 m/s and because of the change in the phase difference angle this peak velocity is reached 3 ms after the beginning of arcing, between the maximum of the Lorentz force and the maximum of the magnetic field. The onset of arc movement commences 1.18 ms after beginning of the arcing cycle and rises rapidly to a maximum.

6.1.3.2 HIGH PEAK CURRENT ARC SIMULATION

The high peak current computer simulations are for 18 kA. Several normalised magnetic fields are investigated with two different phase angles.

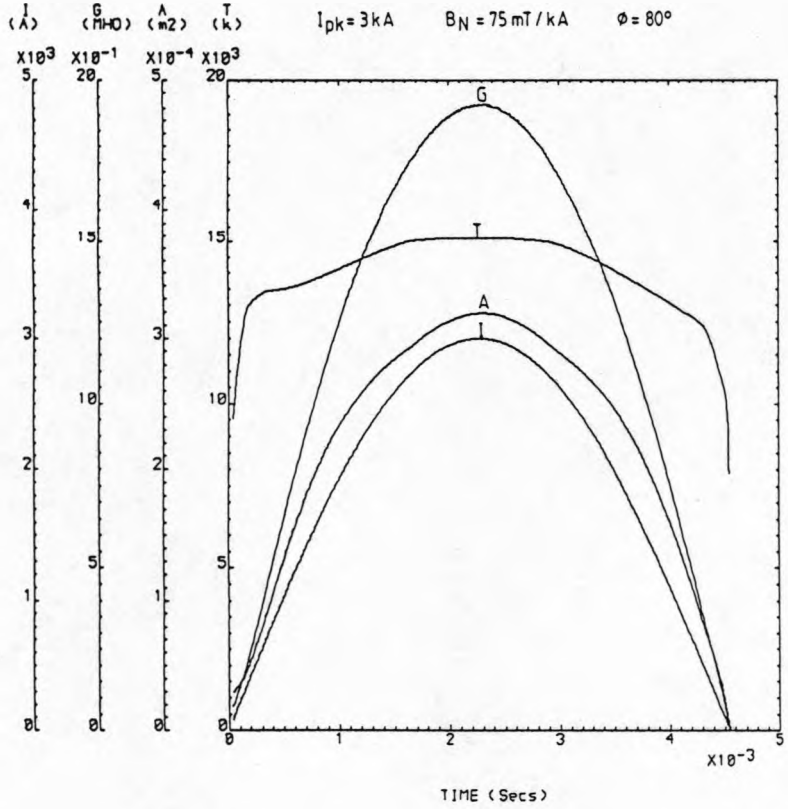

FIGURE 6·10 SIMULATED ARCING SHOWING ARC TEMPERATURE, AREA AND CONDUCTANCE

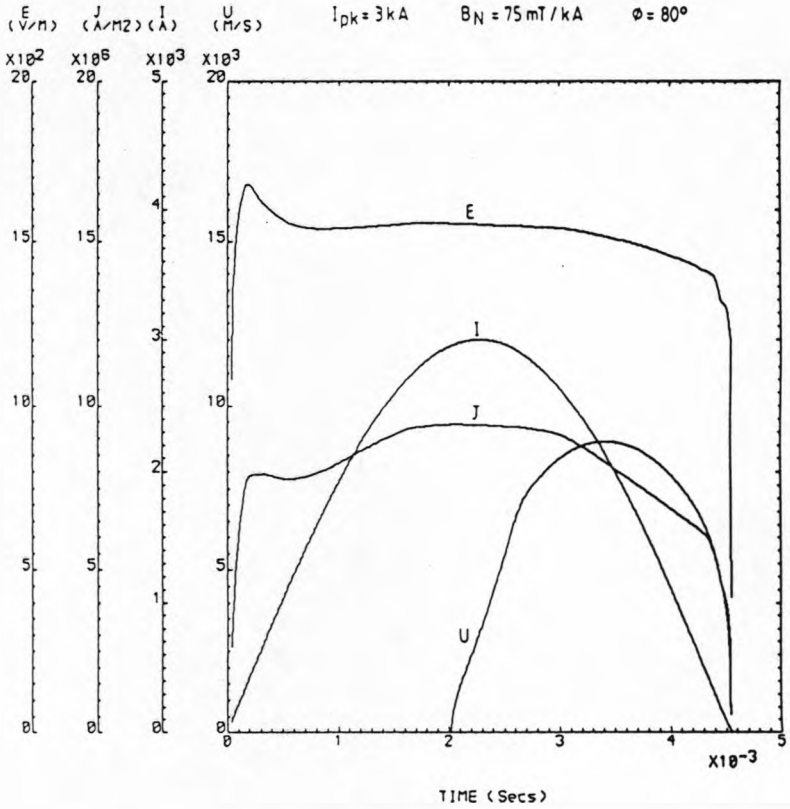

FIGURE 6·11. RESULTS SHOWING ARC VELOCITY, CURRENT DENSITY AND ELECTRIC FIELD FOR COMPUTER SIMULATION

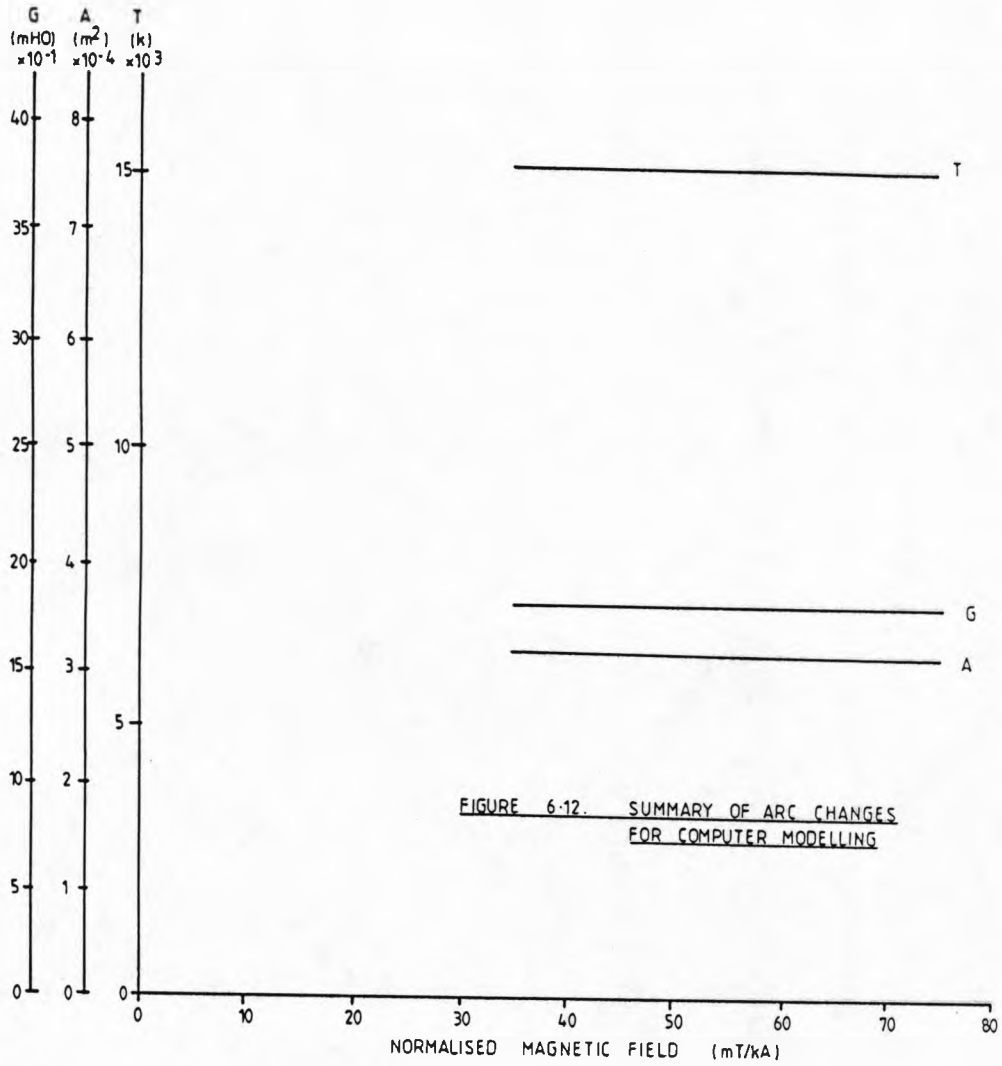

FIGURE 6·12. SUMMARY OF ARC CHANGES FOR COMPUTER MODELLING

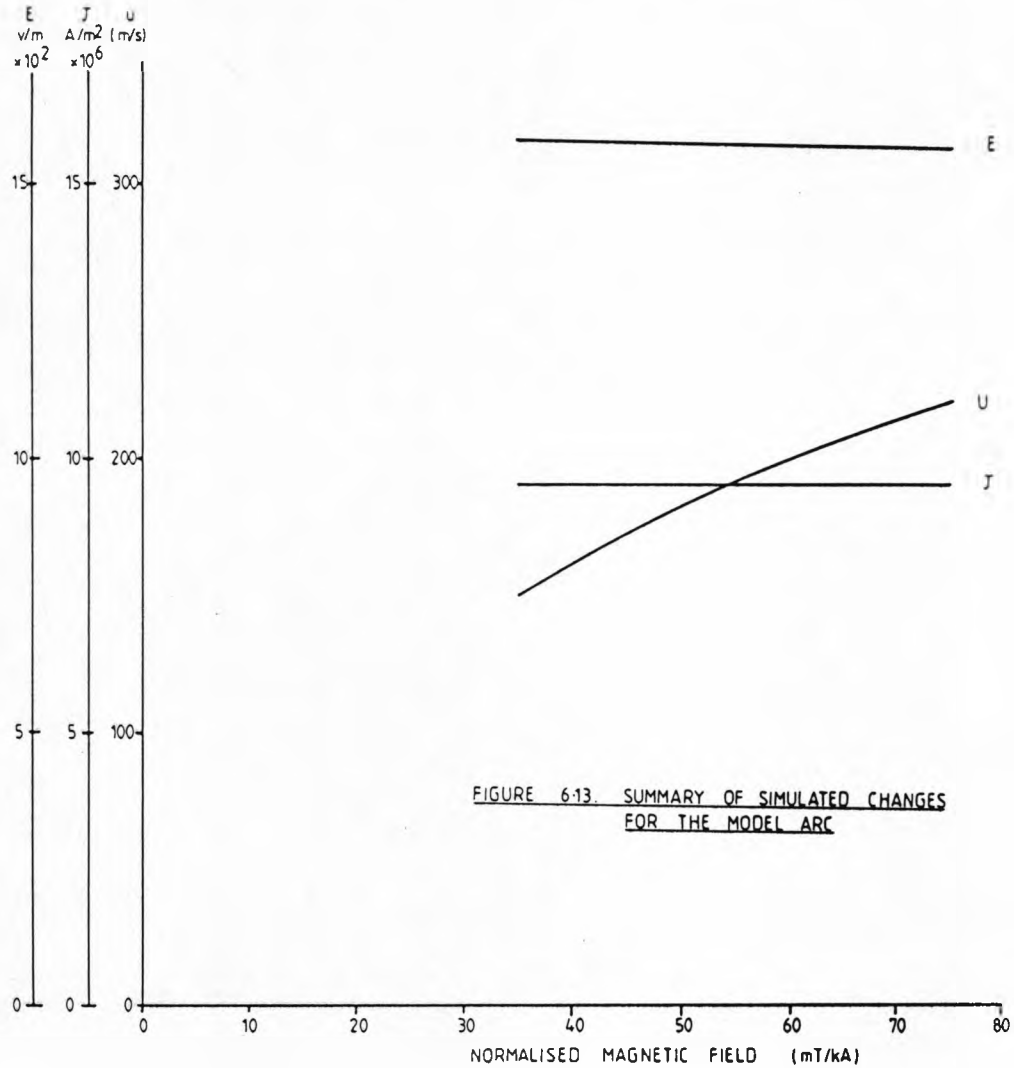

FIGURE 6·13. SUMMARY OF SIMULATED CHANGES FOR THE MODEL ARC

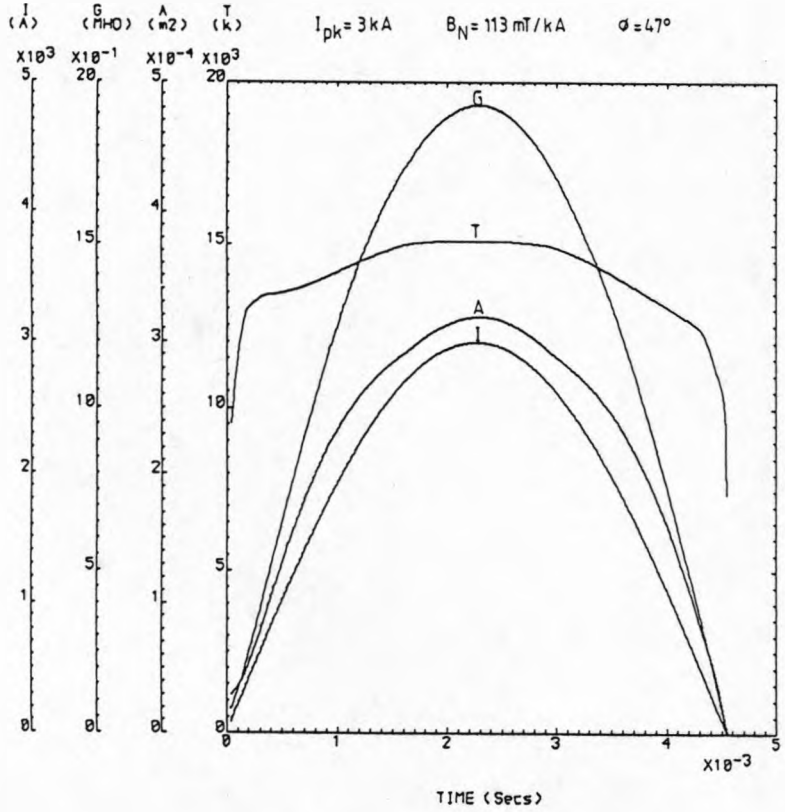

FIGURE 6·14. SIMULATED ARC RESULTS SHOWING ARC TEMPERATURE, AREA AND CONDUCTANCE

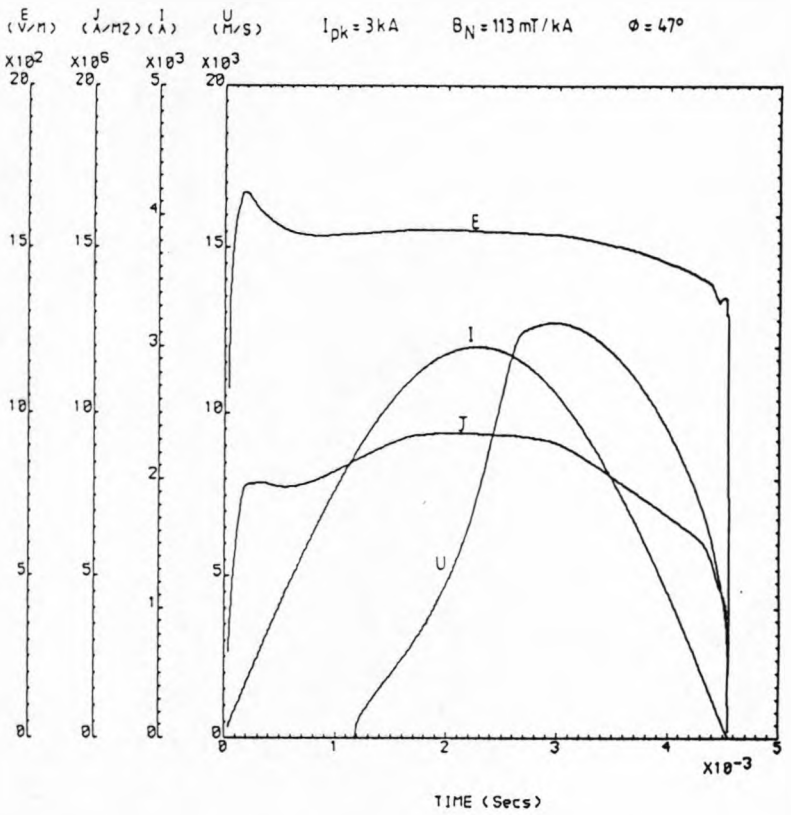

FIGURE 6·15. ARC VELOCITY, CURRENT DENSITY AND ELECTRIC FIELD RESULTS

6.1.3.2.1 80° PHASE DIFFERENCE ANGLE

Figures (6.16 and 6.17) show the results of an 18kA peak current arc rotated by a 35 mT/kA normalised magnetic field with an 80° phase lag. These results have the same distinctive features as those for the 3 kA peak current results but differ in magnitude.

The arc temperature has risen from 15,000 to 15,600°k and has a flatter profile than the 3kA case. The arc area has a more sinusoidal character and has a maximum of 1.8 x 10^{-3} m^2 value at peak current. The arc's conductance has risen from 1.8 mho/m to 11.5 mho/m at peak current.

The current density nolonger remains constant during the half cycle but has a negative slope towards current zero. The average current density is 1 x 10^7 A/M^2 but varies over 4 ms of arcing by 2 x 10^6 A/M^2. The electric field has an average value of 1.56 kv/m but has a transient peak of 1.94 kv/m at the beginning of the cycle. The arc begins to rotate earlier at 2ms into the arcing cycle and peaks at 3.4 ms with a increased maximum value of 630 m/s.

The results from other arcing condition with different flux density are shown on figures (6.18, 6.19), (6.20, 6.21) and correspond to normalised flux densities of 55 mT/kA and 75 mT/kA respectively.

Figures (6.22, 6.23) are a summary of the high current simulated arcing. There is little change in the arc's parameters at peak current except that the arc's velocity increases over the flux density range. Also an extinction peak becomes increasingly apparent on the electric field curves as the flux density increases.

6.1.3.2.2 47° PHASE DIFFERENCE ANGLE

The same trend is repeated for these conditions as for the 80° phase difference results from a low magnetic flux density of 35 mT/kA to a high one of 113 mT/kA the arc's parameter remain constant except the velocity and are similar to those results for the 80° phase difference angle. The arc's velocity varies over this range from 760 m/s for a 35 mT/kA normalised field to 1100 m/s for a 113 mT/kA field. The onset of this velocity is at the same point in time as for the 3kA simulation and reaches a maximum at the same time midway between peak Lorentz force and peak magnetic flux.

6.1.3.3. MAGNETIC FIELD INFLUENCE UPON THE ARC'S BEHAVIOUR

For a given peak current the magnetic field variation over the range 35 mT/kA - 113 mT/kA for both phase difference angles did not change the arc's parameters by any significant amount except for the arc's velocity.

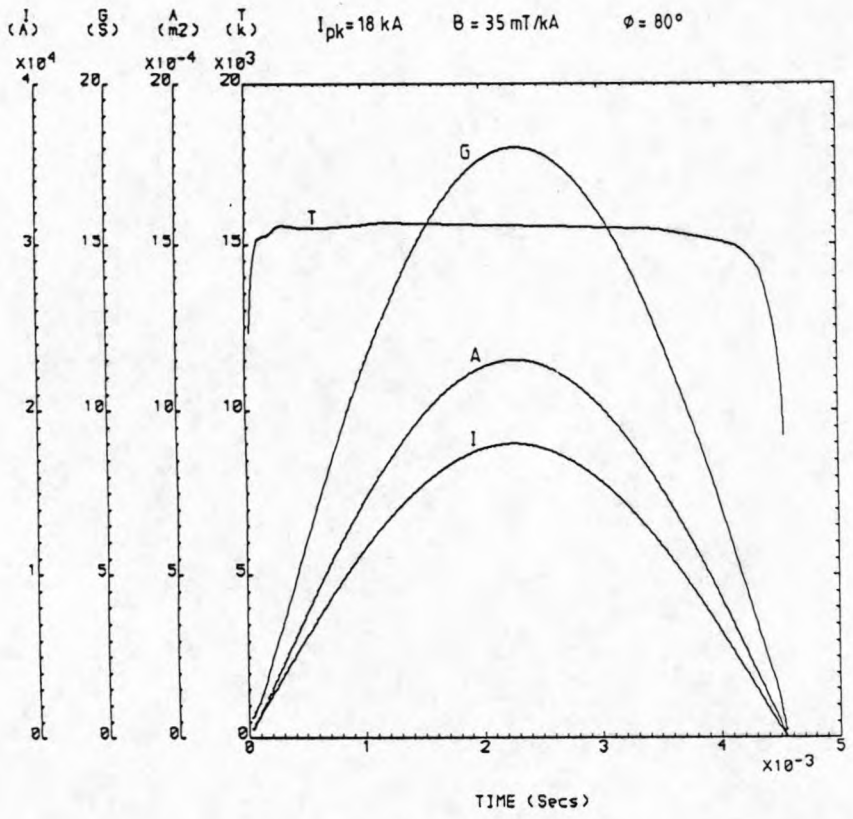

FIGURE 6·16. PEAK CURRENT ARC BEHAVIOUR

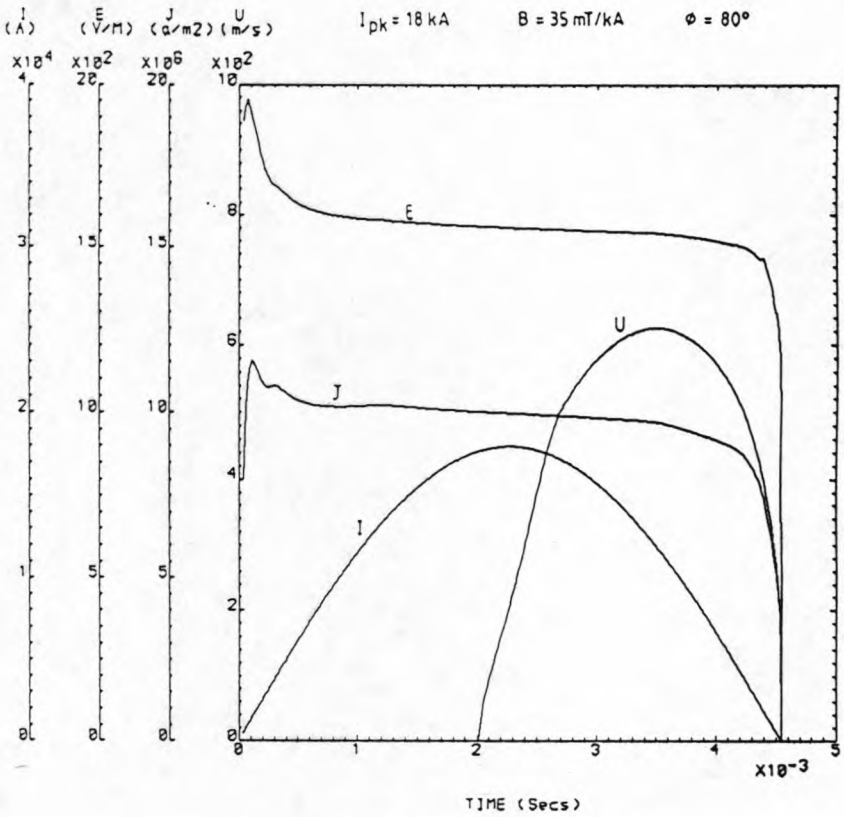

FIGURE 6·17. PEAK CURRENT ARC BEHAVIOUR

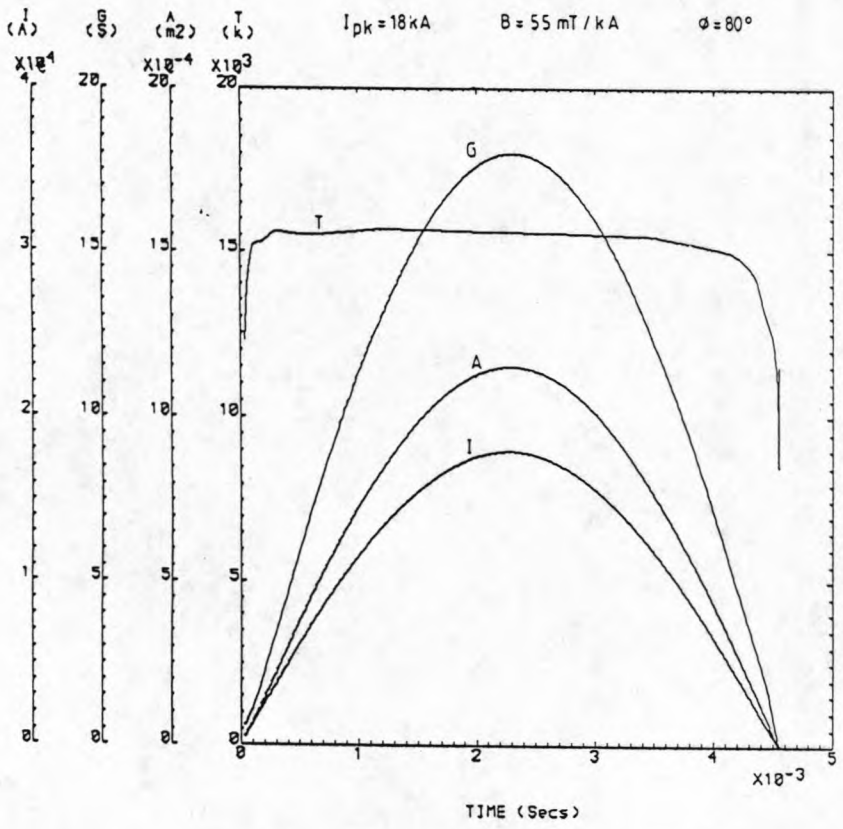

FIGURE 6·18. PEAK CURRENT ARC PREDICTION

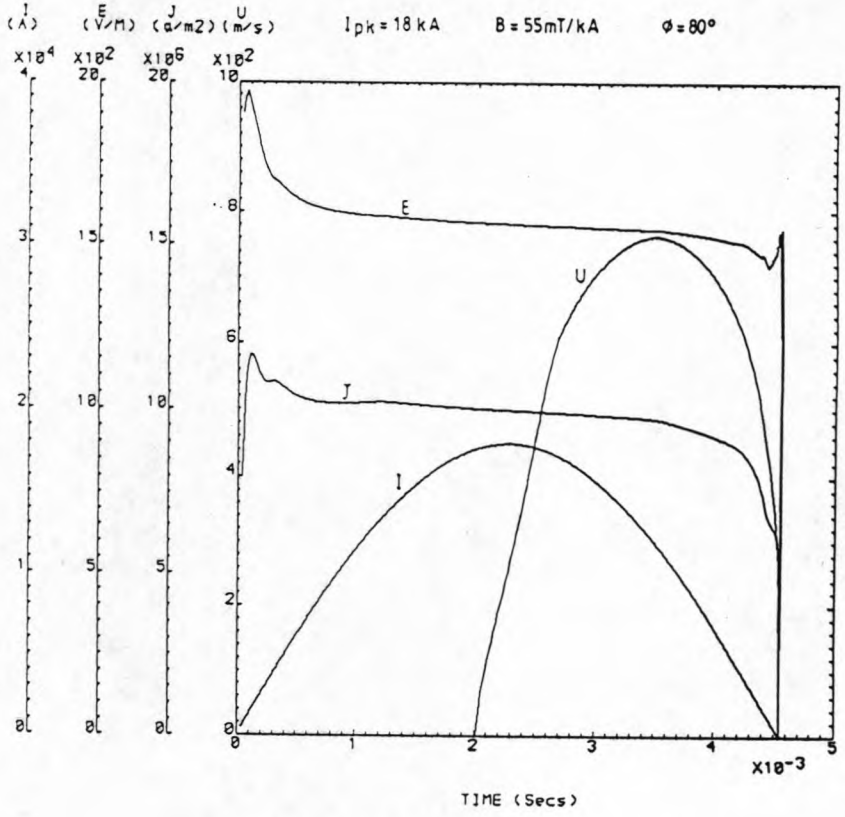

FIGURE 6·19. PEAK CURRENT ARC PREDICTION

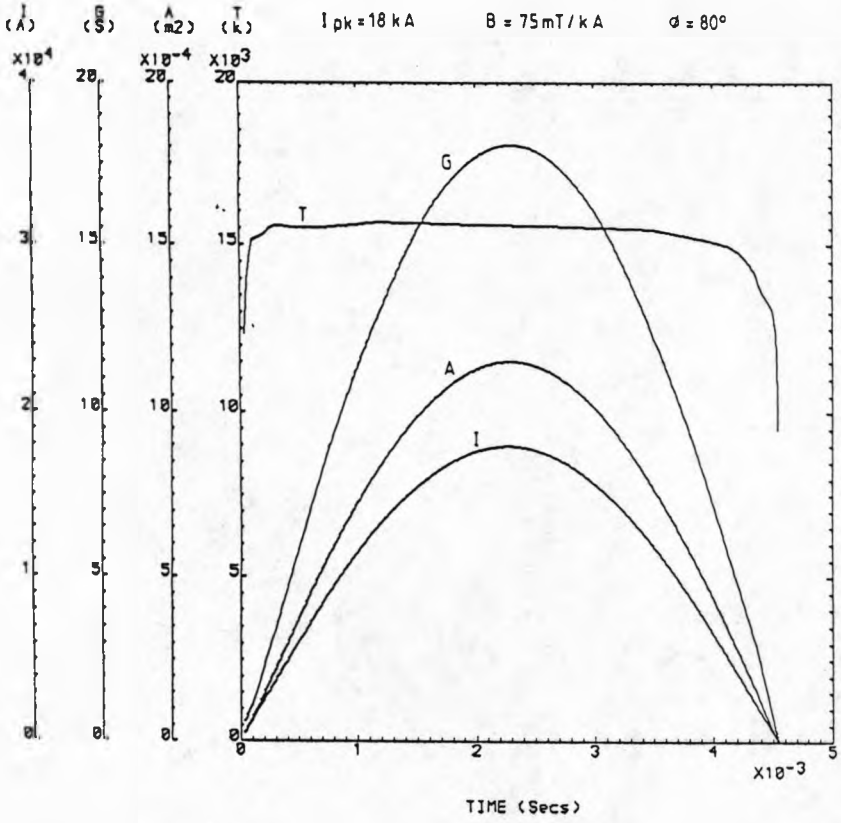

FIGURE 6·20. ARC BEHAVIOUR

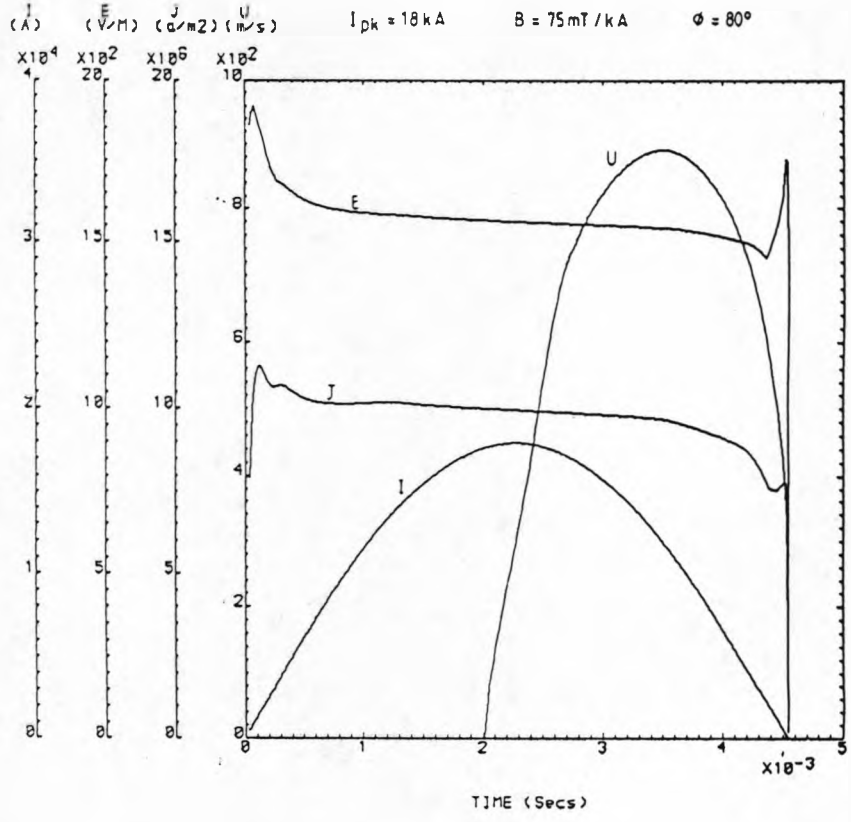

FIGURE 6·21. ARC BEHAVIOUR

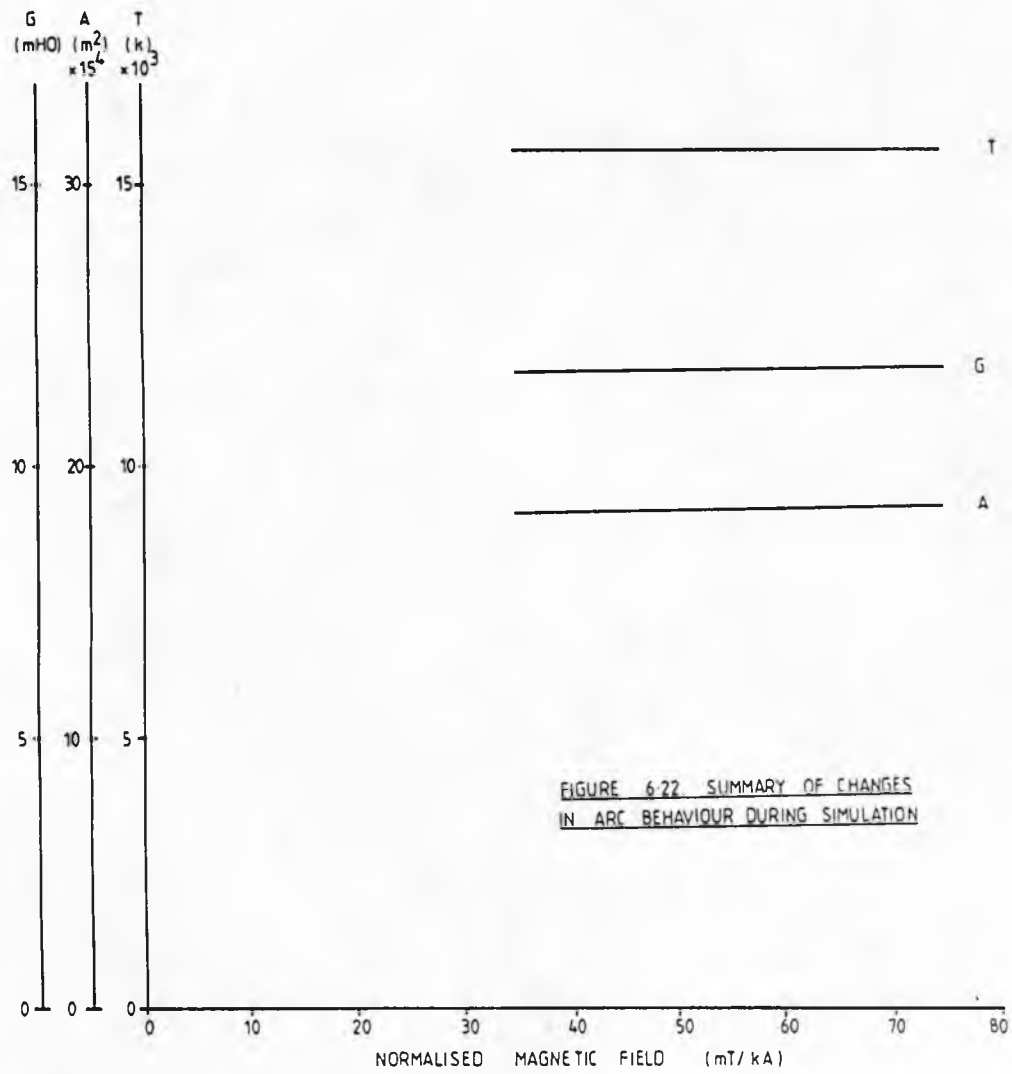

FIGURE 6·22. SUMMARY OF CHANGES IN ARC BEHAVIOUR DURING SIMULATION

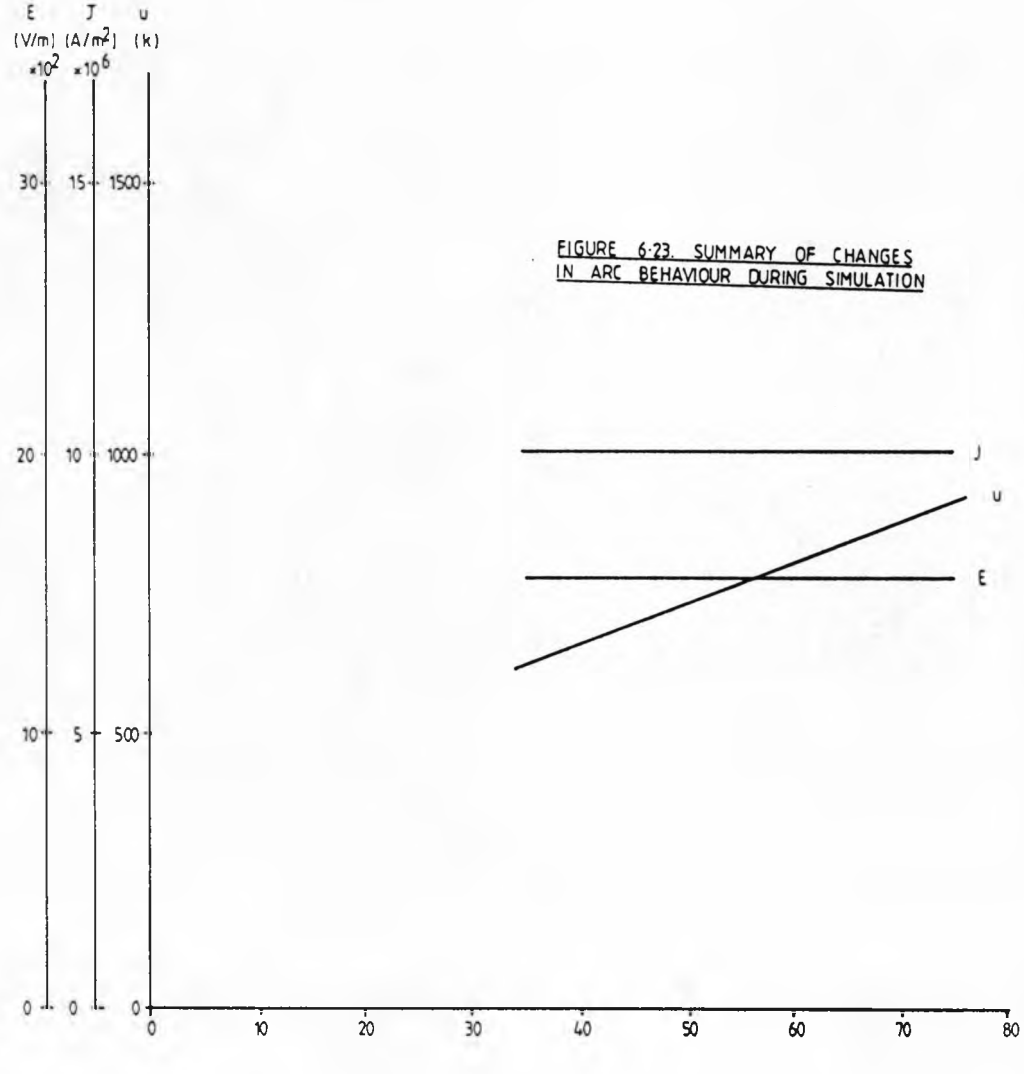

FIGURE 6·23. SUMMARY OF CHANGES IN ARC BEHAVIOUR DURING SIMULATION

However, there is a change in these parameters when the peak current is increased from 3 kA to 18 kA reflecting the rise in ohmic heating of the arc core. Changes in the magnetic field at this higher current cause no effect upon the arc's parameters except for the arc's velocity.

6.1.3.4 COMPARISON OF SIMULATED RESULTS WITH EXPERIMENTAL RESULTS

6.1.3.4.1 LOW CURRENT COMPARISON

Figure (6.24) compares the predicted and measured arc areas for an 80° phase difference are condition and 35 mT/kA magnetic field. The experimental area is an average one corresponding to an average value for the whole length at individual times. Both sets of results show the same trend throughout the half cycle although there is a small difference in the magnitudes. Nonetheless the overall agreement between the measured and calculated areas is good.

Since no temperature measurements are available for the rotary arc a comparison can only be made with results for other SF_6 arcs. These comparisons show a similar trend and the maximum averaged temperature is reasonable.

The conductance per meter length of arc rises and falls

as the power input into the arc increases and decreases this is observed both in the predicted values and experimental values. Experimentally a typical value for the conductance at peak current for the same conditions is 1.4 mho/m, compared with the predicted value of 1.92 mho/m. The agreement between these conductances is therefore reasonable.

Figure (6.25) compares other parameters for the same conditions as for figure (6.24). The predicted current and the experimentally observed current densities show reasonable although not complete agreement. Agreement at the beginning and end of the arcing cycle is not so good.

This descrepency arises from two problems; the first is that there are situations where it is difficult to determine from records the luminous boundary of the arc column due for instance to turbulance and swirl effects. The second reason is associated with the approximate nature of the arc modelling and simplified description of the arc's boundary.

The electric field of 1550 v/m predicted at peak current is somewhat low compared with the experimental value of 2350 v/m. This is probably due to an overestimation of the arc's temperature during the half cycle. The experimental electric field indicates that this temperature should be 12,000-13,000°k which would appear

somewhat low compared with values for axisymmetric arcs.

There are also differences between the predicted and experimental arc velocities, although the trends are similar. The differences between experiment and theory are firstly manifest in the time at which the arc begins rotating. This is later for the predicted velocity probably due to the transient magnetic field within the arc coil (Section 4.1.1) which is ignored in the arc modelling. Secondly the rate of rise of the arc's velocity is more pronounced for the theorectical simulation possibly due to the neglect of hot and cool gas mixing within the arcing environment. Thirdly the maximum predicted velocity is reached sooner possible due to an overestimate of the surrounding gas temperature.

Results for arcing condition of 3 kA, 113 mT/kA and 47° phase difference angle show similar trends to those at 80°. The same discrepencies are apparent arising from the same approximate assumptions.

6.1.3.4.2 HIGH CURRENT ARCING

Figures (6.26, 6.27) show the simulated parameters for an 18 kA, 35 mT/kA, 80° phase difference angle together with experimental data.

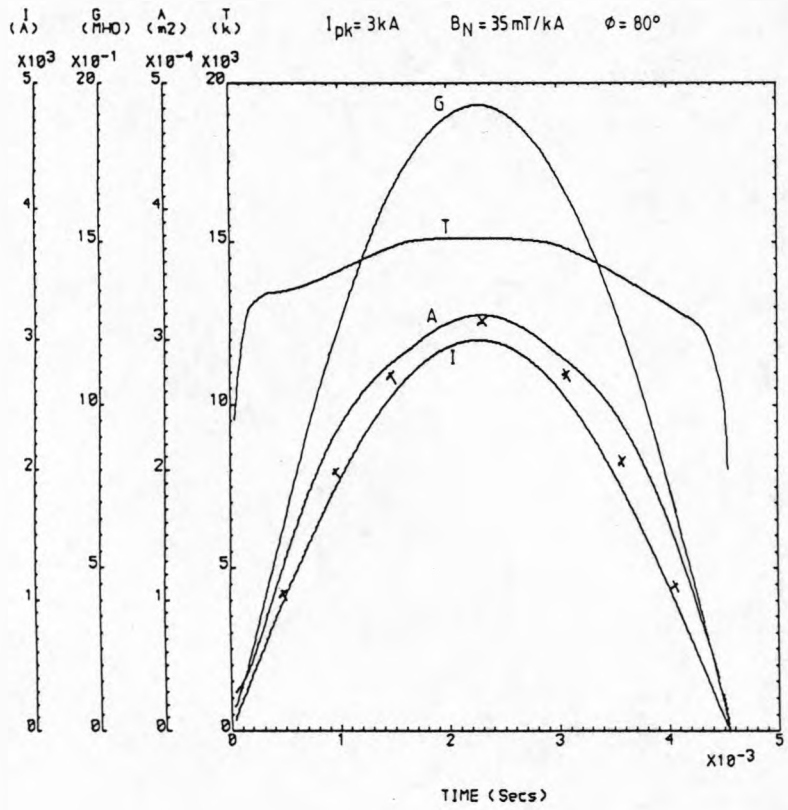

FIGURE 6·24. COMPARISON OF SIMULATED AND ACTUAL ARC BEHAVIOUR

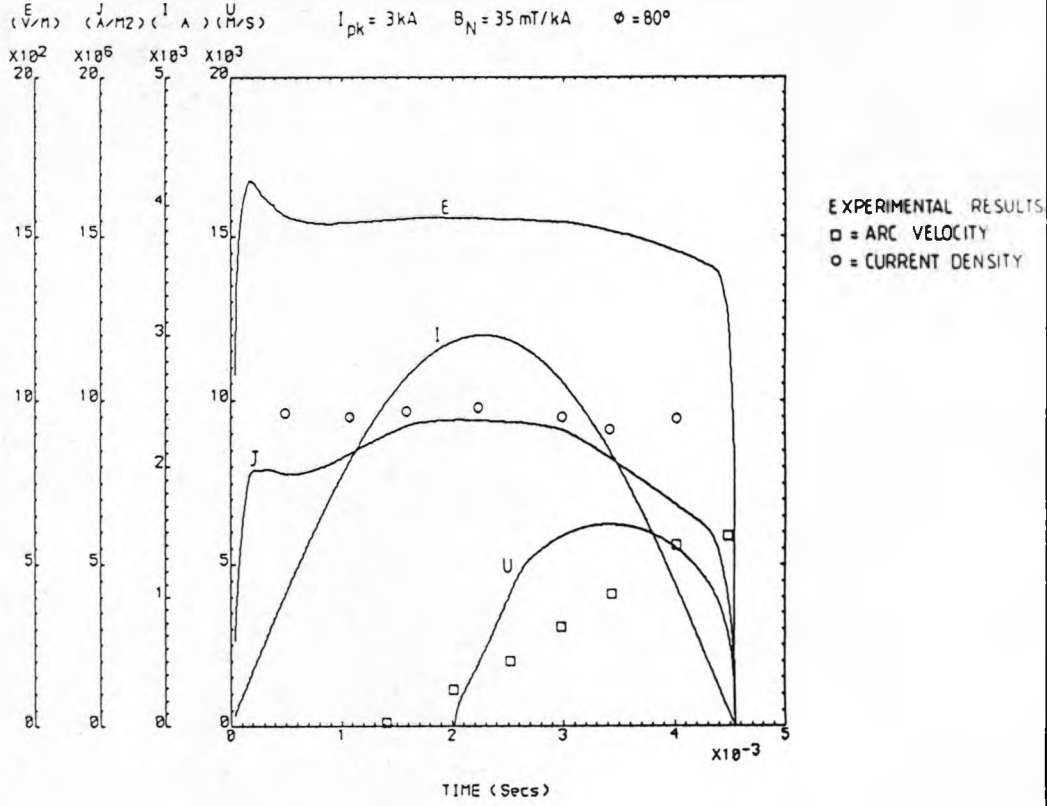

FIGURE 6·25. COMPARISON OF EXPERIMENTAL AND SIMULATED RESULTS

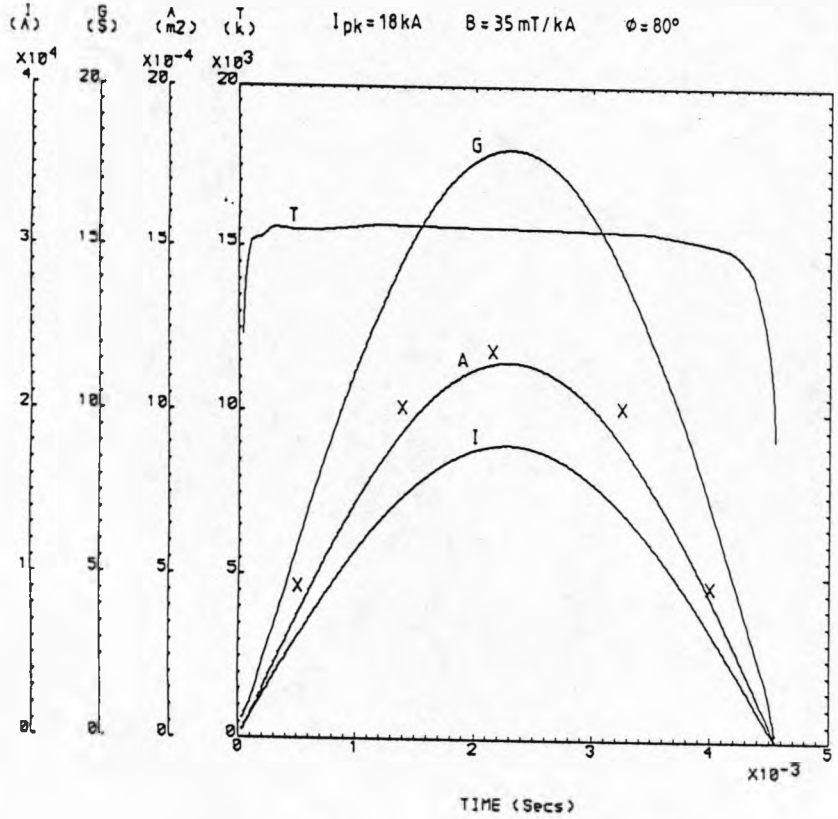

X = EXPERIMENTAL AREA

FIGURE 6·26 COMPARISON OF EXPERIMENTAL AND THEORETICAL RESULTS

o = EXPERIMENTAL CURRENT DENSITY

□ = EXPERIMENTAL ARC VELOCITY

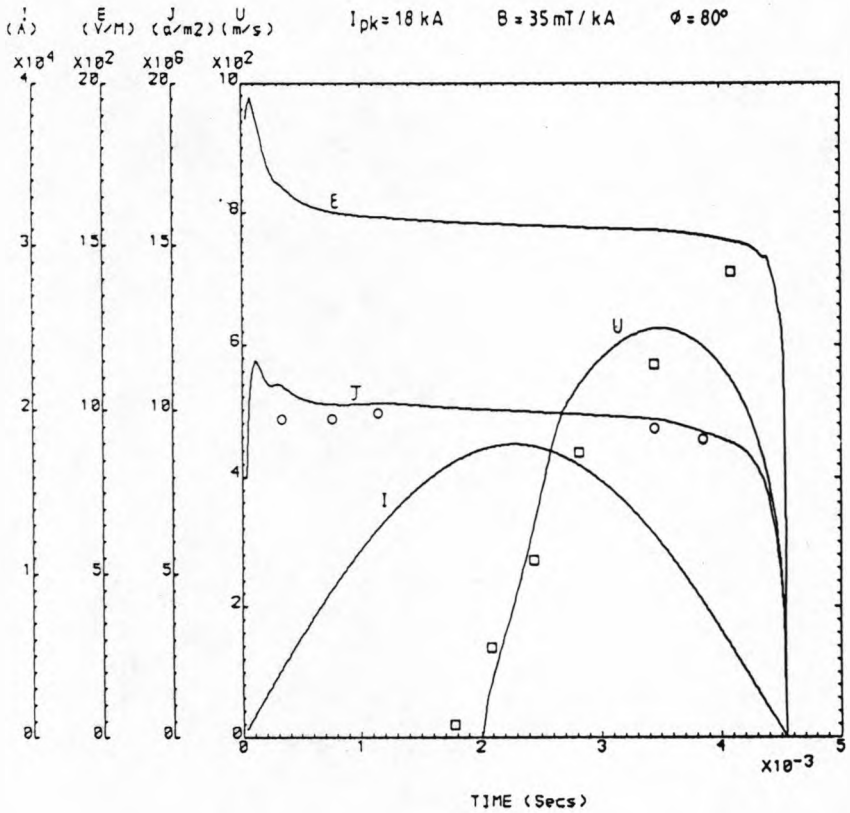

FIGURE 6·27. COMPARISON OF EXPERIMENT AND THEORETICAL RESULTS

Similar trends in the comparison between theory and experiment exist at high current as existed at lower currents. Figure (6.26) shows good agreement for the two arc areas but the arc's conductance is over estimated by 3.0 mho/m. However at high peak currents there is better correlation between the current densities over the whole of the arcing cyle. The electric field is underestimated at peak current being 1.6 kV/m compared to an experimental value of 2.7 kV/m. Using the experimental electric field and current density the temperature of the arc column can be estimated as again being 12,000°k-13,000°k this is lower than that predicted.

The arc velocity prediction shows similar trends as at the lower current. However the magnitude of the predicted velocity is lower than that observed experimentally possible due to underestimating the surrounding gas temperature at this high current.

6.1.3.4.3 CONCLUDING COMMENTS

Although some parameters are somewhat over or under estimated the complex problems presented by a non-axisymmetric rotating arc column in a nonuniform, out-of-phase magnetic field have been broadly overcome with the result that an approximate model is established which can predict general trends and produce reasonable

results.

Before the computer model can be improved further information about the temperature of the surrounding gas and the turbulent effects of mixing requires experimental investigation.

6.2 CURRENT ZERO MODEL

To investigate the reigntion behaviour of the arc after current zero for various dv/dt values, the formulation of the equations governing the arc's behaviour must be changed from a current controlled input to a voltage input. Essentially the differential equations remain the same but the power input now becomes a function of dv/dt.

During the current zero period it becomes even more necessary to monitor the magnitudes of the empirical convection and the thermal conduction. In the current zero region the dominance of the convection losses will decrease and conduction losses will dominate. This change in the type of loss is attributed to the reduction in the arc's velocity prior to and during current zero due to the rapid decay in the Lorentz driving force principally caused by the decay in arc current. Figure (6.28) shows schematically the approximate domains of convection and conduction losses.

This schematic also shows what happens when the arc column reignites and once again convection becomes the dominant loss between the two.

The solution of the same differential equations for the time period after current zero shows the versitility of the initial equations and this method has the potential to predict the thermal performance behaviour of the rotating arc interrupter.

The dv/dt from the synthetic testing circuit is simulated by a linear rising voltage after cyrrent zero. The response of the arc column during this period is monitored.

6.2.1 MODIFICATION OF DIFFERENTIAL EQUATIONS

In order to describe the current zero period one modification is required to each differential equation. For the core equation the modification is to the power input term which changes using ohm's law from

$$\frac{I^2\sigma}{A} \qquad \text{to}$$

$$V^2\sigma A \qquad (6.21)$$

This is the power input per unit length of arc column.

The modification to the boundary equation is similar and affects the net radiation loss term. This changes from

$$\frac{\alpha I^2}{\sigma A} \qquad \text{to} \qquad \alpha V^2 \sigma A \qquad (6.22)$$

This now represents the net radiation loss per unit arc length controlled by the voltage across the arc column.

The differential equation for the arc's velocity is also modified. The input term is changes from

$$\frac{iB}{\bar{\rho}A} \qquad \text{to} \qquad \frac{V\sigma B}{\bar{\rho}} \qquad (6.23)$$

The three modified arc equations are therefore recast in the following form.

CORE:
$$\rho A \frac{\delta h}{\delta t} = V^2 \sigma A - \varepsilon A - \frac{2\Delta T k}{r_o^2} \qquad (6.24)$$

BOUNDARY:
$$(h - h_i)\frac{\delta A}{\delta t} = \varepsilon A - Ah\frac{\delta \rho}{\delta t} - \alpha V^2 \sigma A - 2(S_0 - S_1)\beta J_1(\beta)\pi - \frac{0.4\pi^{1/2} A^{1/2} k \bar{\rho} U \Delta T}{\mu} \qquad (6.25)$$

VELOCITY:
$$\frac{\delta U}{\delta t} = V\sigma B - \frac{RC_D \rho_\infty U^2}{\bar{\rho}A} - \frac{U}{\bar{\rho}A}\frac{\delta M}{\delta t} \qquad (6.26)$$

6.2.2 COMPUTATION

The computer program consists of two sets of equations. The first set describes the arc's behaviour prior to current zero with the power input control by the inputted current, and the second set describes the behaviour after current zero with an imposed voltage

ramp simulating the recovery voltage from synthetic power circuit.

Computationally the analysis is identical upto current zero. At the time when current zero is reached the power input into the arc is zero ($I(t) = 0$). At this point the second set of equations are used to calculate the arc's behaviour. At this time of transfer the power input into the arc column is zero for both sets of equations, that is as well as $I(t) = 0$ so too $V(t) = 0$. Thus the current zero arc condition determined by the current control form the initial condition for the voltage control calculation. The same method of solution is adopted as for the set of current controlled equations. The flow diagram (Figure 6.29) shows the computational sequence. This flow chart is used sequentially after that shown on Figure (6.5).

The aim of this section is to examine the response of the arc column to various dv/dt's after one half cycle of arcing in order to determine the thermal performance of the arc column in terms of the rate of change of current before current zero and the rate of rise of recovering voltage after current zero.

6.2.2.1 DEFINITION OF REIGNITION

Using a linear voltage after current zero to simulate the rate of rise of recovery voltage in the experimental

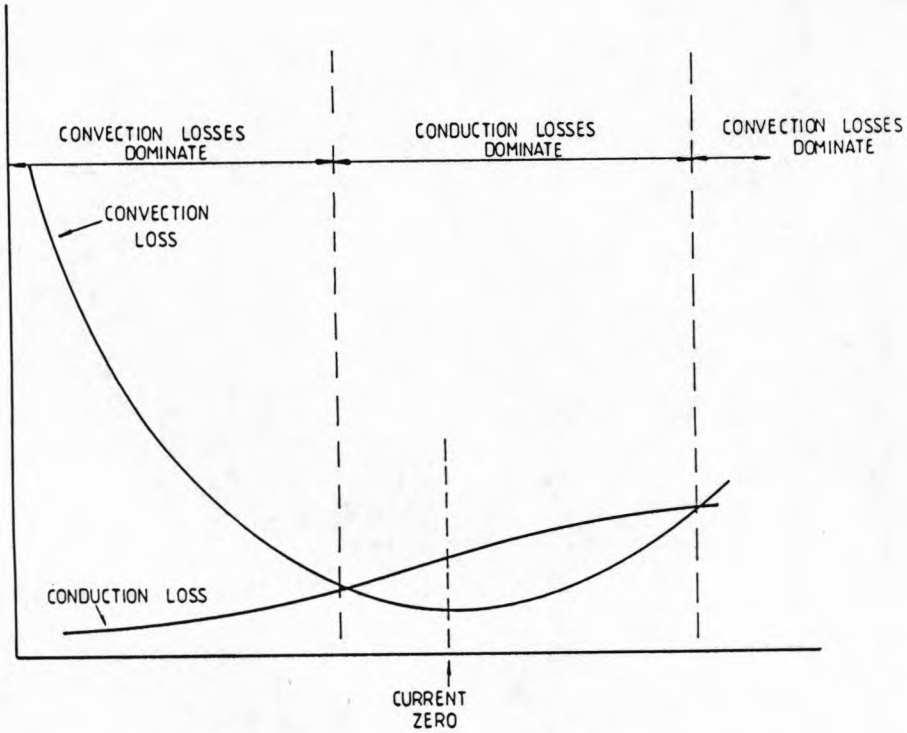

FIGURE 6·28. SCHEMATIC OF ENERGY LOSS DOMINANCE

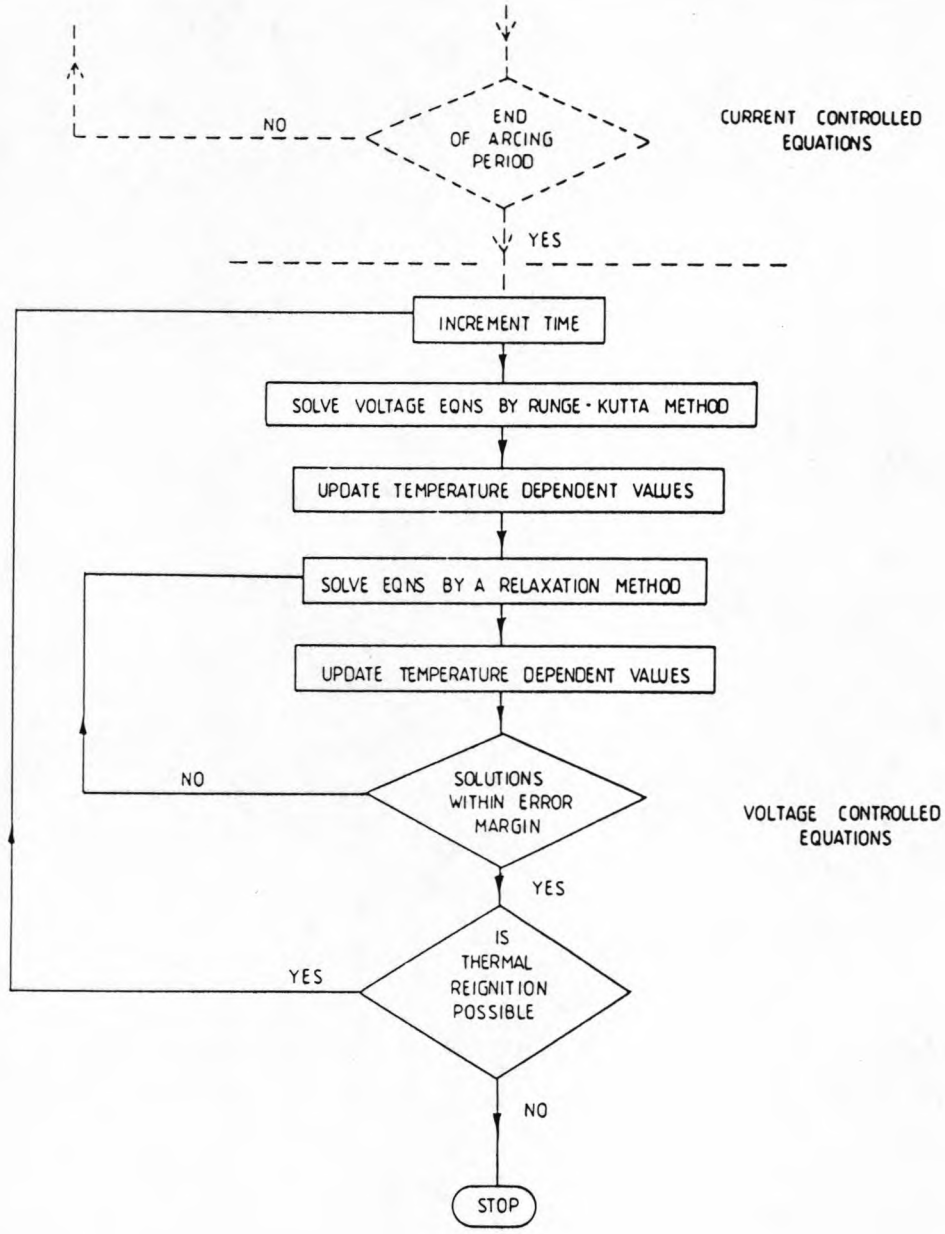

FIGURE 6·29. FLOW CHART FOR COMPUTATION AFTER CURRENT ZERO

circiut causes problems in determining whether the arc has reignited. This is because reignition may still be possible 5 us after current zero when the simulated voltage is larger but the experimental rrrv is oscillating and has decreased. To uniquely specify reignition the time for reignition to occur should be the same as the experimental condition. Experimentally no reignition was observed with the experimental system after 3 us of current zero. This 3 us is therefore the limit allocated to post current zero arc simulation for reignition to occur. If reignition occurs after 3 us and before 5 us then this is adjudged to be a clear but with post arc current flow. Reignition is shown by an increase in the arc's area.

6.2.3 CURRENT ZERO RESULTS

For each set of results there are two graphs. The first shows the arc's temperature, area, conductance and the current whilst the second shows the arc's velocity, electric field, current density and current flow. Two arc currents are investigated in detail 3kA and 18kA peak, for normalised magnetic fields of 35 mT/kA, 55mT/kA, and 75mT/kA and a phase difference angle of 80°.

6.2.3.1 LOW CURRENT ARCING

Results are presented for a 3kA simulated arc in three

magnetic fields and one phase difference angle. Different rates of rise of recovery voltage have been applied at the end of the half cycle of arcing and the arc's response monitored.

6.2.3.1.1 35mT/kA NORMALISED FIELD

Figures (6.30, 6.31) show the arc's behaviour under free recovery conditions ie dv/dt = 0. When the power input has ceased the temperature decays slowly over the next 6μs to 6300°K before arc extinction is complete. Both the arc's area and conductance decay approximately linearly before the arc extinguishes. At current zero the arc temperature is 8000°K, the area is $4.5 \times 10^{-6} m^2$ and the arc velocity is 12m/s.

When a voltage ramp is applied after current zero the arc behaviour is modified as shown on figures (6.32, 6.33). These results are for a rrrv of 550v/μs applied after current zero. Arc reignition does not occur within 3 μs although there is significant post arc current (5 amps, 3 μs after current zero). There is no rise in temperature, increase in arc area nor conductance during this period but there is an increase in the arc's velocity and a rapid increase in current density. This condition represents a clearence with post arc current. If the voltage ramp is maintained then reignition does occur, the arc current increases

rapidly, the arc's temperature, conductance and area increase and there is a marked increase in the arc's velocity.

A higher dv/dt after current zero promotes arc reignition which occurs within a shorter period. Previous to this point of reignition the arc shows no indication that it will reignite (figures 6.34, 6.35), the arc's temperature, area and conductance decay as previously. The increase dv/dt to 650 v/μs significantly increase the power input during the post current zero period. Reignition occurs 4 μs after current zero shown by an increase in the arc's temperature, area and conductance. Although reignition occurs it has not done so within 3 μs, so that for present purposes the arc is described as having marginally cleared but with post arc current.

A further increase in the dv/dt to 750 v/μs reignites the arc within 3 μs of current zero figures (6.36, 6.37). This condition represents arc reignition and is classed as a failure. For this condition as in the other two conditions the arc's temperature following current zero increases at an earlier instant than its area. This phenomenon has been noted for axisymmetric arc's (91) and provides additional confirmation of the validity of this approximate arc model.

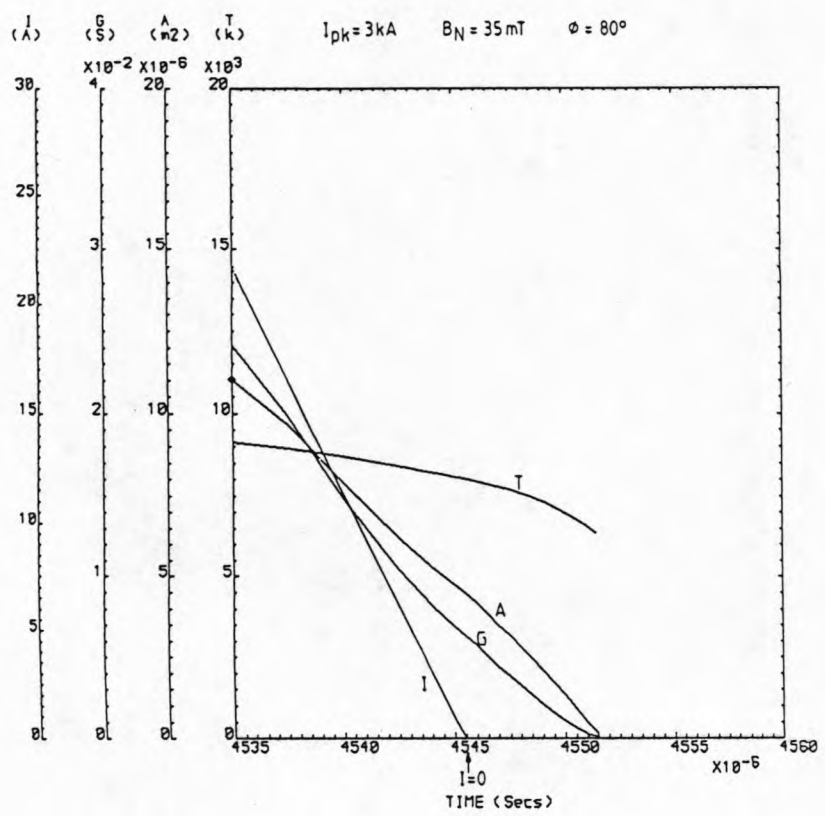

FIGURE 6·30. CURRENT ZERO SIMULATION

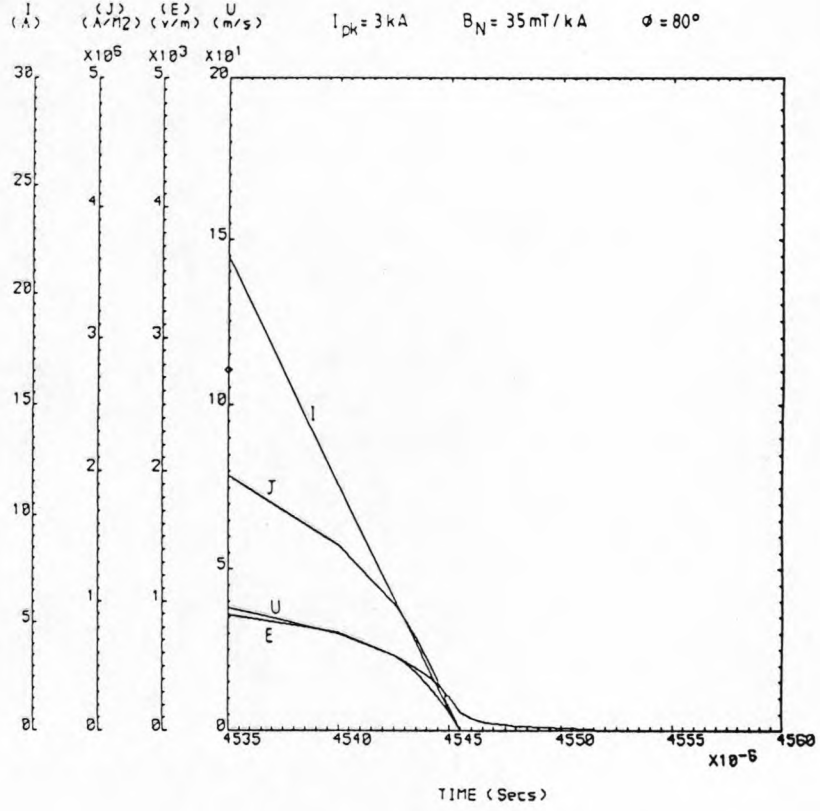

FIGURE 6·31. CURRENT ZERO SIMULATION

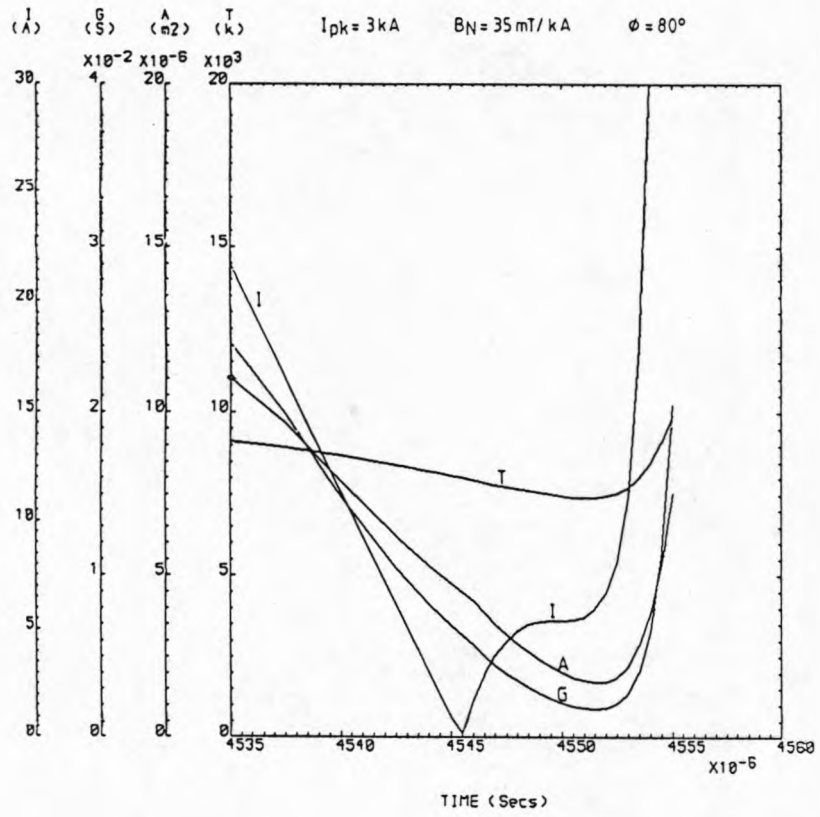

FIGURE 6 32 SIMULATED RESPONSE TO A Dv/DT = 550 v/µs

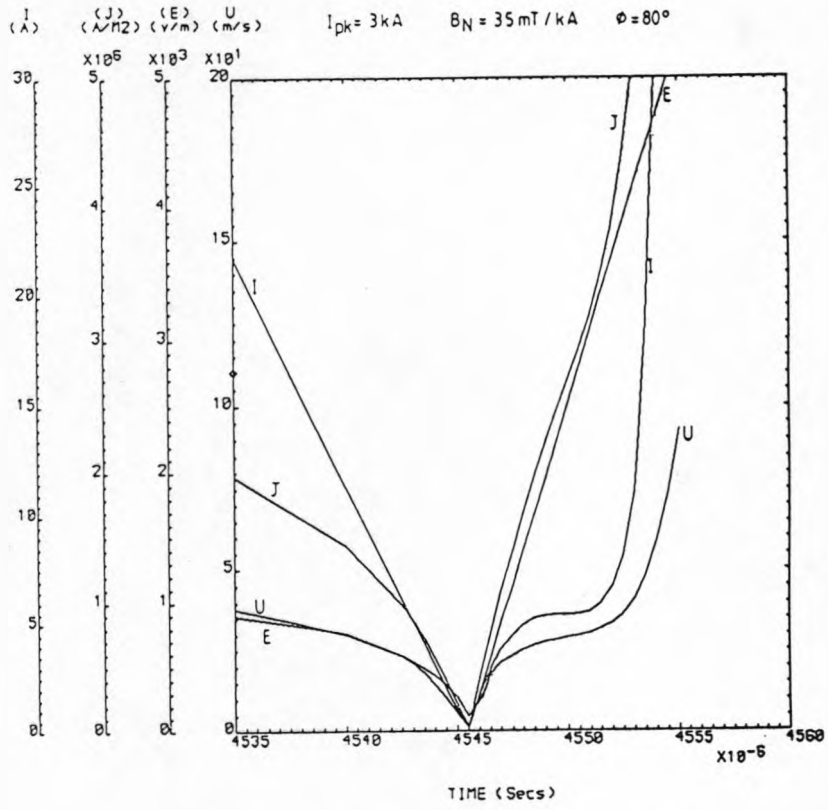

FIGURE 6·33 SIMULATED RESPONSE TO A Dv/DT = 550v/µs

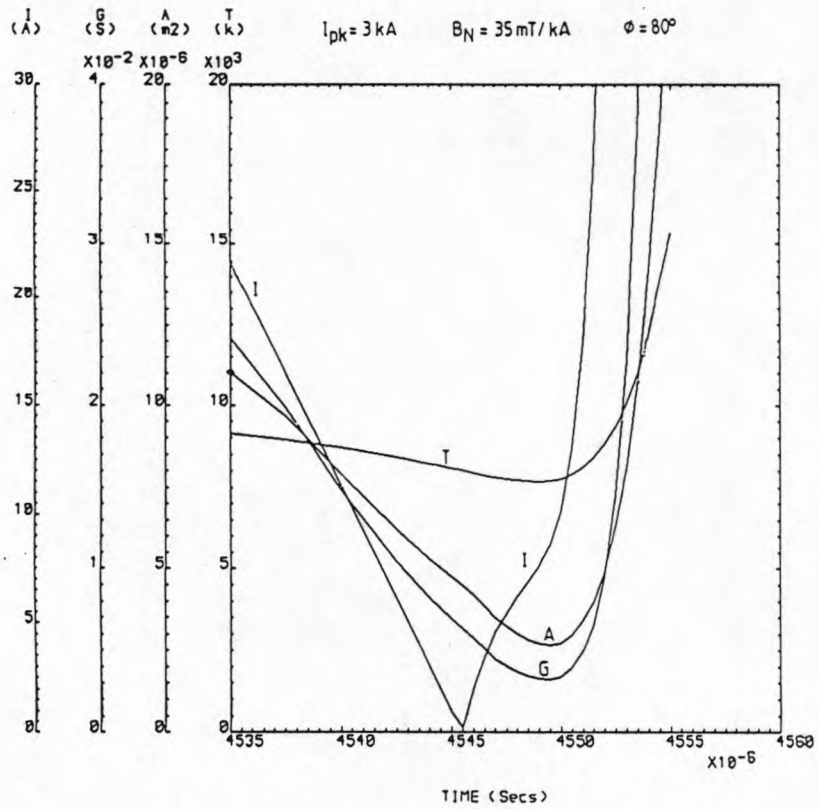

FIGURE 6·34. ARC BEHAVIOUR AFTER CURRENT ZERO FOR A Dv/DT = 650v/μs

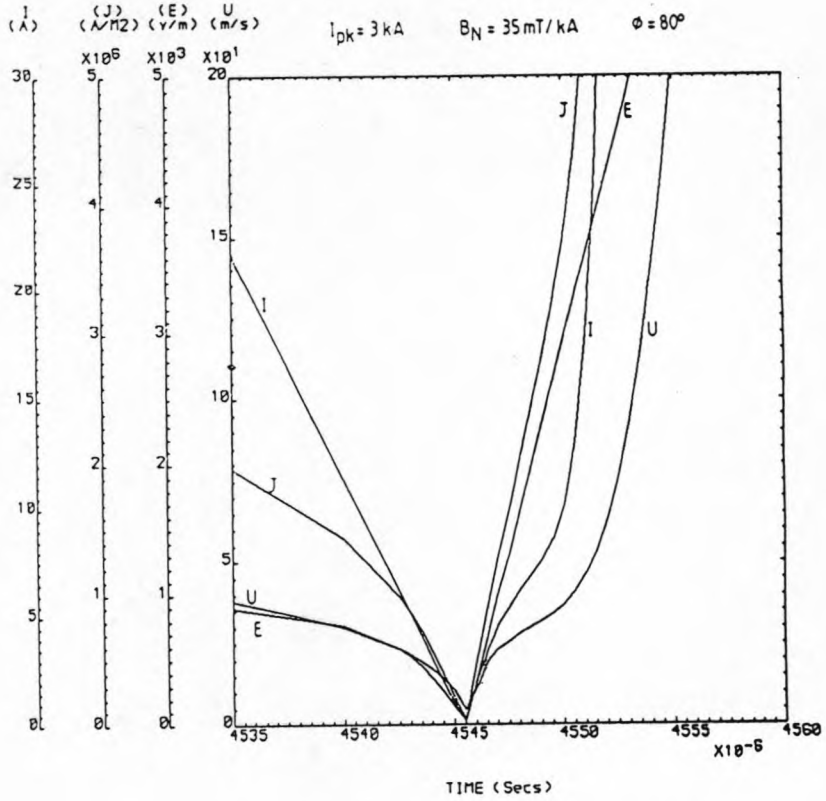

FIGURE 6·35 ARC BEHAVIOUR AFTER CURRENT ZERO FOR A Dv/DT = 650v/μs

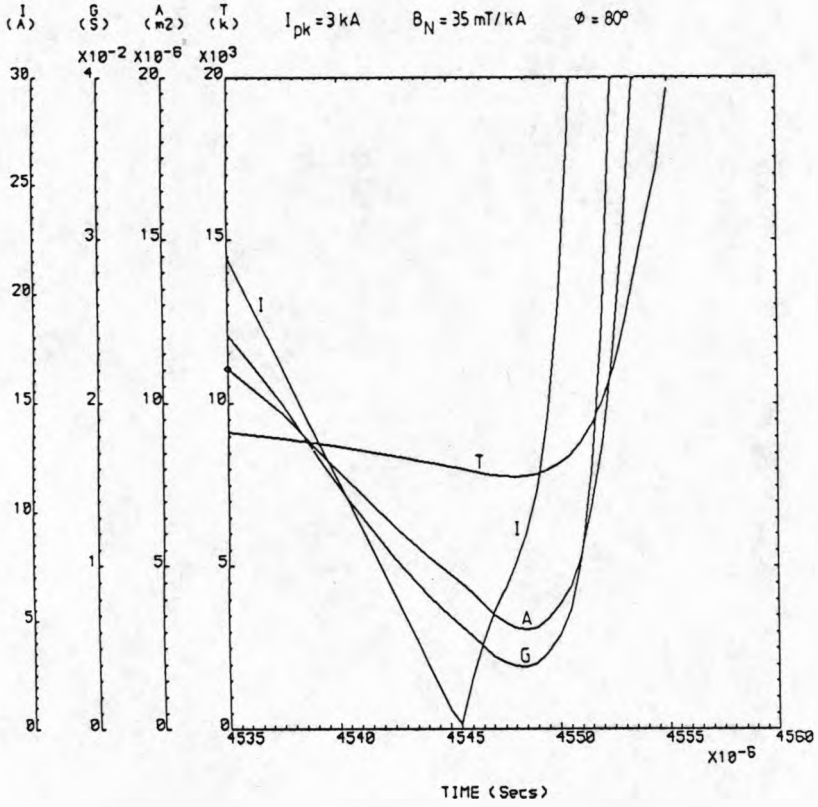

FIGURE 6·36. ARC BEHAVIOUR FOR A Dv/DT = 750 v/µs

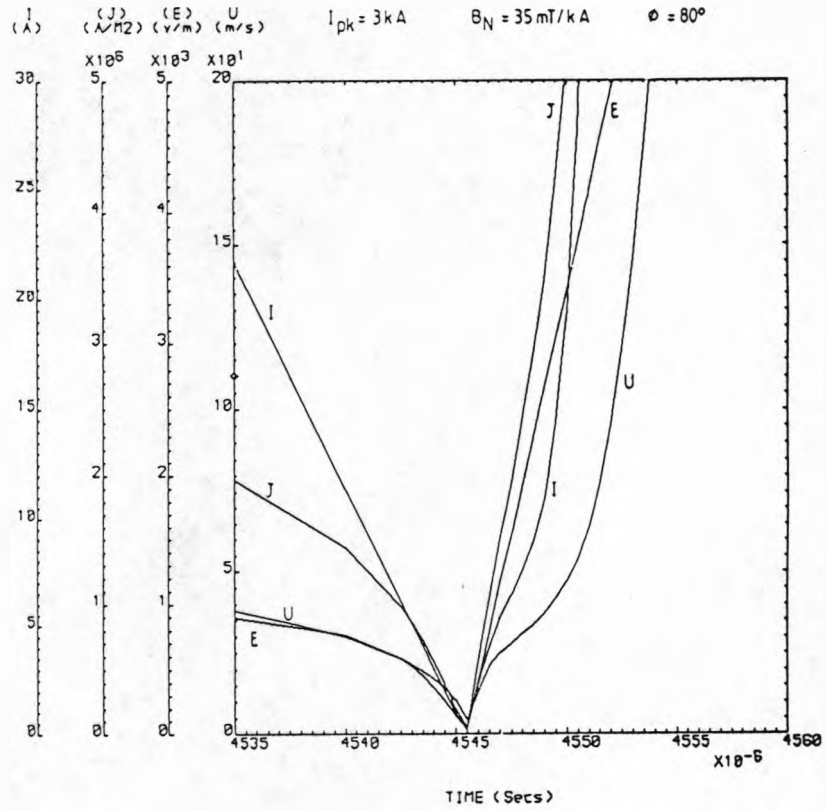

FIGURE 6·37. ARC BEHAVIOUR FOR A Dv/DT = 750v/µs

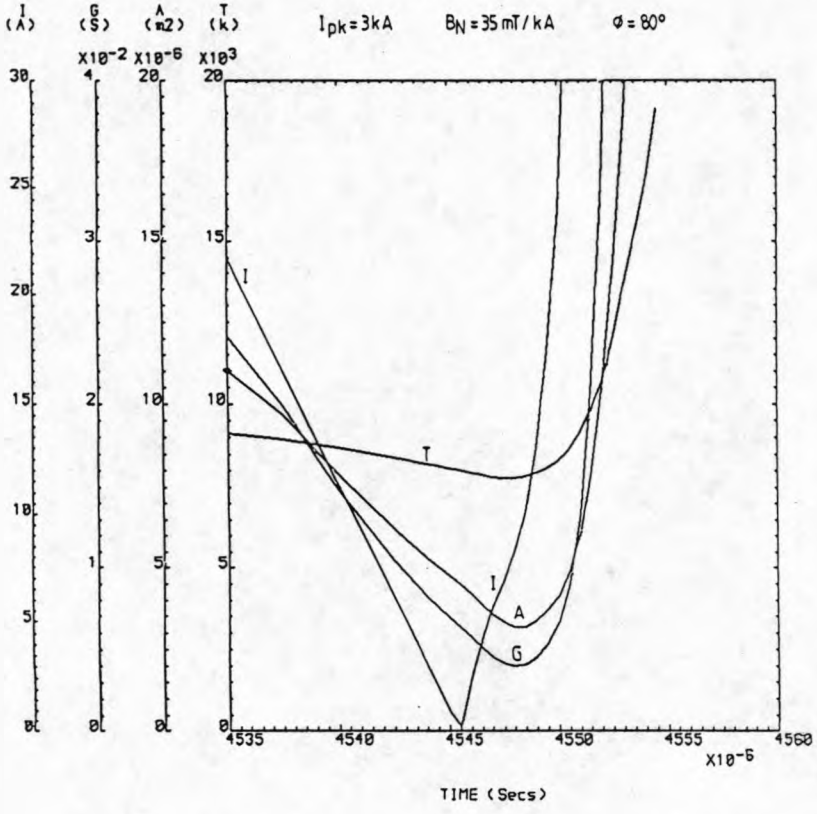

FIGURE 6·38. ARC REIGNITION BY COMPUTER SIMULATION

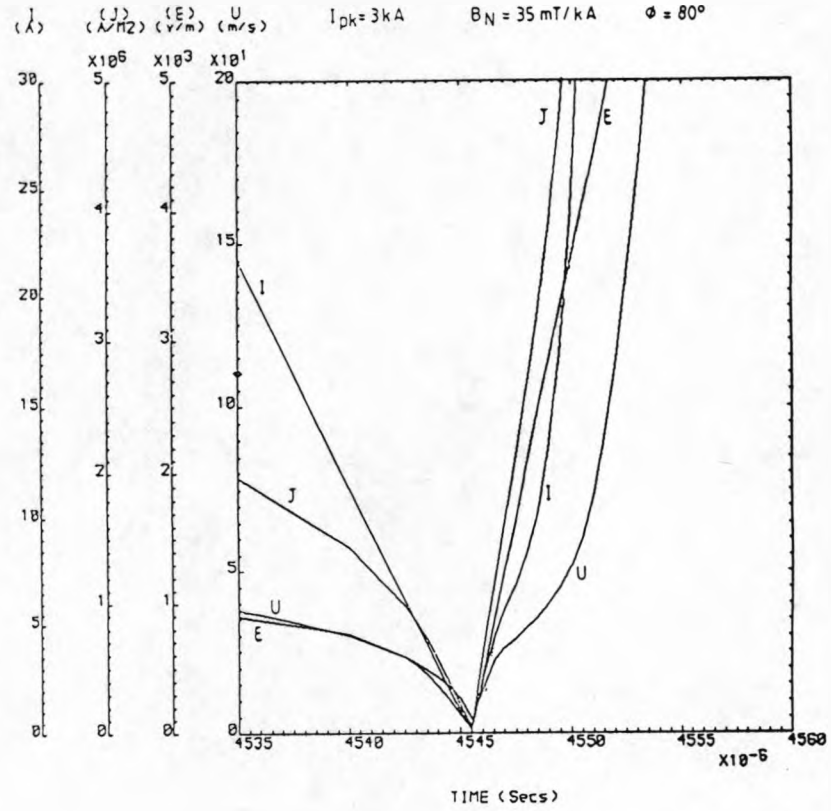

FIGURE 6·39 ARC REIGNITION BY COMPUTER SIMULATION

An increase in the dV/dt to 800 v/μs causes the reignition to occur 0.5 μs earlier (figures 6.38, 6.39). Reignition is similar to those described above. Thus for this particular arcing condition the simulation yields a critical dv/dt of between 650v/μs and 750 v/μs (di/dt = 2.1 A/μs).

6.2.3.1.2 55mT/kA NORMALISED FIELD

The results for a 55 mT/kA normalised magnetic field show similar characteristics to the 35 mT/kA results. Figures (6.40, 6.41) show the arc's behaviour during free recovery. The arc extingushes 2.5 μs after current zero during which time the arc's temperature, area, and conductance decay more rapid than for the previous condition.

Imposing a 1.4 kV/μs voltage ramp after current zero causes post arc current (figures 6.42, 6.43). This current reaches a maximum of 2.0 amps and flows for 3.5 μs before the arc completely extingushes. The rate of decay of temperature, area and concuctance decrease during this flow of post arc current. An increase in the dv/dt to 1.6 kV/μs causes the arc column to reignite within 3 us (figures 6.44, 6.45). Again the arc's temperature increases before its area. After reignition the arc current increases rapidly.

The critical dv/dt for this simulated arcing condition is between 1.4 kV/ μs and 1.6 kV/μs.

6.2.3.1.3 75 mT/kA NORMALISED FIELD

Figures (6.46, 6.47) show the arc's behaviour under free recovery conditions for a still higher driving field. Complete extinction of the arc is reached within 2.5 μs after current zero. The decay in the arc's temperature, area, conductance and velocity follow the same trends as the previous results for lower magnetic flux densities.

The critical rate of rise of withstand voltage for this condition is 2.9 kV/μs (figures 6.48, 6.49). Reignition for this case occures 2.5 μs after current zero, the arc current, area and temperature rising rapidly.

6.2.3.1.4 113mT/kA NORMALISED FIELD AND A 47° PHASE DIFFERENCE ANGLE

The results for the critical dv/dt with a driving magnetic flux of 113 mT/kA are shown on figures (6.50, 6.51). The results exhibit the same trends as for the 80° phase difference conditions. It is particularly noteworthy that during reignition the arc temperature shows a tendency to increase before the arc area.

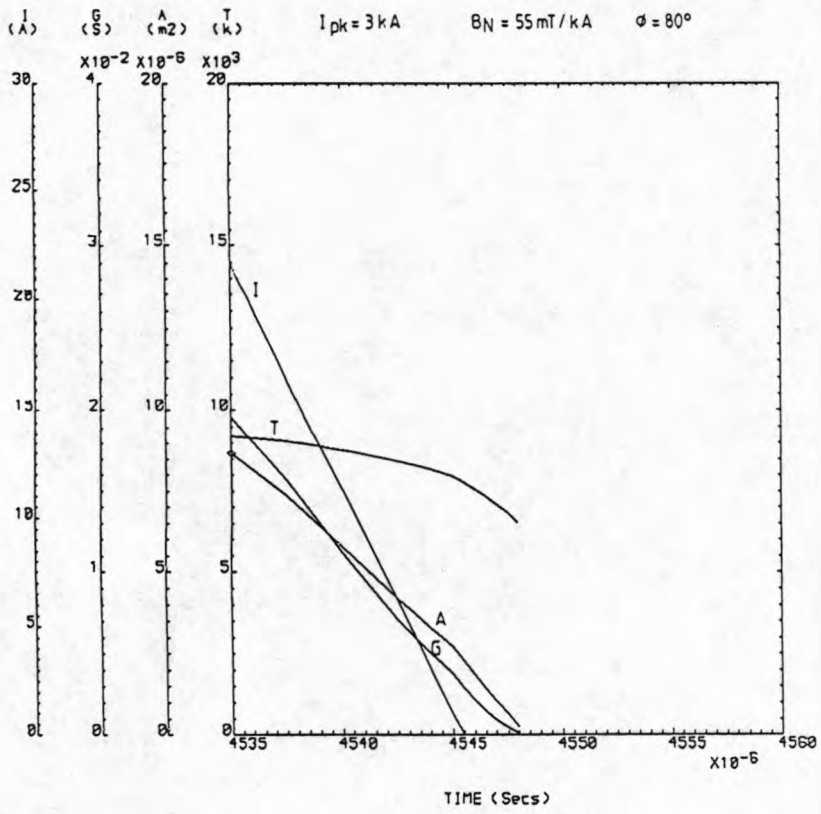

FIGURE 6·40. ARC RECOVERY SIMULATION

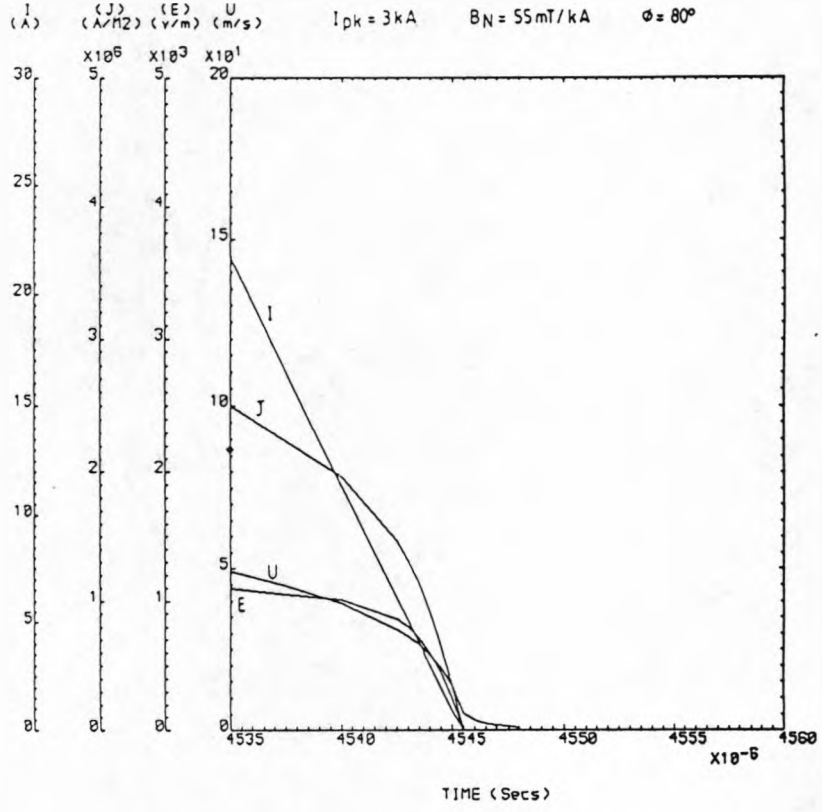

FIGURE 6·41. ARC RECOVERY SIMULATION

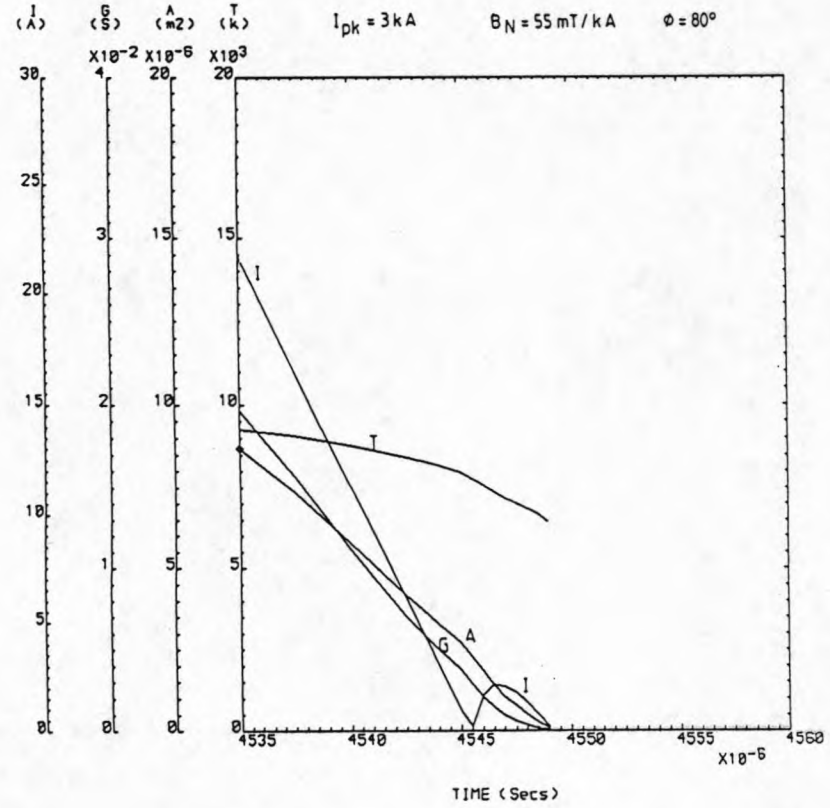

FIGURE 6·42. CLEARENCE WITH POST ARC CURRENT

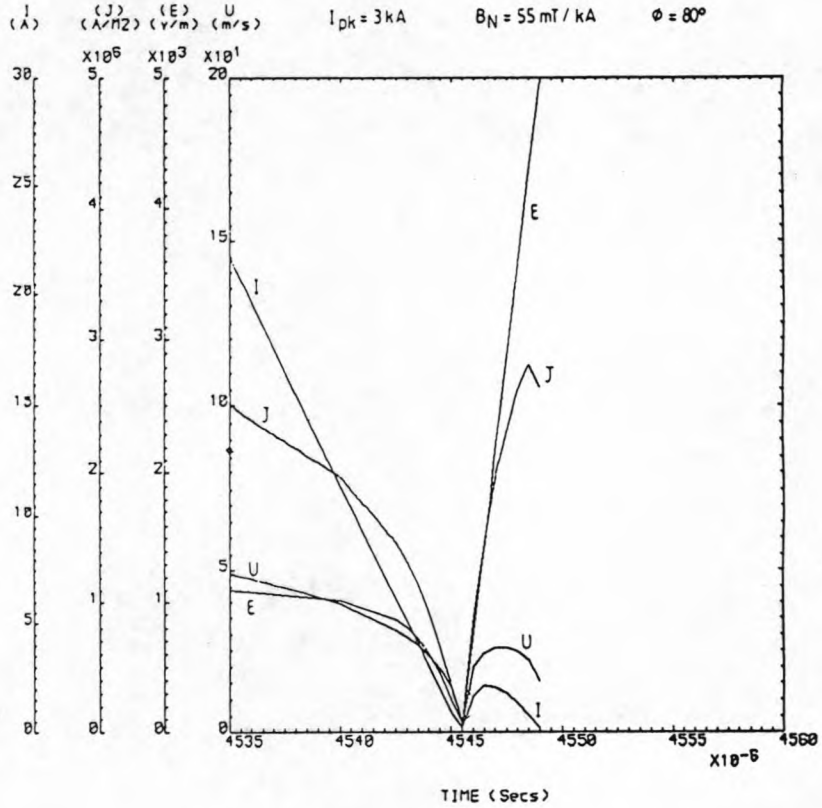

FIGURE 6·43. CLEARENCE WITH POST ARC CURRENT

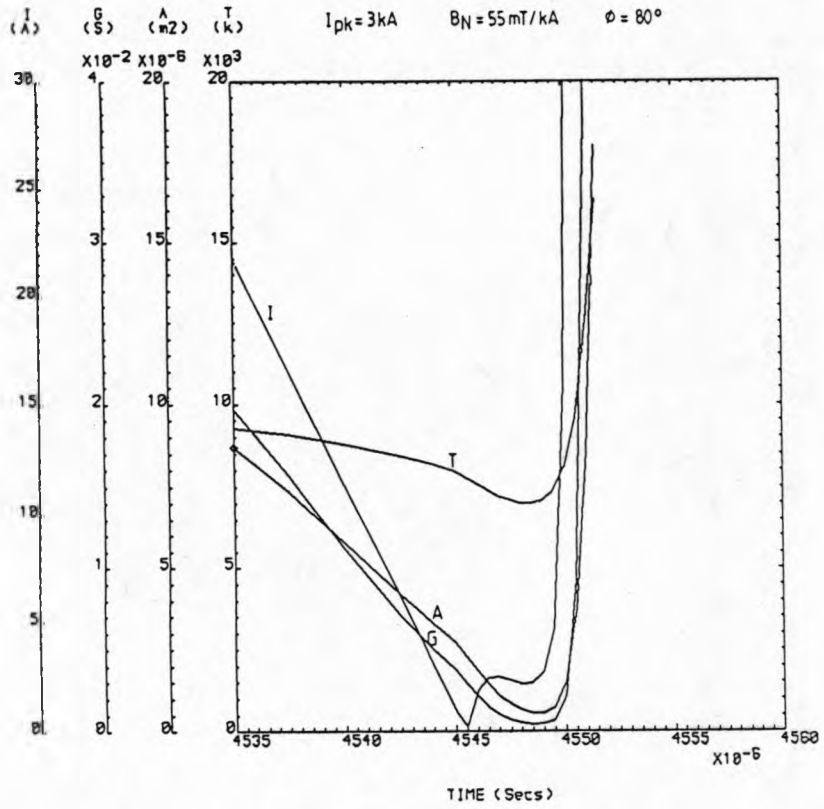

FIGURE 6·44. ARC REIGNITION

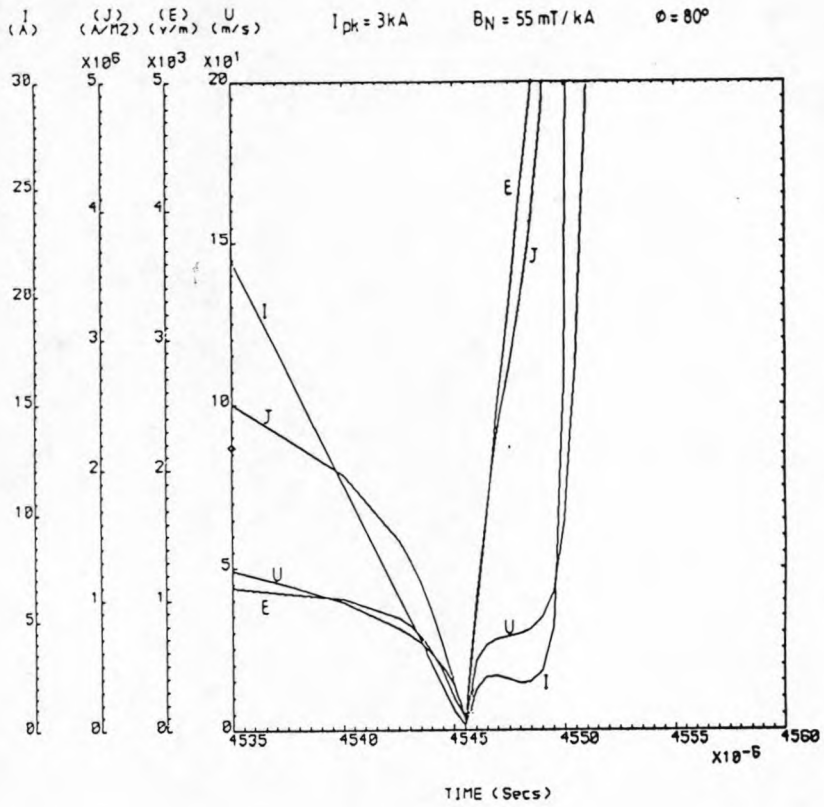

FIGURE 6·45. ARC REIGNITION

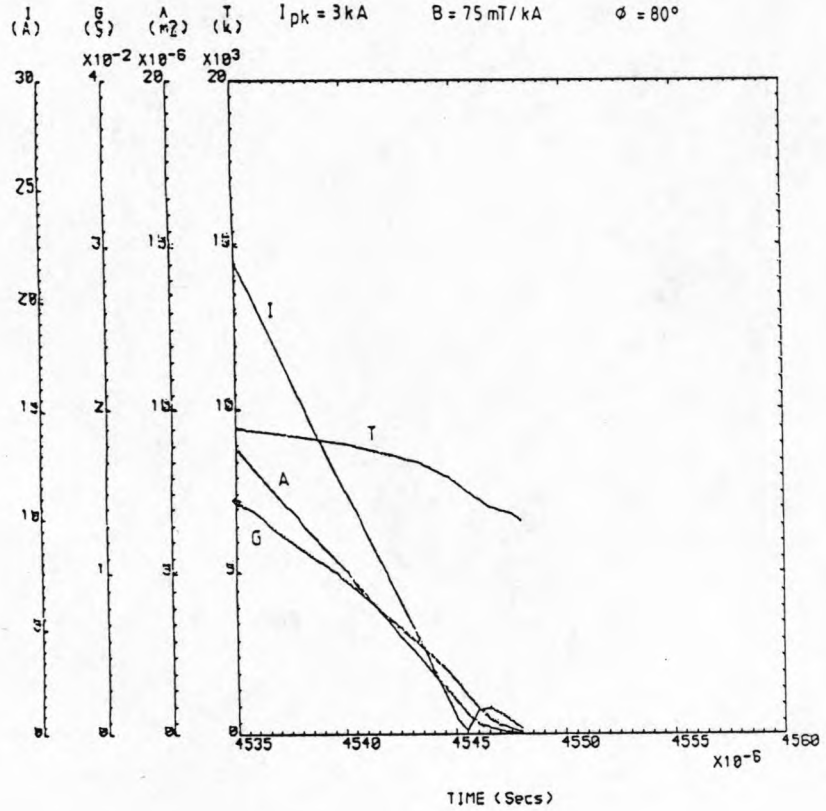

FIGURE 6·46. CURRENT ZERO BEHAVIOUR

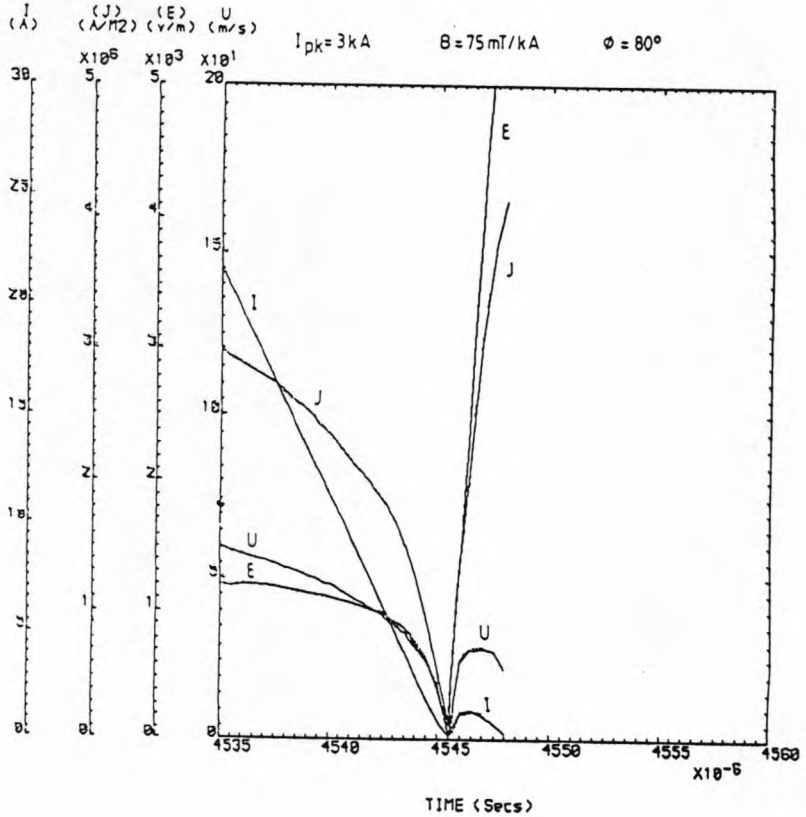

FIGURE 6·47. CURRENT ZERO BEHAVIOUR

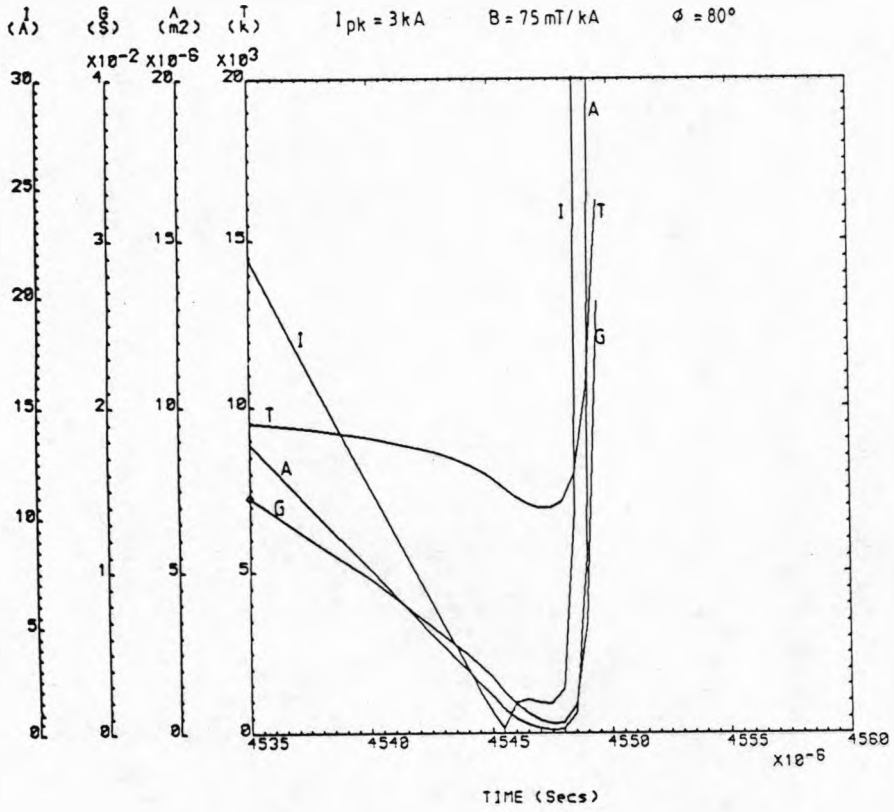

FIGURE 6·4·8 CURRENT ZERO BEHAVIOUR

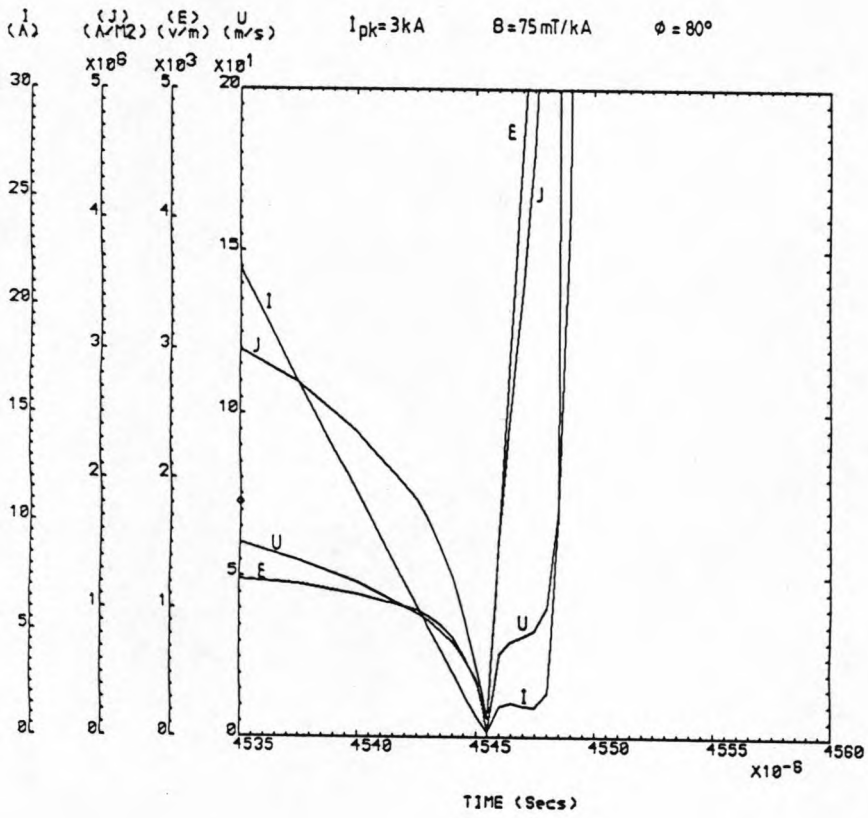

FIGURE 6·4·9 CURRENT ZERO BEHAVIOUR

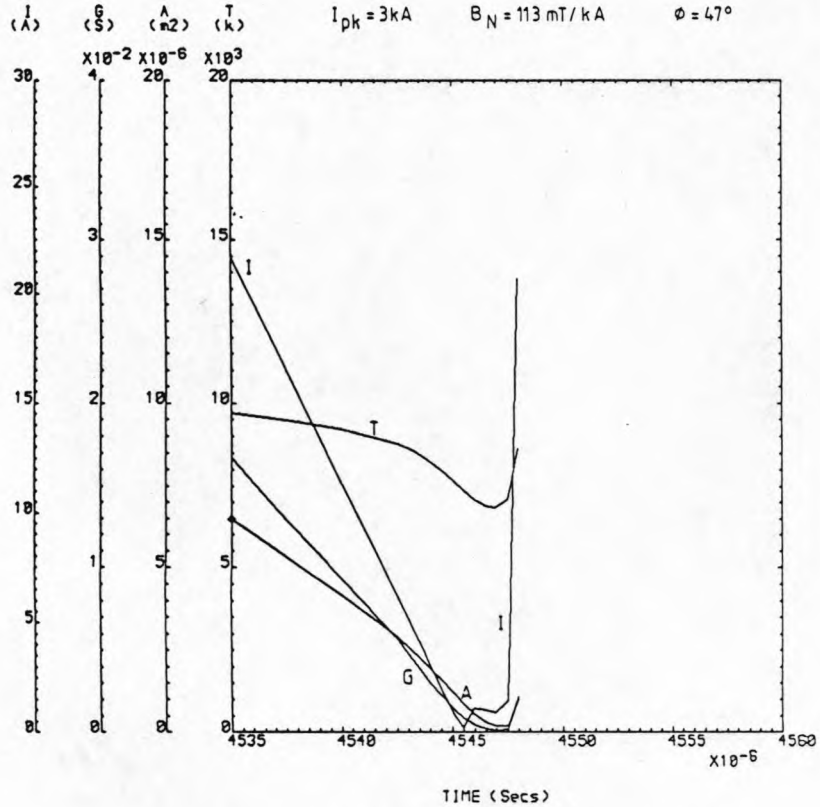

FIGURE 6·50. CRITICAL ARC REIGNITION CONDITION

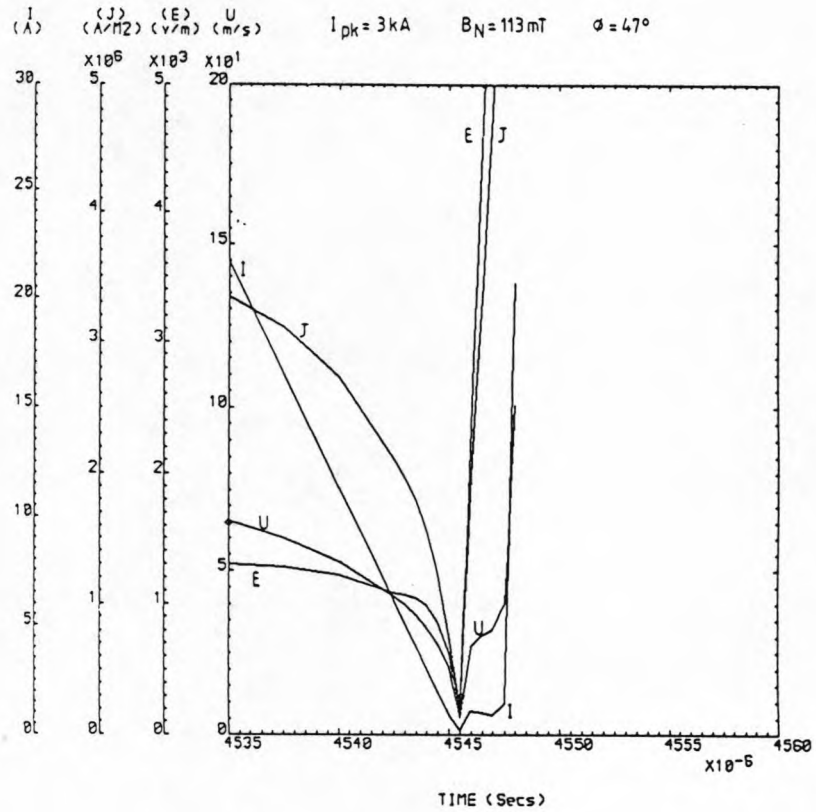

FIGURE 6·51. CRITICAL ARC REIGNITION CONDITION

6.2.3.1.5 SUMMARY OF LOW CURRENT RESULTS

The simulations for low curent arcs for various magnetic flux conditions show similar trends to those observed experimentally. An estimate of the arc's area at current zero from image converter photography is 3 x $10^{-6}m^2$ which compares well with the theoretically simulated values for the same condition. There is a similar agreement between the conductance of each type of arc and also agreement between the simulated arc temperature at current zero and that for axisymetric arcs (48).

An increase in magnetic field strength lowers the arc's temperature, area, velocity and conductance at current zero figure (6.52), the decrease in conductance and area being particularly pronounced. It is expected that there would be a decrease in the arc's temperature, area and conductance because of the increased velocity during the high current phase of arcing which increases the convective power losses from the arc column. The lower arc velocity which is recorded for a higher magnetic filed at current zero is due to the increase in the rate of change of mass within the arc column and is manifest by the smaller arc area and lower arc temperature at current zero. A similar trend is exhibited by the 47° phase difference results.

6.2.3.2 HIGH CURRENT ARCING

The behaviour of the arc at current zero following higher peak current arcing has been simulated in the same way as for the low current arc. Similar trends to those observed for the low current arcing conditions were apparent except there is a difference in the magnitude of the arcs parameters. A sample of the current zero results are presented for one condition (55T/kA and 80° phase difference angle) for two rates of rise of recovery voltage (free recovery and critical rrrv). On figures (6.53, 6.54 and figures 6.55 and 6.56).

6.2.3.2.1 FREE RECOVERY CONDITION

Under free recovery conditions the arc extinguishes in 5μs after current zero (figure 6.53). Although the stored energy at this current is larger than for the lower current case the loss of energy from the arc column has increased and this is manifest as a higher arc temperature and arc area. There is an increase in core radiation loss because of the increase in temperature and an increase in convection losses due to a higher arc velocity during this period.

Figures (6.53, 6.54) show the variation in the various arc parameters during current zero. The trends are

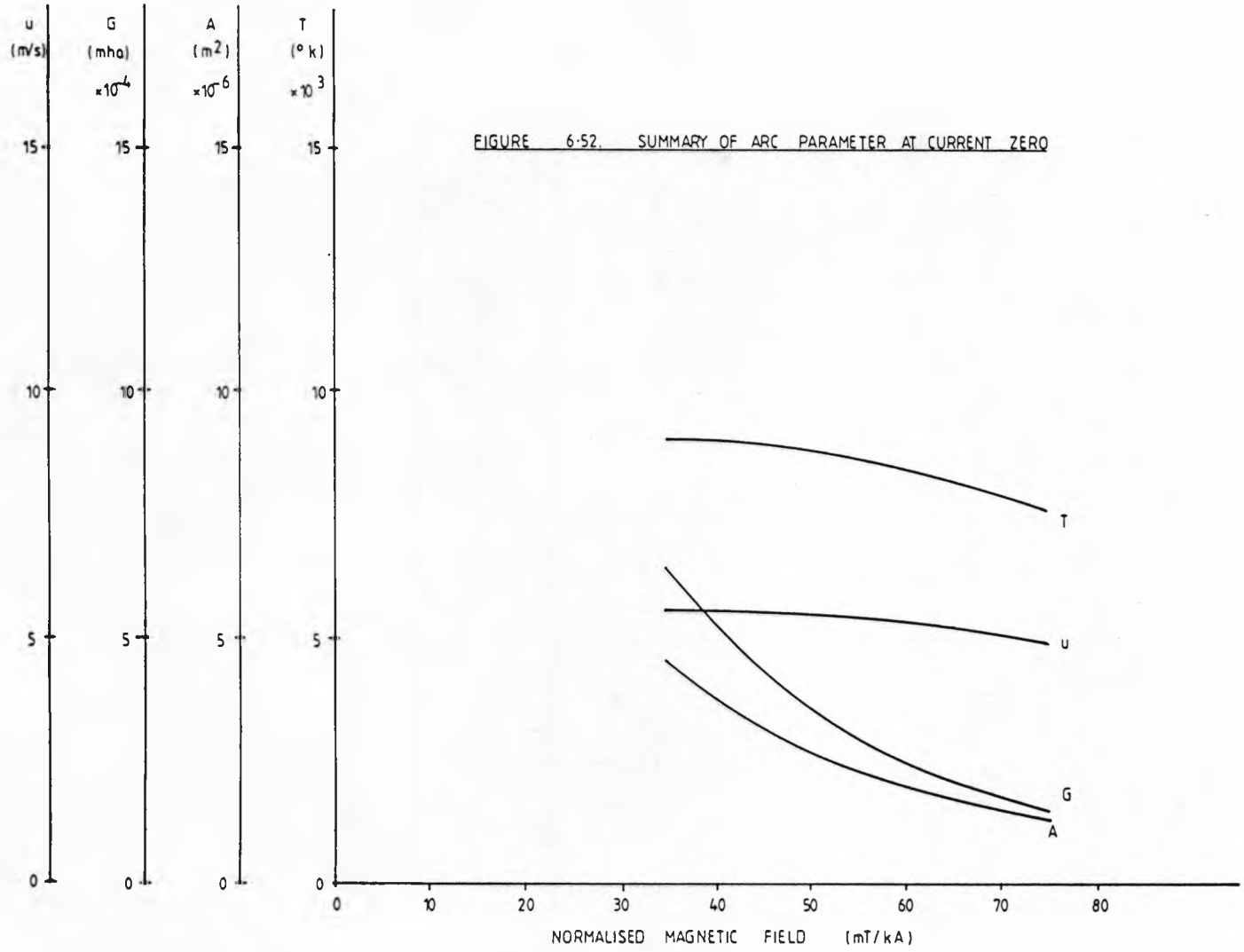

FIGURE 6·52. SUMMARY OF ARC PARAMETER AT CURRENT ZERO

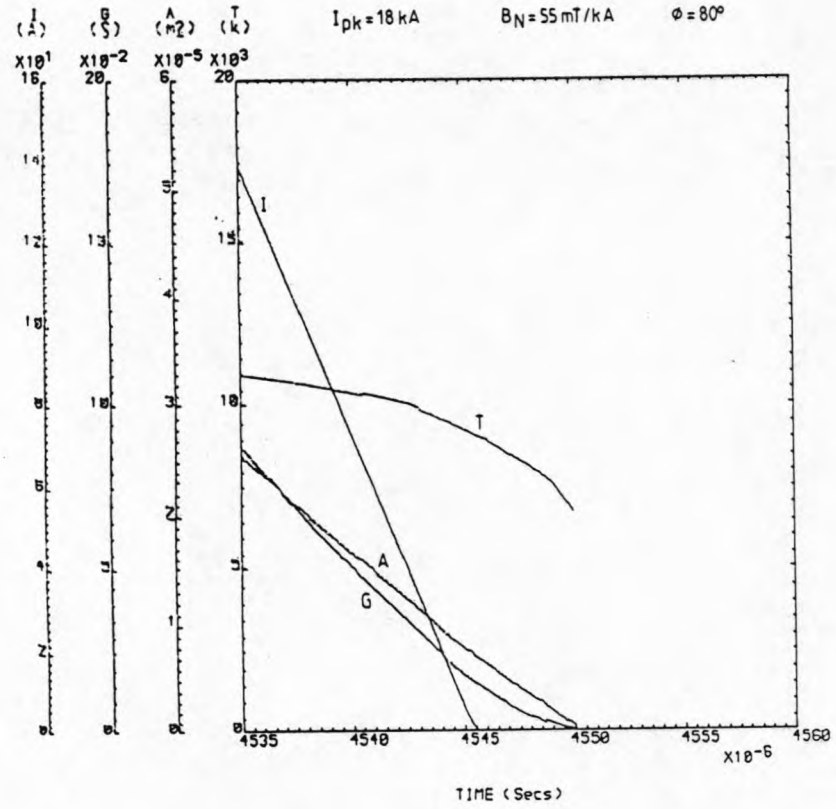

FIGURE 6.53. ARC FREE RECOVERY

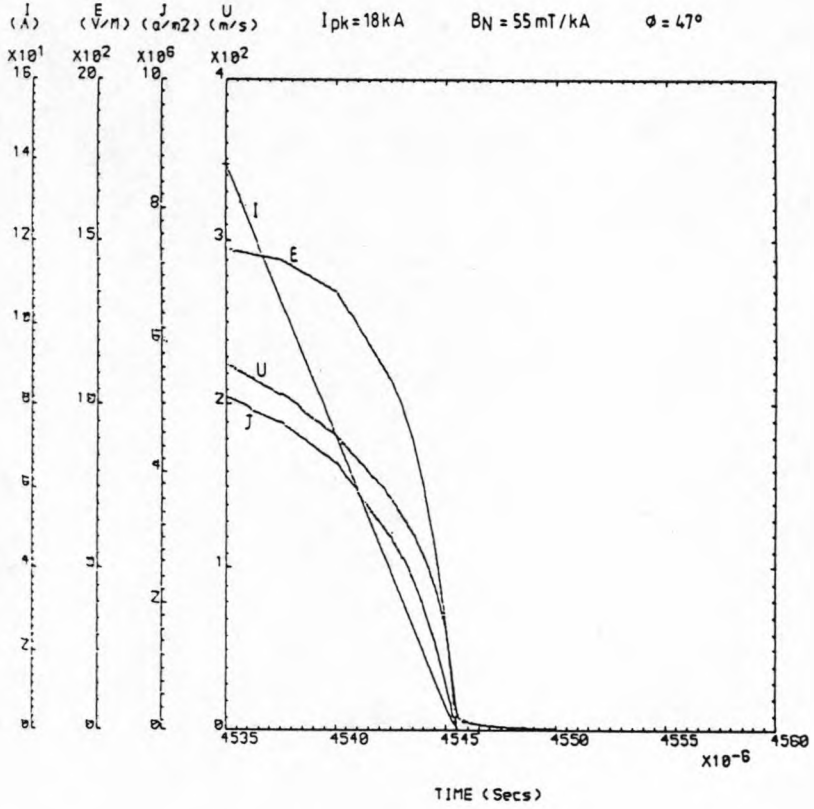

FIGURE 6.54. ARC FREE RECOVERY

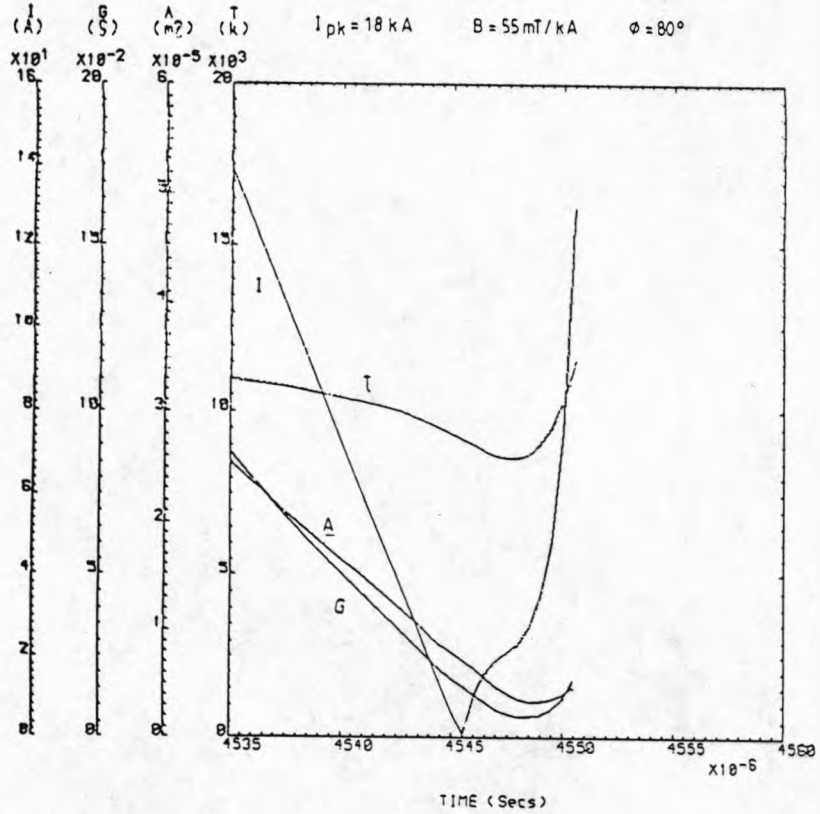

FIGURE 6·55. CURRENT ZERO BEHAVIOUR

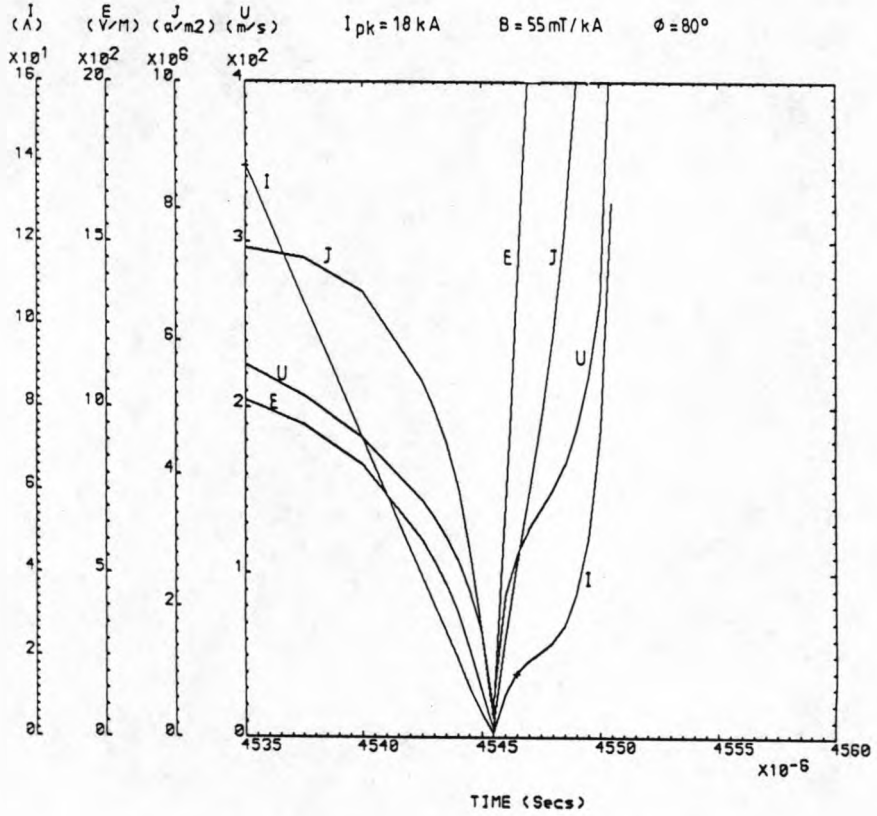

FIGURE 6·56. CURRENT ZERO BEHAVIOUR

similar to the previous low current conditions in that the arc temperature, area, conductance and velocity decrease towards current zero but have a finite value at current zero. The decay in these parameters continues after current zero until arc extinction. The remaining parameters of electric field, current density and current of course decrease to zero at current zero.

6.2.3.2.2 CRITICAL RATE OF RISE OF RECOVERY VOLTAGE

Figures (6.55, 6.56) show the effect of a critical rate of rise of recovery voltage on an arc with 18kA peak current, 55mT/kA normalised magnetic field, an 80°phase difference angle and 1.3v/μs rate of rise of recovery voltage. The response of the post arc current is immediate, rising rapidly to 2 amps in the first micro-second of current zero. However, the arc temperature does not increase for a further micro-second followed by an increase in the arc's area yet another micro-second later. During this period the arc's velocity and current density both rise rapidly.

6.2.3.2.3 SUMMARY OF CHANGES AT CURRENT ZERO

A summary of the arc parameter values at current zero are shown on figure (6.57) for an 80° phase difference between exciting current and magnetic flux density. There are similar trends as exhibited for the lower current condition except there is a rise in arc

temperature with an increased normalised magnetic field. The smaller arc area at larger magnetic fields is a result of more efficient arc conditioning during the high current phase of arcing by the increase arc velocity. The lower arc velocity recorded for a larger magnetic filed at current zero is due to the larger rate of change of mass and also because of the small mass of the arc at this point in time. One micro-second before current zero a higher arc velocity is recorded with a higher magnetic field.

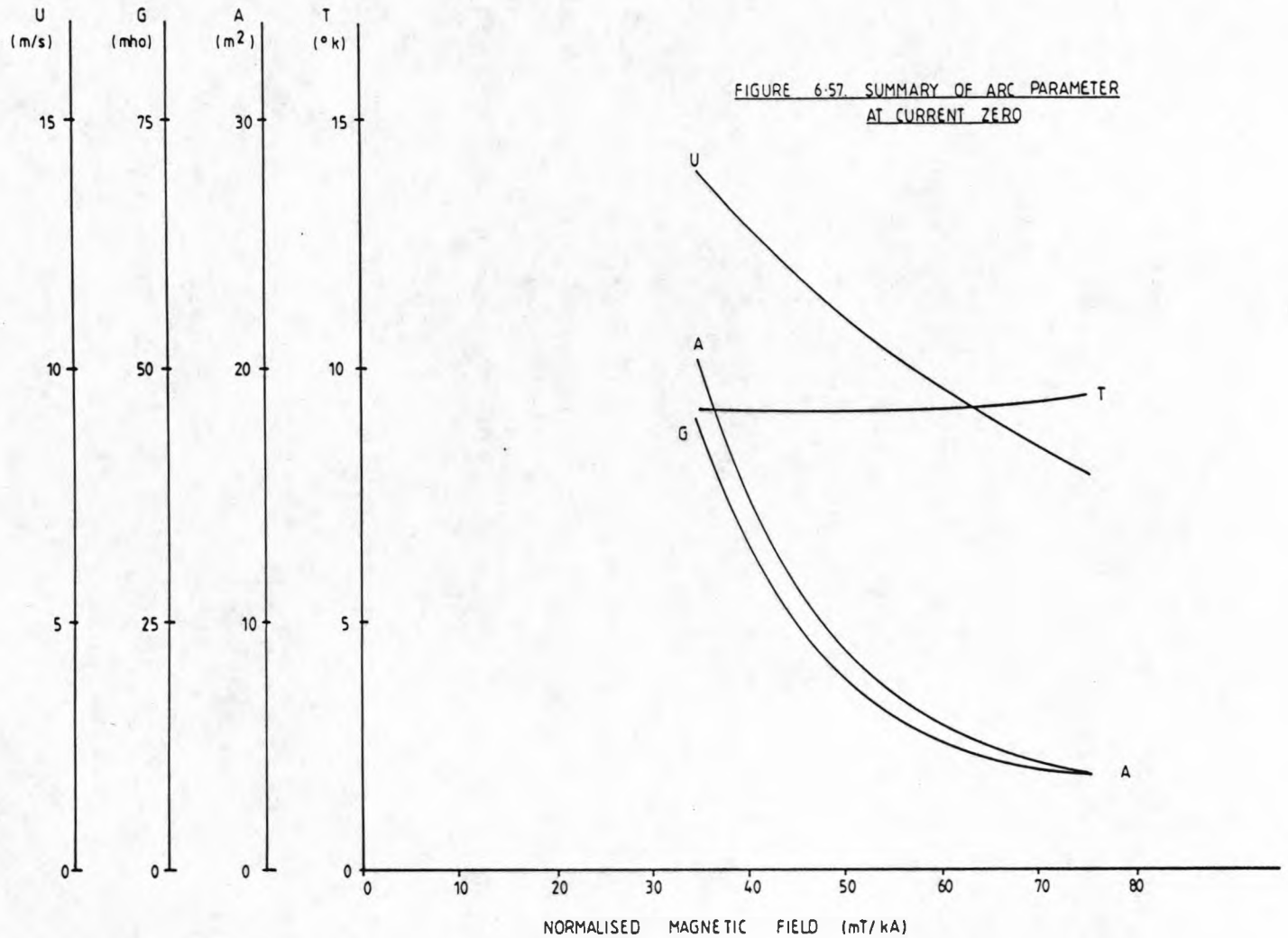

FIGURE 6·57. SUMMARY OF ARC PARAMETER AT CURRENT ZERO

7.0 CONCLUSION

The behaviour of a rotating arc discharge through stationary SF_6 is a complex interaction of many arc, areodynamic and thermodynamic parameters. Experimental investigations highlighted some of this complex interaction and identifies the most influential parameters.

One important parameter is the magnetic flux. This is highly non-uniform within the arcing voluming and has a temporal variation which has a transient exponential component. At any instant in time the magnetic field can be resolved into three components, each component is mutually orthoganol to each other. The axial component is the most dominant and has the most control over the arcs movement. However, the radial component does have some influence upon the arcs movement and is responsible inpart for moving the arc column axially into the arcing coil. Another mechanism for producing axial movement arises from instability considerations. When an arc column is placed in a strong enough magnetic field movement of the arc column can occur, under certain conditions, in the same or reverse direction as the imposed magnetic field. This instability together with the Lorentzian axial force can move the arc column beyond the mid-axial position of the arcing coil to the other end of the arcing coil.

This has the overall effect of lengthening the arc column during this time. Coupled with the rotational force the arc column becomes a spiral or helical shape within the arc volume.

A simple model is used to predict the arcs shape for the dominating magnetic field when all other forces and instabilities are negligible. The results show that the electrode effects the arc's shape considerably. However, this model shows the behaviour of the arc's shape for changes in the magnetic flux non-uniformity and highlights those changes which can be made to the magnetic field to obtain a desired arc shape.

The arc's velocity is also related to the interaction of the magnetic field and the arc current. This is controlled largely by the principal magnetic field and the inherent phase difference between the exciting current (arc current) and the resulting magnetic flux. Empirical relationships show the large dependency upon the strength of the magnetic field and the phase difference angle and the smaller influence of the arc current. This is also shown by the model used to describe the arcs velocity. The model is based upon the rate of change of momentum caused by an imbalance between the dominant Lorentz force and the areodynamic retarding forces.

This model demonstrates the influences which the areodynamic properties of arc column have on its velocity. The thermodynamic properties of the surrounding gaseous medium are also investigated. These two sets of properties are important factors in determining the arc's velocity by controlling the retarding force acting upon the arc column.

Experimentally the arc's velocity is measured by high speed photography, discrete voltage probing and fibre optic techniques. The results from all three sets of measurements were consistant. The empirical relationships derived from these results are in agreement with the equation describing the arc's motion over the current, magnetic flux and phase angle ranges investigated.

Investigation of the current zero behaviour of the arc column identified those parameters which influenced the arc's thermal performance criterion during this period. The important parameters during this period are shown to be the magnetic flux density and the phase difference angle. An empirical equation shows the relationship between the critical rate of rise of recovery voltage as a function of the rate of change of arc current, magnetic flux density and phase difference angle. Results show that a large magnetic flux density increases the critical withstand voltage after current

zero for a given di/dt, similar an 80° phase difference angle for given di/dt and magnetic flux density enables the arc column to withstand a greater rate of rise of recovery voltage after current zero.

Photographic evidence during this current zero period shows that the arc shape changes very little during one event but there can be considerable shot to shot variation manifest as an increase in arc length and shape. Despite this fluctuation the critical rate of rise of recovery voltage is independent of the arc length.

Beyond current zero if reignition occurs the arc rapidly decelerates and accelerates in the reverse direction when the Lorentzian driving force reverses (as a consequence of the reverse flow of the arc current). Photographs show that the arc column becomes extremely twisted by this reversing process, but quickly re-establishes an involute shape in this reverse direction.

With the information gained through the experimental work here and from the experience of other authors, an approximate model of a rotating arc is presented. This model is based on theoretical equations describing the arcs energy, momentum and radiation conservation during one half cycle of arcing and has sufficient detail to

describe the arcs behaviour during current zero. To model the arc column from a purely theoretical angle is extremely difficult and recoarse is made to reduce the number of unknown parameters which experimentally are extremely difficult to measure by using a blend of theory and empirism.

The model considers the arc column and its interaction with the surrounding gas. The results obtained from a computer solution using mathematical relaxation routines and a fourth order Runge-Kutta analysis, show reasonable agreement with the experimental results during the half cycle. The model can predict the arc's area, temperature, velocity and critical withstand voltage for a given set of input conditions and is able to compute reasonable values for at least the experimental range of investigations.

From this work it is possible to use an approximate model to predict the behaviour of a rotating arc discharge in SF_6. However, this model at present cannot be purely theoretical but recoarse has to be made to experimental empirism. It is possible to obtain reasonably accurate results from such an approach as presented here.

8. ACKNOWLEDGEMENTS

The author wishes to express his appreciation to the staff at the Department of Electrical Engineering and Electronics, university of Liverpool for their help during this work. I would like to give special appreciation to my supervisor Dr. G. R. Jones for his patience, invaluable help and encouragement during this work and to Dr. M. T. C. Fang for his encouragement on the theoretical work. I thank Y. Sixsmith, T. Burke and K.Davies for their help in the preparation of this thesis.

9. APPENDIX.

Nomenclature	Symbol	Definition
Thermal	θ_δ	$\int_0^\infty (1-\rho/\rho_\infty)\, 2\pi r\, dr$
Displacement	θ_d	$\int_0^\infty (1-\rho v/\rho_\infty v_\infty)\, 2\pi r\, dr$
Momentum	θ_m	$\int_0^\infty (\rho v^2/\rho^* v^{*2})\,(1-v_\infty/v)\, 2\pi r\, dr$
Magnetic	θ_B	$\pi r_1^2 \exp[-2\int_0^1 (B/B_1)^2\,(r/r_1)\, d(r/r_1)]$
Enthalpy	θ_Δ	$\int_0^\infty (\rho h/\rho^* h^*)\,(1-h_\infty/h)\, 2\pi r\, dr$
Enthalpy flux	θ_h	$\int_0^\infty (\rho v h/\rho^* v^* h^*)\,(1-h_\infty/h)\, 2\pi r\, dr$
Kinetic energy	θ_{ke}	$\int_0^\infty (\rho v^3/\rho^* v^{*3})\,(1-v_\infty^2/v^2)\, 2\pi r\, dr$
Radiation	θ_Q	$\int_0^\infty (Q/Q^*)\, 2\pi r\, dr$
Conductance	θ_c	$\int_0^\infty (\sigma/\sigma^*)\, 2\pi r\, dr$

Table A1.

APPENDIX 1

MAGNETIC FIELD CALCULATION

The magnetic field at a point P from a current conducting cylindrical copper bar is;

$$B = \iiint \frac{\mu}{4\pi} \frac{\underline{J} \times \hat{\underline{r}}}{r^2} \, dv \qquad A1$$

J = current density (A/m^2)

B = flux density at P (T)

μ = permeability of medium (H/m)

$\hat{\underline{r}}$ = unit vector from element to P

r = distance from dv to P (m)

dv = infinitesimal element of volume (m^3)

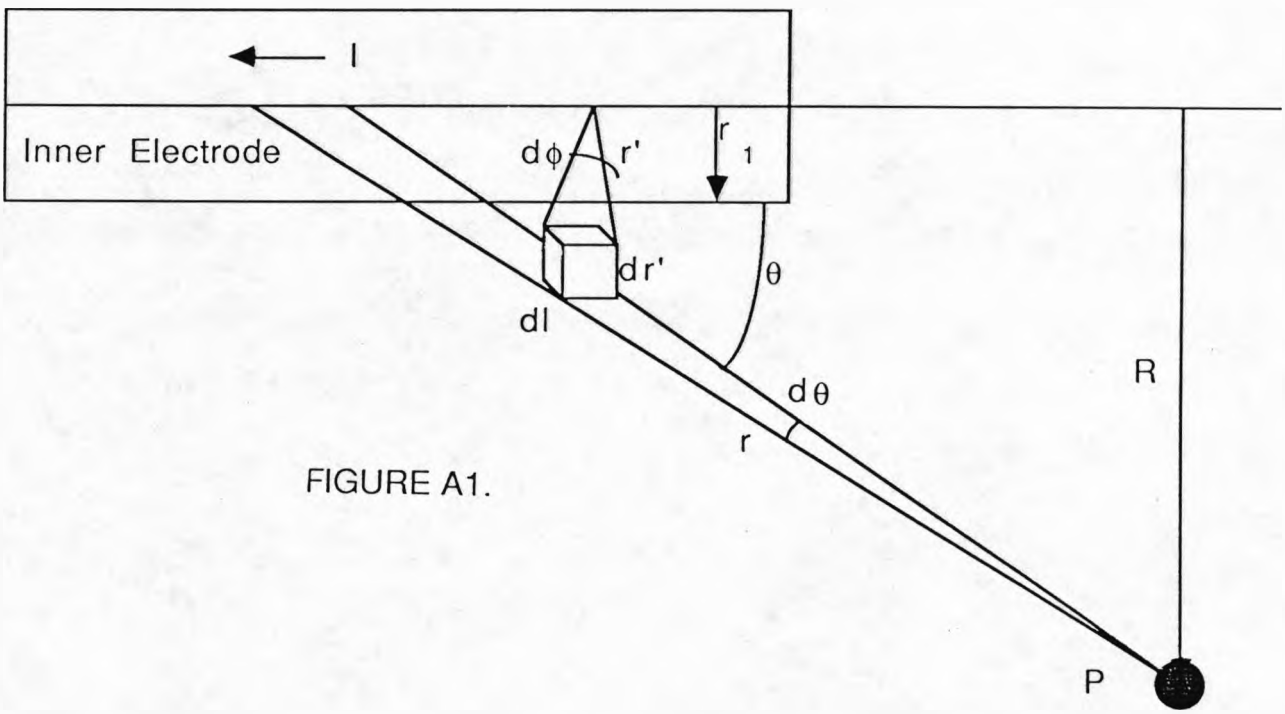

FIGURE A1.

For $R \geq r_1$ then

$$dv = r'd\phi dr'dl \qquad A2$$

Substituting A2 into A1

$$B = \frac{\mu}{4\pi}\int_{l_1}^{l_2} dl \int_0^{r_1} dr' \int_0^{2\pi} \frac{J\sin\theta\, r'd\phi}{r^2} \qquad A3$$

$$B = \frac{\mu}{4\pi}\int_{l_1}^{l_2} \frac{I\sin\theta dl}{r^2} \qquad A4$$

Making the following substitutions into A4

$$\sin\theta dl = rd\theta \qquad R = r\sin\theta$$

$$B = \frac{\mu I}{4\pi R}\int_{\theta_1}^{\theta_2} \sin\theta d\theta$$

$$B = \frac{\mu I}{4\pi R}\left[-\cos\theta\right]_{\theta_1}^{\theta_2} \qquad A5$$

APPENDIX 2

AVERAGE THERMAL DIFFUSIVITY FOR SF_6

The solution of equation (5.15) for the region $-r < x < r$ (where $-r$ and r represents the arc's boundary), is

$$\lambda t/R^2 = f[\chi]$$

$f[\chi]$ is obtained by graphical means (figure A2). For this particular case T/T_0 is 0.95 and $f[\chi] = 0.13$.

From Kopainsky and Schade the most pessimistic λ can be calculated from their experimental results.

The time for one arc rotation is 0.138 mS for an arc radius of 4.25×10^3 m. The thermal diffusivity is calculated as 17.0×10^{-3} m^2/s.

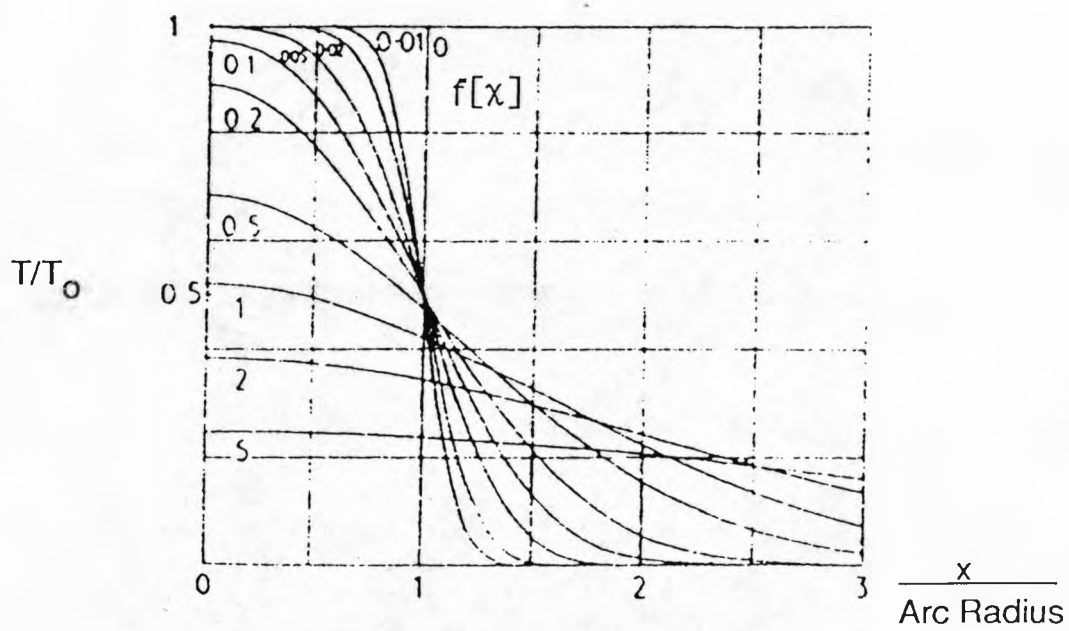

Figure (A2)

The subsequent calculation of the time of the wake temperature to decay from 2000° k to 1900° k is

$$t = \frac{f[\chi]R^2(t)}{\lambda}$$

10. REFERENCES

1. Guile, Arc Electrode Phonomena. proc.IEE,IEE Reviews vol 118, no. 9R, 1971.

2. Block, M.J. and Fenkelnburg,W.,Z. Naturforsch 1953, 8A.

3. Eckler, G., Technical report for US Dept, of navy. FTRI 1959.

4. Unpublished seminars by G.R. Jones L'pool University. (1984).

5. Maccker H . Z.phys., 1955,141,pp198-216.

6. Cassie, M. Arc rupture and circuit severity, a new theory. CIGRE Paper No.102 (1939)

7. Mayr,O. Arch. Elekrotech 37, 1943.

8. Browne T., A study of AC arc behaviour near current zero by means of mathematical models. AIEE Trans., 67 Pt.I (1948).

9. Lee, T.H-Jappl. Phys., 1957,28 pp920

10. Lee, T.H. J.Appl. Phys., 1959,30,pp166-171.

11. Swanson B.W. and Roidt,R.E., Boundary layer analysis of an SF6 circuit breaker arc. IEEE Trans PAS-90, 1970.

12. Swanson, B.W., Roidt, R.E., and Browne, T., Arc cooling and short line fault interruption. IEEE Trans. PAS-90, 1970.

13. Swanson, B.W., Roidt, R.E., and Browne,T., Thermal Analysis of an SF6 circuit breaker arc IEE Trans. PAS-91, 1972

14. Swanson, B.W., and Roidt, R.E., Some numerical solutions of the boundary layer equation for an SF6 arc.IEE vol 59, 1971.

15. Swanson B.w., Roidt., R.E., and Browne, T. A Thermal arc model for short line fault interruption. ET-Z-A BD93. 1972.

16. Swanson B. W., A themal analysis of a short line fault interruption IEE Winter power meeting paper C-74,1974.

17. Swanson B.W., Nozzle arc interruption in supersonic flow. IEEE Trans. PA5-96,1977.

18. Topham, D.T., The electrical arc in a constant pressure axial gas flow. J. Phys. D, Vol 4, 1971.

19. Topham, D.T., Scaling laws for interruption of a Gas blast circuit breaker arc with an electric circuit. proc.IEE power vol,119 no. 10, Oct 1972.

20. Topham, D.T., The characteristics of axial flow electric arcs subject to pressure gradiants. J. Phys.D.Appl. Phys, Vol 5, 1972.

21. Hermann, W., and Schade, E., JQSRT 12, page 1257 1972.

22. Hermann, W., Kagelschatz, Niemegerm, Ragaller, Schade. Experimental and theoretical study of a stationary high current arc in a supersonic nozzle flow. J. Phys. D., vol.74, 1974.

23. Hermann, W., Kagelschatz, Niemeyer, Ragaller, Schade. Investigation on the physical phenomena around current zero in H.V. Gas Blast Breakers. IEEE Trans. PA5-95, 1976.

24. Niemeyer and Ragaller. Development of turbulance by the interaction of gas flow within plasmas. Z. Naturfosch, vol 28a,1973.

25. Hermann, Ragaller and Schneider. Theory of high pressure arc in strong axial gas flow. proc. 10th ICPIG 1971.

26. Hermann and Ragaller. Theoretical description of the current interruption in H.V. gas blast circuit breakers. IEEE Trans. PAS-96, 1977.

27. Tuma, D.T. and Fong ,E. Current zero deformation by interaction of the air blast arc with the test circuit IEEE, Trans. PAS, VOL, PAS-99 P,976,1980.

28. Tuma, D.T. and Lowke, J.J. Prediciton of properties of arcs stabilised by forced convertion. J. Appl. phys., vol 46, pp.3361-67, 1975.

29. Richley, E and Tuma, D.T. Free recovery of gas blast arc column, IEEE Trans. on plasma science, vol P5-8, pp 405-410, 1980.

30. Richley, E. and Tuma,D.T., Mechanisims for temperature decay in the feely recovering gas blast arc, IEEE Trans., plasma science, vol. p5-10, pp2-7, 1982.

31. Lowke, J.J. and Ludwig H.C. A simple model for high current arcs stabilised by forced convection, J.Appl. Phys., vol 46, P3352, 1975.

32. El-Akkari, F.R and Tuma, D.T. Simulation of transient and zero current behaviour of arcs stabilised by forced convection, IEEE Trans., PAS, vol.PA5-96, pp 1784-88, 1977..

33. Tuma, D.T. A comparison of the behaviour of SF6 and N2 blast arcs around current zero. IEEE Trans. PAS, vol PA5-99,PP.2129-2137, 1980.

34. Fang, M.T.C. and Brenan, D.A. Current-zero arc model based on forced convection. IEEE Trans., Plasma Science,vol P5-7, PP.217-29, 1979.

35. Malghan,V.R., Fang M.T.C. and Jones, G.R. Investigation of quasi-steady state high current arcs in an orifice airflow, J Appl.Phys., vol.48, pp2331-37, 1977.

36. Cowley, M.D. Integral method of arc analysis. pt.I. J.phys D., Vol.7, pp. 2218-2231, 1974.

37. Chan, S.K., Cowley, M.D. and Fang, M.T.C. Integral method of arc analysis,pt.111. J. Phys.D., Vol 9. pp.1085 -1099, 1976.

38. Chan, S.K., Cowley, M.D. and Fang M.T.C. The DC arc in a supersonic nozzle flow, IEEE Trans, Plasma Science, volPS-6, pp394-405,1978.

39. Fang, M.T.C. Ramakrishnan, S., and Messerle, H.K. Scaling laws for gas blast circuit breaker arcs during the high current phase. IEEE Trans., Plasma Science, vol PS-8, pp.357-62, 1980.

40. Fang, M.T.C. and Newland, D.B. DC Nozzle arcs with mild wall ablation. J. Phys. D. Vol 16 pp. 793-810 1983.

41. Lee., T.H. Plasma physics and the interuption of an electric circuit. proc. IEEE, Vol 57, no.3, 1969.

42. Fang., M.T.C. "A review of gas blast circuit breaker arc modelling. Arc research project report, ULAP-T75, 1983.

43. Maecker H. General description of stationery arc discharges with some experimental arrangements Proc 3rd. Internal Symp. On Electrical Discharges In Gases (venice 1957)

44. Yoon.K.H., and Spindle, H.E., A study of the dynamic response of arcs in various gases. Trans AIEEE (power apparatus and systems), Vol77 PP1634-1642, February 1959.

45. Edels, H and F.H. Ferlon, Theory of a filled tube thermal arc column, Brit J. Appl. Phys., Vol.16, P219, 1965.

46. Fenlon, F.H. Phid. Thesis, University of Liverpool. "Theoretical Studies of Arc Interruption and thermal reignition. 1963.

47. Walmsley.H., Jones. G.R., and Barrault .M.R., "Properties of the Thermal Region of a gas Blast A.C. Arc particularly near current zero. ULAP-T56 March 1978 Liverpool University.

48. Lewis .E., "Private communication."

49. Smith. M.R., Jones G.R., Housby-Smith. C., Barrault. M.R., El-Menshawy.M.F., Jenkins.J.E. Spectrascopic investigations during the current zero period for arcs in an orifice gas flow. Report ULAP-T61 Nov 1978 University of Liverpool.

50. J.J.Lowke and Ludwig H.C., A simple model for high-current arcs stabilised by forced convection, J.Appl. Phys., Vol 46, pp3352-3360 1975.

51. Jones, G.R. and Freeman, G.H., The influence of natural radial convection upon the transient behaviour of a cylindrical arc column. Z. Physik, 229,PP177-191,1969.

52. Chan S.K., Fang M.T.C. and Cowley M.D. Proc IEE 122 pp580-590.

53. Fang M.T.C., Chan S.K., and Cowley M.D. J Phys. 9 1757-1770

54. Walmsley H.L., Jones G.R., IEEE Trans on plasma science. PS-8, 39-49 1980.

55. Uhlenbusch, J., 1976, Physica, 82c:61.

56. Stäblein,H.G., 1977, in "Proceedings, 13th INTERNATIONAL CONFERENCE ON PHENOMENA IN IONISED GASES, BERLIN, INVITED LECTURERS.

57. Jones G.R., and Fang, M.T.C., 1980, Rep. Prog. Phys., 43:1415.

58. Lord, W.T., J. Fluid Mech., 35 689-709. 1969.

59. Hodnett, P.F., The physics of fluids,12,1441-1451 (1969)

60. Hermann,W. and Ragaller,K., proc,. 1xth I.C.P.I.G., BUKAREST 1969, P306.

61. Fucks.W. Bartels,K. Fischer,E., Uhlenbusch,J. ARL report 68-0074 (1968)

62. Fischer, E. Thesis,T.H. Aachen 1967

63. Bartels,K., Thesis, T.H. Aachen 1969

64. Yas'ko,O.I. Br. J. Appl. Phys (J. Phys D) Ser 2 1969 1967

65. Nicolai, L.M., and Kuethe,A.M., Phys. Fluids 12, 2072-82 1969.

66. V.R. Malgham and Benson, D.M., ARL - Report 71-0302 pp 147-168 (1971)

67. Baker, A.J. and Benson D.M., Proc IEEE,59,450-457 (1971)

68. Sebald,N. Proc X11th I.C.P.I.G., EINDHOVEN 1975 PP187.

69. Plessl. A, Appl. Phys. 21. 377-389 (1980).

70. Roman W.C. and Mayr T.W. AIAA Journal 5 (1967)2011.

71. Guile, Naylor and Wells, J. Phys. 3(1970) 931.

72. Guile,A.E., Adams, V.W., Lord,W.T. and Naylor,K.A., Proc.IEE vol 116, No.4. April 1969.

73. Kopainsky, and Schade,E. Appl. Phys.20,147-153(1979).

74 Kopainsky,J. and Schade,E. GAS DISCHARGE CONFERENCE SWANSEA SEPT '76

75. Guile, A.E., and Sloot, J.G.J. Proc.IEE, VOL 122,No6, JUNE 1975

76. Adams V.W. Technical note No. Aero 2915 R.A.E. Sept 1963.

77. Schrade H.O. , IEEE Trans. VOL. PS -1 1973.

78. Bennanson, D.M. and Baker,A.J. AIAA Journal vol 9 no. 8 Aug 1971.

79. Taylor,S. and Wang, B. ULAP INTERNAL REPORT 1981

80. Grundy, J.A. Proc. IEE, VOL 124, No.5 MAY 1977.

81. Park, J.H., J. Res. Natl. Bur. Stand., 1947,39,pp191-212.

82. Silsbee, F.B. Bureau of Standards Journal of research

83. Schwadd, A.V., IEEE Trans. 1970, IM-19, pp2251-2257.

1930, 4,pp73-83

84. *Chapman, A. Ph.D. Thesis Liverpool University 1977.*

85. *D. Chan and Turner, D.T. The Transient Magnet Field of a rotating arc device, Internal Report dept, Electrical Engineering and electronics Liverpool University 1984.*

86. *Schrade H.O., Xth INTERN CONF ON PHENO OF IONISED GASES.*

87. *Wang B., Taylor , S., Blackburn, T.R., Jones, G.R. ULAP REPORT T72 1982.*

88. *Briggs A.C. The contribution of Axial and Radial Components of gas velocity to the thermal interuption capability of a Gas Blast Circuit Breaker. Proc.Vll INT CONF on Gas Discharges and their applications, 1982.*

89. *LOWKE. J.J. Predicisions of Arc Temperature Profiles using approximate Emission coeficients for radiation losses. J Quant. Spectrosc. Radiat. Transfer, Voll4, pplll-122.*

90. *Freeman, G.H., "The transient Behaviour of cylindrical Arc Columns." PH.D. thesis Dec 68 L'Pool university*

91. *Jones G.R. Private Communication 1985.*

92. *Bublievskii, A.F., "An approximate model of an electric Arc in transverse mutually perpendicular aerodynamic and magnetic fields" INZHENERNS-FIZICHESKII ZHURNAL VOL 35 No. 6 pp 1012-1018 Dec 1978.*

93. *Strachan, D.C., Bolton A.W., Jones G.R., and Atkinson,F.B.(1977) UNIVERSITY OF LIVERPOOL RESEARCH REPORT. ULAP-T46.*

94. *Frost and Libermann, Composition and Transport properties of SF6. Proc. IEEE. Vol.59, No.4. 1971.*